

SPIN STRUCTURE OF THE NUCLEON:
PHENOMENOLOGICAL DESIDERATA

THESIS

*Submitted to the University of Madras
as part of the requirements for the award of degree of
DOCTOR OF PHILOSOPHY*



by

D. INDUMATHI

THE INSTITUTE OF MATHEMATICAL SCIENCES
MADRAS 600 113 INDIA
NOVEMBER 1992



THE INSTITUTE OF MATHEMATICAL SCIENCES

Madras 600 113, India.

Ph: 2351856, 2350856

ACKNOWLEDGEMENTS

October 29, 1992

I thank my supervisor

Prof. M.V.N. Murthy

CERTIFICATE

This is to certify that the Ph.D thesis submitted by D. Indumathi to the University of Madras, entitled "Spin Structure of the Nucleon: Phenomenological Desiderata," is a record of bonafide research work done by her under my supervision. The research work presented in this thesis has not been presented in part or full for any Degree, Diploma, Associateship or other similar title. It is further certified that the thesis represents independent work on the part of the candidate and collaboration was necessitated by the nature and scope of the problems dealt with.

Prof. M.V.N. MURTHY



ACKNOWLEDGEMENTS

I thank my supervisor, M.V.N. Murthy for helping me through this thesis with patience. His unfailing optimism and enthusiasm have encouraged me to work harder—I have learnt a great deal from him.

I also thank Ramesh Anishetty, Babaji, HariDass, Sourendu Gupta, Anjan Joshipura, Deepak Mathur, Murthy and J. Pasupathy who have taught me much of the Physics I know. I thank Prakash, Ravindran and Uma Sankar who have so cheerfully listened to my lectures and contributed a great deal to my understanding of Spin Physics.

To the trio—Balaji, Ravi-ji and Shaji—strong proponents of the Other School, from whom I hope to learn more, many thanks.

I thank the Institute of Mathematical Sciences and everybody in it for providing all requisite facilities and generally, a happy and congenial atmosphere. I thank Jayaraman, John, Manas, Manu, Rahul and Vytheeswaran who have helped me in many ways.

I thank my parents, sister and parents-in-law for their constant encouragement and support; also Kamal, Krishna and Shanthi, practically family by now.

And thanks, of course, to Ramanujan without whom this thesis—and much else—would not have been.



CONTENTS

1	Introduction	1
1.0	Background	1
1.1	Motivation	4
1.1.1	Formalism of DIS experiments	5
1.1.2	The EMC results	9
1.1.3	Discussion of results in the Parton Model	12
1.1.4	Consequences of the EMC results	15
1.2	Organisation of the thesis	17
	References	19
<i>pp collision processes: Introduction</i>		
	References	
PART I		
PARTON MODEL PHENOMENOLOGY		23
2	Parametrisation of Densities	26
2.0	Preliminaries	26
2.1	The Constraints	28
2.2	Choice of Parametrisations	29
2.2.1	Parametrisation Type 1	36
2.2.2	Parametrisation Type 2	46
	References	46
3	The Valence Densities	49
3.0	The μ - p semi-inclusive process	49
3.1	Formalism	50
3.2	Numerics	62
3.3	Conclusions	64
3.4	Application to the nuclear EMC effect	64
3.5	Appendix on $\nu\bar{p} \rightarrow \mu hX$	68
	References	69
	<i>pp collision processes: Introduction</i>	70
4	The gluon densities: Intermediate-x region	76
4.0	Direct photon and Drell Yan processes	76
4.1	Formalism	77
4.2	Numerics	89
4.3	The $p\bar{p}$ collision process	101
4.3.1	Numerics	103

5	The gluon densities: Small- x region	108
5.0	The 2-jet production processes	108
5.1	Formalism	109
5.2	Numerics	114
6	The sea densities	125
6.0	The direct diphoton process	125
6.1	Formalism	125
6.2	Numerics	130
6.3	The $p\bar{p}$ collision process	134
	pp collision processes: Conclusion	137
	References	139

PART II

SPIN DEPENDENT STRUCTURE FUNCTION, REVISITED

7	OPE approach to the moments of the spin dependent structure function	143
7.1	The OPE Formalism	144
7.2	Effective equation of motion	145
7.3	Numerical estimates of m_{eff}	146
7.4	Model calculation of matrix elements	148
7.5	Conclusions	155
	References	156
8	The spin dependent structure functions: QCD Sum Rule approach	157
8.1	The Sum Rule	160
8.2	Calculation of $\text{Im}\mathcal{T}_{\mu\nu}$ via the OPE	164
8.3	Conclusion	173
	References	174

APPENDICES

A	$2 \rightarrow 2$ Kinematics	176
A.0	Introduction	176
A.1	The cross-section	178
A.2	Mandelstam variables	180

B	Collection of useful formulae	181
B.0	The QCD Lagrangian	181
B.1	Definitions and normalisation conventions	183
B.2	γ -matrix algebra	187
B.3	Some colour traces and identities	188
B.4	Feynman rules for QCD	189
Background		
C	Deep inelastic scattering phenomena	191
C.0	Introduction	191
C.1	The leptonic tensor, $\mathcal{L}_{\mu\nu}$	194
C.2	The hadronic tensor, $\mathcal{W}^{\mu\nu}$	195
C.3	The cross-section	197
C.4	The asymmetry	200
C.5	Parton model interpretation	201
	References	204
D Kinematics of pp processes		
D.0	Variables in pp processes	205
D.1	Cross-section for $2 \rightarrow 3$ processes	208
D.2	Choice of reference frame	210
E Some details of the Sum Rule method		
E.1	The LHS	212
E.2	The RHS	213
E.3	List of Integrals	215



INTRODUCTION

CONTENTS

Background

Motivation

Organisation of thesis

Nuclear physics arose with the knowledge that the nucleus of an atom is composed of particles with half-integral spin, *protons* and *neutrons*, collectively called *nucleons*. Successive discoveries of more and more elementary structures of matter led to an understanding of the underlying sub-structure of these nucleons. These constituents of the nucleon, labeled collectively as *partons* were shown to account for several of the nucleonic properties. In spite of the great advances made in the understanding of the nucleonic structure, little is known about the distribution of the “*spin*” of the nucleon in terms of the spin of its constituents. An investigation into this problem forms the subject matter of this thesis.

In this chapter, we put these discoveries, both theoretical as well as experimental, regarding the structure of the nucleon in a historical perspective. We then use this to provide motivation as well as background for this study.

1.0 Background

Early parton ideas like the Quark Model of Gell-Mann [1] viewed quarks simply as theoretical constructs, obeying certain symmetry principles which enabled them to make predictions about some static hadronic properties. Quarks were postulated to be particles with fractional charges and half-integer spin. This simple quark model ran into problems [2] immediately when attempting to define the wave function for the proton and neutron. Since these are the lightest baryons, their spatial wave function was assumed to be symmetric, in the

spirit of quark models. However, the observed ratio of the magnetic moments of the neutron and proton indicated that their wave functions were also symmetric in spin-isospin space. This fully symmetric wave function contradicted the notion that the wave function of a system of fermions should be fully antisymmetric under particle exchanges. In order to preserve the spin-statistics connection, a new internal degree of freedom called *colour* [3] was postulated; quarks came in three colours such that the hadronic wave function was explicitly antisymmetric in colour space, thus restoring the desired antisymmetry of the wave function.

Although quarks are coloured, the multiplicity of the observed hadrons exactly matched the counting based simply on the number of charge states allowed. This implied that hadrons were colour singlets and eventually led to the idea of *colour confinement* with no coloured hadrons occurring in nature. The quark model a la Gell-Mann gave a reasonable explanation of the static properties of hadrons; however, it still lacked a knowledge of the underlying dynamics.

In the late '60s, results on deep inelastic scattering (DIS) of high energy electrons off protons at the Stanford Linear Accelerator Centre (SLAC) provided a first look into the deep interior of the nucleon. They established what is now known as *scaling* behaviour: the cross-section for such a process can be expressed as a product of kinematical factors and unknown *structure functions*. These structure functions were found, to a very good approximation, to be independent of dimensional quantities like the momentum transfer and energy transfer in the experiment, [4] but to depend only on a dimensionless combination of these. This scaling behaviour was surprising in view of the fact that the elastic electron-proton cross-sections fall off very rapidly with the squared momentum transfer, Q^2 (approximately as $(1/Q^2)^4$ for large momentum transfers); hence, the inelastic cross-section was expected to be very small. However, scaling had actually been predicted by Bjorken [5] using Current Algebra techniques. It was realised that such behaviour is consistent with

a picture of electrons scattering incoherently off point-like, almost free particles within the nucleon; these were called *partons* and this idea of point-like structures within the nucleon was incorporated into the *parton model* [6]. The angular distribution of scattered electrons in DIS indicated that these partons, relevant to the understanding of DIS, were spin-half fermions and could, in fact, be identified as the quarks that were discussed earlier. Scaling appears naturally in the parton model as a consequence of the absence of a mass scale (partons are massless) in the theory. The parton model was very successful not only in describing DIS phenomena but a host of other experiments involving hadrons at high energies and momentum transfers.

In the meanwhile, great advances were made in the area of non-abelian gauge theories. With that emerged the so-called Standard Model [7] of particle physics. The standard model, as it stands today, is a non-abelian gauge theory based on the group $SU(3)_C \times SU(2) \times U(1)$. This theory, in principle, is supposed to reproduce all known strong, electromagnetic and weak interaction physics. The theory of strong interactions, Quantum Chromodynamics (QCD), [8] forms an integral part of the Standard Model. It is a non-abelian, renormalisable theory with the colour gauge group $SU(3)_C$. It is an asymptotically free theory which implies that the renormalised coupling constant vanishes (logarithmically) as the momentum scale, Q^2 , tends to infinity. The theory also prescribes how corrections can be calculated order by order in the perturbation, with the renormalised coupling constant being the expansion parameter. At low or intermediate energies (with respect to energies involved in nuclear interactions), typically of the order of the nucleon mass, the coupling constant is large and is no longer a good expansion parameter. Hence calculations are reliable only at short distances or at large Q^2 and not in the so-called nonperturbative domain. Nevertheless, there are indications (especially from lattice calculations) that the interquark potential increases with the distance of separation. This is often interpreted as colour confinement and may lead to the occurrence of colour singlet bound states (of baryons and mesons) as

is observed in nature. Hence, QCD is considered to be a perfectly valid theory of strong interactions — it postulates that hadronic matter is made up of coloured, spin-half *quarks* and the interaction between them is mediated by the coloured spin-one *gluons*, both of which are confined and are therefore unobservable.

Asymptotic freedom in QCD provides a natural justification for the success of the naïve parton model as applied to various DIS processes. In addition, QCD provides a systematic method for calculating corrections at finite momentum scales, atleast perturbatively. Calculations in the case of DIS indicated that, in fact, scale invariance of structure functions is approached only asymptotically. Leading corrections, which were called “scaling violations”, are logarithmic. These logarithmic violations of scaling predicted by QCD were actually observed and were a triumph for the theory [9].

The leading order results in QCD for the structure functions have a simple interpretation in the parton model framework [10]. Scaling violations as predicted by QCD are incorporated into a parton model of an interacting field theory, where the interactions between partons destroy scaling logarithmically. All these predictions compare reasonably well with data from various experiments [11].

1.1 Motivation

Early experiments in the study of spin dependent lepton-proton DIS were also begun by the SLAC collaboration [12] in the mid '70s. This process requires both the beam as well as the target to be polarised and so is technically harder to achieve. It was only a few years ago that data in this sector became amenable to a rigorous examination. Hence, current interest in polarised DIS phenomena dates from this time, *i.e.*, with the availability of more data from the European Muon Collaboration (EMC) [13]. To understand why their result stimulated so much controversy and discussion, we first specify in more detail, what exactly they measured.

1.1.1 Formalism of DIS experiments

The process studied is highly inelastic lepton-proton collisions,

$$\vec{\ell} \vec{p} \rightarrow \ell X, \quad (1.1)$$

where the arrows on the initial state lepton and proton indicate that they are longitudinally polarised with respect to the beam direction and X is the (unobserved) debris. The break-up of the proton in the electromagnetic collision process is shown in Fig. (1.1) .

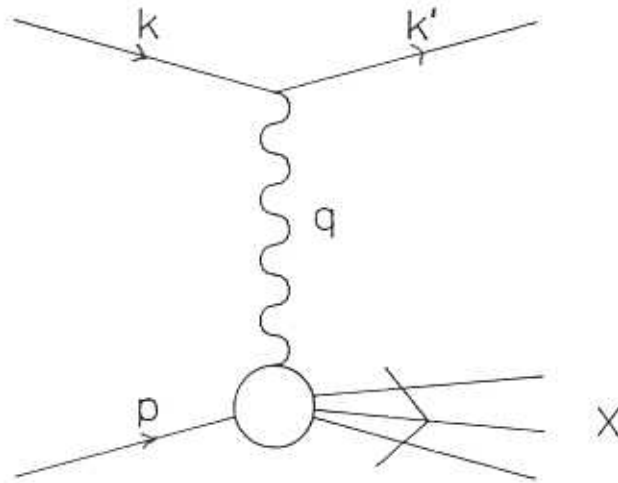


Fig. 1.1 Illustration of the DIS process and the break-up of the proton due to the collision.

The kinematics of this process is dealt with in detail in Appendix C (both for the polarised as well as the unpolarised case). Here, it suffices for us to note that there are two independent kinematical variables in this process and we choose them to be q^2 and ν . Here, q^2 is the square of the momentum transfer from the lepton to the hadron-photon vertex (*i.e.*, q is the momentum of the virtual photon), $q^2 = (k - k')^2$ and $\nu = p \cdot q$, where p is the proton momentum.

The lepton-photon vertex is elementary and well-known, while the photon-hadron vertex is not. The latter is parametrised in terms of unknown *structure functions* which can be determined from experiment. The number of independent structure functions is fixed by the number of non-vanishing, independent helicity amplitudes for forward virtual Compton scattering (remembering that the process is parity and time-reversal invariant). There are two unpolarised and two polarised structure functions in this case, labeled W_1 and W_2 in the unpolarised case and G_1 and G_2 for the polarised case. (Again, see Appendix C for details.)

The cross-section combinations that were measured by the EMC and SLAC groups were

$$\begin{aligned} \frac{d\sigma}{dQ^2 d\nu} (\uparrow\downarrow - \uparrow\uparrow) &= \frac{4\pi\alpha^2}{E^2 Q^2} \left\{ (E + E' \cos\theta) M_p G_1 - Q^2 G_2 \right\}; \\ \frac{d\sigma}{dQ^2 d\nu} (\uparrow\downarrow + \uparrow\uparrow) &= \frac{8\pi\alpha^2 E'}{Q^4 E} \left\{ 2W_1 \sin^2(\theta/2) + W_2 \cos^2(\theta/2) \right\}. \end{aligned} \quad (1.3)$$

Here, the arrows indicate the configuration when the lepton and proton are polarised parallel ($\uparrow\uparrow$) and antiparallel ($\uparrow\downarrow$) to each other. The laboratory lepton scattering angle is θ while E and E' are the initial and final lepton lab energies; $Q^2 = -q^2$ and α , as usual, is the fine structure constant.

Scaling implies that the structure functions appearing in the expression for the cross-section are not separately functions of q^2 and ν , but rather of their ratio. In fact, they are dimensionless functions of a single *Bjorken scaling variable*, x , defined in the scaling limit as

$$\lim_{\substack{-q^2 \rightarrow \infty \\ \nu \rightarrow \infty}} \frac{-q^2}{2\nu} \equiv x, \quad 0 < x \leq 1. \quad (1.2)$$

Specifically, in the above limit, the scaling behaviour is as follows:

$$\begin{aligned} M_p W_1(q^2, \nu) &\rightarrow F_1(x); & (\nu/M_p) W_2 &\rightarrow F_2(x); \\ M_p \nu G_1(q^2, \nu) &\rightarrow g_1(x); & (\nu^2/M_p) G_2 &\rightarrow g_2(x). \end{aligned}$$

Here, M_p is the mass of the nucleon. The cross-section for the process can then be expressed in terms of these *scaling structure functions*, $F_i(x)$ and $g_i(x)$.

Since the sum and difference of the different spin-configured cross-sections have common kinematical factors, what was measured was the *polarisation asymmetry*, so that errors due to over-all normalisation factors were reduced. This asymmetry can be expressed as

$$A^{\mu p} \equiv \frac{d\sigma(\uparrow\downarrow - \uparrow\uparrow)}{d\sigma(\uparrow\downarrow + \uparrow\uparrow)}, \quad (1.4)$$

where the cross-sections are differential with respect to Q^2 and ν as shown in eq. (1.3). The cross-sections can be reexpressed, using the optical theorem, in terms of the photoabsorption cross-section into states with $J_z = J = 1/2, 3/2$, denoted as σ_J , where the "massive" photon can be either transverse (helicity = ± 1) or scalar (helicity = 0) and J denotes the total angular momentum of the photon-nucleon system. In fact, the asymmetry can be written in terms of the transverse asymmetry for absorption of transverse photons, A_1 , given by

$$A_1 \equiv \frac{\sigma_{1/2}^T - \sigma_{3/2}^T}{\sigma_{1/2}^T + \sigma_{3/2}^T} = \frac{\nu G_1 - Q^2 G_2}{W_1} \quad (1.5)$$

as

$$A^{\mu p} \simeq D A_1, \quad (1.6)$$

where D is a depolarisation factor of the virtual photon.

In writing eq. (1.6), various approximations (kinematical as well as parton model based) have been used; for details refer Appendix C. We just add that the structure function of interest is given in terms of the scaling structure functions by

$$g_1(x) = A_1(x) F_1(x) = \frac{A_1 F_2}{2x(1+R)}, \quad (1.7)$$

while g_2 is zero in the parton model [14]. Here, R is the ratio of longitudinal to transverse unpolarised photoabsorption cross-sections which vanishes in the scaling limit.

Problems started when the data for A_1 , supplemented with the known data for $F_1(x)$ in that region was compared with the parton model expression [15] for $g_1(x)$, written in terms of *quark distribution functions*:

$$\begin{aligned} g_1(x) &\equiv \frac{1}{2} \sum_f e_f^2 \tilde{q}_f(x); \\ F_1(x) &\equiv \frac{1}{2} \sum_f e_f^2 q_f(x). \end{aligned} \quad (1.8)$$

Within the parton model, the Bjorken variable, x , has the interpretation of being the fraction of momentum of the parent hadron that the parton carries. The sum runs over quark and antiquark flavours; e_f is the charge of the f -flavour quark. Here q is the sum and \tilde{q} the difference of the positive and negative helicity quark distribution functions:

$$\begin{aligned} \tilde{q}_f(x) &= q_f^+(x) - q_f^-(x); \\ q_f(x) &= q_f^+(x) + q_f^-(x). \end{aligned}$$

Here, $q_f^+(x)$ is interpreted as the number of f -flavour quarks with momentum fraction between x and $(x+dx)$ of the parent proton, whose spin is aligned with that of the parent proton, while $q_f^-(x)$ is the number in the same momentum interval whose spins are opposed to that of the parent hadron.

The expression in eq. (1.8) for g_1 follows from angular momentum conservation: a spin-half parton can only absorb a photon of opposite helicity,

$$\gamma^\uparrow q^\uparrow \rightarrow q^\uparrow.$$

Hence, within the parton model, the photoabsorption cross-section, $\sigma_{1/2}$, which gets contributions only from the antiparallel configuration shown above, is proportional to the number of positive helicity quarks, while $\sigma_{3/2}$ is proportional to the number of negative helicity quarks. Hence,

$$A_1 = \frac{\sum e_f^2 \tilde{q}_f(x)}{\sum e_f^2 q_f(x)}. \quad (1.9)$$

We complete this list of definitions by introducing the n -th moment of the structure function, g_1 ,

$$G_n \equiv \int_0^1 dx x^{n-1} g_1(x) . \quad (1.10)$$

There exist sum rules for the first moment of the proton and neutron spin dependent structure functions. One of these is the Bjorken Sum Rule [16]:

$$\int_0^1 dx (g_1^p(x) - g_1^n(x)) = \frac{1}{6} g_A (1 - \alpha_s/\pi) , \quad (1.11)$$

where g_A is the ratio of the axial vector to vector coupling constants in nucleon beta-decay. Later, Ellis and Jaffe [17] assumed exact $SU(3)$ flavour symmetry as well as a net zero strange quark polarisation in the sea to obtain separate sum rules for the moments of g_1^p and g_1^n in terms of F and D , the antisymmetric and symmetric $SU(3)$ couplings (see Appendix C for details).

1.1.2 The EMC results

In the EMC experiment, polarised positive muons produced from pion decay were accelerated and scattered off a polarised ammonia target with a large number of free protons in a fixed target set-up. Target polarisation of about 75–80% and beam polarisation of nearly 80% was achieved. (Polarisation was defined with respect to the beam direction as the reference z -axis). Data was taken in the kinematical range $0.01 \leq x \leq 0.7$ and $2.5 \leq Q^2(\text{GeV}^2) \leq 80$. Scaling (constant value over the Q^2 range measured) was indeed observed. Several precautions were taken to ensure the accuracy of data [13] which was extrapolated using the assumptions [18],

$$\begin{aligned} A_1 &\xrightarrow{x \rightarrow 1} 1 ; \\ A_1 &\xrightarrow{x \rightarrow 0} 0 . \end{aligned}$$

The first moment of the combination $\sum_f \tilde{q}_f(x)$ is the helicity content of the quark and so should be finite. The integrability condition on this leads to the second result above.

This yielded $g_1(x)$ at a mean $\langle Q^2 \rangle = 10.7 \text{GeV}^2$ with F_2 taken from unpolarised data [19]. Their result is reproduced in Fig. (1.2). The convergence of

the data for small- x was also well-tested, *i.e.*, the assumption, $A_1(0) \rightarrow 0$ (See Fig. (1.3)). After such suitable checks, the moment of $g_1^p(x)$ was quoted to be (combined with the SLAC data [20], [12])

$$G_1^p \equiv \int_0^1 dx g_1^p(x) = 0.126 \pm 0.010(\text{stat}) \pm 0.015(\text{syst}) .$$

The first error is statistical, while the second is due to systematic errors coming from uncertainties in R , A_2 (see Appendix C), the fraction of free protons interacting in the experiment, etc.

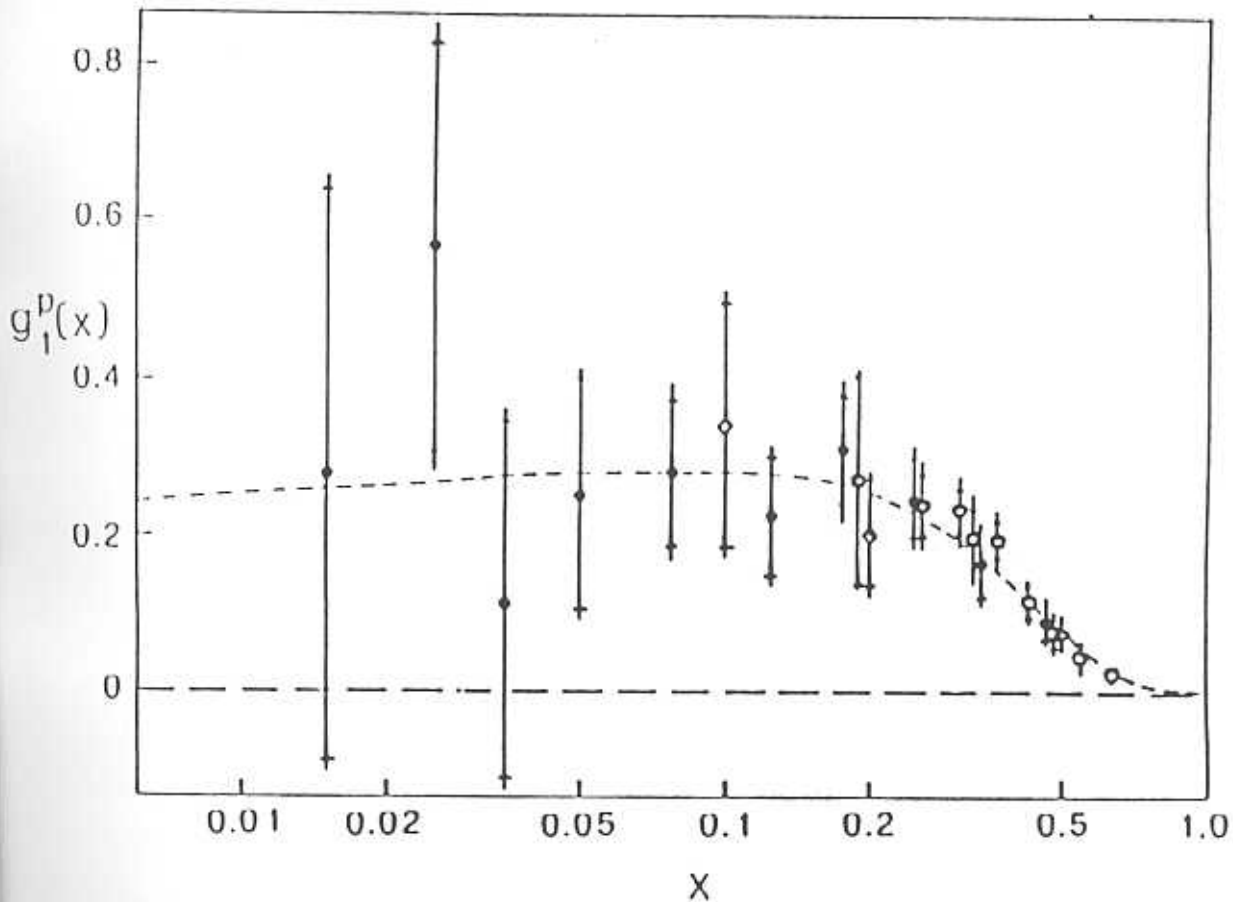


Fig. 1.2 The structure function, $g_1^p(x)$, is plotted as a function of the Bjorken variable, x . Solid dots represent the EMC [13] data, while the SLAC data is represented by open circles (ref. [20]) and diamonds (ref. [12]).

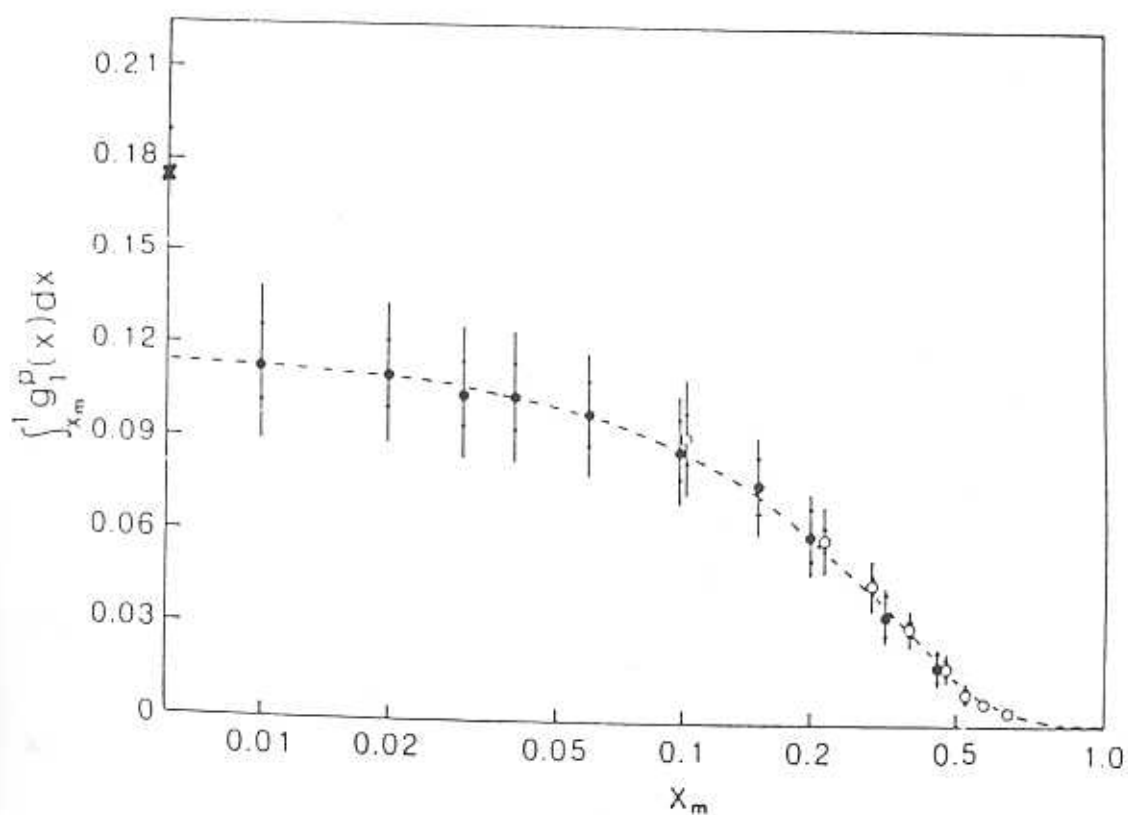


Fig. 1.3 $\int_{x_m}^1 dx g_1^p(x)$ is plotted versus x_m to show convergence of the data. Solid and open circles refer to EMC and SLAC data respectively. The point $(0, 0.174)$ marked with a cross is the Ellis-Jaffe prediction [17] for the first moment of this structure function.

1.1.3 Discussion of results in the Parton Model

In general, G_1^p can be expressed in terms of the (proton) matrix elements of the axial-vector operators,

$$A_i^\mu = \bar{\psi} \gamma^\mu \gamma_5 \frac{\lambda_i}{2} \psi; \quad i = 1, \dots, 8, \quad (1.12)$$

where λ_i are the generators of the flavour group $SU(3)_f$. (The analogous expressions for the spin independent case involve the corresponding vector operators). Their matrix elements can be expressed as

$$\langle p, S | A_i^\mu | p, S \rangle = 2M_p a_i S^\mu,$$

where S^μ is the proton spin vector and the a_i are unknown factors which may be related to the F and D coupling constants using $SU(3)$ symmetry. In fact, G_1^p can be expressed in terms of only the diagonal elements, a_3 , a_8 and a_0 . The last corresponds to the singlet current contribution, with λ_i being replaced by unity in eq. (1.12), while the first two are non-singlet contributions having the following form using $SU(3)$ symmetry:

$$a_3 = g_A = F + D; \quad a_8 = \frac{g_8}{\sqrt{3}} = \frac{1}{\sqrt{3}} (3F - D). \quad (1.13)$$

There is no prediction for the singlet contribution, a_0 .

In terms of these, the first moment of g_1^p in the parton model can be written as

$$G_1^p = \frac{1}{12} \left(a_3 + \frac{a_8}{\sqrt{3}} \right) \left(1 - \frac{\alpha_s}{\pi} \right) + 2\sqrt{\frac{2}{3}} a_0 \left(1 - \frac{33 - 8f \alpha_s}{33 - 2f \pi} \right),$$

where the singlet (a_0) and non-singlet contributions have different leading order ($\mathcal{O}(\alpha_s)$) QCD corrections, as they obey different Q^2 evolution equations [10]. Note that the α_s correction to the singlet piece is also dependent on the number of flavours, f .

Now, g_A and g_8 and hence a_3 and a_8 can be measured from the beta-decay of nucleons and hyperons [21]. However, a_0 is not known. Hence, Ellis and Jaffe [17] assumed that the contribution from strange quarks was zero, or,

$a_0 = \sqrt{2}a_8$. With this assumption, their prediction for G_1^p is, with $\alpha_s(Q^2 = 10.7\text{GeV}^2) = 0.27 \pm 0.02$,

$$G_1^{p,\text{EJ}} = 0.174 \pm 0.005 .$$

This number is indicated in Fig. (1.3) and is seen to be *inconsistent with the measured value*. This was the first surprising result coming from the EMC.

The unknown a_0 can be extracted, knowing the value of G_1^p from this experiment. This yields

$$a_0 = 0.09 \pm 0.076 \pm 0.113 .$$

This result is fairly insensitive to the value of a_8 which is not very well measured, especially as $SU(3)$ flavour symmetry is not exact [22]. The EMC claim that "any uncertainty from possible magnitude of $SU(3)_f$ symmetry breaking effects is much smaller than experimental errors."

To proceed further, we invoke parton model results. The a_i , $i = 0, 3, 8$, can be written in terms of the quark spin contributions. Define

$$\Delta q_f \equiv \int_0^1 dx [\tilde{q}_f(x) + \tilde{\bar{q}}_f(x)] \quad (1.14)$$

to be the spin contribution to the proton of the f -flavour quark and antiquark. For the case of three flavours, we have

$$\begin{aligned} a_3 &= \Delta u - \Delta d ; \\ a_8 &= \frac{1}{\sqrt{3}} [\Delta u + \Delta d - 2\Delta s] ; \\ a_0 &= \sqrt{\frac{2}{3}} [\Delta u + \Delta d + \Delta s] . \end{aligned}$$

Note that the Ellis-Jaffe assumption is equivalent to the statement $\Delta s = 0$.

Using the values of a_0 , a_3 and a_8 listed above, we can solve for the Δq_i , or equivalently, for the mean z -component of the spin carried by each quark flavour in a polarised proton with $\langle S_z \rangle_p = +1/2$. We get

$$\begin{aligned} \langle S_z \rangle_u &= 0.391 \pm 0.016 \pm 0.023 ; \\ \langle S_z \rangle_d &= -0.236 \pm 0.016 \pm 0.023 ; \\ \langle S_z \rangle_s &= -0.095 \pm 0.016 \pm 0.023 , \end{aligned}$$

where $\langle S_z \rangle_q = \Delta q/2$, so that the contribution to the proton spin is

$$\langle S_z \rangle_{\text{quark}} = \frac{1}{2} \sqrt{\frac{3}{2}} a_0 = \frac{1}{2} (\Delta u + \Delta d + \Delta s) = 0.060 \pm 0.047 \pm 0.069. \quad (1.15)$$

The naïve quark model, with three quarks bound into a proton predicts that the entire spin of the proton is carried by these three quarks. This idea is incorporated into the parton model containing infinite number of quarks and antiquarks by stating that there is an excess of three quarks over the antiquarks in a nucleon and hence the difference of moments of the quark and antiquark distributions (which gives the difference in number of quarks and antiquarks) is three, *i.e.*,

$$\sum_f \int dx (q_f - \bar{q}_f) \equiv \sum_f \int dx q_V(x) = 3$$

and these are identified as the quarks of the quark model. Hence, $(q_f - \bar{q}_f)$ gives the *valence* distribution in a nucleon. The corresponding parton model expectation is then that these valence quarks carry most of the proton spin. With this in mind, the result of eq. (1.15) is indeed surprising: the *u*-quarks are indeed mostly positively polarised as expected, but the net quark contribution to the spin of the proton is only $(12 \pm 9 \pm 14)\%$, *i.e.*, nearly vanishing. Thus, the valence contribution is almost exactly canceled by the sea contribution.

It is true that corresponding results in unpolarised DIS indicates that the gluon carries no charge, but about half the momentum of the proton. This, however, is not surprising as, in a sense, the gluons also have to move, in order to “keep up” with the proton! However, spin can be thought of as a static property of the proton. In view of the phenomenal success of the static quark model in describing properties of the nucleon such as the ratio of proton and neutron magnetic moments by assuming that the entire spin of the nucleon is carried by the valence quarks, this result, that the sea quarks carry non-negligible spin, forces a critical reexamination of the assumptions in these models.

These two unexpected results of the EMC, namely

1. the observed violation of the Ellis-Jaffe Sum Rule implying $\Delta s \neq 0$ and

2. vanishing quark contribution to the proton spin, implying possibly large contributions from the gluons and/or orbital angular momentum, as opposed to naïve expectations

have variously been described as a "proton-spin crisis."

1.1.4 Consequences of the EMC results

Several explanations of the EMC results and the apparent failure of the parton model have been proposed. These include Skyrme model analyses, where the proton spin is accounted for mostly by the orbital angular momentum [23] of the quarks; the veracity of the data has also been questioned [24] as well as the dropping of the term involving the $g_2(x)$ structure function [25] in the expression for the asymmetry. This data has also been cited as being evidence against QCD [25]. A calculation using the QCD Sum Rule technique, however, seems to satisfactorily account for [26] the measured value of G_1^p .

One of the earliest analyses indicating that the total spin contribution of quarks practically vanishes was due to Glück and Reya [27]. Unlike the unpolarised case where only quarks and gluons contribute to the momentum of the proton, in the polarised case, there is the added complication of the orbital angular momentum, \mathcal{L}_z , of the partons. Hence, *a priori*, the simplicity of the parton model description of the unpolarised sector is not present in the polarised case. Since the total contribution to the proton spin can come from its constituents as well as their relative orbital angular momentum, we have the sum rule,

$$\frac{1}{2} \sum_f \Delta q_f + \Delta g + \mathcal{L}_z = \frac{1}{2} \equiv \langle S_z \rangle_p. \quad (1.16)$$

Thus, the EMC result allows for a large gluon contribution to the proton spin.

Apart from the need for obtaining data with improved statistics over a larger kinematical region, it seems important to sort out theoretical ambiguities by carefully defining the various structure functions and parton distributions involved. This would enable us to probe the nucleon spin content

through other processes. This becomes specially important as many difficulties in understanding the spin structure of the proton arise from the fact that a measurement of $g_1^p(x)$ alone cannot completely determine all the parton distributions. As in the case of unpolarised densities, other experiments are needed in order to determine the various unknown quantities to sufficient accuracy in order to make definite statements regarding the different spin dependent quark distributions.

Several calculations [28] have pointed out that the gluon contribution to the first moment of $g_1^p(x)$ (to leading order) through a “triangle-diagram axial-anomaly”-like diagram. Further, the Altarelli-Parisi evolution equations [10] in Q^2 indicate that, to first order in α_s , the quantity $\alpha_s \Delta g$ is conserved (where Δg is the moment of the spin dependent gluon distribution and is the contribution of the gluons to the spin of the proton, analogous to eq. (1.14) for the quarks); hence, Δg can be large at the Q^2 ranges accessed in the EMC experiment and so the gluon contribution to the DIS asymmetry may be non-negligible. Because of the nature of definition of the structure functions [29], [15], which we shall deal with in more detail in the next chapter, this implies that what was measured was not just the quark contribution to G_1^p , but also the (large) gluonic contribution appearing through the singlet (sea) quark contribution. To put it simply, next-to-leading order corrections to the spin dependent structure function are large and cannot be ignored. This is possibly why the naïve parton model failed to explain the EMC result.

Since Δq does not evolve in Q^2 [10], \mathcal{L}_z must decrease with Q^2 exactly as Δg increases with it, in order to satisfy eq. (1.16), as its RHS is trivially conserved. Hence, at the intermediate Q^2 ranges of the experiment, \mathcal{L}_z can also be large. That $\alpha_s \Delta g$ is constant to leading order is a QCD result; hence, the statements about large Δg and \mathcal{L}_z hold even here. However, the claim that this implies a redefinition of G_1^p in terms of Δq and Δg [30], as

$$G_1^p \equiv \frac{1}{2} \sum_f e_f^2 \left[\Delta q - \frac{\alpha_s}{2\pi} \Delta g \right]$$

is made strictly within the parton model. Furthermore, this result is also scheme-dependent [31].

There have been several results for evaluating G_1^p in different renormalisation schemes; Bodwin and Qiu [32] were the first to discuss the question of interpretation and definition of the quark distribution functions in different ultraviolet-regularisation schemes in view of the EMC result. Later, it was found, using other techniques like OPE, factorisation, etc., [33], [34], [35], that the gluonic correction to the first moment of $g_1^p(x)$ either vanished or agreed with the Altarelli result, depending on the renormalisation scheme used. The most important conclusions drawn were:

1. Parton distributions defined beyond the leading order are not unique. Provided the same set of definitions are used in both the polarised and the unpolarised sector, meaningful parton densities can still be constructed, *within a given renormalisation scheme*, in a given model [32].
2. More data is required in order to study the distribution of the nucleon spin in terms of its constituents; specifically, measurements of combinations of parton densities, other than what was measured by the EMC, are needed in order to settle this question.

With these two points in mind, we now begin a presentation of our work.

1.2 Organisation of the thesis

The thesis is organised in two parts. The first part, titled "Parton Model Phenomenology" deals with, as the title indicates, a study of polarisation asymmetries which, we show, will shed more light on the spin content of the proton. Specifically, what is presented is a complete set of processes that yield information on the spin dependent valence quark, gluon and sea quark distributions within the proton. A parametrisation of these densities, consistent with corresponding unpolarised densities as well as currently available data and other theoretical inputs, has been developed in Chapter 2. This is later

used in order to demonstrate the dependence of these asymmetries on the various spin dependent densities. Due to reasons presented earlier (which we again discuss in more detail in the next chapter), the parton densities themselves are defined upto next-to-leading order (of order $\mathcal{O}(\alpha_s \equiv g_s^2/4\pi)$) where required. Chapter 3 discusses extraction of the spin dependent valence quark densities in semi-inclusive DIS process, while Chapters 4–6 deal with extraction of the gluon and sea quark spin dependent densities in polarised pp collision processes. All cross-sections are computed in leading order QCD with massless partons. Conclusions common to all chapters are drawn at the end of this part.

The second part deals with a study of the nucleon spin dependent structure functions, $g_1(x)$ and $g_2(x)$, as well as their moments. Chapter 7 discusses the higher moments of the spin dependent structure function, $g_1^p(x)$, using the OPE technique. It is shown that a mass scale typical of the quark model scale emerges from the ratios of these moments. Support for results obtained is provided in a non-perturbative Bag Model. In Chapter 8, we attempt to evaluate the nucleon structure functions, $g_1(x)$ and $g_2(x)$, within the Sum Rule [36] approach. Here, the aim is to try to evaluate the x -dependent structure function itself in a kinematical range that is experimentally accessible and theoretically viable.

Everywhere, appendices have been used in order to keep the thesis self-contained as much as possible, even when the contents of the appendices are well-known text-book material. We have endeavoured to fill in pertinent details in these appendices where-ever possible, rather than interrupt the continuity of presentation. Certain ideas/facts which appear only once and are not directly germane to the core of the thesis have been merely presented with appropriate references, but have not been derived.

The contents of this thesis have appeared in the references [37], [38], [39], [40], [41], [42] and [43].

References

- [1] This was due to M. Gell-Mann and G. Zweig. The original paper of Gell-Mann is reprinted in M. Gell-Mann and Y. Ne'eman, *The Eight-fold Way*, Benjamin, New York, 1964
- [2] Ta-Pei Cheng and Ling-Fong Li, in *Gauge Theories of Elementary Particle Physics*, Clarendon Press, Oxford, 1984
- [3] O.W. Greenberg, *Phys. Rev. Lett.* **13** (1964) 598
- [4] E.D. Bloom *et al.*, *Phys. Rev. Lett.* **23** (1969) 930.
For more discussion of the data, see S.B. Treiman, R. Jackiw and D.J. Gross in *Current Algebra and its Applications*, Princeton Univ. Press, 1972, pg. 281
- [5] J.D. Bjorken, *Phys. Rev.* **179** (1969) 1547
- [6] J.D. Bjorken and E.A. Paschos, *Phys. Rev.* **185** (1969) 1975; R.P. Feynman, *Phys. Rev. Lett.* **23** (1969) 1415; also in *Photon Hadron Interactions*, Pub: Benjamin, Reading, Massachusetts, 1972
- [7] S.L. Glashow, *Nucl. Phys.* **22** (1961) 579; S. Weinberg, *Phys. Rev. Lett.* **19** (1967) 1264; A. Salam, in *Elementary Particle Physics*, Nobel Symposium No.8, ed: N. Svartholm, Almquist and Wilsell, Stockholm
- [8] H.D. Politzer, *Phys. Rev. Lett.* **30** (1973) 1346; *Phys. Rep.* **C14** (1974) 129; D. Gross and F. Wilczek, *Phys. Rev. Lett.* **30** (1973) 1340; *Phys. Rev.* **D8** (1973) 3633; S. Weinberg, *Phys. Rev. Lett.* **31** (1973) 494
- [9] H.L. Anderson *et al.*, *Phys. Rev. Lett.* **38** (1977) 1450; B.C. Barish *et al.*, *Phys. Rev. Lett.* **40** (1978) 1414
- [10] G. Altarelli and G. Parisi, *Nucl. Phys.* **B126** (1977) 298
- [11] T. Sloan, G. Smadja and R. Voss, *Phys. Rep.* **162** (1988) 45

- [12] M.J. Alguard *et al.*, SLAC-Yale 80 E80 Collaboration, Phys. Rev. Lett. **37** (1976) 1261; **41** (1978) 70
- [13] J. Ashman *et al.*, The EM Collaboration, Phys. Lett. **B206** (1988) 364; Nucl. Phys. **B328** (1989) 1
- [14] There are several controversies regarding this little-known structure function. While $g_2(x)$ is zero in the parton model as it depends on the mass and transverse momentum of the quarks, which are both zero, in the OPE, it is only the first moment of $g_2(x)$ that vanishes. We anyway ignore this structure function for the present; in a later section (QCD Sum Rule), we show that indeed this does not appear in the same order as $g_1(x)$.
- [15] V. Gupta, S.M. Paranjape and H.S. Mani, Pramana **14** (1980) 119; see G. Altarelli, R.K. Ellis and G. Martinelli, Nucl. Phys. **B143** (1978) 521 for the corresponding spin independent quantities.
- [16] J.D. Bjorken, Phys. Rev. **148** (1966) 1467
- [17] J. Ellis and R.L. Jaffe, Phys. Rev. **D9** (1974) 1444; **E: D10** (1974) 1669; for an independent derivation using $SU(6)$ current algebra, see A.S. Joshipura and P. Roy, Nucl. Phys. **B116** (1976) 591
- [18] The QCD prediction is due to G. Farrar and J.D. Jackson, Phys. Rev. Lett. **35** (1975) 1416
- [19] J.J. Aubert *et al.*, The EM Collaboration, Nucl. Phys. **B259** (1985) 189
- [20] G. Baum *et al.*, SLAC-Yale E80 Collaboration, Phys. Rev. Lett. **51** (1983) 1135; see also reference [12] above.
- [21] The particle data book (1991) specifies $g_A = 1.261 \pm 0.004$ and $g_8 = 0.584 \pm 0.018$.
- [22] The original EMC data uses the value $g_8 = 0.683 \pm 0.035$ due to M. Bourquin *et al.*, Z. Phys. **C21** (1983) 27

- [23] J. Ellis and M. Karliner, Phys. Lett. **B213** (1988) 73
- [24] F.E. Close and R.G. Roberts, Phys. Rev. Lett. **60** (1988) 1471
- [25] G. Preparata and J. Soffer, Phys. Rev. Lett. **61** (1988) 1167
- [26] S. Gupta, M.V.N. Murthy and J. Pasupathy, Phys. Rev. **D39** (1989) 2547;
C.B. Chiu, J. Pasupathy and S.L. Wilson, Phys. Rev. **D32** (1985) 1786
- [27] M. Glück and E. Reya, Z. Phys. **C39** (1989) 569
- [28] R.L. Jaffe, Phys. Lett. **B193** (1987) 101
R.D. Carlitz, J.C. Collins and A.H. Mueller, Phys. Lett. **B214** (1988) 229.
G. Altarelli and G.G. Ross, Phys. Lett. **B212** (1988) 391.
A.V. Efremov and O.V. Teryaev, Preprint JINR EL-88-287.
C.S. Lam and Bing-An Li, Phys. Rev. **D25** (1982) 683.
- [29] See the reference to Altarelli *et al.* in [15]
- [30] G. Altarelli and G.G. Ross in reference [28] above
- [31] It is well-known that there is no unique definition of parton densities beyond the leading order; see, for instance, [15]
- [32] G.T. Bodwin and J. Qiu, preprint ANL-HEP-PR-89-83
- [33] A. Manohar, Phys. Rev. Lett. **66** (1991) 289
- [34] The weak case was addressed by
Prakash Mathews and V. Ravindran, Phys. Lett. **B278** (1992) 175;
preprint IMSc/91/32, to appear in the Int. J. Mod. Phys. A
W. Vogelsang and A. Weber, Nucl. Phys. **B362** (1991) 3
- [35] U. Ellwanger, Phys. Lett. **B259** (1991) 469

- [36] M.A. Shifman, A.I. Vainshtein and V.I. Zakharov, Nucl. Phys. **B147** (1979) 385
- [37] S. Gupta, D. Indumathi and M.V.N. Murthy, Z. Phys. **C42** (1989) 493
- [38] S. Gupta, D. Indumathi and M.V.N. Murthy, Z. Phys. **C47** (1990) 227
- [39] D. Indumathi, M.V.N. Murthy and V. Ravindran, preprint, IMSc/91/31, to appear in Z. Phys. C 1992
- [40] D. Indumathi and M.V.N. Murthy, Extended Abstract, DAE Symposium, Aligarh, 1989
- [41] D. Indumathi, M.V.N. Murthy and V. Ravindran, Mod. Phys. Lett. **A14** (1990) 1125
- [42] D. Indumathi, M.V.N. Murthy and V. Ravindran, Int. J. Mod. Phys. **A6** (1991) 3933
- [43] D. Indumathi, Inst. of Mathematical Sciences, preprint IMSc/92/47

PART I

PARTON MODEL PHENOMENOLOGY

At the outset, we wish to emphasise that the cross-sections (both spin dependent as well as spin independent) for the processes we shall consider, have all been calculated and are well-known. The rôle of this section is then to demonstrate that these processes possess various properties that will help in understanding the spin composition of the nucleon, *within the confines of the parton model*. To do that, it is necessary to understand why we confine ourselves so and also to put into perspective, historically relevant details regarding the parton densities.

Having accepted that the naïve parton model fails to explain the EMC data, it is a foregone conclusion that we must now go beyond the leading order. The complication that arises with this step is two-fold. First of all, when we go beyond the naïve parton model, we no longer have a picture of zero-mass partons with zero-momentum-component transverse to that of the parent proton. In other words, the helicity representation of the states is not a good representation. Though this can be largely ignored, the other, more important problem at finite Q^2 is that of the definition of the parton densities and their relation to the structure functions. The fact is that there exists *no unique definition of the parton densities* beyond the leading order. In fact, they become prescription-dependent. To first order in α_s , the splitting functions that appear in the Q^2 -evolution equations [1] for the parton densities are renormalisation-scheme independent. However, the corresponding quantity of order α_s that appears in the Q^2 -dependent expression for the parton densities/structure functions is not just the splitting function, but also contains constant (Q^2 -independent) pieces which are renormalisation-scheme dependent. The choice of definition of the parton densities then becomes one of convenience; this was pointed out by Altarelli *et al.* [2]. Strictly speaking, this means that different approaches — say parton model and OPE — need not have a one-to-one correspondence at the level of identification of the densities, but only need match in the case of observables like the structure functions. However, within a given approach, the densities must be consistently defined.

This means, for instance, that the definition of the quark densities should be consistent with the following identification:

$$\begin{aligned}q(x) &= q^+(x) + q^-(x); \\ \tilde{q}(x) &= q^+(x) - q^-(x),\end{aligned}$$

and so also for the gluon.

Having defined a consistent set of polarised and unpolarised densities, we can then go on to a study of various processes in order to extract more information about the manner in which these partonic constituents contribute to the spin of the nucleon.

We have preferred the above verbose description of the problem at hand over a mathematical one for two reasons. Firstly, to specifically exhibit the Q^2 dependence of the parton densities/structure functions in various models and renormalisation schemes will take us far away from the discussion at hand; it is more in keeping as part of a review or book. Secondly, with the specific choice of the quark parton model in which we will work, we shall specify these Q^2 dependences of the densities along with their parametrisations in the next chapter. This, we hope, is sufficient to illustrate our statements.

We begin the next chapter with a discussion of the expressions for the next-to-leading order structure functions — both polarised and unpolarised. We shall specifically concentrate on the quark parton model and comment on other approaches appropriately. After defining the densities and their parametrisation, we use them to analyse, in succeeding chapters, various other processes that sensitively depend on the spin dependent parton densities.

References

- [1] G. Altarelli and G. Parisi, Nucl. Phys. **B126** (1977) 298
- [2] G. Altarelli, R.K. Ellis and G. Martinelli, Nucl. Phys. **B143** (1978) 521

PARAMETRISATION OF DENSITIES

CONTENTS

Preliminaries

The Constraints

Choice of Parametrisations

In this chapter, we set up typical parametrisations of the (unknown) spin dependent parton densities, consistent with the known spin independent ones. To do this, we use the EMC result [1] for $g_1^p(x)$ and its first moment as well as several theoretical constraints on various density combinations. We find that, by combining all constraints, there are still several free parameters, on which bounds can be placed. We shall use different values of these parameters to study the x -dependence of the various densities.

From Chapter 3 onward, we present asymmetries in several processes involving polarised beam-polarised target scattering. Using the parametrisations developed here, we will be able to establish which spin dependent density(ies) these asymmetries are sensitive to and which they will thus be able to probe. The parametrisations thus enable us to *quantify* the dependences of the asymmetries on these densities.

2.0 Preliminaries

We construct the parametrisations in the limit of nearly free, massless partons. Hence gluons have only two helicity states due to transverse polarisation. (There are anyway only two helicity states for the spin-half quarks). In the parton model, the momenta of the partons are assumed to lie entirely in the direction of the parent momentum with negligible transverse momentum. In this limit, the Bjorken variable, x , has the interpretation of being the *fraction*

of the parent hadron momentum that the parton carries. The distribution in x of the number of quarks, $q(x)$, can then be interpreted as the probability of finding a quark with momentum fraction between x and $(x + dx)$. An analogous definition holds for the gluon distribution. Since we are interested in the spin or the helicity parton distributions, we define $q_f^+(x)$ to be the density of positive helicity quarks of flavour f , with momentum fraction between x and $(x + dx)$ and $q_f^-(x)$ to be that of the negative helicity quarks. Here, by positive helicity we mean that the spin of the quark is aligned with that of the parent hadron (See Fig. (2.1)). There are two well-defined density combinations:

$$\begin{aligned} q_f(x) &\equiv q_f^+(x) + q_f^-(x), \text{ the spin independent density and} \\ \tilde{q}_f(x) &\equiv q_f^+(x) - q_f^-(x), \text{ the spin dependent one.} \end{aligned} \quad (2.1)$$

A similar definition holds for antiquarks and gluons. Clearly, $q(x)$ (or $g(x)$) gives the number density of quarks (or gluons) in the momentum range x and $(x + dx)$, while $\tilde{q}(x)$ (or $\tilde{g}(x)$) is the difference of helicity densities and thus defines the helicity or spin dependent density. The contribution of these to the proton spin involves the moments of these densities; we define them to be

$$\begin{aligned} \Delta q_f &\equiv \int dx (\tilde{q}_f(x) + \tilde{\bar{q}}_f(x)) ; \\ \Delta g &\equiv \int dx \tilde{g}(x) . \end{aligned} \quad (2.2)$$

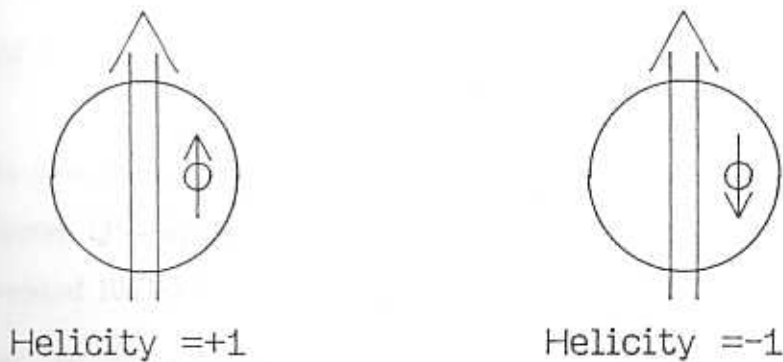


Fig. 2.1 This illustrates our notation for parton helicities.

Then $\Delta q_f/2$ is the contribution of the f -flavour quark to the hadron spin and Δg is the corresponding gluonic contribution.

In the spin independent sector, the quark and antiquark density for every flavour is parametrised as

$$q^f = q_V^f + q_s^f; \quad \bar{q}^f = q_s^f, \quad f = u, d, s,$$

where q_V is the valence contribution and q_s is the sea contribution. The valence contribution is defined to be the difference in quark and antiquark distributions, as discussed in Chapter 1. An analogous equation holds in the spin-dependent sector, where we define \tilde{q}^f and $\tilde{\bar{q}}^f$ as

$$\tilde{q}^f = \tilde{q}_V^f + \tilde{q}_s^f; \quad \tilde{\bar{q}}^f = \tilde{q}_s^f, \quad f = u, d, s.$$

The Q^2 dependence of these densities is theoretically well-studied [2]. The form of the spin-independent densities that we use are from Eichten et al. [3]. Similar results are also obtained upon using the parametrisation of Sloan et al. [4].

2.1 The Constraints

We first state all the constraints on the spin dependent densities:

1. The densities should reproduce the EMC result [1] for the first moment of the spin-dependent proton structure function, $g_1^p(x)$, i.e.,

$$G_1^p \equiv \int_0^1 g_1^p(x) dx = 0.126 \pm 0.010(\text{stat}) \pm 0.015(\text{syst}); \quad \langle Q^2 \rangle = 10.7 \text{ GeV}^2. \quad (2.3)$$

In view of the large (approximately 20%) errors in this result, we shall ignore Q^2 -dependence of the densities and assume an average Q^2 of around 10 GeV^2 .

2. The Bjorken Sum Rule [5]: This relates the difference in the moments of the proton and neutron spin-dependent structure functions to the axial vector coupling constant, g_A .

$$\Delta \Sigma + \int_0^1 dx (g_1^p(x) - g_1^n(x)) = \frac{g_A}{6} (1 - \alpha_s/\pi).$$

Assuming Isospin invariance [6], this translates to $\Delta u - \Delta d = g_A$ in terms of parton densities.

3. We assume the validity of the Carlitz-Kaur parametrisation [7] which relates the spin-dependent valence densities, \tilde{u}_V and \tilde{d}_V , to the *spin-independent* densities u_V , d_V via a spin dilution function, $\cos 2\phi(x)$, which involves a single parameter, γ . [See Table 2.1]
4. In addition, the following constraints exist *independent* of any specific models or assumptions used:
 - The spin-dependent densities should be integrable, as their first moments are interpreted as the finite contributions to the proton spin.
 - Define a parton asymmetry,

$$A^Q = \tilde{Q}(x)/Q(x); \quad Q = q_f, \bar{q}_f, g.$$

Then, $|A^Q| \leq 1$ for all x as the helicity dependent densities are positive definite (See the definitions of the densities in eq. (2.1)).

- Further, from the definition of the densities in eq. (2.1), Q and \tilde{Q} must vanish, at large- x , at the same rate, i.e., Q and \tilde{Q} should fall off as the same power of $(1-x)$ as $x \rightarrow 1$.

2.2 Choice of Parametrisations

With the constraints listed above, the most obvious forms of parametrisations are those listed in Table 2.1 (See [8]).

Use of both the Bjorken Sum Rule and Carlitz-Kaur parametrisation fixes not only the moments Δu_V and Δd_V (see eq. (2.2)), but also \tilde{u}_V and \tilde{d}_V individually, as $\cos 2\phi$ is a known 1-parameter function. This leads to an interesting observation on $SU(3)$ -symmetric models. $SU(3)$ symmetry implies the existence of the constraint (on the other non-singlet combination)

$$\Delta u + \Delta d - 2\Delta s = g_8 \quad \Rightarrow \quad \Delta u_V + \Delta d_V = g_8,$$

since the moments of the sea quark densities are equal, *i.e.*, $\Delta u_s = \Delta d_s = \Delta s_s$. Here g_8 is an $SU(3)$ octet coupling constant, measured in hyperon beta decay. This, along with the Bjorken Sum Rule implies

$$\Delta u_V = \frac{g_A + g_8}{2}; \quad \Delta d_V = \frac{g_8 - g_A}{2}.$$

Using the currently known values [9] for g_A and g_8 , we find that it is impossible to satisfy both of the above equations for a single value of the parameter, γ .

The Spin Independent Densities	
EHLQ set: $Q^2 = 5\text{GeV}^2, \Lambda = 200 \text{ MeV}$	Sloan set: $Q^2 = 15\text{GeV}^2, \Lambda = 90 \text{ MeV}$
$xu_V(x) = 1.78x^{0.5}(1-x)^{3.5}$	$xu_V(x) = 2.75x^{0.588}(1-x)^{2.69}$
$xd_V(x) = 0.67x^{0.4}(1-x)^{4.5}$	$xd_V(x) = 8.53x^{1.03}(1-x)^{6.87}$
$xu_s(x) = 0.182(1-x)^{8.54}$	$xu_s(x) = 0.229(1-x)^{14.6}$
$xd_s(x) = xu_s(x)$	$xd_s(x) = xu_s(x)$
$xs_s(x) = \eta xu_s(x); \eta = 0.445$	$xs_s(x) = \eta xu_s(x); \eta = 0.5$
$xg(x) = 2.62(1 + 3.5x)(1-x)^{5.9}$	$xg(x) = 4.548(1-x)^{7.5}$
The Spin Dependent Densities	
$x\tilde{u}_V(x) = \left(xu_V(x) - \frac{2}{3}xd_V(x)\right) \cos 2\phi(x)$ $x\tilde{d}_V(x) = -\frac{1}{3}xd_V(x) \cos 2\phi(x)$ $\cos 2\phi(x) = \left\{1 + \gamma \frac{\sqrt{(1-x)}}{x^{0.1}}\right\}^{-1}$	
$x\tilde{u}_s(x) = \tilde{N}_s x^\beta (1-x)^{8.54}$ $x\tilde{d}_s(x) = x\tilde{u}_s(x)$ $x\tilde{s}_s(x) = \eta x\tilde{u}_s(x); \eta = 0.445$ $x\tilde{g}(x) = \tilde{N}_g x^\alpha (1 + \tilde{a}x)(1-x)^{5.9}$ $\alpha, \beta > 0$	$x\tilde{u}_s(x) = \tilde{N}_s x^\beta (1-x)^{14.6}$ $x\tilde{d}_s(x) = x\tilde{u}_s(x)$ $x\tilde{s}_s(x) = \eta x\tilde{u}_s(x); \eta = 0.5$ $x\tilde{g}(x) = \tilde{N}_g x^\alpha (1-x)^{7.5}$ $\alpha, \beta > 0$

Table 2.1 The set of spin independent and spin dependent densities for the two sets of parametrisations due to EHLQ [3] and Sloan [4].

Hence, if we retain the Carlitz-Kaur parametrisation, we must give up the g_8 equation, i.e., $SU(3)$ symmetry (See ref. [8]).

Ofcourse, one could equally well give up the Carlitz-Kaur parametrisation, but in view of the fact that $SU(3)$ symmetry is known to be broken in the spin-independent sector (the momentum fraction carried by the strange quarks is half that carried by the up-type quarks in the sea), we prefer to retain the former.

To proceed, the value of γ in Table 2.1 is chosen to satisfy the Bjorken Sum Rule, but not the g_8 equation. The valence sector is thus completely fixed, with no free parameter. (There is no valence strange quark distribution). The spin dependent valence u - and d - quark distributions are shown as functions of x in Fig. (2.2) for both sets of unpolarised density parametrisations (due to EHLQ as well as Sloan). We have also plotted the EMC data for comparison with the valence contribution to $g_1^p(x)$. We see that at large x values, the structure function value is saturated by the valence contribution.

The magnitudes of \tilde{u}_s and \tilde{s}_s can at most be as large as u_s and s_s (since the partonic asymmetries are all bounded by unity). This means that, in the sea sector, the $SU(3)$ symmetry breaking parameter is at most as large as the spin independent one; we assume them to be equal, i.e., we use

$$\tilde{u}_s = \tilde{d}_s ; \quad \tilde{s}_s = \eta \tilde{u}_s ; \quad \eta \simeq 1/2 .$$

Hence, there are in general, only four unknown spin dependent densities (\tilde{u}_V , \tilde{d}_V , \tilde{u}_s and \tilde{g}). Since use of the Carlitz-Kaur prescription fixes the valence sector, Δu_s , which is a measure of the sea polarisation, can be fixed using the EMC result for G_1^p . In order to invoke this result, we need to express g_1^p in terms of parton densities. This depends on the exact definition of the structure function in terms of the parton densities.

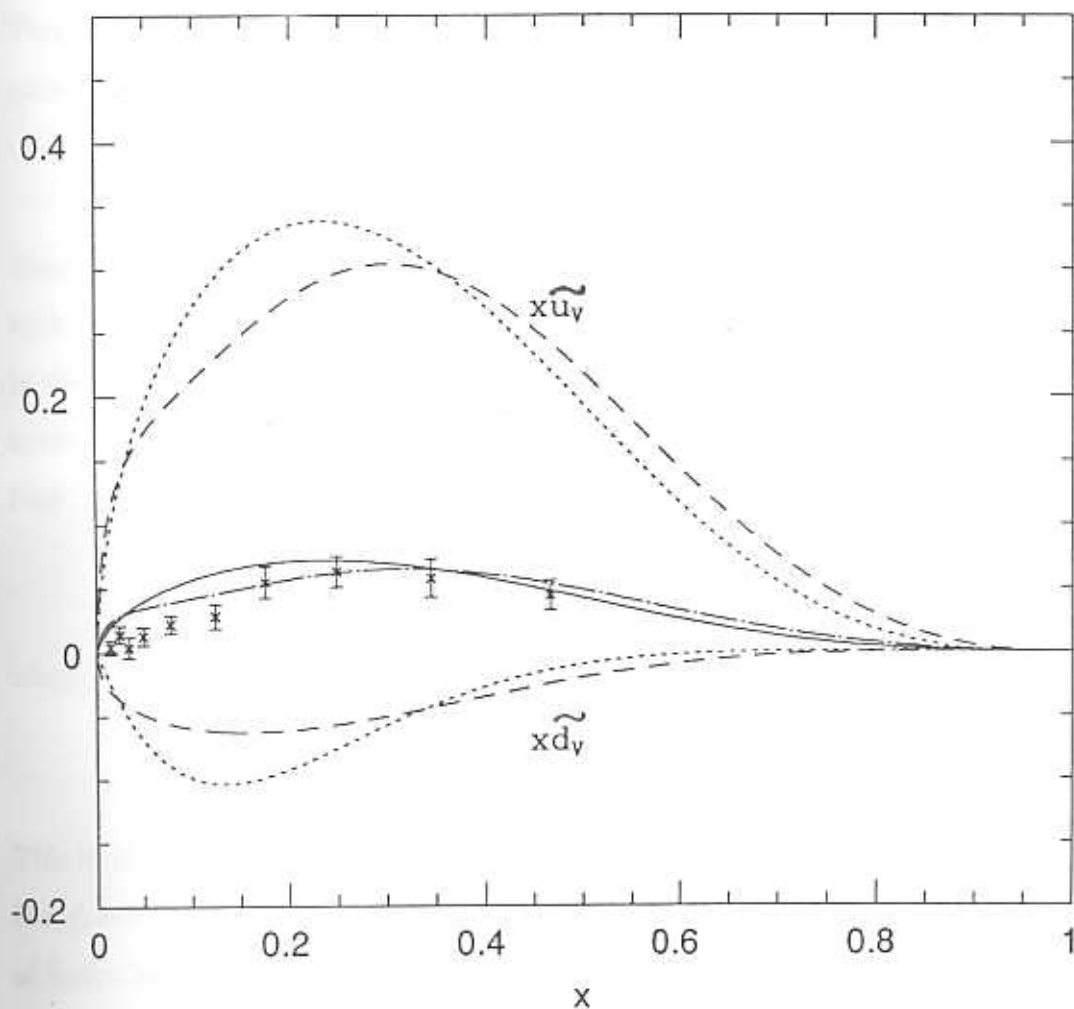


Fig. 2.2 The spin dependent valence densities are plotted as a function of x for EHLQ (dotted line) and Sloan (dashed line) parametrisations. The solid and dot-dash line represent the pure valence contribution of the two sets to $xg_1^p(x)$ for which the EMC data is also shown.

As seen in Chapter 1, the new interpretation includes an ‘anomaly-like’ contribution [10] to G_1^p coming from the gluons:

$$G_1^p = \frac{1}{2} \left\{ \sum_f e_f^2 \left(\Delta q_f - \frac{\alpha_s}{2\pi} \Delta g \right) \right\}. \quad (2.4)$$

This is because the leading order Q^2 evolution equations for the spin dependent parton densities [11] states that

$$\frac{d}{dt} \Delta \Sigma = 0; \quad \frac{d}{dt} (\alpha_s \Delta g) = \frac{\alpha_s^2}{\pi} \Delta \Sigma,$$

where $\Delta \Sigma$ is the sum of the flavour spin contributions and $t = \ln(Q^2/\mu^2)$, with μ the subtraction scale. In other words, $\alpha_s \Delta g$ is conserved to first order in the running coupling constant, α_s . Even to second order in α_s , $\alpha_s \Delta g$ is approximately conserved as the EMC experiment indicates $\Delta \Sigma$ is vanishing. Now, α_s at one-loop level vanishes logarithmically with Q^2 as

$$\alpha_s(Q^2) = \frac{12\pi}{(33 - 2f) \ln(Q^2/\Lambda^2)}, \quad (2.5)$$

where Λ is defined for f flavours through

$$b \alpha_s(0) \ln(\mu^2/\Lambda^2) = 1; \quad b = \frac{(33 - 2f)}{12\pi}.$$

This implies that Δg increases (also logarithmically) with Q^2 . Hence, though the gluonic contribution to the spin dependent structure function, $g_1^p(x)$, is of higher order in α_s than the quark contribution, there are potentially large gluonic contributions to the first moment of this structure function. This may explain the unexpected results of the EMC [10] and was the motivation behind the redefinition,

$$\Delta q \rightarrow \Delta q' - \frac{\alpha_s}{2\pi} \Delta g$$

with $\Delta q'$ being identified as the ‘true’ quark contribution in eq. (2.4).

This means that G_1^p yields an estimate of Δu_s only in the case where the (first) moment of the gluonic contribution to the structure function, $g_1^p(x)$, vanishes. Otherwise, since Δq_f and Δg both appear in the same expression

for G_1^p , eq. (2.4) only relates these quantities but does not separately determine their values. (The valence sector is completely defined; the only unknowns in this equation are Δu_s and Δg). On the other hand, since $\Delta\Sigma$ is conserved, a large Δg value implies also a correspondingly large value of the orbital angular momentum, \mathcal{L}_z in order to satisfy the "proton spin sum rule" in eq. (1.16), where the sum over $\langle S_z \rangle_q/2$ is identified as $\Delta\Sigma$. This means that we have already lost sight of the naïve parton model picture with zero net orbital angular momentum. Hence, the EMC result seems to imply that not only are the sea quark and gluon spin dependent densities possibly larger than expected, but the orbital angular momentum also may be large. Evidently it becomes important to *separately* establish the valence, sea and gluon contributions.

Consequently, we see now the importance of including terms that *a priori* seem to contribute only at sub-leading level, i.e., at $\mathcal{O}(\alpha_s)$ to the moment of g_1^p . However, such a procedure presents its own difficulties. The $\mathcal{O}(\alpha_s)$ contributions to the structure functions are scheme-dependent, as stated earlier; we, however, need a definition of parton densities that is "process independent." Since the definition of parton densities beyond the leading order is not unique, we are, in essence, free to choose them in such a way that the gluon contribution to $g_1^p(x)$ is either vanishing or non-vanishing.

The expression for $g_1^p(x)$ within the parton model is [2]

$$g_1(x, Q^2) = \frac{1}{2} \sum_f e_f^2 \int_x^1 \frac{dy}{y} \left(\tilde{q}(y, Q^2) \left[\delta\left(1 - \frac{x}{y}\right) + A\left(\frac{x}{y}\right) \right] + \tilde{g}(y, Q^2) B\left(\frac{x}{y}\right) \right), \quad (2.6)$$

where the parton densities already include the Q^2 -dependent splitting function factors. The Q^2 -independent $\mathcal{O}(\alpha_s)$ corrections to the quark and gluon terms are given by A and B respectively:

$$A(z) = \frac{\alpha_s}{2\pi} \left(f_{q,2}(z) - \frac{4}{3}(1+z) \right), \quad (2.7a)$$

where

$$f_{q,2}(z) = \frac{4}{3} \left(1 + 3z - \frac{3}{2} \frac{1}{(1-z)_+} - \frac{2(1+z^2)}{1-z} \ln z - \frac{2\pi^2}{3} \delta(1-z) \right) \quad (2.7b)$$

where the + prescription in the term $1/(1-z)_+$ indicates that the pole contribution at $z=1$ must be removed:

$$\int dz \frac{f(z)}{(1-z)_+} \equiv \int dz \frac{f(z) - f(1)}{1-z}.$$

Note that the leading behaviour of $g_1^p(x)$ and the spin independent structure function, $F_1(x)$, is the same. Also, the infrared (IR) singularities coming from a parton collinearly emitting another parton have been removed by taking the quarks off-shell and suitably regularising the expressions. (See refs. [2], [12]).

The gluon term is given in the QCD-corrected parton model by

$$B(z) = \frac{\alpha_s}{2\pi} (1-2z)(1+\ln z). \quad (2.8)$$

This result is also obtained via the OPE in the momentum subtraction scheme (MOM), while the \overline{MS} scheme gives a result [13]

$$B(z) = \frac{\alpha_s}{2\pi} \left((1-2z) \ln \left(\frac{z}{1-z} \right) + 3 - 4z \right). \quad (2.9)$$

Note that the sum in eq. (2.6) is over quarks and antiquarks; hence, the total gluonic contribution to $g_1^p(x)$ is twice that given in either eqs. (2.8) or (2.9). Furthermore, the gluon contribution starts at $\mathcal{O}(\alpha_s)$, but we have seen that this can still contribute significantly to G_1^p . Gluons contribute an amount $(-\alpha_s/2\pi)\Delta g$ to the moment of g_1^p because of eq. (2.8) so that eq. (2.4) is satisfied; eq. (2.9), though, yields a vanishing gluon contribution to the moment of g_1^p which corresponds to the naïve parton model expectation (*i.e.*, without the gluon term in eq. (2.4)).

Finally, we emphasise that it is the asymmetry, $A^{\mu p}$ that is finite as $x \rightarrow 0$; the only constraint on $g_1^p(x)$ is that it should be integrable and satisfy the constraints listed above. We point this out in view of the fact that the EMC [1] has fitted a form of $g_1^p(x)$ that seems to vanish at small- x , which need not be the case [14].

Hence, the EMC result for G_1^p only relates Δu_s and Δg and does not determine them individually when using eq (2.8) but actually fixes Δu_s [15]

when we use eq. (2.9). Without showing a preference for either case, we parametrise the densities both ways. We refer to the former as parametrisation Type 1 and the latter as parametrisation Type 2. We begin with the Type 1 parametrisation.

2.2.1 Parametrisation Type 1

Here, eq. (2.4) applies. For the EHLQ set of unpolarised density distributions, we have $\gamma = 0.2468$ (see Table 2.2). Hence,

$$\Delta u_V = 1.021; \quad \Delta d_V = -0.240$$

satisfying the Bjorken Sum Rule. Then using eq. (2.4) and the EMC result for G_1^p in eq (2.3), we get

$$\frac{3\alpha_s}{\pi} \Delta g - (10 + 2\eta) \Delta u_s = 1.576. \quad (2.10)$$

We evaluate α_s at $Q^2 = 5 \text{ GeV}^2$ and $\Lambda_{QCD} = 200 \text{ MeV}$, at which the unpolarised densities are parametrised, using eq. (2.5) for α_s . We choose to fix Δg by setting Δu_s as a free parameter. Hence, in the sea-sector, there are two free parameters, \tilde{N}_s and β (see Table 2.1). Now, from the form of parametrisation of the densities shown in Table 2.1, we have

$$\Delta u_s \equiv \int dx \tilde{u}_s(x) = \tilde{N}_s B(\beta, \xi + 1),$$

where $\xi = 8.54$ is the (common) exponent of $(1-x)$ in the expressions for u_s and \tilde{u}_s ; B stands for the beta-function. We can trade Δu_s for \tilde{N}_s ; hence, the two free parameters in the sea sector are β and Δu_s .

Once Δu_s is fixed, Δg gets fixed from eq. (2.10). Now, Δg has three free parameters, \tilde{N}_g , \tilde{a} and α (see Table 2.1):

$$\begin{aligned} x\tilde{g}(x) &= \tilde{N}_g x^\alpha (1 + \tilde{a}x)(1-x)^\zeta \\ xg(x) &= N_g (1 + ax)(1-x)^\zeta \end{aligned}$$

where the spin independent density, g , is known. Also, Δg is given by

$$\Delta g = \tilde{N}_g B(\alpha, \zeta + 1) \left[1 + \frac{\tilde{a}\alpha}{\alpha + \zeta + 1} \right],$$

Hence \bar{N}_g gets fixed, leaving only two free parameters, \hat{a} and α . It is more convenient to use α and $A^g(1)$, which is the gluon asymmetry, \bar{g}/g at $x = 1$.

Parametrisation Type 1: EHLQ		
$\gamma = 0.2468$; hence, $\Delta u_V = 1.021$, $\Delta d_V = -0.240$		
	Parameter values	Resulting Spin Contributions
Set (a)	$\Delta u_s = -0.2$, $\beta = 0.3622$, $\alpha = 0.50571$, $A^g(1) = -1$	$\Delta u = 0.62$, $\Delta d = -0.64$, $\Delta s = -0.178$, $\Delta g = -2.18$
Set (b)	$\Delta u_s = -0.133$, $\beta = 0.4476$, $\alpha = 1.0767$, $A^g(1) = 1$	$\Delta u = 0.75$, $\Delta d = -0.51$, $\Delta s = -0.118$, $\Delta g = 0.46$
Set (c)	$\Delta u_s = -0.1$, $\beta = 0.5135$, $\alpha = 0.5688$, $A^g(1) = 1$	$\Delta u = 0.82$, $\Delta d = -0.44$, $\Delta s = -0.089$, $\Delta g = -1.76$
Set (d)	$\Delta u_s = -0.05$, $\beta = 0.6958$, $\alpha = 0.36744$, $A^g(1) = 1$	$\Delta u = 0.92$, $\Delta d = -0.34$, $\Delta s = -0.045$, $\Delta g = 3.73$
Set (e)	$\Delta u_s = +0.05$, $\beta = 0.6958$, $\alpha = 0.2262$, $A^g(1) = 1$	$\Delta u = 1.12$, $\Delta d = -0.14$, $\Delta s = 0.045$, $\Delta g = 7.68$
Parametrisation Type 1: Sloan		
$\gamma = 0.2539$; hence, $\Delta u_V = 1.007$, $\Delta d_V = -0.254$		
	Parameter values	Resulting Spin Contributions
Set (f)	$\Delta u_s = -0.2$, $\beta = 0.3706$, $\alpha = 0.4223$	$\Delta u = 0.61$, $\Delta d = -0.65$, $\Delta s = -0.2$, $\Delta g = -3.92$
Set (g)	$\Delta u_s = -0.1$, $\beta = 0.5075$, $\alpha = 0.5515$	$\Delta u = 0.81$, $\Delta d = -0.45$, $\Delta s = -0.1$, $\Delta g = 2.29$
Set (h)	$\Delta u_s = -0.05$, $\beta = 0.6667$, $\alpha = 0.3558$	$\Delta u = 0.91$, $\Delta d = -0.35$, $\Delta s = -0.05$, $\Delta g = 5.39$

Table 2.2 The actual values of parameters that we will use are listed for both EHLQ and Sloan sets for Type 1 parametrisation. These results have been obtained *without* using the x -dependent form of the structure function, g_1^p , but only its moment.

This is related to \bar{a} by

$$A^g(1) = \frac{\bar{N}_g(1 + \bar{a})}{N_g(1 + a)}.$$

This is useful when we make sure that we satisfy the constraint, $|A^g(x)| \leq 1$.

So, altogether there are four free parameters, Δu_s , β , α and $A^g(1)$. These are to be chosen to satisfy the constraints

$$|A^Q(x)| \leq 1 \quad \text{for all } x; \quad A^Q = \tilde{Q}(x)/Q(x); \quad Q = q_s, g,$$

as well as the EMC data for the structure function and its expression in eqs. (2.6)-(2.8).

Hence the task is to use the expression in eq. (2.6) for $g_1^p(x)$, write it in terms of the four free parameters and use the data points to best-fit them. The most important constraint is that the parton asymmetries are all ≤ 1 . The logic required to check for this is as follows:

- The sea density case

It is straightforward to check that $|A^Q(x)| \leq 1$ for all x . The sea quark asymmetry is defined as

$$A^s(x) = \frac{\bar{N}_s x^\beta}{N_s}$$

and is an increasing function of x . Hence, provided $|A^s(x=1)| \leq 1$, the constraint is always satisfied. So, the requirement is that

$$|\bar{N}_s| \leq N_s \quad \text{or} \quad \left| \frac{\Delta u_s}{B(\beta, \xi + 1)} \right| \leq N_s$$

for the choice of β and Δu_s to be acceptable.

- The gluon density case

The situation is slightly more complicated in the gluon sector, because of larger number of parameters. We have

$$A^g(x) = \frac{\bar{N}_g x^\alpha (1 + \bar{a}x)}{N_g(1 + ax)}.$$

To make sure that $|A^g(x)| \leq 1$ always, we have to find the extrema of $|A^g|$ and check that these values are ≤ 1 . There are two extrema satisfying

$$\frac{\partial A^g}{\partial x} = 0$$

which are the solutions of

$$px^2 + qx + r = 0;$$

$$p = a\tilde{a}\alpha, \quad q = \tilde{a}(\alpha + 1) + a(\alpha - 1), \quad r = \alpha.$$

Let us call these solutions x_{min} and x_{max} . Recall $A(x = 0) = 0$, by definition. The procedure is as follows:

- Check if x_{min} lies within the range $[0,1]$. If so, check if the asymmetry at that value, $A^g(x_{min})$, has a modulus ≤ 1 . If so,
- Check if x_{max} lies within the range $[0,1]$. If so, check if the asymmetry at that value, $A^g(x_{max})$, has a modulus ≤ 1 . If both these conditions are valid, the choice of parameters is allowed.
- If either (or both) solution(s) lies outside the valid interval, or else is complex, the value of the asymmetry at that point is irrelevant. For example, if both solutions lie outside the interval $[0,1]$, then that choice of parameters is always allowed, provided, ofcourse, that $|A^g(x = 1)| \leq 1$.

For the case of the Sloan parametrisation, the entire procedure goes through as above, except that the spin dependent gluon parametrisation (which is similar to the sea quark parametrisation), is easier to handle. Hence, there are four free parameters in the EHLQ case (β , α , Δu , and $A^g(1)$), while there are only three in the Sloan case (as $A^g(1)$ is known once Δu , and α are fixed). Typical parameter values for both cases have been listed in Table 2.2. The limits on these parameters are shown in Fig. (2.3). Note that Δg can be both positive or negative. The sea quark spin dependent densities have been plotted as a function of x in Figs. (2.4a) and (2.4b) for the different parametrisation

sets of Table 2.2 for the EHLQ and Sloan parametrisation of the unpolarised densities.

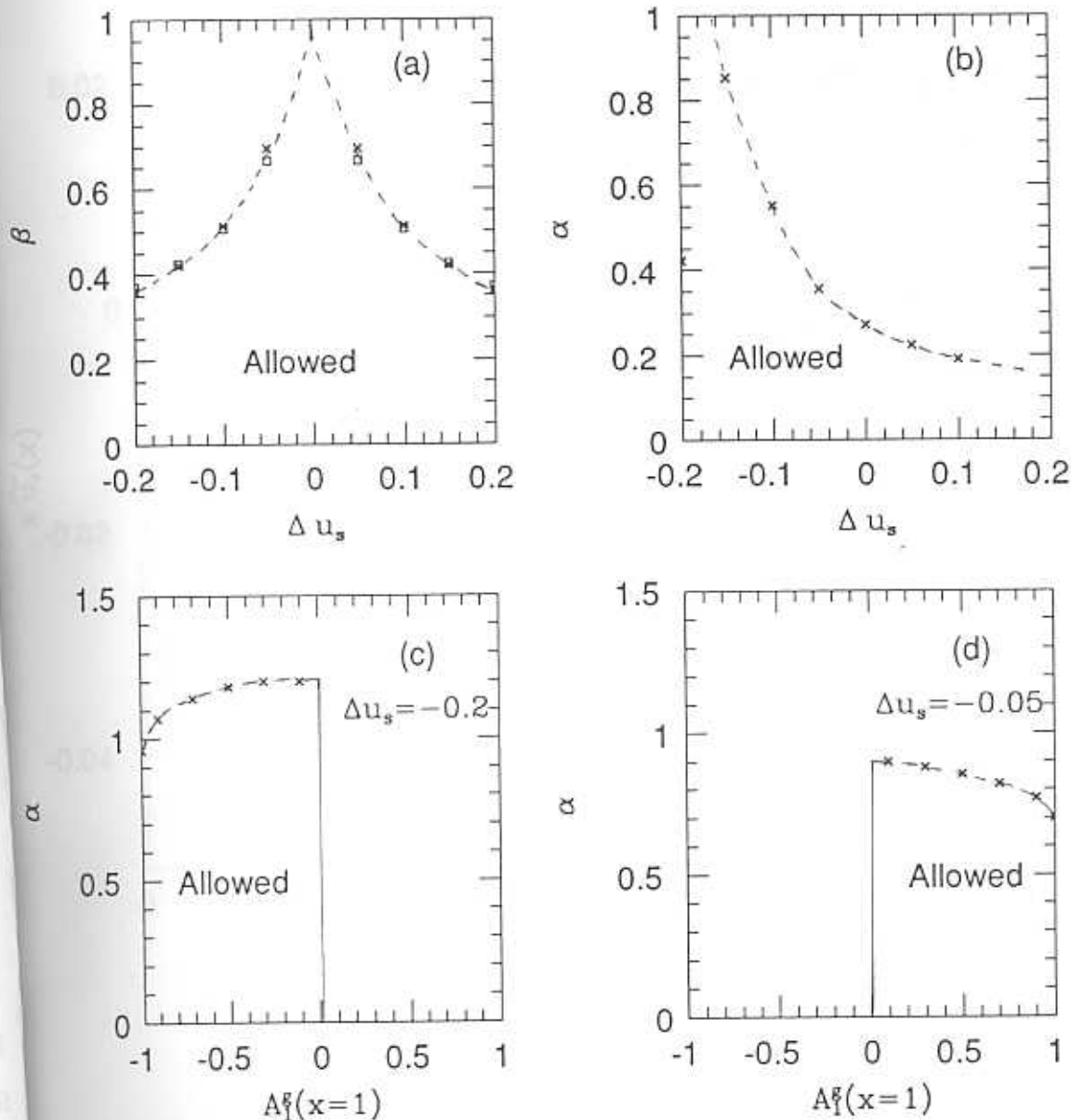


Fig. 2.3 Limits on the various free parameters for parametrisation type 1.

Fig. (a) shows the allowed region of Δu_s and β for the EHLQ (x) and Sloan (o) sets of unpolarised densities. Fig. (b) shows the limits on α in the Sloan case. Figs. (c) and (d) show the behaviour of the two parameters, α and $A^g(x=1)$ for the EHLQ set of unpolarised densities.

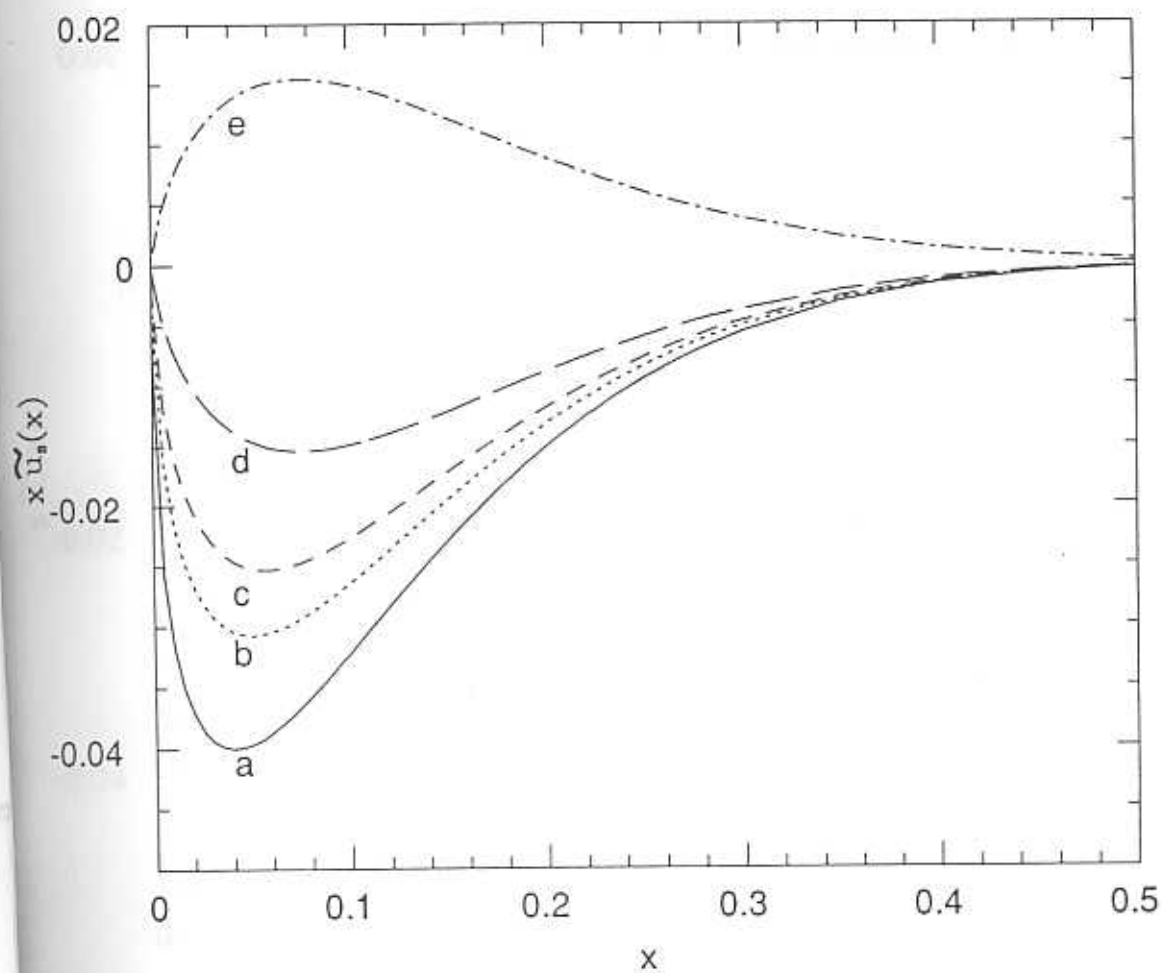


Fig. 2.4a Curves marked (a) to (e) show $x \bar{u}_2$ as a function of x for EHLQ Type 1 parametrisations. See Table 2.2 for details.

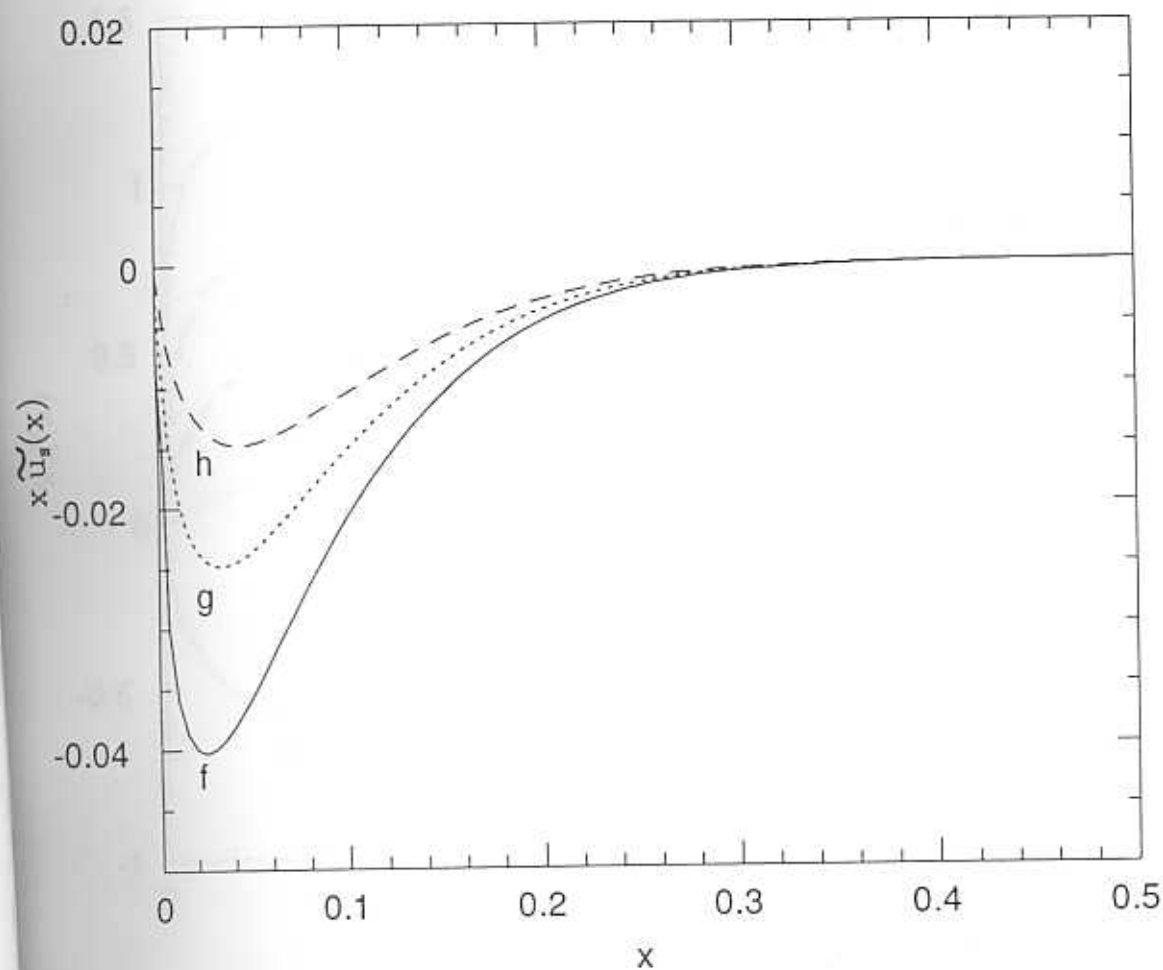


Fig. 2.4b Curves marked (f) to (h) show $x \tilde{u}_t$ as a function of x for Sloan Type 1 parametrisations. These are similar to the EHLQ sets. See Table 2.2 for details.

The corresponding spin dependent gluon densities have been plotted in Figs. (2.5a) and (2.5b). We see that the Sloan set has very similar behaviour to the EHLQ one and so we shall use the latter set alone in what follows.

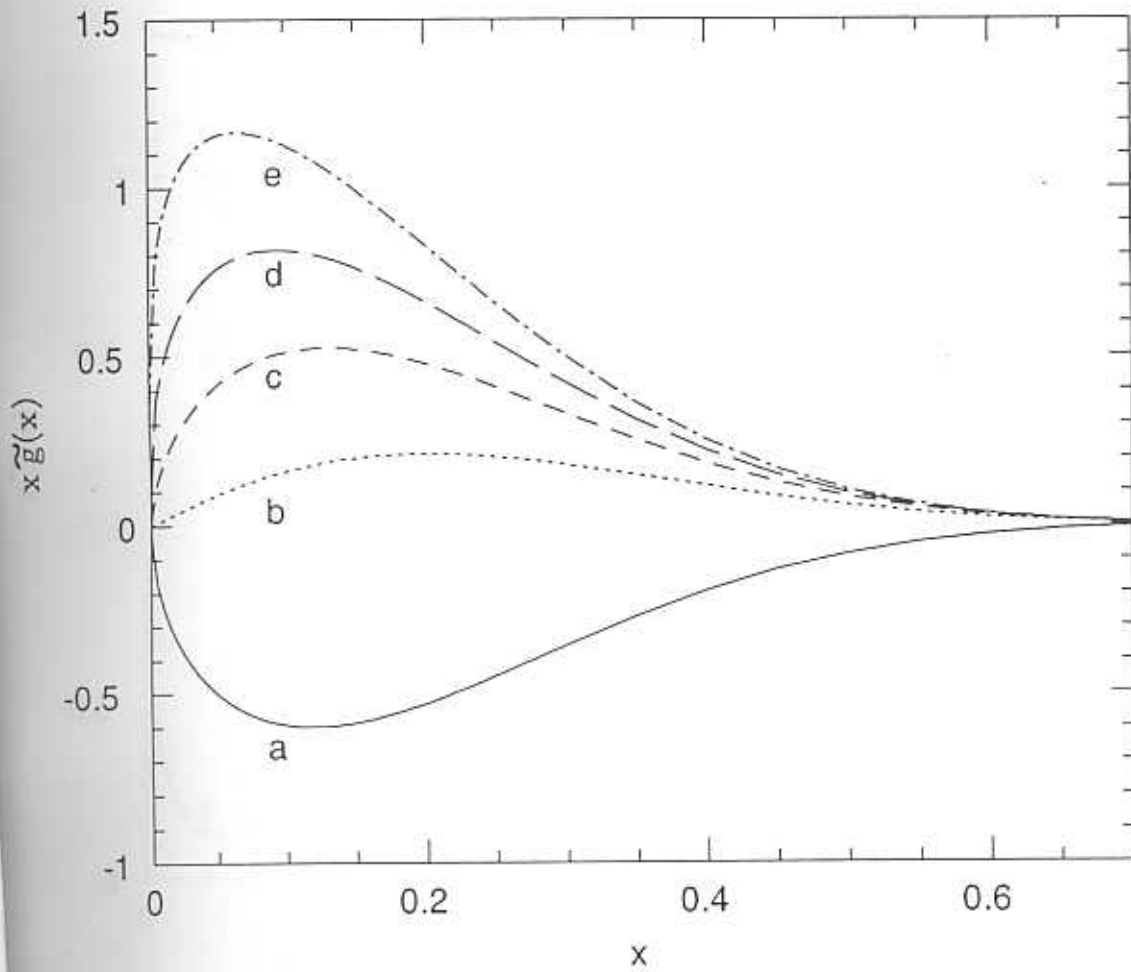


Fig. 2.5a The same as Fig. 2.4a, but for $x\tilde{g}$.

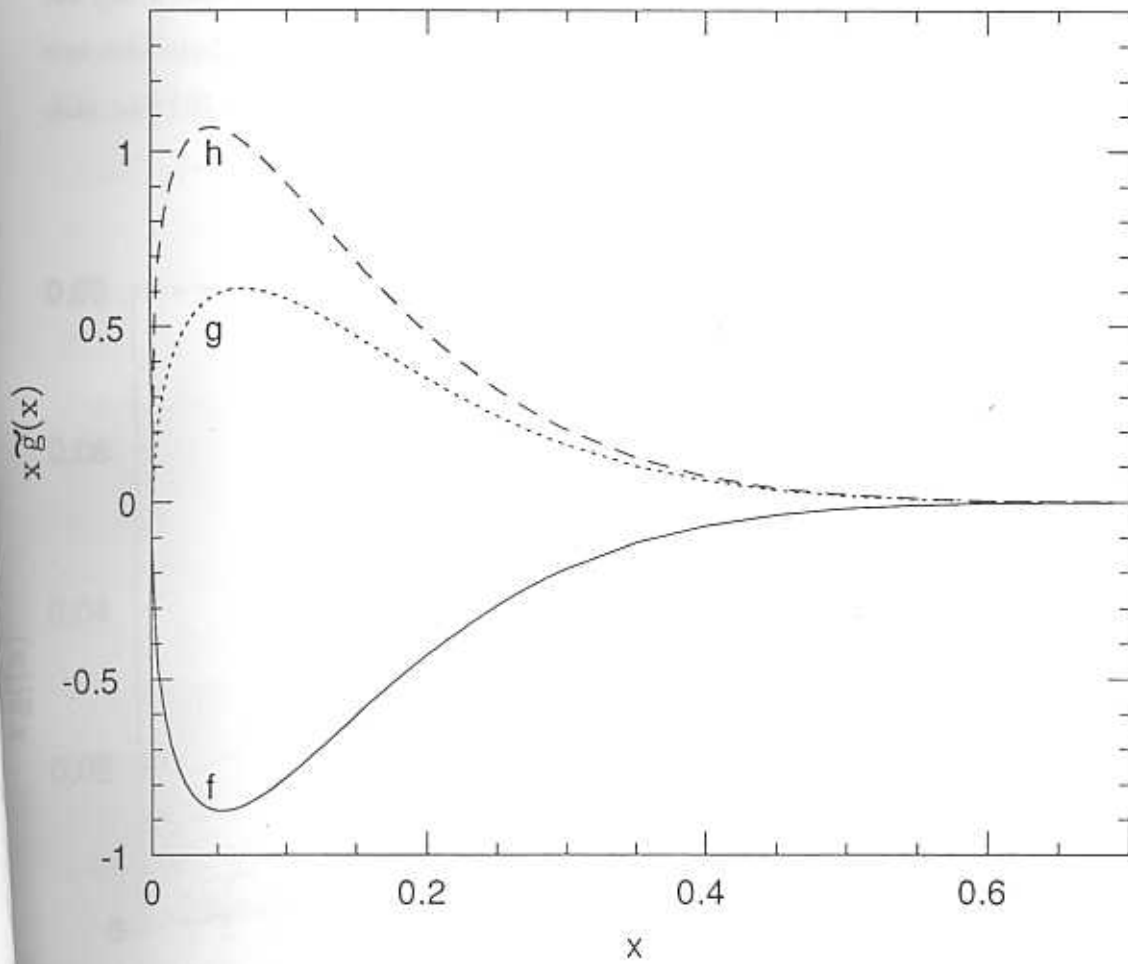


Fig. 2.5b The same as Fig. 2.4b, but for $x\tilde{g}$.

Finally, $xg_1^p(x)$ has been plotted in Fig. (2.6) where the solid curve is the EMC fit to the data, which has also been shown. We see that curve (e) corresponding to very large Δg or equivalently positive Δu , does not fit the data for any choice of parameters. This indicates that positive sea or strange quark spin contributions are unfavoured. Here, we have neglected $\mathcal{O}(\alpha_s)$ corrections to the quark contribution. Furthermore, the *spin independent* structure function was evaluated only to leading order as this is sufficient to fit the unpolarised data well [16].

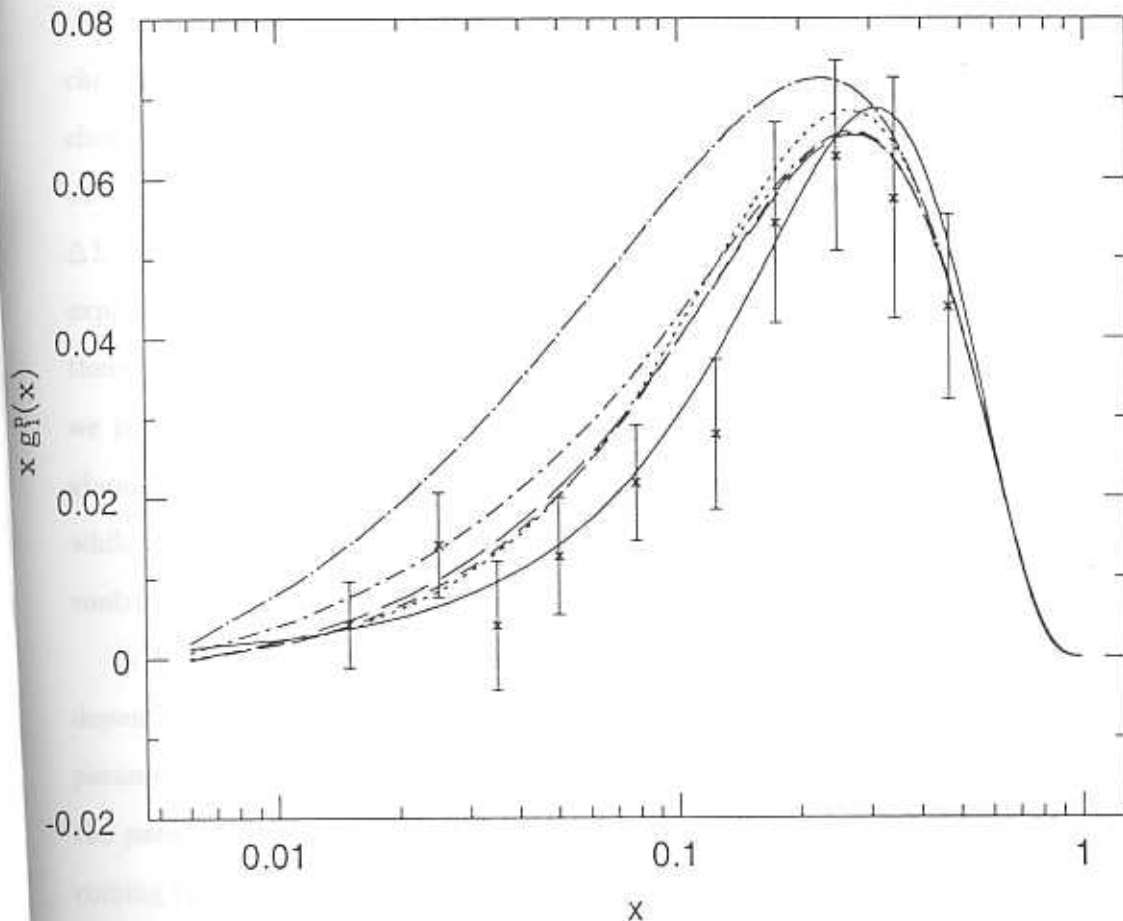


Fig. 2.6 $x g_1^p$ is shown for the EHLQ parametrisation sets (a) to (e) of Table 2.2 as a function of x . The EMC data is shown for comparison. Curve (e) does not fit the data.

2.2.2 Parametrisation Type 2

Here, the valence sector remains the same as in the type 1 case; only the sea and gluon sectors are changed. If we use the naïve parton model interpretation of the moment of the structure function in terms of the parton densities, then the equation

$$G_1^p \equiv \int_0^1 g_1^p(x) = 1/2 \sum_f e_f^2 \Delta q_f, \quad f = u, d, s,$$

fixes Δu_s as Δu_V and Δd_V are known. Hence, unlike in the case of the type 1 parametrisation, Δu_s is not a variable. However, there is no way to directly fix Δg ; we have to appeal to the proton spin sum rule (eq. (1.16)); if we choose \mathcal{L}_2 to be zero, Δg comes out to be around half. However, different choices of Δg , again both positive and negative, are allowed. Once Δg is chosen, everything else proceeds as in parametrisation type 1. In either case, we find $\Delta u_s \simeq -0.14$ for EHLQ as well as Sloan parametrisation sets, so that $\Delta \Sigma \simeq 0$. The choice $\mathcal{L}_2 = 0$ with no gluon contribution to G_1^p has been explicitly mentioned as it corresponds to the naïve expectation. Otherwise, there is no advantage of this parametrisation over the other type; in fact, we prefer the former (Type 1 parametrisation) as it separately contains the gluon contribution to the first moment of $g_1^p(x)$, which we know to be large, while the latter (Type 2 parametrisation) includes this potentially large gluon contribution in the definition of the spin dependent sea densities.

With this, we conclude our description of the parametrisation of the spin dependent densities. We see from the figures that the Sloan and EHLQ parametrisations yield similar results; we therefore choose the EHLQ set and the parametrisation Type 1 with which to discuss the asymmetries in forthcoming chapters.

References

- [1] J. Ashman *et al.*, The EM Collaboration, Phys. Lett. **B206** (1988) 364;

- Nucl. Phys. **B328** (1989) 1
- [2] V. Gupta, S.M. Paranjape and H.S. Mani, *Pramana* **14** (1980) 119; see also [12] for the corresponding spin independent quantities
- [3] Eichten et al. EHLQ, *Rev. Mod. Phys.* **56** (1984) 579.
- [4] T. Sloan, G. Smadja and R. Voss, *Phys. Rep.* **162** (1988) 45
- [5] J.D. Bjorken, *Phys. Rev.* **148** (1966) 1467; *Phys. Rev. D* **1** (1970) 1376
- [6] Recently isospin violation was observed through a measurement of the Gottfried Sum Rule; the consequent possible isospin violation of the sea has been ignored here as it is small compared to the errors in this experiment. Later parametrisations must however incorporate this as the quality of DIS data improves.
- [7] R. Carlitz and J. Kaur, *Phys. Rev. Lett.* **38** (1977) 673.
J. Kaur, *Nucl. Phys.* **B128** (1977) 219.
- [8] S. Gupta, J. Pasupathy and J. Szwed, *Z. Phys.* **C46** (1990) 111.
D. Indumathi, M.V.N. Murthy and V. Ravindran, 2-jet production in polarised pp collisions, preprint, IMSc/91/31
- [9] Particle Data Group, *Phys. Lett.* **B239** (1990).
The values we use, based on nucleon and Σ^- decay data, are $g_A = 1.261 \pm 0.004$ and $g_8 = 0.584 \pm 0.018$; if one includes data from Λ^0 decay, the value of g_8 decreases somewhat, but is still consistent, within error-bars, with what we have used.
- [10] See the references in Chapter 1
- [11] G. Altarelli and G. Parisi, *Nucl. Phys.* **B126** (1977) 298
- [12] G. Altarelli, R.K. Ellis and G. Martinelli, *Nucl. Phys.* **B143** (1978) 521

- [13] S.D. Bass, B.L. Ioffe, N.N. Nikolaev and A.W. Thomas, preprint DFTT-7/91 (1991)

See also U. Ellwanger referenced in Chapter 1

- [14] F.E. Close and R.G. Roberts, Phys. Rev. Lett. 60 (1988) 1471

- [15] This is where we differ from [8] the first reference in [8]

- [16] This needs careful handling; a redefinition of the spin dependent densities in the expression for $g_1^p(x)$ forces a corresponding redefinition of the spin independent densities so that the intuitive picture of q being the sum and \tilde{q} being the difference of the helicity densities holds. However, any such redefinitions affect the result for F_1 only at next-to-leading order and so we ignore them.

THE VALENCE DENSITIES

C O N T E N T S

The $\mu - p$ semi-inclusive process	
Formalism	
Numerics	
Application to the nuclear EMC effect	
Appendix: The νp DIS process	

3.0 The μ - p semi-inclusive process

In Chapter 1 we studied the polarised $\vec{\mu}$ - \vec{p} DIS process and corresponding data from the EMC and SLAC experiments. We will now look at different processes to see what more information can be gathered.

As a natural extension of the electromagnetic inclusive, polarised μp DIS process, we have semi-inclusive hadroproduction [1]. This is represented by

$$\vec{\mu} \vec{p} \longrightarrow \mu h^{\pm} X$$

where the arrows on the initial state particles denote longitudinal polarisation as usual, and h is a (charged) hadron; charged rather than neutral so that its experimental identification is easier. This process is an exact analogue of the inclusive DIS experiment, with a single particle being tagged in the final state debris. Some preliminary data is already available from the EMC. The final state polarisations are not detected as usual; it is enough if any two particles involved in the process are polarised. We consider the following three processes:

$$\begin{aligned}
 \vec{\mu} \vec{p} &\rightarrow \mu \pi^{\pm} X ; \\
 \vec{\mu} \vec{p} &\rightarrow \mu K^{\pm} X ; \\
 \vec{\mu} \vec{p} &\rightarrow \mu p(\bar{p}) X .
 \end{aligned}
 \tag{3.2}$$

We shall set up the asymmetries corresponding to these processes as defined in eq. (1.4):

$$A \equiv \frac{d\sigma(\uparrow\downarrow - \uparrow\uparrow)}{d\sigma(\uparrow\downarrow + \uparrow\uparrow)}, \quad (3.1)$$

but the cross-sections appearing in this expression are no longer just particle production cross-sections, but combinations of them such that a measurement of the asymmetry directly yields the spin dependent valence parton densities alone. Specifically, differences in rates of production of charge conjugates, i.e., h^+ and h^- , are sensitive to the valence densities in the proton. Once such an experiment is performed, therefore, the valence part will be fixed; it will then be possible to focus on just the sea densities which is the sector in which the ambiguities/controversies in this field are confined. Of course, the inclusive νp weak DIS process directly gives information on the sea densities [2]; however, such experiments are difficult to perform due to problems with obtaining monoenergetic ν beams. (Hence errors are larger in such experiments.)

The difference in cross-section between the production of h^+ and h^- factorises into the product of the valence quark density and the difference of quark and antiquark fragmentation functions. This fact was used initially to study the unknown fragmentation functions in unpolarised DIS hadroproduction. Hence the polarised experiment may be performed with very little effort; in fact, as stated before, preliminary data already exists. This is important, especially in view of the fact that we discuss polarised $\vec{p}\vec{p}$ collisions in the following Chapters, where the experimental feasibility is obvious only in fixed-target experiments, not in colliders.

3.1 Formalism

The cross-section for the processes listed in eq.(3.2) is related to the cross-section for a parton (that scatters off the polarised muon in the subprocess) to fragment into a hadron. Hence, the semi inclusive process is again represented at the subprocess level by

$$\mu q \rightarrow \mu q$$

where q is a parton, except that we now require the final state quark to fragment (or hadronise) into a specific kind of hadron, either π , K or p . To incorporate this constraint, in the parton model, we introduce a fragmentation function, $D_q^h(z)$. Quarks have colour and are confined; hence, they must fragment into hadrons with unit probability. That is,

$$\int D_q^h(z) dz = 1 .$$

This leads to the interpretation of the fragmentation function as a probability distribution—the probability that a parton, q , with momentum k , “fragments” into a hadron, h , with momentum, $z k$. This is depicted in Fig. (3.1).

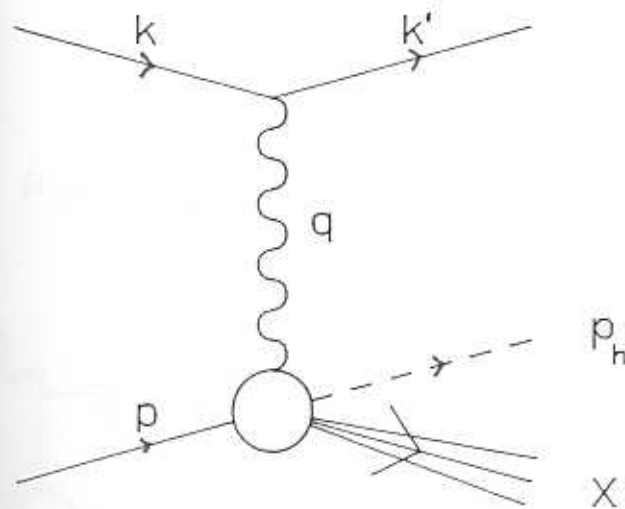


Fig. 3.1 This illustrates hadroproduction in semi-inclusive DIS processes.

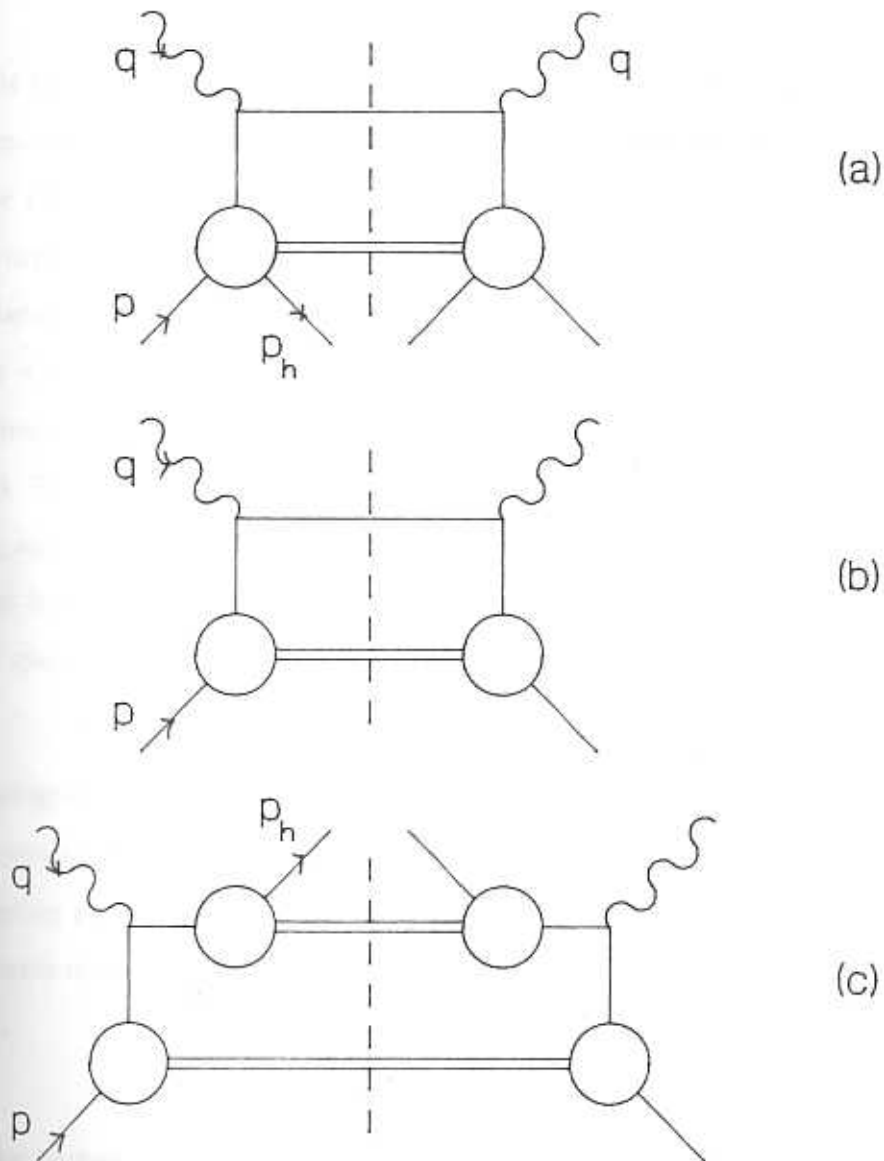


Fig. 3.2 Fig. (a) corresponds to Target fragmentation, Fig. (c) to Current fragmentation and Fig. (b) is the total inclusive cross-section (see text for details). The figure is reproduced from *An Introduction to Quarks and Partons*, F.E. Close, Academic Press, London, 1979.

In general, the hadron momentum may have some transverse components with respect to the momentum of the parton from which it was produced. Then,

$$z \equiv \frac{p_n \cdot p_h}{p_n \cdot q}, \quad (3.3)$$

where p_n is the initial nucleon momentum. There are two possible sources of the hadron. One is in the target debris, and the other, the struck quark. In the former case, (referred to as target fragmentation) the produced hadron does not carry any information about the DIS process; it is a recoil particle of the $\vec{\mu} \vec{p}$ interaction coming from the proton debris, X , and so has a momentum fraction, $z < 0$. In the latter case, it is the quark interacting with the photon that hadronises into the hadron, h (current fragmentation) with $z > 0$ (see Fig. (3.2)). This is the process we are interested in.

Hence, apart from the usual DIS kinematical variables, Q^2 and ν (or x and y), we also have the three-momentum of the hadron, h . This is because, in the phase space factor,

$$dQ = \sum_i \frac{d^3 p_i}{(2\pi)^3 2E_i}, \quad (3.4)$$

we have integrated out all but the $i = h$ momenta. When p_h is also integrated over, the result corresponds to the inclusive DIS cross-section.

Expressing p_h in terms of its longitudinal and transverse components, (z , p_T^2), the semi-inclusive cross-section is differential with respect to four variables, *i.e.*,

$$d\sigma(\vec{\mu} \vec{p} \rightarrow \mu h X) \equiv \frac{d^4 \sigma}{dx dy dz dp_T^2}.$$

Within the parton model, this process is approximated as consisting of two parts: first, the photon incoherently interacts with a nearly-free quark—this corresponds to the usual DIS process with variables x and y . Then, this struck quark (which now has a large momentum due to the large momentum transfer in the process, and is therefore well separated from the nucleon fragments) produces a hadron, h , of momentum fraction, z . The assumption made in the parton model is that the parton fragmentation proceeds independently

of the DIS process, *i.e.*, independently of x and y and is represented by the probability density (fragmentation function), D_q^h , which is a function of the hadron momentum alone:

$$D_q^h \equiv D_q^h(z, p_T^2)$$

and is independent of the target used. In what follows, we assume D_q^h to be a function of z alone, as the fragmentation functions are expected to be fairly insensitive to the small p_T picked up during the hadronisation process. (Recall that p_T is the transverse component of the hadron momentum with respect to the momentum of the parent parton; the hadron is part of the debris which is a "jet" confined to a narrow cone around the parton's momentum direction.)

Finally, we have the constraint,

$$\sum_h \int_0^1 dz z D_q^h(z) = 1, \quad q \equiv q, \bar{q} \quad (3.5)$$

which is the momentum conservation relation due to the constraints that

- a quark has to hadronise with probability one and
- the momenta of the hadrons it goes into should add up to its own momentum.

In terms of these fragmentation functions, the cross-section for the process, $\mu p \rightarrow \mu h^\pm X$, is given by

$$\begin{aligned} \frac{d\sigma}{dx dy dz}(\mu p \rightarrow \mu h^\pm X) &= \sum_q \frac{d\sigma}{dx dy}(\mu p \rightarrow \mu X) [D_q^h(z)] \\ &= \mathcal{A} \sum_{f, \bar{f}} e_f^2 q_f(x) D_f^h(z), \end{aligned} \quad (3.6)$$

where \mathcal{A} includes kinematical factors and the squared matrix elements and the sum runs over both quark and antiquark flavours. Notice that q 's refer to quark-antiquark densities inside the proton which interacts in the process while D_f^h carries information on the final state hadron.

Since we are interested in polarised μp scattering, we define the cross-sections,

$$d\sigma^h(\uparrow\uparrow) \text{ and } d\sigma^h(\uparrow\downarrow).$$

The former corresponds to deep inelastic hadroproduction when both the initial particles are longitudinally polarised parallel to each other (say, along the z -axis or the beam direction) and the latter corresponds to an antiparallel spin configuration. We now have to express $q(x)$ and $D_q^h(z)$ suitably, to accommodate the spin dependence.

As in inclusive $\vec{\mu} \vec{p}$ DIS, we define the spin independent and spin dependent parton density combinations, $q_f(x)$ and $\tilde{q}_f(x)$. Consider first, the production of $h = \pi, K$, i.e., spinless meson production. Obviously,

$$D_{f+}^h(z) = D_{f-}^h(z) = D_f^h(z); \quad h = \pi, K. \quad (3.7)$$

Eq. (3.7) states that the probability for a positive helicity parton to produce a spinless hadron equals that for a negative helicity parton, *at every* z .

Using eq. (3.7) and the density combinations $q_f(x)$ and $\tilde{q}_f(x)$ to express the spin dependences in the hadroproduction cross-section, we have

$$\begin{aligned} \frac{d\sigma^h}{dx dy dz}(\uparrow\downarrow) &= A \sum_f e_f^2 q_f^+(x) D_f^h(z); \\ \frac{d\sigma^h}{dx dy dz}(\uparrow\uparrow) &= A \sum_f e_f^2 q_f^-(x) D_f^h(z). \end{aligned} \quad (3.8)$$

Again, the notation is the same as in inclusive DIS, where $(\uparrow\downarrow)$ and $(\uparrow\uparrow)$ refer to antiparallel and parallel beam-target polarisation configurations respectively and q^+ and q^- refer to positive and negative helicity quarks whose spins are respectively aligned and opposed to that of the parent hadron. When integrated over z , as stated earlier, eq. (3.8) corresponds exactly to polarised, inclusive DIS.

As before, we define the combinations:

$$\begin{aligned} \tilde{\sigma}^h &= \frac{d\sigma^h}{dx dy dz}(\uparrow\downarrow) - \frac{d\sigma^h}{dx dy dz}(\uparrow\uparrow); \\ d\sigma^h &= \frac{d\sigma^h}{dx dy dz}(\uparrow\downarrow) + \frac{d\sigma^h}{dx dy dz}(\uparrow\uparrow). \end{aligned}$$

We get

$$\begin{aligned}\widetilde{d\sigma}^h &= \mathcal{A} \sum_f e_f^2 \bar{q}_f(x) D_f^h(z); \\ d\sigma^h &= \mathcal{A} \sum_f e_f^2 q_f(x) D_f^h(z).\end{aligned}\tag{3.9}$$

At first sight, it seems, from eq. (3.9), that we have gained no further insight into the parton contributions to the nucleon spin; in fact, we seem to be worse off than before as we do not know the fragmentation functions. However, we observe that

- the fragmentation functions are independent of the polarisation configuration of the initial state
- they are also the only quantities that carry information on the produced hadron;

hence, the combination

$$d\sigma^{h^+} - d\sigma^{h^-}$$

is proportional to

$$q_f D_f^{h^+}(z) - \bar{q}_f D_f^{h^-}(z),$$

where we have not displayed charge factors for the sake of clarity. Since h^+ and h^- are charge conjugates (+ and - refer to the charges of the mesons and are not to be confused with the spins), invariance under charge conjugation symmetry implies

$$D_f^{h^+}(z) = D_f^{h^-}(z).\tag{3.10}$$

Then the contribution to $(d\sigma^{h^+} - d\sigma^{h^-})$ of quarks and antiquarks of a given flavour is

$$\begin{aligned}& \left[q_f D_f^{h^+} + \bar{q}_f D_f^{h^+} \right] - \left[q_f D_f^{h^-} + \bar{q}_f D_f^{h^-} \right], \\ &= (q_f - \bar{q}_f) \left[D_f^{h^+}(z) - D_f^{h^-}(z) \right], \\ &= q_v(x) \left[D_f^{h^+}(z) - D_f^{h^-}(z) \right],\end{aligned}\tag{3.11}$$

where we have used eq. (3.10). Hence, the combination, $d\sigma^{h^+} - d\sigma^{h^-}$ is proportional always to the valence quark densities weighted, ofcourse, by charge

factors. Hence, if we set up the asymmetry for the cross-section combinations

$$\begin{aligned} \Delta N^h &\equiv d\sigma^{h^+} - d\sigma^{h^-}, \\ \widetilde{\Delta N}^h &\equiv \widetilde{d}\sigma^{h^+} - \widetilde{d}\sigma^{h^-}, \end{aligned}$$

instead of for just $d\sigma^{h^+}$ or $d\sigma^{h^-}$, the result will be proportional to the valence quark densities alone. Since there is no sea quark contribution, gluons also do not contribute and hence this asymmetry will measure the contribution to nucleon spin coming from only the valence densities.

We still have to worry about the unknown fragmentation functions, which are not as well determined from experiments as the quark distribution functions. However, in what follows, we shall see that we can relate the various fragmentation functions using charge conjugation and isospin invariance, such that the resulting expression for the asymmetry is *independent* of these unknown fragmentation functions. We begin with K^- -production.

There are six fragmentation functions for the K^+ . They are

$$D_u^{K^+}, D_{\bar{u}}^{K^+}, D_d^{K^+}, D_{\bar{d}}^{K^+}, D_s^{K^+}, D_{\bar{s}}^{K^+},$$

and analogously six for the K^- . Charge conjugation symmetry relates them according to eq. (3.10) so that there are only six fragmentation functions in all for the K^+ and the K^- ; these we write in terms of the K^+ fragmentation functions alone as

$$D_f^{K^+}(z) = D_{\bar{f}}^{K^-}(z) \equiv D_f^K(z).$$

The various cross-sections can be written in terms of these. Then, according to eq. (3.11), the cross-section combinations of interest to us are as follows:

$$\begin{aligned} \Delta N^K &\equiv d\sigma^{K^+} - d\sigma^{K^-} \\ &= \frac{A}{9} \left\{ 4(u - \bar{u}) [D_u - D_{\bar{u}}] + (d - \bar{d}) [D_d - D_{\bar{d}}] + \right. \\ &\quad \left. (s - \bar{s}) [D_s - D_{\bar{s}}] \right\}; \end{aligned} \quad (3.12)$$

$$\begin{aligned} \widetilde{\Delta N}^K &\equiv \widetilde{d}\sigma^{K^+} - \widetilde{d}\sigma^{K^-} \\ &= \frac{A}{9} \left\{ 4(\bar{u} - \bar{\bar{u}}) [D_u - D_{\bar{u}}] + (\bar{d} - \bar{\bar{d}}) [D_d - D_{\bar{d}}] + \right. \\ &\quad \left. (\bar{s} - \bar{\bar{s}}) [D_s - D_{\bar{s}}] \right\}, \end{aligned} \quad (3.13)$$

where the dependences on x and z of the densities and the fragmentation functions respectively as well as the superscript, K , in the fragmentation functions have been suppressed for convenience. Notice that the strange quark contribution vanishes as the valence combinations, $(s - \bar{s})$ and $(\tilde{s} - \bar{\tilde{s}})$, are zero in the nucleon. We also use the approximation of equality of unfavoured fragmentation; in this case, this implies that

$$D_d^K(z) = D_{\bar{d}}^K(z).$$

Since d quarks are present only through $d\bar{d}$ pairs in the sea of the K^+ which is a $(u\bar{s})$ valence-quark bound state, this is a reasonable assumption. Then, eqs. (3.12) and (3.13) reduce to

$$\begin{aligned}\Delta N^K &= \frac{A}{9} \left\{ 4 u_V (D_u - D_{\bar{u}}) \right\}; \\ \widetilde{\Delta N}^K &= \frac{A}{9} \left\{ 4 \widetilde{u}_V (D_u - D_{\bar{u}}) \right\}.\end{aligned}$$

So the asymmetry, defined analogous to eq. (3.1) as

$$A^K(x, z) \equiv \frac{\widetilde{\Delta N}^K}{\Delta N^K}$$

becomes

$$\begin{aligned}A^K(x, z) &= \frac{\widetilde{u}_V(x) (D_u - D_{\bar{u}})(z)}{u_V(x) (D_u - D_{\bar{u}})(z)} \\ &= \frac{\widetilde{u}_V(x)}{u_V(x)}\end{aligned}\tag{3.14}$$

and is thus independent of the unknown fragmentation functions; in fact, it depends on the u -quark valence density alone. Since the unpolarised u -quark valence density is known, measurement of the asymmetry in polarised DIS K -production directly gives the spin dependent u -quark valence density.

A similar procedure for the case of π -production gives

$$\begin{aligned}\Delta N^\pi &= \frac{A}{9} \left\{ 4 u_V (D_u - D_{\bar{u}}) + d_V (D_d - D_{\bar{d}}) \right\}; \\ \widetilde{\Delta N}^\pi &= \frac{A}{9} \left\{ 4 \widetilde{u}_V (D_u - D_{\bar{u}}) + \widetilde{d}_V (D_d - D_{\bar{d}}) \right\},\end{aligned}$$

where the superscript on $D_f(z)$ should now be π . Since u and d are in the valence of π , we cannot drop either of them as we did in the case of

K -production; however, isospin symmetry between π^+ and π^- gives us

$$D_u^{\pi^+} = D_d^{\pi^-}; \quad D_d^{\pi^+} = D_u^{\pi^-},$$

which, together with eq. (3.10) that states charge conjugation invariance, yields the following relations between the various fragmentation functions:

$$\begin{aligned} D_{\bar{u}}^{\pi^-} \stackrel{C}{=} D_u^{\pi^+} \stackrel{I}{=} D_d^{\pi^-} \stackrel{C}{=} D_d^{\pi^+}, \quad \text{which we denote by } D_u^\pi \text{ and} \\ D_u^{\pi^-} \stackrel{C}{=} D_{\bar{u}}^{\pi^+} \stackrel{I}{=} D_{\bar{d}}^{\pi^-} \stackrel{C}{=} D_{\bar{d}}^{\pi^+}, \quad \text{which we denote by } D_{\bar{u}}^\pi. \end{aligned} \quad (3.15)$$

(Here, C and I indicate charge conjugation and isospin operations respectively.) Then,

$$\begin{aligned} \Delta N^\pi &= \frac{A}{9} \left\{ (4u_V - d_V) (D_u - D_{\bar{u}}) \right\}; \\ \widetilde{\Delta N}^\pi &= \frac{A}{9} \left\{ (4\bar{u}_V - \bar{d}_V) (D_u - D_{\bar{u}}) \right\}. \end{aligned}$$

Hence, the asymmetry in the pion case, which is the ratio of $\widetilde{\Delta N}^\pi$ and ΔN^π , is

$$A^\pi(x, z) = \frac{4\bar{u}_V(x) - \bar{d}_V(x)}{4u_V(x) - d_V(x)}. \quad (3.16)$$

Again, we see that the fragmentation functions, *i.e.*, the z -dependence cancels. Since \bar{u}_V is directly measurable in K -production, polarised DIS π -production will yield information on \bar{d}_V . Since d_V is positive (it is a probability density) and \bar{d}_V is expected to be negative over most of the x -range, A^π has a larger numerator and smaller denominator than A^K and so A^π will be larger than A^K . Hence, the relative magnitudes of A^K and A^π can also indicate the sign of the spin dependent valence d -quark contribution.

Since d_V is less than u_V at all x , (recall d_V is suppressed by a factor $(1-x)$ relative to u_V), we rewrite the asymmetry in terms of the ratios,

$$f(x) = \frac{d_V(x)}{4u_V(x)}, \quad \rho_u = \frac{\bar{u}_V(x)}{u_V(x)}, \quad \rho_d = \frac{\bar{d}_V(x)}{d_V(x)}, \quad (3.17)$$

all of whose magnitudes are less than unity. We have

$$A^\pi \simeq \rho_u + (\rho_u - \rho_d) (f + f^2), \quad (3.18)$$

where we have retained terms upto order f^2 only, as f is small. Since A^K in eq. (3.14) equals ρ_u ,

$$A^\pi - A^K \simeq f (\rho_u - \rho_d) .$$

When the hadron detected in the final state is a proton, the fragmentation functions need to be carefully defined as protons carry spin of half a unit ($\hbar/2$). The key point to note here is that the final state polarisation is not detected, so a summation over the proton spin must be carried out.

In the subprocess, the polarised initial state quark interacts with the photon and, because of fermion helicity conservation at the photon-fermion vertex, goes into a final state quark with definite polarisation. For example, a helicity (-1) photon interacts with a quark whose spin is aligned with the photon direction only:

$$\gamma^{\downarrow} q^{\uparrow} \rightarrow q^{\uparrow} .$$

This final state quark of definite helicity then fragments into the proton. Let $D_{f+}^{p+}(z)$ be the probability for a positive helicity quark to fragment into a positive helicity proton (neglecting its mass for the moment) with a momentum fraction, z . Similarly, q^+ can fragment into p^- . Since the proton polarisation is not detected, we have to sum the probability that this q^+ fragments into p^+ or p^- . This is expressed as

$$D_{f+}^p(z) \equiv D_{f+}^{p+}(z) + D_{f+}^{p-}(z) .$$

$D_{f-}^p(z)$ is similarly defined by replacing q^+ by q^- in the above equation. However, the probability of a q^+ fragmenting into an unpolarised proton with spin down, *i.e.*, p^{\downarrow} , is the same as that of q^- producing p^{\uparrow} , by definition, *i.e.*

$$D_{f+}^{p\downarrow} = D_{f-}^{p\uparrow} ; \quad D_{f-}^{p\downarrow} = D_{f+}^{p\uparrow} .$$

Hence, we have the following relations:

$$D_{f+}^p = D_{f+}^{p+} + D_{f-}^{p\downarrow} \equiv D_f^{p+} .$$



Also, we have thus generally

$$D_{f+}^p = D_{f-}^{p1} + D_{f+}^{p1} \equiv D_f^{p1},$$

i.e., a sum over the final state proton spin directions is equivalent to a sum taken over parent quark helicities. Hence, we define

$$\begin{aligned} D_{f+}^p(z) &= D_f^{p1}(z) = D_f^{p1}(z) \\ &\equiv D_f^p(z), \end{aligned}$$

since the probability for an unpolarised quark, q , to fragment into a proton of either polarisation is just the probability that it fragments into that proton at all. Similarly,

$$D_{f-}^p(z) \equiv D_f^p(z),$$

so that again the fragmentation functions are insensitive to the initial state spin, as they ought to be. The asymmetry is given by

$$A^p = \frac{4 \tilde{u}_V (D_u - D_{\bar{u}}) + \tilde{d}_V (D_d - D_{\bar{d}})}{4 u_V (D_u - D_{\bar{u}}) + d_V (D_d - D_{\bar{d}})} \quad (3.19)$$

The further assumption that [3]

$$(D_u - D_{\bar{u}}) = (D_d - D_{\bar{d}})$$

for a proton leads to a factorisation of the fragmentation functions as before and we get

$$A^p(x, z) \simeq \frac{4 \tilde{u}_V(x) + \tilde{d}_V(x)}{4 u_V(x) + d_V(x)}$$

Rewriting in terms of f , ρ_u and ρ_d as defined in eq. (3.17), we have

$$A^p \simeq \rho_u - (\rho_u - \rho_d) (f - f^2),$$

where we have again retained terms upto order f^2 only, as f is small. We observe that

$$\begin{aligned} A^\pi + A^p &\simeq 2 \rho_u + f^2 (\rho_u - \rho_d) \\ &\simeq 2 A^K \end{aligned} \quad (3.20)$$

to a very good approximation.

We have thus generally established that asymmetries in polarised deep inelastic μp hadroproduction yield information on the spin dependent valence densities. Symmetry arguments were used to cancel the z -dependence of these asymmetries which appear as ratios of fragmentation functions. This was possible as these were the only quantities in the cross-section that contained any z -dependence. Since very little is known about these fragmentation functions, we should also test that that our results are not spoiled by possible x -dependences of fragmentation functions. Experimental evidence indicates [4] that, if such effects are present, they are the same for hadrons related by charge conjugation. Since we are constructing asymmetries involving the differences of particle-antiparticle production cross-sections, it is likely that such x -dependences will cancel out to a good approximation. In the next section, we shall use the parametrisations of Chapter 2 for the valence densities to study the magnitude and sign of these asymmetries.

3.2 Numerics

We have parametrised the spin dependent valence densities in terms of a single one-parameter function, $\cos 2\phi$. The asymmetries constructed in the previous section can be expressed in terms of this "spin dilution factor" as

$$\begin{aligned} A^K &= \cos 2\phi(x) \left(1 - \frac{2}{3} f(x)\right); \\ A^\pi &= \cos 2\phi(x) \left(1 - \frac{1}{3} f(x) - \frac{1}{12} f^2(x)\right); \\ A^p &= \cos 2\phi(x) \left(1 - f(x) + \frac{1}{4} f^2(x)\right). \end{aligned} \quad (3.21)$$

Hence, every asymmetry is positive. Further, the fit to $\cos 2\phi$ obtained from the EMC data yields large values for these asymmetries over most of the x -range, including the small- x region, where sensitive and accurate data is needed in order to resolve the controversies generated by the EMC experiment. Further, Fig. (3.3) shows [7] that $(A^\pi + A^p)/2$ equals A^K to within few percent over the entire x -range.

3.3 Conclusions

We conclude that the results of the present work which in study any experimental set up to study the process by including the effect of the

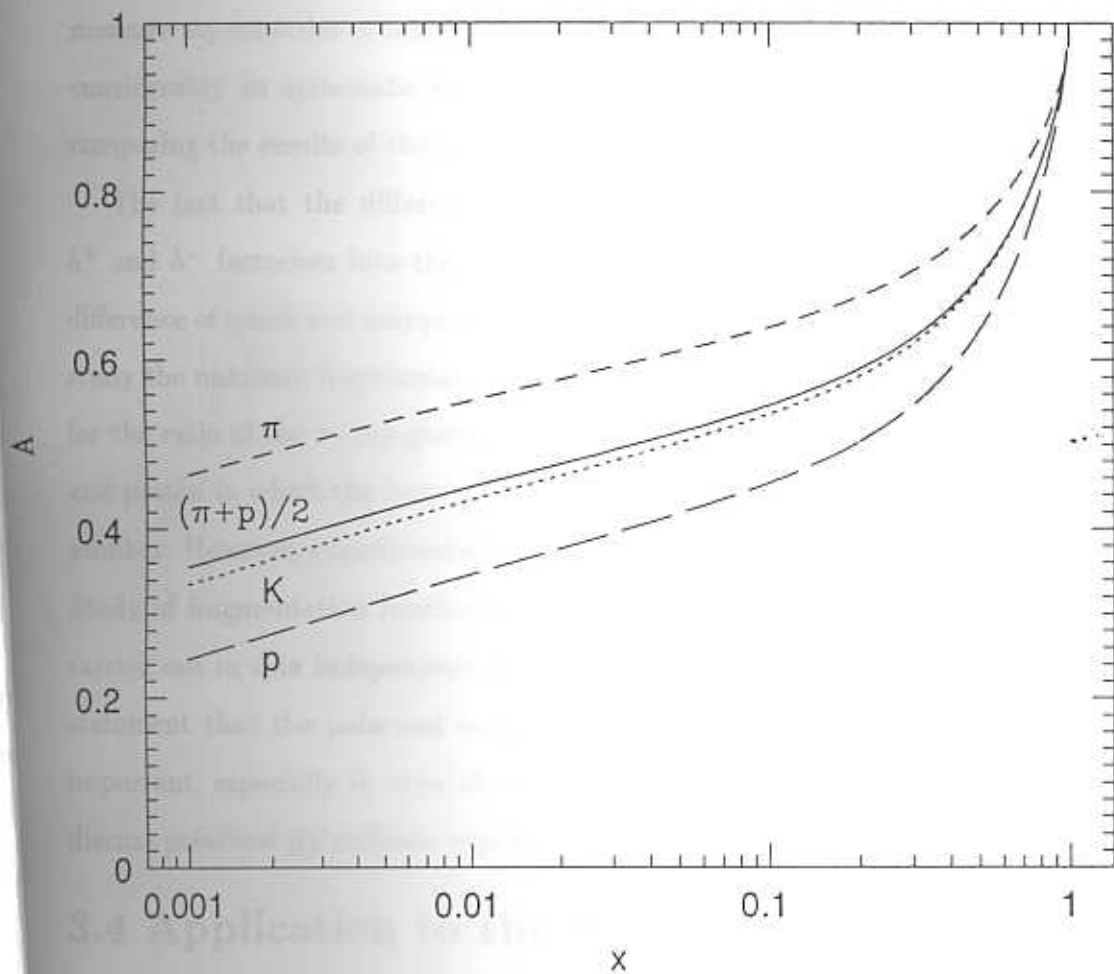


Fig. 3.3 The asymmetries in semi-inclusive K , π and p production. Note that the solid line corresponding to $(\pi + p)/2$ equals the asymmetry for K to within a few percent over the entire x -range.

3.3 Conclusions

We conclude that polarised deep inelastic charged hadroproduction is a good process with which to study the spin dependent valence densities. In fact, any experiment set up to study polarised DIS can immediately measure this process by including final state hadron detection. Use of a single set-up to measure asymmetries in inclusive as well as semi-inclusive DIS will cut down considerably on systematic errors and will thus allow the sea densities (on comparing the results of the two experiments) to be extracted more reliably.

The fact that the difference in cross-section between the production of h^+ and h^- factorises into the product of the valence quark density and the difference of quark and antiquark fragmentation functions was used initially to study the unknown fragmentation functions. Later, sum rules were derived [1] for the ratio of the x -integrated DIS π -production cross-sections in neutron and proton in which the fragmentation functions cancel and the ratio is just a number. However, experimental verification of these sum rules is yet to come. Study of fragmentation functions and their z -dependence has recently been carried out in spin independent DIS hadroproduction [4]. This reinforces the statement that the polarised experiment may be performed easily. This is important, especially in view of the fact that in the following Chapters, we discuss polarised $\vec{p}\vec{p}$ collision experiments which are harder to perform.

3.4 Application to the Nuclear EMC Effect

As an application of the technique described in section (3.1), we discuss the valence nuclear EMC effect [8]. Although not central to this thesis, this topic forms a good application of the analysis presented above. The EMC effect is the observation, first made by the European Muon Collaboration [5] that the structure function of a nucleon found in a nucleus of mass number A and that of a free nucleon are nontrivially different. This is shown in Fig. (3.4), where the ratio of the nuclear (Fe and Cu) and nucleon (Deuteron) structure functions, $F_2(x)$, is plotted as a function of x .

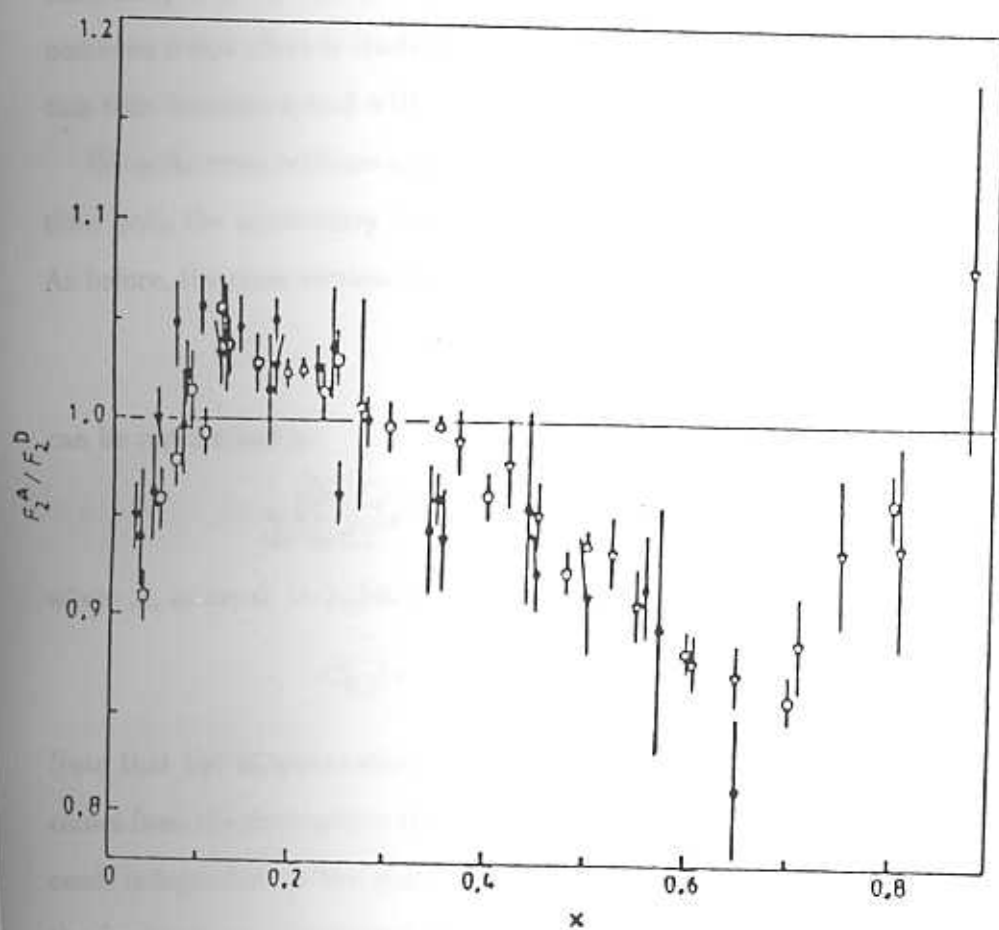


Fig. 3.4 Combined data from EMC, SLAC and BCDMS collaborations on the EMC effect from the review by R.P. Bickerstaff and A.W. Thomas, in reference [5] above.

The ratio is seen to be less than one for large $x \simeq 0.4 - 0.8$ as well as in the very small- x region ≤ 0.05 . The latter effect is called shadowing and is not yet well understood. Although there is no consensus explanation for the A -dependence of the structure functions, the field has narrowed to two candidates—nuclear smearing and fermi rescaling models. However, neither completely explains the data [6]. One may gain more insight into this phenomenon if this effect is studied on individual parton densities. Hadroproduction then becomes a tool with which to study the “valence EMC effect.”

We write cross-sections analogous to polarised deep inelastic hadroproduction; here, the asymmetry is the ratio of nuclear and nucleon cross-sections. As before, the cross-section for muon-nucleon/nuclear scattering

$$\mu(N, A) \rightarrow \mu h X$$

can be represented as

$$\frac{d\sigma}{dx dy dz}(\mu N, A \rightarrow \mu h X) = \mathcal{A} \mathcal{L}_{N,A}^h(x, z),$$

where \mathcal{A} , as usual, includes kinematical variables and \mathcal{L}^h is given by

$$\mathcal{L}_{N,A}^h(x, z) = \sum_f e_f^2 q_f^{N,A}(x) D_f^h(z).$$

Note that the fragmentation functions are independent of the target. This comes from the assumption that, in DIS, the quark fragmentation process proceeds independent of the scattering — the latter is an x -dependent process; the former is a z -dependent one. Effectively, this means that the hadronisation process is indifferent to the source of the parent quark. Given a quark with large momentum, the probability that a hadron with a momentum fraction, z , can be found in its debris is fixed. The large-momentum condition is required to ensure that the struck parton does not interact with the target debris.

With this realisation of the A -independence of the fragmentation functions, it becomes clear that the procedure applied earlier in this section also holds here.

Defining

$$\Delta N^h \equiv \frac{d\sigma}{dx dy dz}(\mu D \rightarrow \mu h^+ X) - \frac{d\sigma}{dx dy dz}(\mu D \rightarrow \mu h^- X),$$

as before, and

$$\Delta A^h \equiv \frac{d\sigma}{dx dy dz}(\mu A \rightarrow \mu h^+ X) - \frac{d\sigma}{dx dy dz}(\mu A \rightarrow \mu h^- X),$$

we immediately see that both ΔA and ΔN depend on valence densities alone and also that their ratio (on using charge conjugation and isospin invariance) will be independent of the z -dependent fragmentation functions. For an isoscalar target of mass, A , and the deuteron, D , isospin invariance implies

$$u^p(x) = d^{\bar{p}}(x).$$

Further, using

$$s - \bar{s} = 0 \quad \text{and} \quad D_d = D_{\bar{d}}$$

as before, we obtain, for K -production,

$$\begin{aligned} \Delta N^K &= \frac{A}{9} \left\{ 4 (u_V^N + d_V^N) (D_u - D_{\bar{u}}) \right\}; \\ \Delta A^K &= \frac{A}{9} \left\{ 4 (u_V^A + d_V^A) (D_u - D_{\bar{u}}) \right\}, \end{aligned}$$

where the latter equation is for an isoscalar target of mass number, A . Then the EMC asymmetry for K -production is

$$A_K^{EMC} \equiv \frac{\Delta A^K}{\Delta N^K} = \frac{u_V^A + d_V^A}{u_V^N + d_V^N} = A_{\pi}^{EMC} = A_p^{EMC}.$$

The asymmetries for π and p production are the same as for K -production as we are considering an isoscalar target; hence, the only combination of densities that appears is the isoscalar one, namely, $(u + d)$. We have chosen this combination because this is what is experimentally measured. Hence, the u - and d -valence EMC effects cannot be separated. However, on comparison with the usual EMC effect, *i.e.*,

$$\rho^{EMC} = \frac{F_2^A}{F_2^D} = \frac{\sum_f e_f^2 q_f^A(x)}{\sum_f e_f^2 q_f^D(x)},$$

we see that ρ^{EMC} must match the valence asymmetry, A^{EMC} at large- x , where sea densities are negligible. This will be a test of the assumed A -independence of the fragmentation functions. Once this is established, comparison of the small- x data will yield information on $q_{sea}^A(x)$. That A^{EMC} measures only the valence quark combination is true for all x -values. Define

$$V \equiv u_V + d_V .$$

Then, from the form of the parametrisation of the parton densities suggested in Chapter 2, (assuming that it holds for nuclear targets as well), we have

$$\rho^{EMC} = \frac{V^A + \chi \sigma^A}{V^N + \chi \sigma^N}; \quad \chi = 22/5,$$

where the superscripts refer to nucleus and nucleon targets and σ is the sea quark density (called u_s in Chapter 2). The semi inclusive asymmetry is given by

$$A^{EMC} = \frac{V^A}{V^N} .$$

Hence, we have the relation between the EMC asymmetries in DIS and semi-inclusive DIS:

$$\rho^{EMC} \left\{ 1 + \frac{\chi \sigma^N}{V^N} \right\} = A^{EMC} + \frac{\chi \sigma^A}{V^A} .$$

The LHS of this equation is expressed in terms of known quantities; hence, a measurement of the asymmetry in semi-inclusive DIS, A^{EMC} , will yield information on σ^A . Since shadowing is a small- x phenomenon, it will also throw light on possible sources of this effect.

3.5 Appendix on $\nu \vec{p} \rightarrow \mu h X$

For completeness, we present a brief discussion of semi-inclusive hadroproduction (π production) in neutrino-proton polarised DIS,

$$\nu(\bar{\nu}) \vec{p} \rightarrow \mu^\pm h^\pm X .$$

This experiment is harder to perform. We redefine the polarisation asymmetries to be

$$A_h^{\nu p} = \frac{d\sigma(\uparrow\uparrow) + d\sigma(\downarrow\downarrow) - d\sigma(\uparrow\downarrow) - d\sigma(\downarrow\uparrow)}{d\sigma(\uparrow\uparrow) + d\sigma(\downarrow\downarrow) + d\sigma(\uparrow\downarrow) + d\sigma(\downarrow\uparrow)} ,$$

where the first arrow refers to the (longitudinal) polarisation of ν and the second to that of the proton. (ν^{\uparrow} represents an antineutrino.) Then, define the difference in production rates of π^+ and π^- to be

$$d\sigma = d\sigma^{\pi^+} - d\sigma^{\pi^-}.$$

Assuming the Cabibbo angle to be zero, the corresponding asymmetry is

$$A_{\pi}^{\nu p} = \frac{(1-y)^2 \bar{u}_V(x) - \bar{d}_V(x)}{(1-y)^2 u_V(x) - d_V(x)}.$$

Again, the fragmentation functions cancel, exactly as in $\bar{\mu} \bar{p}$ scattering. The factor, $(1-y)^2$ appears on account of the nontrivial angular dependence of the cross-section in νq^{\uparrow} (or $\bar{\nu} q^{\uparrow}$) scattering.

References

- [1] M. Gronau, F. Ravndal and Y. Zarmi, Nucl. Phys. **B51** (1973) 611
- [2] V. Ravishankar, Nucl. Phys. **B374** (1992) 309
- [3] The error due to using this approximation rather than $D_u - D_{\bar{u}} = 2(D_d - D_{\bar{d}})$ is less than three percent; see references [4] and [7] below.
- [4] M. Arneodo *et al.*, EMC, Nucl. Phys. **B321** (1989) 541
- [5] The first observation of this effect was made by J.J. Aubert *et al.*, The EMC, Phys. Lett. **B123** (1983) 275; for later data, see the review by R.P. Bickerstaff and A.W. Thomas, J. Phys. **G15** (1989) 1523
- [6] S. Gupta and M.V.N. Murthy, Mod. Phys. Lett **A4** (1989) 11
- [7] S. Gupta, D. Indumathi and M.V.N. Murthy, Z. Phys. **C47** (1990) 227
- [8] D. Indumathi and M.V.N. Murthy, Extended Abstract, DAE Symposium, Aligarh, 1989

pp COLLISION PROCESSES: INTRODUCTION

Spin dependent quark and gluon densities can be extracted from hard scattering experiments with polarised beam and targets, or by measuring final state polarisations [1]. Extracting spin dependent densities through experiments measuring final state angular distribution is difficult in fixed target experiments. This can be seen, for example, from recent measurements of the angular distribution of muon pairs in unpolarised Drell-Yan process [2]. Therefore we study spin dependences in experiments with polarised beams and targets. We have just discussed the rôle of polarised DIS processes in studying spin dependent parton densities. In the remainder of this Parton Model Phenomenology section, we discuss various asymmetries in polarised $\bar{\mu}\bar{\nu}$ scattering—in particular, large- p_T phenomena. One of the most important ingredients in resolving the proton spin puzzle is the extent of gluon polarisation within the proton. pp collisions provide an important tool to extract the gluon spin dependent density. Unlike in DIS, where the gluon contribution arises as a correction to the basic process, here the diagrams involving gluons contribute at leading order. These large p_T processes are most easily observed, as the final states, which are tagged in the experiment, are well separated (angularly) from the forward-moving components of the beam which did not undergo any collision. The processes that we consider, therefore, are those in which the collision causes the final state particle to have large transverse momentum with respect to the incident beam direction.

Here, we consider two protons colliding and so both the interaction vertices are nontrivial, unlike in $\bar{\mu}\bar{\nu}$ DIS where the electron-photon vertex is an elementary one. We apply the factorisation assumption in which the complicated hadron-hadron interaction is reduced to the interaction of one parton from each proton with the others remaining spectators in the process. In this assumption, the cross-section for the process “factors” into the product

of the cross-section for the underlying parton subprocess and the probability distributions of the initial partons, *i.e.*,

$$\frac{d\sigma}{dx_1 dx_2 dW} = \sum_i q_1(x_1) q_2(x_2) \frac{d\hat{\sigma}_{12}^i}{dW} . \quad (4.0.1)$$

The underlying processes are all of the type with two particles interacting in the initial state and the sum is over all possible contributing subprocesses giving rise to the required final states. Here, x_1 is the fraction of momentum of one of the protons that is carried by one interacting parton and x_2 is the momentum fraction of the parton belonging to the other proton. Note, however, that x_1 and x_2 are *not* observables, although we sometimes refer to them as Bjorken scaling variables. We shall discuss this aspect in greater detail later on. A $2 \rightarrow 2$ elementary subprocess is a function of the single Mandelstam variable, \hat{t} (see Appendix A), while a $2 \rightarrow 3$ subprocess (as occurs in the Drell Yan process) typically depends on more. These dependences are represented as W in eq. (4.0.1). Carets on variables indicate that they are subprocess variables. The subscript (12) on the subprocess cross-section indicates that the cross-section corresponds to that for the interaction of particles q_1 and q_2 , which may be quarks or gluons.

All processes that we study in pp collision process involve final states with large transverse momentum, p_T , to facilitate detection. The scattered particles in the final state can be γ , q or g . The processes involving production of (1 or 2) photons are called *direct photon* production processes as the photon is produced directly at the elementary parton-parton vertex during scattering. “Massive photon” production, in which the massive photon goes into a lepton pair, say $\mu^+ \mu^-$, is also called the Drell Yan process, while q , g in the final state produce a number of hadrons in a narrow cone centered about that parton direction, called a *jet*. What is important is the qualitative observation that the final state particles emerge with $p_T \neq 0$.

In the succeeding chapters, we shall write down asymmetries corresponding to all these processes. For these $\vec{p}\vec{p}$ collision processes, the asymmetry is

defined analogous to eq. (1.4) as

$$A \equiv \frac{d\sigma(\uparrow\downarrow) - d\sigma(\uparrow\uparrow)}{d\sigma(\uparrow\downarrow) + d\sigma(\uparrow\uparrow)}, \quad (4.0.2)$$

where the parallel ($\uparrow\uparrow$) and anti-parallel ($\uparrow\downarrow$) configurations refer to proton pp polarisations instead of to μp as in eq. (1.4) and the cross-sections are as differential as we choose.

Consider the contribution of a given subprocess. This is the differential parton subprocess cross-section, $d\hat{\sigma}$ multiplied by the probability distribution for each parton. There are four parton helicity combinations, viz., $(++)$, $(+-)$, $(-+)$ and $(--)$. Recall that a “+” helicity parton has its spin aligned with that of its parent hadron, while a “-” helicity has its spin opposed. Obviously, when the parent proton polarisation direction is flipped, a “+” parton becomes a “-” parton and *vice versa*, by definition. However, in the parton frame, the relative spin directions of the two partons remains the same, as the *parton* helicity was not flipped. (What we have is essentially a redefinition.) In other words, the subprocess cross-sections are the same for the two cases:

$$\begin{aligned} d\hat{\sigma}(++) &= d\hat{\sigma}(--); \\ d\hat{\sigma}(+-) &= d\hat{\sigma}(-+), \end{aligned} \quad (4.0.3)$$

where these subprocess cross-sections are differential with respect to the set of variables, W . This set will be explicitly defined for each process. This implies that, if $d\sigma(\uparrow\uparrow)$ is given by

$$\begin{aligned} d\sigma(\uparrow\uparrow) &= q_1^+ q_2^+ d\hat{\sigma}(++) + q_1^+ q_2^- d\hat{\sigma}(+-) \\ &\quad + q_1^- q_2^+ d\hat{\sigma}(-+) + q_1^- q_2^- d\hat{\sigma}(--), \end{aligned}$$

then $d\sigma(\uparrow\downarrow)$ is given by flipping the sign on the second parton density, *i.e.*,

$$\begin{aligned} d\sigma(\uparrow\downarrow) &= q_1^+ q_2^- d\hat{\sigma}(++) + q_1^+ q_2^+ d\hat{\sigma}(+-) \\ &\quad + q_1^- q_2^- d\hat{\sigma}(-+) + q_1^- q_2^+ d\hat{\sigma}(--). \end{aligned}$$

Here, we have dropped the subscript (12) on $d\hat{\sigma}$ as well as the argument x_1 of q_1 and x_2 of q_2 for convenience. Using eq. (4.0.3), the difference in cross-sections

is

$$\begin{aligned} d\sigma(\uparrow\downarrow) - d\sigma(\uparrow\uparrow) &= (q_1^+ - q_1^-) (q_2^+ - q_2^-) (d\hat{\sigma}^{+-} - d\hat{\sigma}^{++}) \\ &\equiv \tilde{q}_1(x_1) \tilde{q}_2(x_2) \tilde{d}\hat{\sigma} , \end{aligned}$$

while the sum of the two polarisation cross-sections (which is twice the unpolarised cross-section) is

$$\begin{aligned} d\sigma(\uparrow\downarrow) + d\sigma(\uparrow\uparrow) &= (q_1^+ + q_1^-) (q_2^+ + q_2^-) (d\hat{\sigma}^{+-} + d\hat{\sigma}^{++}) \\ &\equiv q_1(x_1) q_2(x_2) d\hat{\sigma} . \end{aligned}$$

Hence, the numerator of the asymmetry is related to the spin dependent parton density combination and the spin dependent subprocess cross-section:

$$\tilde{d}\hat{\sigma} \equiv d\sigma^{+-} - d\sigma^{++}$$

while the denominator is related to the spin independent density and the spin summed subprocess cross-section:

$$d\hat{\sigma} \equiv d\sigma^{+-} + d\sigma^{++} .$$

This result is generically true for $\vec{p}\vec{p}$ scattering where the concerned subprocesses all involve interaction of two particles in the initial state. Hence, the asymmetry in $\vec{p}\vec{p}$ scattering can be symbolically written as

$$A = \frac{\sum \tilde{q}_1(x_1) \tilde{q}_2(x_2) \tilde{d}\hat{\sigma}}{\sum q_1(x_1) q_2(x_2) d\hat{\sigma}} , \tag{4.0.4}$$

where the sum is over all possible contributing subprocesses.

Note that the definition of the densities that we have used in earlier chapters is crucial to the definition of cross-sections in eq. (4.0.4) . With the QCD corrected parton model definition of densities with both quarks and gluons contributing to the structure function g_1^p as defined in eq. (2.6), namely,

$$g_1(x, Q^2) = \frac{1}{2} \sum_f e_f^2 \int_x^1 \frac{dy}{y} \left(\tilde{q}(y, Q^2) \left[\delta(1 - \frac{x}{y}) + A(\frac{x}{y}) \right] + \bar{g}(y, Q^2) B(\frac{x}{y}) \right) ,$$

the $d\hat{\sigma}$ that occurs in eq. (4.0.4) is precisely the subprocess cross-section as defined; however, if we use the naïve definition of g_1^p involving only quarks,

namely

$$g_1(x, Q^2) = \frac{1}{2} \sum_f e_f^2 \bar{q}(x, Q^2),$$

where the entire α_s contribution from both quarks as well as gluons has been lumped into the definition of the quark density, $d\hat{\sigma}$ is not the relevant pp subprocess cross-section, but has some $\mathcal{O}(\alpha_s)$ terms subtracted out. This is because, for example in the Drell Yan process, the quark density to $\mathcal{O}(\alpha_s)$ in the subprocess cross-sections has the same Q^2 dependence (splitting functions) as in DIS [6], but the constant terms (like A and B above) are different. However, we want the definition of the parton densities to be independent of the process being studied and to be a property of the nucleon. Implementing the DIS definition of the quark density to $\mathcal{O}(\alpha_s)$ in Drell Yan then means correcting for this difference in the Q^2 independent pieces between Drell Yan and DIS.

Crudely, without displaying the actual expressions involved, if the definition of the spin dependent quark density to $\mathcal{O}(\alpha_s)$ is

$$q = N(1 + \alpha_s P)$$

and the quantity that appears in DY is $N(1 + \alpha_s R)$, then we can identify this as

$$\begin{aligned} N(1 + \alpha_s R) &= N(1 + \alpha_s P)(1 + \alpha_s(R - P) + \dots) \\ &= q(1 + \alpha_s(R - P)) + \mathcal{O}(\alpha_s^2). \end{aligned}$$

Since we are interested in the $\mathcal{O}(\alpha_s)$ process (the leading order DY process has zero p_T), the "cross-section," $d\hat{\sigma}$, occurring in this case would be the quantity $(R - P)$ or, in other words, the usual DY cross-section with a corresponding term occurring in the DIS cross-section (at that order) subtracted out. Here, however we use definitions of parton densities such that the sub-process cross-sections in pp collisions are to be used as they are, without corrections being required due to the choice of definition of the densities that multiply them in the expression for the hadronic cross-section. We have just used the above discussion to indicate that care must be taken in defining and using densities

at the next-to-leading order. We shall not discuss this in any more detail. A very clear discussion as well as the next-to-leading order expressions in the case of unpolarised DY production has been provided by Altarelli, Martinelli and Stirling in ref. [6]. The polarised case has recently been studied by Prakash and Ravindran [7] both within the parton model as well as within the operator product and factorisation approach.

However, we stress that provided we use a proper definition of parton densities and correspondingly define $d\hat{\sigma}$ that appears in the expression for the hadronic cross-section and asymmetry, the form of the asymmetry equation (eq. (4.0.4)) remains the same. Choice of model/scheme is just a convenience and does not alter the physics.

We shall study this asymmetry in eq. (4.0.4) for various spin dependent processes. We shall show that the one-photon and Drell-Yan as well as the two-jet production processes are all sensitive to the spin dependent gluon density, the first two at larger values of Bjorken x (either x_1 or x_2), and the latter in the small- x region. On the other hand, the two-photon process is sensitive to gluon as well as sea densities. Knowing the spin dependent gluon density from the former will enable the sea density to be extracted from the two-photon experiment. An experimental complication is that the luminosities are likely to be smaller than those obtained with unpolarised beams. As a result, errors in measurement are likely to be higher. This can be seen in the case of polarised DIS itself, where the errors are around 25%. Results on asymmetries must be examined with this in mind.

We now discuss these processes in detail. We begin with direct photon and Drell-Yan production at large transverse momentum in polarised $\vec{p}\vec{p}$ as well as $\vec{p}\vec{\bar{p}}$ collisions. Common conclusions as well as references are provided at the end of the pp collisions section, *i.e.*, after Chapter 6.

THE GLUON DENSITIES: INTERMEDIATE-X REGION

CONTENTS

Direct Photon and Drell Yan processes

Formalism

Numerics

The $\vec{p}\vec{p}$ collision process

4.0 Direct Photon and Drell Yan processes

The processes we consider here both produce final states at large transverse momentum:

$$\vec{p} + \vec{p} \rightarrow \gamma + \text{jet} + X \quad (\text{Direct Photon}),$$

and

$$\vec{p} + \vec{p} \rightarrow (\mu^+ \mu^-) + \text{jet} + X \quad (\text{Drell Yan}),$$

The latter, which is called the Drell-Yan (DY) process, proceeds just as the former Direct Photon ($D\gamma$) production process, but with the production of a massive photon that goes into a di-muon pair. In both cases, the large transverse momentum of the photon (or the di-muon pair) is balanced by a corresponding jet. As usual, X corresponds to the (unobserved) debris. We shall show [3], [4] that both these processes are sensitive to the spin dependent gluon density and can thus be used to study this crucial density. This is essential in order to resolve the different parton contributions to the proton spin. We first set up expressions for the asymmetries and later use the parametrisations for the spin dependent densities set up in Chapter 2 to substantiate our claims with numerical simulations of these asymmetries.

4.1 Formalism

We begin with direct photon production ($D\gamma$) at large p_T . We are interested in computing the asymmetry [5] corresponding to eq. (4.0.3) for this process. In the leading order, there are two subprocesses; they are

$$qg \rightarrow \gamma q; \quad \text{and}$$

$$q\bar{q} \rightarrow \gamma g.$$

The former is the *Compton* and the latter is the *Annihilation* diagram.

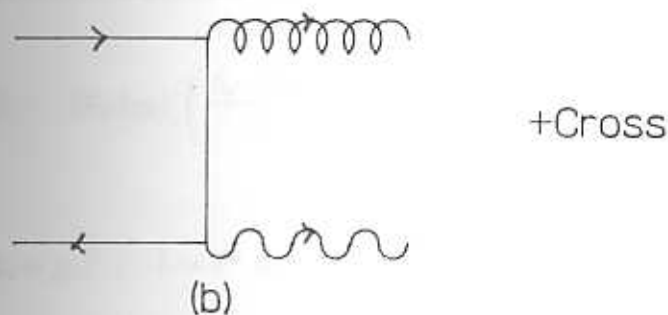
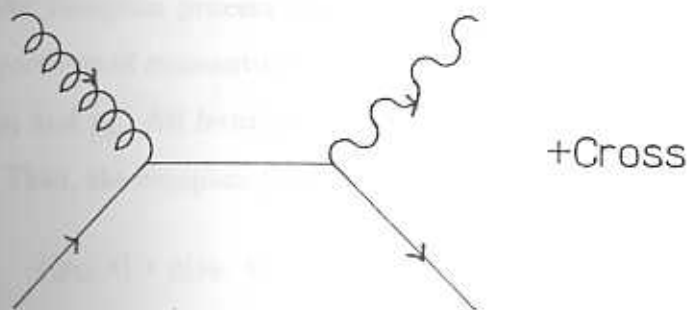


Fig. 4.1 The leading contributions to the Direct Photon process: (a) Compton, (b) Annihilation.

Both are of the $2 \rightarrow 2$ type and hence the subprocess cross-sections are differential with respect to the single Mandelstam variable, \hat{t} (see Appendix A for details of kinematics).

From the discussion in the introduction to this pp collisions section, we know that we are interested in the computation of the subprocess cross-sections, $\frac{d\hat{\sigma}}{d\hat{t}}(h h')$, ($h, h' = +, -$), where h and h' are the helicities of the initial state partons. The helicities of the final state partons are not observed and are therefore summed over. We outline the details of the computation in the case of the Compton process shown in Fig. (4.1). Our convention is that the initial particles of momentum p_1 and p_2 scatter into the final particles of momentum p_3 and p_4 . All fermion helicities are denoted by λ and boson helicities by h . Then, the compton process can be represented as

$$q(p_1, \lambda) + g(p_2, h) \rightarrow \gamma(p_3, h') + q(p_4, \lambda')$$

with λ' and h' ultimately summed over. We use the identities and relations given in Appendix B and obtain

$$\frac{d\hat{\sigma}}{d\hat{t}}(\text{compton}) = \frac{\pi \alpha \alpha_s}{\hat{s}^2} \sum_f e_f^2 |M|^2,$$

where the matrix element is a sum of the contributions of the direct and crossed channels,

$$M = -i \bar{u}_{\lambda'}(p_4) \left(\frac{\not{p}_4 \not{p}_2 \not{p}_1}{\hat{s}} + \frac{\not{p}_1 \not{p}_2 \not{p}_4}{\hat{t}} \right) u_{\lambda}(p_1),$$

where

$$\hat{s} = S^2 \equiv (p_1 + p_2)^2; \quad \hat{t} = T^2 \equiv (p_1 - p_3)^2; \quad \hat{u} = U^2 \equiv (p_1 - p_4)^2$$

are the usual Mandelstam variables, satisfying the relation,

$$\hat{s} + \hat{t} + \hat{u} = 0,$$

as we have neglected the parton masses. Then, the matrix element squared can be expressed as

$$|M|^2 \equiv T_h^{\mu\nu} T_{h'}^{\rho\sigma} H_{\mu\nu\rho\sigma},$$

$$\text{with } H_{\mu\nu\rho\sigma} = \frac{1}{4} (1 + \lambda\lambda') S_{\mu\nu\rho\sigma} + \frac{1}{4} (\lambda + \lambda') A_{\mu\nu\rho\sigma} .$$

The symmetric piece of $H_{\mu\nu\rho\sigma}$ is given by

$$S_{\mu\nu\rho\sigma} = \text{Tr} (\not{p}_4 [\]_{\rho\mu} \not{p}_1 [\]_{\nu\sigma})$$

and the antisymmetric part by

$$A_{\mu\nu\rho\sigma} = \text{Tr} (\gamma_5 \not{p}_4 [\]_{\rho\mu} \not{p}_1 [\]_{\nu\sigma}) ,$$

where

$$[\]_{ab} = \frac{\gamma_a \not{s} \gamma_b}{\hat{s}} + \frac{\gamma_b \not{t} \gamma_a}{\hat{t}}$$

and the T 's contain the ϵ -dependence:

$$\begin{aligned} T_{\mu\nu}^h &= \epsilon_h^\mu \epsilon_h^{*\nu} ; \\ T_{\rho\sigma}^{h'} &= \epsilon_{h'}^\rho \epsilon_{h'}^{*\sigma} . \end{aligned}$$

Using the formulae of Appendix B for evaluating T 's, we get, on summing over the final state polarisations,

$$\sum_{\lambda', h'} |M|^2 = -2(1 + \lambda h) \left(\frac{\hat{s}}{\hat{t}} + \frac{\hat{t}}{\hat{s}} \right) + 4 \lambda h \frac{\hat{t}}{\hat{s}} .$$

As expected, the cross-section depends only on the product of the initial state helicities. Introducing the colour factor ($C_F = 1/6$), we get, for the compton subprocess,

$$\frac{d\hat{\sigma}^C}{d\hat{t}}(\lambda h) = \frac{\pi \alpha \alpha_s}{\hat{s}^2} \frac{1}{3} \left\{ -(1 + \lambda h) \left(\frac{\hat{s}}{\hat{t}} + \frac{\hat{t}}{\hat{s}} \right) + 2 \lambda h \frac{\hat{t}}{\hat{s}} \right\} . \quad (4.1)$$

Note that we have dropped the summation over initial quark flavours weighted by the quark charges. We will include this with the density dependent part. A similar calculation for the annihilation diagram of Fig. (4.1) gives (with a colour factor of $C_F = 4/9$),

$$\frac{d\hat{\sigma}^A}{d\hat{t}}(\lambda \lambda') = \frac{\pi \alpha \alpha_s}{\hat{s}^2} \frac{8}{9} \left\{ (1 - \lambda \lambda') \left(\frac{\hat{t}}{\hat{u}} + \frac{\hat{u}}{\hat{t}} \right) \right\} . \quad (4.2)$$

This is most easily obtained by retaining the λ' dependence in the previous calculation (compton case) and using crossing symmetry ($s \leftrightarrow t$, $u \leftrightarrow u$, $\lambda \leftrightarrow \lambda$, $\lambda' \leftrightarrow -\lambda'$, $h \leftrightarrow -h$, $h' \leftrightarrow h'$).

To compute the asymmetry, we need to evaluate the combinations $\widetilde{d\hat{\sigma}}$ and $d\hat{\sigma}$, which are the difference and sum of the helicity cross-sections,

$$\frac{d\hat{\sigma}}{dt}(+-) \quad \text{and} \quad \frac{d\hat{\sigma}}{dt}(++)$$

respectively. (Here, $(+-)$ and $(++)$ refer to λh in the qg process and $\lambda \lambda'$ in the $q\bar{q}$ process.) These are listed in Table 4.1.

Finally, we observe that the interacting partons could have come from either proton (target or projectile) and so we have to sum over both configurations. This procedure ($x_1 \leftrightarrow x_2$) effectively interchanges \hat{t} and \hat{u} . Then, the summed cross-section, i.e., the denominator of the asymmetry can be written as

$$\begin{aligned} d\sigma^{D\gamma} &\equiv \frac{d\sigma}{dx_1 dx_2 dt}(\uparrow\downarrow) + \frac{d\sigma}{dx_1 dx_2 dt}(\uparrow\uparrow) \\ &= H_0(x_1, x_2) d\hat{\sigma}^A + G_1(x_1, x_2) d\hat{\sigma}^C + G_2(x_1, x_2) d\hat{\sigma}^{C'}, \end{aligned} \quad (4.4)$$

where

$$d\hat{\sigma}^\alpha \equiv \left(\frac{d\hat{\sigma}^\alpha}{dt}(+-) + \frac{d\hat{\sigma}^\alpha}{dt}(++) \right); \quad \alpha = A, C, C' \quad (4.5)$$

are the parton cross-sections listed in Table 4.1 and the structure function factors, H_0 and $G_{1,2}$, are given by

$$\begin{aligned} H_0(x_1, x_2) &= \sum_f e_f^2 \left(q_f^T(x_1) \bar{q}_f^P(x_2) + \bar{q}_f^T(x_1) q_f^P(x_2) \right), \\ G_1(x_1, x_2) &= g^T(x_1) \sum_f e_f^2 \left(q_f^P(x_2) + \bar{q}_f^P(x_2) \right) \equiv 2g^T(x_1) F_1^P(x_2), \\ G_2(x_1, x_2) &= G_1(x_2, x_1) \equiv 2F_1^T(x_1) g^P(x_2). \end{aligned} \quad (4.6)$$

Here, x_1 is defined as the momentum fraction of the parton coming from the target T and x_2 that from the projectile P . The labels, T and P , are irrelevant for the $\vec{p}\vec{p}$ (identical particles) collision process under consideration here, but will be useful for the case of $\vec{p}\vec{\bar{p}}$ which we shall discuss later. The labels, *target* and *projectile*, are just a convenient means of distinguishing the two protons and do not imply that this discussion is restricted to the case of fixed-target experiments only; it is also valid for collider beams.

Further, by including the partonic charge factors in the structure function definitions, we have obtained a nice form for the compton contribution. Everywhere, f indicates a sum over quark flavours, u, d, s , only and *not over the antiquarks*, which are included explicitly. By definition, $d\hat{\sigma}$ is twice the unpolarised cross-section.

Similarly, the numerator of the asymmetry is expressed in terms of spin dependent quantities as

$$\begin{aligned}\widetilde{d\sigma}^{D\gamma} &\equiv \frac{d\sigma}{dx_1 dx_2 dt}(\uparrow\downarrow) - \frac{d\sigma}{dx_1 dx_2 dt}(\uparrow\uparrow) \\ &= \widetilde{H}_0(x_1, x_2) d\hat{\sigma}^A \phi^A + \widetilde{G}_1(x_1, x_2) d\hat{\sigma}^C \phi^C + \widetilde{G}_2(x_1, x_2) d\hat{\sigma}^{C'} \phi^{C'},\end{aligned}\quad (4.7)$$

Subprocess	Direct Photon	Drell-Yan
(α)	$d\hat{\sigma}^\alpha$	
A	$\frac{16}{9} \left(\frac{u^2 + t^2}{tu} \right)$	$\frac{16}{27} \left(\frac{u^2 + t^2 + 2M^2 s}{tu} \right)$
C	$-\frac{2}{3} \left(\frac{s^2 + t^2}{ts} \right)$	$-\frac{2}{9} \left(\frac{s^2 + t^2 + 2M^2 u}{ts} \right)$
C'	$-\frac{2}{3} \left(\frac{s^2 + u^2}{us} \right)$	$-\frac{2}{9} \left(\frac{s^2 + u^2 + 2M^2 t}{us} \right)$
(α)	ϕ^α	
A	1	1
C	$-\left(\frac{s^2 - t^2}{s^2 + t^2} \right)$	$-\left(\frac{s^2 - t^2 - 2M^2(s - t)}{s^2 + t^2 + 2M^2 u} \right)$
C'	$-\left(\frac{s^2 - u^2}{s^2 + u^2} \right)$	$-\left(\frac{s^2 - u^2 - 2M^2(s - u)}{s^2 + u^2 + 2M^2 t} \right)$

Table 4.1 Subprocess cross-sections for compton and annihilation diagrams in $D\gamma$ and DY processes. The $D\gamma$ cross-section is expressed in terms of $d\hat{\sigma}^\alpha \equiv \left(\frac{\pi\alpha_s\alpha_e}{s^2} \right)^{-1} \left(\frac{d\hat{\sigma}^\alpha}{dt}(+ -) + \frac{d\hat{\sigma}^\alpha}{dt}(+ +) \right)$ where $\alpha = A, C, C'$, and in the case of DY, $d\hat{\sigma}^\alpha \equiv \left(\frac{\alpha_s^2\alpha_e}{s^2 M^2} \right)^{-1} \left(\frac{d\hat{\sigma}^\alpha}{dt dM^2}(+ -) + \frac{d\hat{\sigma}^\alpha}{dt dM^2}(+ +) \right) \cdot \phi^\alpha$ is defined in eq. (4.8). Carets on the Mandelstam variables have been deleted for the sake of clarity.

where the spin dependent partonic cross-section is given by

$$d\hat{\sigma}^\alpha \phi^\alpha \equiv \widetilde{d\hat{\sigma}}^\alpha = \left(\frac{d\hat{\sigma}^\alpha}{d\hat{t}} (+-) - \frac{d\hat{\sigma}^\alpha}{d\hat{t}} (++) \right) ; \quad \alpha = A, C, C' \quad (4.8)$$

with ϕ^α listed in Table 4.1. The structure function factors are analogous to the spin summed case, but expressed now in terms of spin dependent quantities:

$$\begin{aligned} \widetilde{H}_0(x_1, x_2) &= \sum_f e_f^2 \left(\widetilde{q}_f^T(x_1) \widetilde{q}_f^P(x_2) + \widetilde{q}_f^T(x_1) \widetilde{q}_f^P(x_2) \right) , \\ \widetilde{G}_1(x_1, x_2) &= \widetilde{g}^T(x_1) \sum_f e_f^2 \left(\widetilde{q}_f^P(x_2) + \widetilde{q}_f^P(x_2) \right) \equiv 2 \widetilde{g}^T(x_1) g_1^P(x_2) , \\ \widetilde{G}_2(x_1, x_2) &= \widetilde{G}_1(x_2, x_1) \equiv 2 g_1^T(x_1) \widetilde{g}^P(x_2) . \end{aligned} \quad (4.9)$$

Differences in sign between the expressions in eq. (4.9) and corresponding expressions in refs. [3], [4] are merely because the asymmetry is defined with opposite sign in the two cases.

In both the spin-symmetric as well as the spin-antisymmetric cases, $d\hat{\sigma}^A = d\hat{\sigma}^{A'}$, *i.e.*, the annihilation diagram is symmetric in \hat{t} and \hat{u} as can be seen from Fig. (4.1). So we have clubbed the two contributions together. As in the unpolarised case, the structure function factor for the compton contribution simplifies greatly and is, in fact, directly proportional to the spin dependent structure function, $g_1^P(x)$, of the proton.

We now discuss the Drell-Yan (DY) process. The underlying subprocesses here are the same as those for the $D\gamma$ process, with the final state photon being massive, its mass, M^2 , being the invariant mass squared of the dilepton pair, *i.e.*,

$$M^2 = (p_{\ell^+} + p_{\ell^-})^2 \simeq 2 p_{\ell^+} \cdot p_{\ell^-} .$$

Hence the structure function factors for the DY process are identical to those for the $D\gamma$ process. However, the subprocess cross-sections differ. This is because, kinematically, there are now three particles in the final state (see Fig. (4.2)). Such a process can be described in terms of two invariants and two angles (see Appendix D). To visualise this simply, each of the DY subprocesses

can be expressed as a combination of two processes, *viz.*,

$$(1) : k_1 k_2 \rightarrow \gamma^* k_3 ;$$

$$(2) : \gamma^* \rightarrow \ell^+ \ell^- .$$

The former is a $2 \rightarrow 2$ process, while the latter is a $1 \rightarrow 2$ decay process. The lowest order DY process also shown in Fig. (4.2), is the $2 \rightarrow 2$ annihilation diagram with only leptons in the final state. However, such a process has no large net p_T and we ignore such contributions.

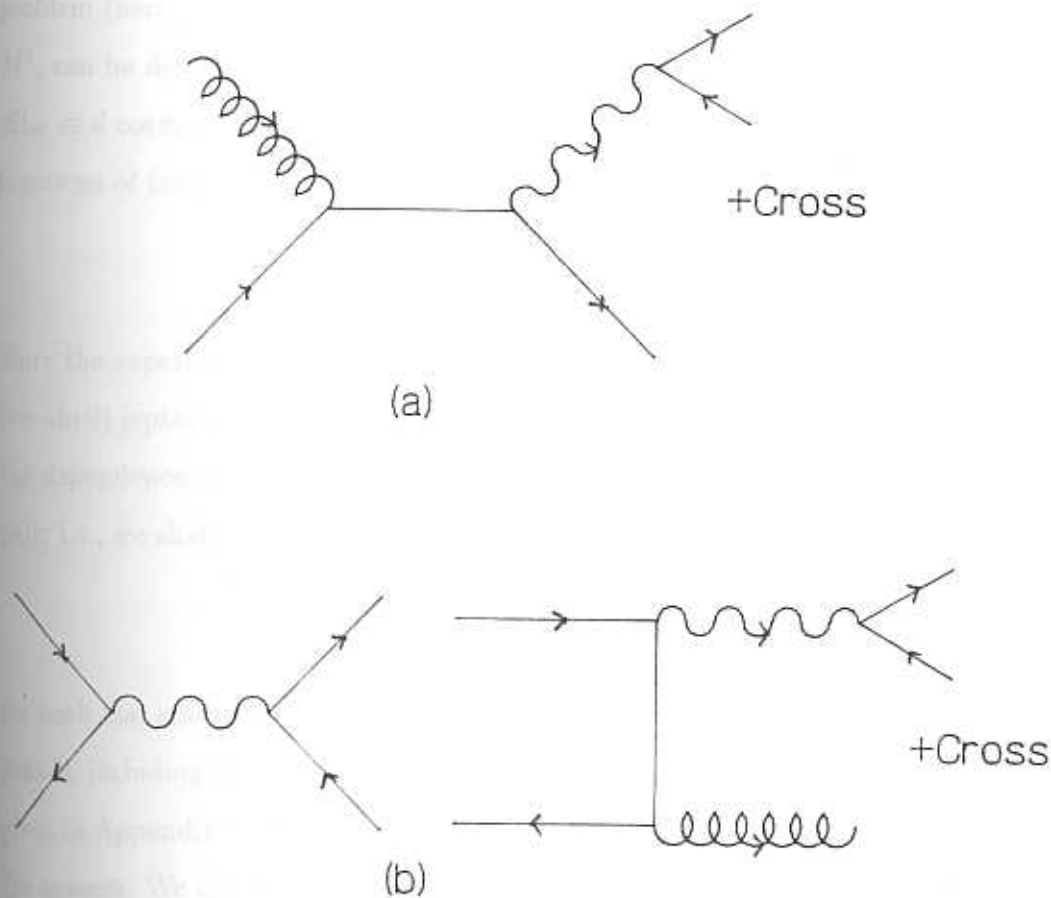


Fig. 4.2 The leading order contributions to the Drell Yan process: (a) Compton, (b) Annihilation. Also shown is the lowest order (zero p_T) annihilation graph.

Kinematically, the intermediate state in the three body process can be explicitly introduced by means of the identity,

$$\begin{aligned} 1 &= \int dM^2 \int \frac{d^3 p_\gamma}{(2\pi)^3 2E_\gamma} \delta^4(p_\gamma - p_{\ell^+} - p_{\ell^-}) \\ &\equiv \int dM^2 \int d^4 p_\gamma \delta^4(p_\gamma - p_{\ell^+} - p_{\ell^-}) \delta(p_\gamma^2 - M^2). \end{aligned} \quad (4.10)$$

(For details, see Appendix D). Then, the $2 \rightarrow 2$ process has, as we know, exactly one independent variable, $\hat{t} (= (k_1 - p_\gamma)^2 \equiv (k_3 - k_2)^2)$ and depends on the initial energy, $\hat{s} (= (k_1 + k_2)^2)$, of the process and the masses in the problem (here, only M^2). The decay of the massive photon of variable mass, M^2 , can be described in terms of the solid angle of either of the leptons, say, $d\Omega_{\ell^+} \equiv d \cos \theta_{\ell^+} d\phi_{\ell^+}$. Hence, the cross-sections for the DY subprocesses are functions of four variables, namely, \hat{t} , M^2 , $\cos \theta_{\ell^+}$ and ϕ_{ℓ^+} , *i.e.*, we have

$$d\hat{\sigma}^{DY} \equiv \frac{d\hat{\sigma}}{d\hat{t} dM^2 d\Omega_{\ell^+}}.$$

Since the experimental signature for this process is the presence of a large p_T (on-shell) lepton pair (say, $\mu^+ \mu^-$) with a balancing jet, we shall integrate out the dependence of the cross-section on the angular coördinates of the lepton pair; *i.e.*, we shall obtain expressions for

$$\frac{d\hat{\sigma}}{d\hat{t} dM^2} \equiv \int d\Omega_{\ell^+} d\hat{\sigma}^{DY}$$

for both the annihilation as well as the compton subprocesses. Kinematical details, including reference frames in which the calculation is carried out, are given in Appendix D. Note that the colour factors are identical to those in the $D\gamma$ process. We obtain, for the compton process of Fig. (4.2),

$$\frac{d\hat{\sigma}^C}{d\hat{t} dM^2}(\lambda, h) = \frac{\alpha^2 \alpha_s}{\hat{s}^2 M^2} \frac{1}{9} \left\{ - (1 + \lambda h) \left(\frac{\hat{s}}{\hat{t}} + \frac{\hat{t}}{\hat{s}} + \frac{2 M^2 \hat{u}}{\hat{t} \hat{s}} \right) + 2\lambda h \frac{(M^2 - \hat{t})^2}{\hat{t} \hat{s}} \right\} \quad (4.11)$$

while for the annihilation diagram of Fig. (4.2), we have

$$\frac{d\hat{\sigma}^A}{d\hat{t} dM^2}(\lambda \lambda') = \frac{\alpha^2 \alpha_s}{\hat{s}^2 M^2} \frac{8}{27} \left\{ (1 - \lambda \lambda') \left(\frac{\hat{t}}{\hat{u}} + \frac{\hat{u}}{\hat{t}} + \frac{2 M^2 \hat{s}}{\hat{t} \hat{u}} \right) \right\}. \quad (4.12)$$

Again, the partonic charge factor, namely, e_f^2 , and the sum over quark flavours have been absorbed into the structure function factor definitions.

From eqs. (4.11) and (4.12), we obtain the quantities of interest

$$d\hat{\sigma}^\alpha(+ -), \quad d\hat{\sigma}^\alpha(+ +); \quad \alpha = A, C, C'$$

and their sum and difference. These are listed in Table 4.1 along with the information on $D\gamma$.

We are now in a position to compute the asymmetry,

$$A^P \equiv \frac{\tilde{d}\sigma^P}{d\sigma^P}, \quad (4.13)$$

where the process, P , can be $D\gamma$ or DY . We can evaluate eq. (4.13) using the parametrisations developed earlier for the spin dependent parton densities and the subprocess cross-sections listed in Table 4.1. If we do so, we shall certainly find that, typically, both the $D\gamma$ and the DY processes sensitively depend on the spin dependent gluon density.

However, instead of parametrising both the (unknown) spin dependent gluon density as well as the spin dependent sea quark density, we can choose appropriate phase space regions where the sea contribution is negligible. From the discussion following eq. (2.1) in Chapter 2, we know that $\tilde{\sigma}(x)$ and \tilde{q} (or equivalently g_1) fall off with x at the same rate as σ and q (or F_1) — hence, if we can neglect σ/F_1 in some parts of phase space, then we can also neglect $\tilde{\sigma}/g_1$ in that same region.

In other words, we shall assume that the compton contribution dominates the cross-section (in both the numerator as well as the denominator of the asymmetry) and so, as a first approximation, we shall ignore the contribution coming from the annihilation diagrams. We later estimate errors due to this as well as the region of phase space for which this approximation is valid. Then the asymmetry simplifies to its zeroth order form:

$$A_0^P(x_1, x_2) = \frac{2g_1(x_1)\tilde{g}(x_2)\phi^C d\hat{\sigma}^C + 2g_1(x_2)\tilde{g}(x_1)\phi^{C'} d\hat{\sigma}^{C'}}{2F_1(x_1)g(x_2)d\hat{\sigma}^C + 2F_1(x_2)g(x_1)d\hat{\sigma}^{C'}}. \quad (4.14)$$

Hence, the observation that the compton subprocess structure function factor has a simple expression in terms of the proton structure functions, g_1 and F_1 , (along with dropping the annihilation contribution) results in an expression for the asymmetry that involves only one unknown quantity, namely, the spin dependent gluon density, $\tilde{g}(x)$. Hence, a measurement of the asymmetry in $D\gamma$ and DY processes provides a direct measurement of $\tilde{g}(x)$.

A further simplification occurs when we choose $x_1 = x_2 \equiv x$, which corresponds to the configuration with the photon and jet being back-to-back in the hadronic CM frame (as well as, ofcourse, in the parton CM frame, where they always should); the parton densities factorise out and the asymmetry becomes

$$\begin{aligned} A_0^P(x) &= \frac{g_1(x) \tilde{g}(x)}{F_1(x) g(x)} \left[\frac{\phi^C d\hat{\sigma}^C + \phi^{C'} d\hat{\sigma}^{C'}}{d\hat{\sigma}^C + d\hat{\sigma}^{C'}} \right] \\ &\equiv A^{\mu p}(x) A^g(x) \phi . \end{aligned} \quad (4.15)$$

We see from eq. (4.15) that the leading order asymmetry in these processes factors into a product of the gluon asymmetry, $A^g \equiv \tilde{g}(x)/g(x)$, the DIS asymmetry, $A^{\mu p}$, (which has been directly measured by the EMC) and a parton-level asymmetry ϕ , (which is calculable in QCD). Hence, in the region of phase space where our approximation is valid, A_0 is a measure of the spin dependent gluon density, as stated before. This result is *independent of the interpretation of the EMC result*. By this we mean that, given a definition of the spin dependent proton structure function, g_1 , within (say) the parton model, as we have done in Chapter 2, that same quantity appears in the expression for the leading order asymmetry in the processes under consideration.

In DY, the choice $x_1 = x_2 = x$ is possible for a fixed M^2 only at a given value of x and not throughout phase space. If we vary x , M^2 also changes, to accomodate $x_1 = x_2 = x$. In the special configuration of 90° scattering (in the CM of hadrons), when $d\hat{\sigma}^C = d\hat{\sigma}^{C'}$, the expression for the asymmetry in eq. (4.15) is true for *all* x for both DY and $D\gamma$ production. Further, the asymmetry in direct photon production, $A^{D\gamma}$, is *independent* of the beam direction (i.e., of \hat{s}), while it depends only on the ratio, $\tau (= M^2/s)$, in Drell-Yan.

We shall therefore, for the sake of clarity/simplicity, choose this configuration for all numerical illustrations here-after and comment on other configurations when necessary.

We now work out the corrections to A_0 in eq. (4.14) from annihilation terms. We reëxpress H_0 and \widetilde{H}_0 in terms of F_1 (or g_1) and σ (or $\tilde{\sigma}$) as

$$\begin{aligned} H_0 &= 2F_1(x_1)\sigma(x_2) + 2\sigma(x_1)F_1(x_2) - \frac{23}{18}\sigma(x_1)\sigma(x_2); \\ \widetilde{H}_0 &= 2g_1(x_1)\tilde{\sigma}(x_2) + 2\tilde{\sigma}(x_1)g_1(x_2) - \frac{23}{18}\tilde{\sigma}(x_1)\tilde{\sigma}(x_2), \end{aligned} \quad (4.16)$$

where the sea density is $\sigma = u_s = d_s = s_s/\eta$ and we have used $\eta = 1/2$ [8], [9]. We see that the introduction of H_0 in the expression for the asymmetry brings in the added complication of one more unknown quantity, $\tilde{\sigma}$.

In the configuration with $x_1 = x_2 = x$ and 90° scattering, the corrections due to inclusion of the annihilation terms can be written in powers of an expansion parameter,

$$\beta = \frac{d\hat{\sigma}^A}{d\hat{\sigma}^C} \frac{\sigma(x)}{g(x)}, \quad (4.17)$$

and our expressions are valid in those phase space regions where $\beta \ll 1$ (i.e., the annihilation terms are small compared to the compton terms). Since β is expressed in terms of known spin independent densities, it can be evaluated. On including the annihilation terms, then, the denominator of the total asymmetry (eq. (4.4)) is

$$d\sigma \equiv 4 F_1 g d\hat{\sigma}^C \left[1 + \beta \left(1 - \frac{23\sigma}{72F_1} \right) \right].$$

Since σ/F_1 is small (and is further multiplied by the factor β which is also small), it can be dropped. Then the total asymmetry is

$$A^P = \frac{A_0}{1 + \beta} \left[1 + \frac{\tilde{\sigma}}{g} \frac{d\hat{\sigma}^A}{d\hat{\sigma}^C} \frac{\phi^A}{\phi^C} \right],$$

where we have dropped terms containing $\tilde{\sigma}/\widetilde{g}_1$ just as we dropped the corresponding spin independent term. Retaining terms upto $\mathcal{O}(\beta)$, we have

$$A_{\beta}^{D\gamma, DY} = A_0 - \beta A^{\mu\nu} \left\{ A^g \phi^C - A^\sigma \phi^A \right\}. \quad (4.18)$$

Here, $A^\sigma \equiv \tilde{\sigma}/\sigma$, analogous to A^g .

Notice that, even with the inclusion of the annihilation terms, it is still possible to express the cross-section (or asymmetry) in terms of the DIS asymmetry, A^{np} and the gluonic and sea quark asymmetries, A^g and A^σ . We see from eq. (4.18) why β is a good expansion parameter: since every asymmetry is bounded by one, the coefficients of the power series in β are bounded and the approximation is valid where β is small.

Hence, the particular configuration of $x_1 = x_2 = x$ allows a neat factorisation of both the DY and D γ asymmetries, which are then expressible in terms of A^{np} , A^g and A^σ alone; *i.e.*, they do not explicitly depend on the *individual* parton densities, u_V , d_V , u_s and g . In this sense, the asymmetry, as we have formulated it (subject to phase space constraints) clearly exhibits its dependence on the gluon and sea quark densities, without needing to resort to the entire technical power of the parametrisation we developed in Chapter 2.

Before we begin the numerical analysis of these two processes, we need to define the kinematical observables. So far, we have been using the (independent) variables x_1 , x_2 and \hat{t} for D γ and x_1 , x_2 , \hat{t} and M^2 or τ for DY. Although this is a perfectly valid choice, these are not the quantities that are observed experimentally. In fact, in a configuration where (say) the two particles are colliding head-on (CM of the protons), the observed quantities are the (different) scattering angles of the photon (or lepton pair) and balancing jet, as well as their (common) transverse momenta. Remember that the photon and jet come out back-to-back only in the CM of the partons. Their p_T in both frames, however, always balance each other. We therefore transform to the set of observables (y_1, y_2, x_T) , which are an equally valid set. Here, y_1 and y_2 are the rapidities of the photon and jet and $x_T = 2p_T/\sqrt{s}$, where p_T is the transverse momentum and $0 \leq x_T \leq 1$. (For details regarding the definition of these variables, see Appendix D). Such a transformation involves a Jacobean from one set of variables to another and uniformly affects both the sum, $d\sigma$, as well as the difference, $\tilde{d}\sigma$, of cross-sections. Hence, the expression, eq. (4.13),

for the asymmetry remains unchanged. So, we use the equations for the asymmetry just as they are; it is enough to know (x_1, x_2, \hat{t}) in terms of (y_1, y_2, x_T) . Details of this are given in Appendix D. We have

$$\frac{d\sigma}{dx_T dy_1 dy_2} = \frac{\hat{s}}{2} x_T \frac{d\sigma}{dx_1 dx_2 d\hat{t}}.$$

Hence, the asymmetry is given by

$$A(y_1, y_2, x_T) = \frac{\widetilde{d\sigma}/(dx_T dy_1 dy_2)}{d\sigma/(dx_T dy_1 dy_2)} = \frac{\widetilde{d\sigma}/(dx_1 dx_2 d\hat{t})}{d\sigma/(dx_1 dx_2 d\hat{t})}.$$

The cross-sections are further differential with respect to M^2 for DY. The configuration we have chosen corresponds to

$$\begin{aligned} x_1 = x_2 &= x \equiv \frac{1}{2} (x_T \cosh y_2 + \bar{x}_T \cosh y_1) ; \\ \cos \hat{\phi} &= -\tanh y_2 = \frac{x^2 + \tau}{x^2 - \tau} \tanh y_1 . \end{aligned}$$

Here,

$$\bar{x}_T^2 = x_T^2 + 4\tau ; \quad \tau = M^2/s .$$

For the direct photon, $\tau = 0$. Hence, $x_1 = x_2 \Rightarrow y_1 = -y_2 = y$, *i.e.*, the photon and jet are back-to-back in the CM of hadrons as well. In principle, therefore, we can choose to work with an appropriate y where the production rates are high and accessible to the experiment.

In the case of the DY process, we have $M_{max}^2 = \hat{s}$, *i.e.*, $\tau_{max} = x_1 x_2 = x^2$, from energy momentum conservation in the subprocess. So, in the $(x-\tau)$ phase space, the region $\tau > x^2$ is unphysical. In the special case where $y_1 = y_2 = 0$ we have $x = (x_T + \bar{x}_T)/2$.

4.2 Numerics

We use the Type I parametrisation developed in Chapter 2 for the EHLQ type of unpolarised densities. These are the parametrisation sets (a)-(d). The set (e), as we recall, does not fit the EMC DIS data for $g_1^p(x)$ and so we ignore it. We now use these parametrisations of the spin dependent as well as spin independent densities in order to quantify the dependence of the $D\gamma$ and DY symmetries on these.

We begin with the $D\gamma$ process and study the region in which our approximation for the asymmetry in eq. (4.14) is valid. In Fig. (4.3) we plot the expansion parameter, β , as a function of x for $D\gamma$ in the configuration where $x_1 = x_2 = x$ and the centre-of-mass angle, ϕ , varies between 30° and 90° . We see that the correction is small (≤ 0.1) for large ϕ for small x -values, eg., for $x \geq 0.1$ for $\phi = 90^\circ$ and increases with decreasing ϕ . However, recall that the cross-sections themselves are larger at smaller scattering angles.

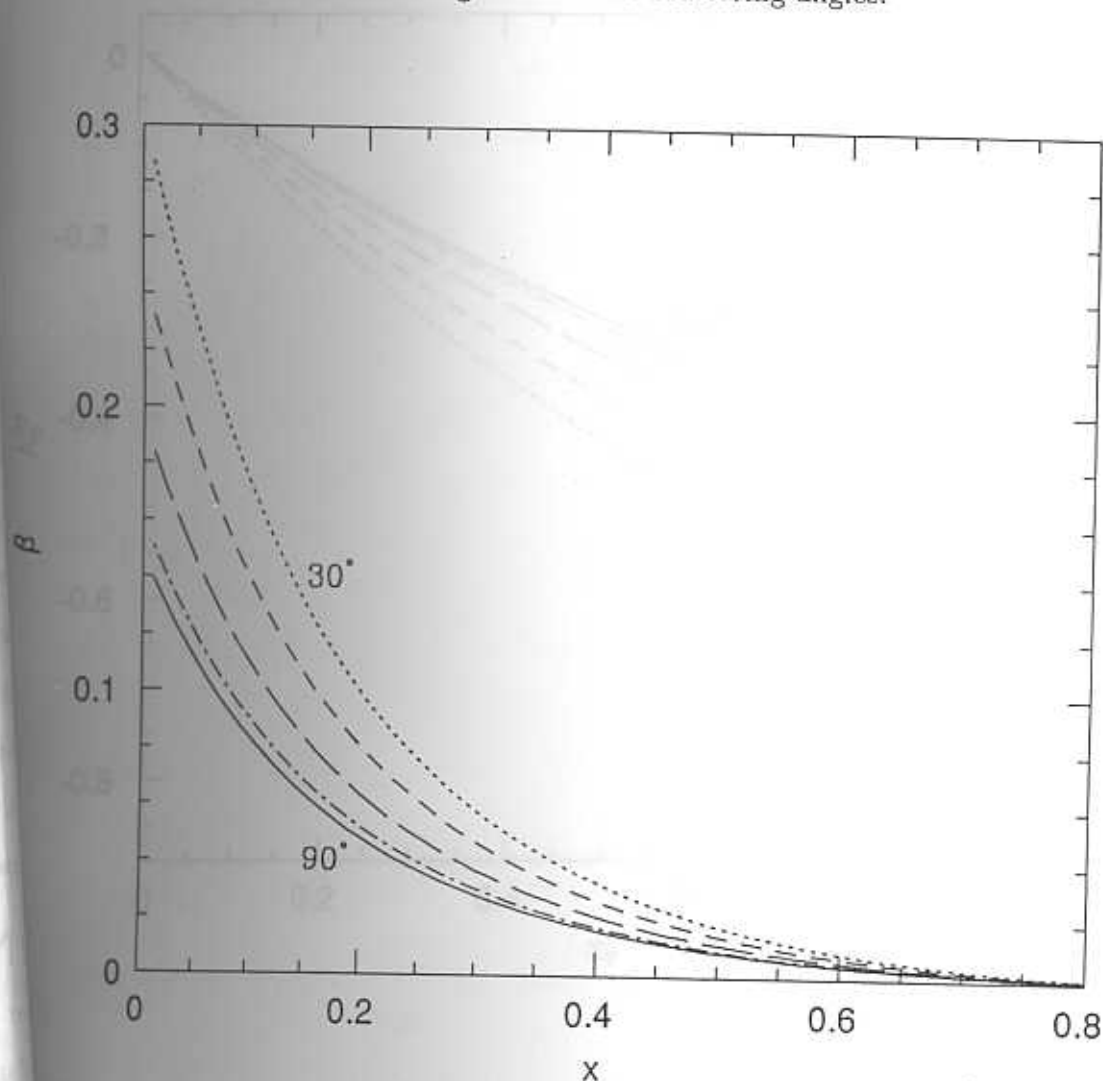


Fig. 4.3 The expansion parameter, β , as a function of x in $D\gamma$ process in pp collisions for different CM scattering angles, $\hat{\phi} = 30^\circ - 90^\circ$ in steps of 15° .

Hence, the approximation we have used for the asymmetry in eq. (4.14) holds in this allowed region. The corresponding asymmetry is plotted for parametrisation type (d) (EHLQ set) as a function of x_T for different angles in Fig. (4.4). We see that the asymmetry is maximum for minimum ϕ .

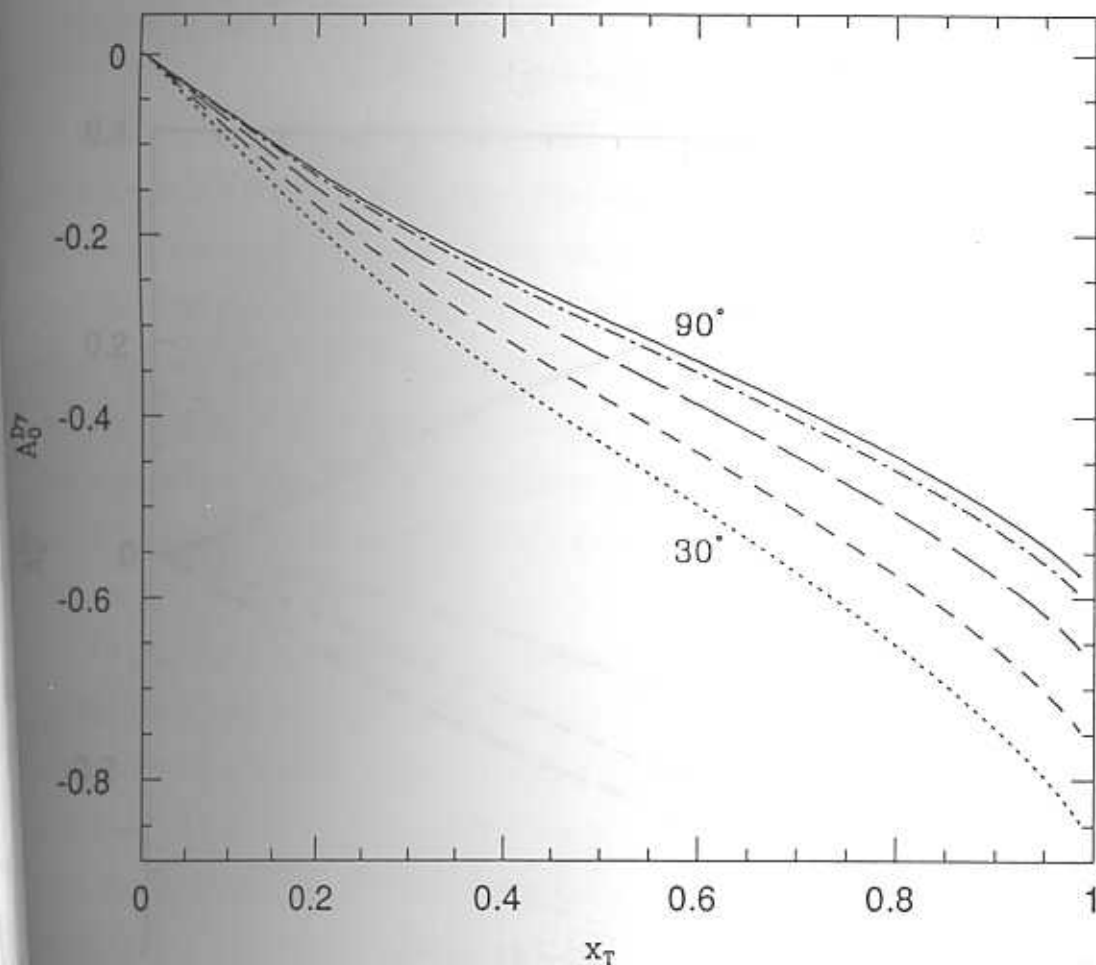


Fig. 4.4 The zero-order asymmetry in $pp D\gamma$ process plotted as a function of x_T for different $\hat{\phi}$ values as described in the caption to Fig. (4.3). Parametrisation type (d) has been used for the spin dependent densities (see text for details).

The dependence of this zero order asymmetry on the gluon parametrisation can be seen very well from Fig. (4.5), where it is seen that for different parametrisation sets, the asymmetry drastically varies between positive and negative values. (We have used $\hat{\phi} = 90^\circ$ or $y_1 = y_2 = 0$). Recall that the different parametrisation sets all give similar values for $g_1^p(x)$ (they were so chosen!).

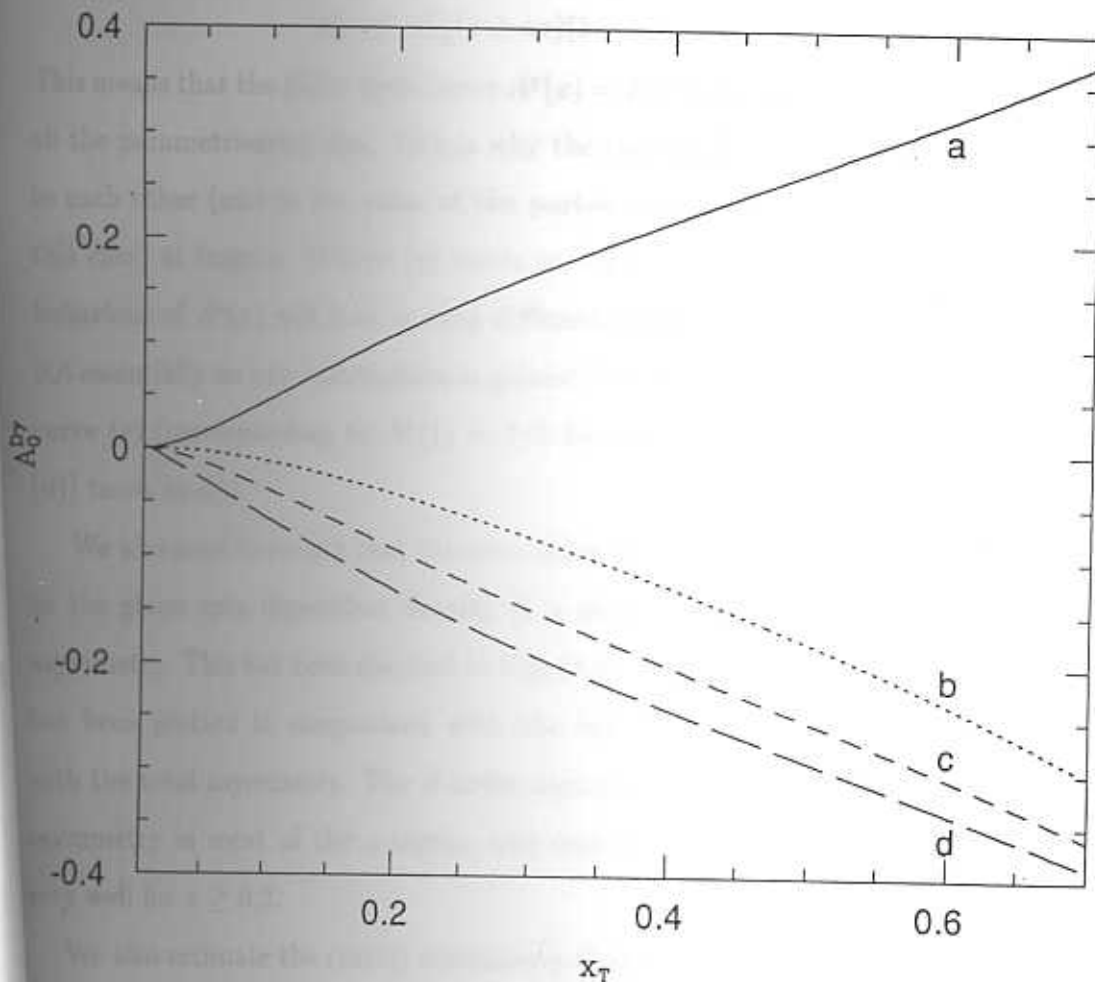


Fig. 4.5 The zero-order asymmetry in $pp D\gamma$ process plotted as a function of x_T for $\hat{\phi} = 90^\circ$ for spin dependent parametrisations type (a)-(d).

Hence, in the expression for the zero order asymmetry, for a given angle ϕ , the asymmetry $A^{pp}(x)$ and the parton asymmetry ϕ are the same for all parametrisation types and so the curves in Fig. (4.5) show differences *only* due to changes in \tilde{g} and will therefore be sensitive to this quantity. This also fixes the *sign* of \tilde{g} and hence of the gluon polarisation as being the negative of the sign of the $D\gamma$ asymmetry. This is important as the sign of \tilde{g} and Δg has not yet been established. Further, in our parametrisation we have used a simple behaviour for \tilde{g} :

$$\begin{aligned} x\tilde{g} &= \pm N_g x^\alpha (1+ax)(1-x)^\zeta \\ xg &= N_g (1+ax)(1-x)^\zeta . \end{aligned}$$

This means that the gluon asymmetry $A^g(x) = \tilde{g}/g$ has a value ± 1 at $x = 1$ for all the parametrisation sets. This is why the curves (b)–(d) in Fig. (4.5) tend to each other (and to the value of the parton asymmetry, ϕ , equal to 0.6 in this case) at large x . (Curve (a) tends to $-\phi$). Choice of a different $x \rightarrow 1$ behaviour of $A^g(x)$ will lead to very different large- x behaviour in Fig. (4.5), but essentially no new information is gained. See for example Fig. (4.6), where curve (e) (corresponding to $A^g(1) = 1/2$ for the same value of Δg as curve (d)) tends to $\phi/2$.

We also need to ensure that the zero-order asymmetry which is so sensitive to the gluon spin dependent density is a good approximation to the total asymmetry. This has been checked in Fig. (4.7) where the β -order asymmetry has been plotted in comparison with the zero-order asymmetry as well as with the total asymmetry. The β order asymmetry is seen to equal the total asymmetry in most of the x -region and matches the zero order asymmetry very well for $x \geq 0.2$.

We also estimate the (total) asymmetry that would be measured in an experiment where the jet is not observed. The computation is for 800 GeV fixed target beam energy. The cross-sections appearing in the asymmetry equation are now doubly differential (with respect to x_T and y_1 and we choose $y_1 = 0$) with y_2 left free and integrated over. In order to perform the integration, we

have to put back the Jacobean in the transformation from the set of variables (x_1, x_2, t) to (x_T, y_1, y_2) and make sure that overall kinematical factors are included as they will affect the integration.

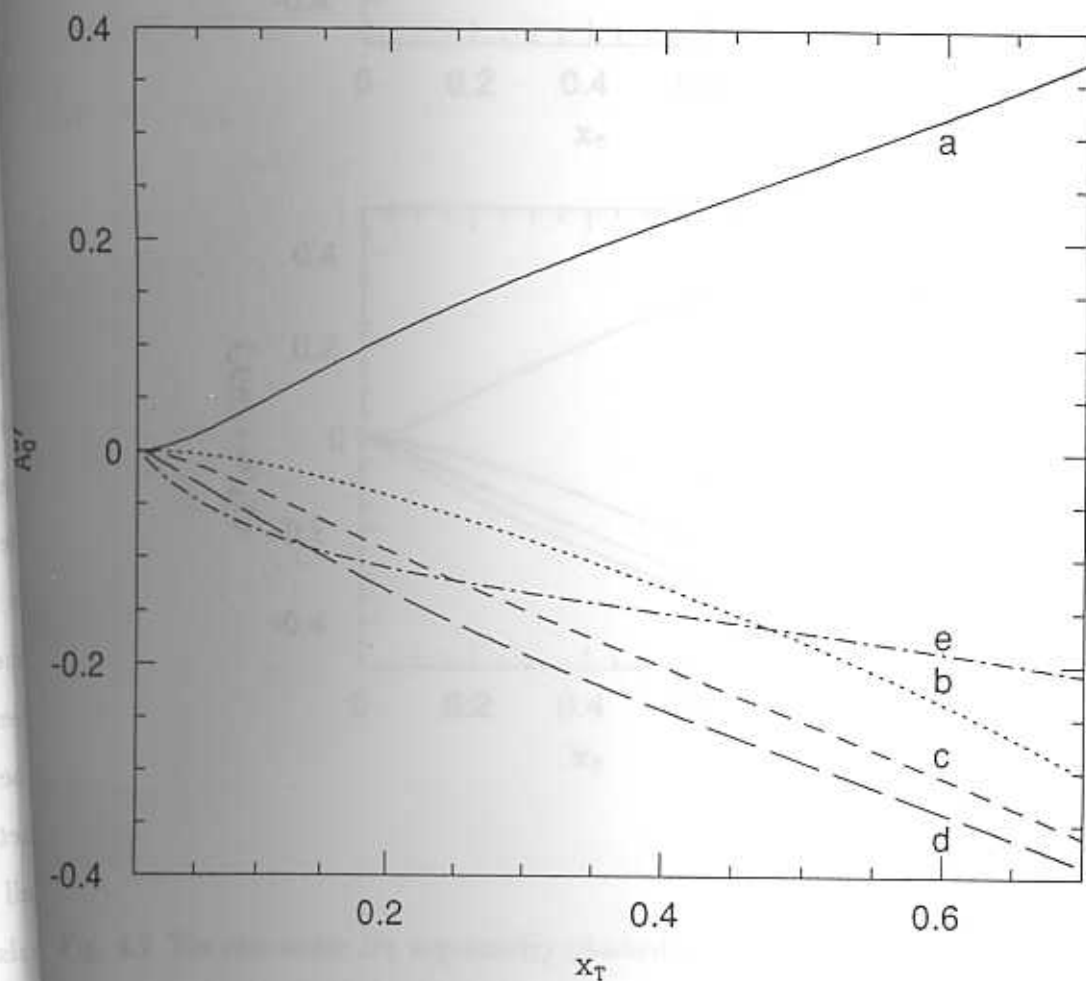


Fig. 4.6 The same as Fig. (4.5) with an extra spin dependent parametrisation type corresponding to curve (e) demonstrating the effect of changing $A^g(x=1)$ from 1 to $1/2$.

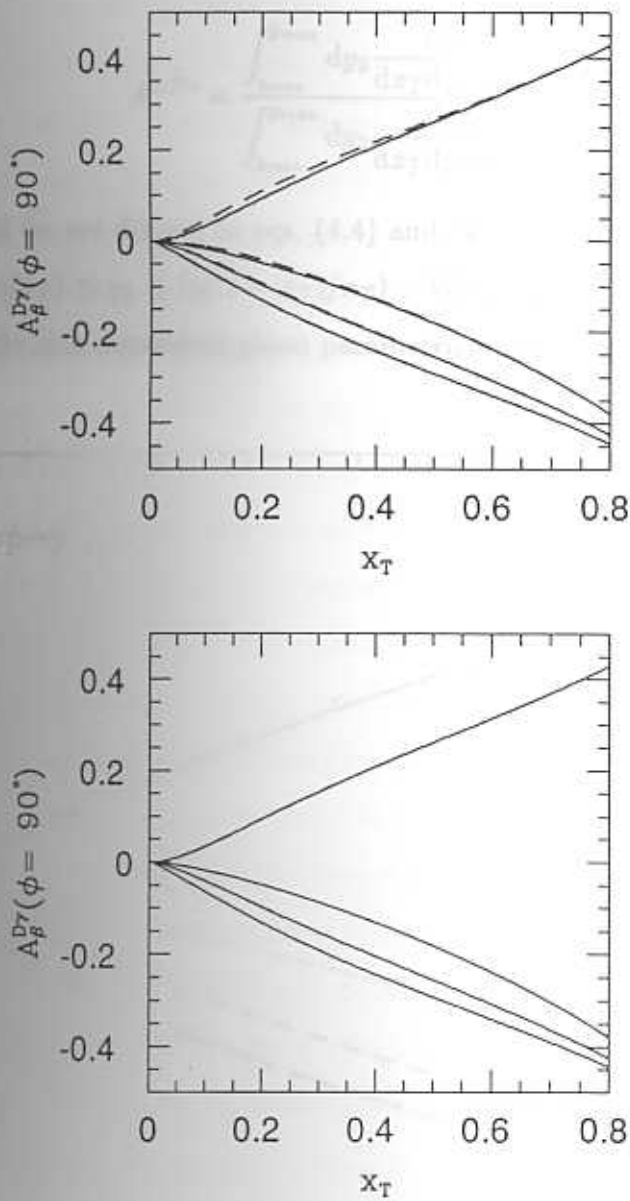


Fig. 4.7 The zero order $D\gamma$ asymmetry (dashed curves) plotted as a function of x_T along with the β order result (solid curves). The zero order result is a good approximation over most of the x -range. The lower figure shows A_{β} along with the total asymmetry, which corresponds so closely that it is not visible in the graph.

We define the semi-integrated asymmetry as

$$A^{2,D\gamma} = \frac{\int_{y_{\min}}^{y_{\max}} dy_2 \frac{\widetilde{d\sigma}}{dx_T dy_1 dy_2}}{\int_{y_{\min}}^{y_{\max}} dy_2 \frac{d\sigma}{dx_T dy_1 dy_2}}, \quad (4.19)$$

where $d\sigma$ and $\widetilde{d\sigma}$ are defined in eqs. (4.4) and (4.7) and the limits on y_2 are $-\ln((2-x_T)/x_T) \leq y_2 \leq \ln((2-x_T)/x_T)$. We find that $A^{2,D\gamma}$ is also very sensitive to the spin dependent gluon parametrisation (see Fig. (4.8)).

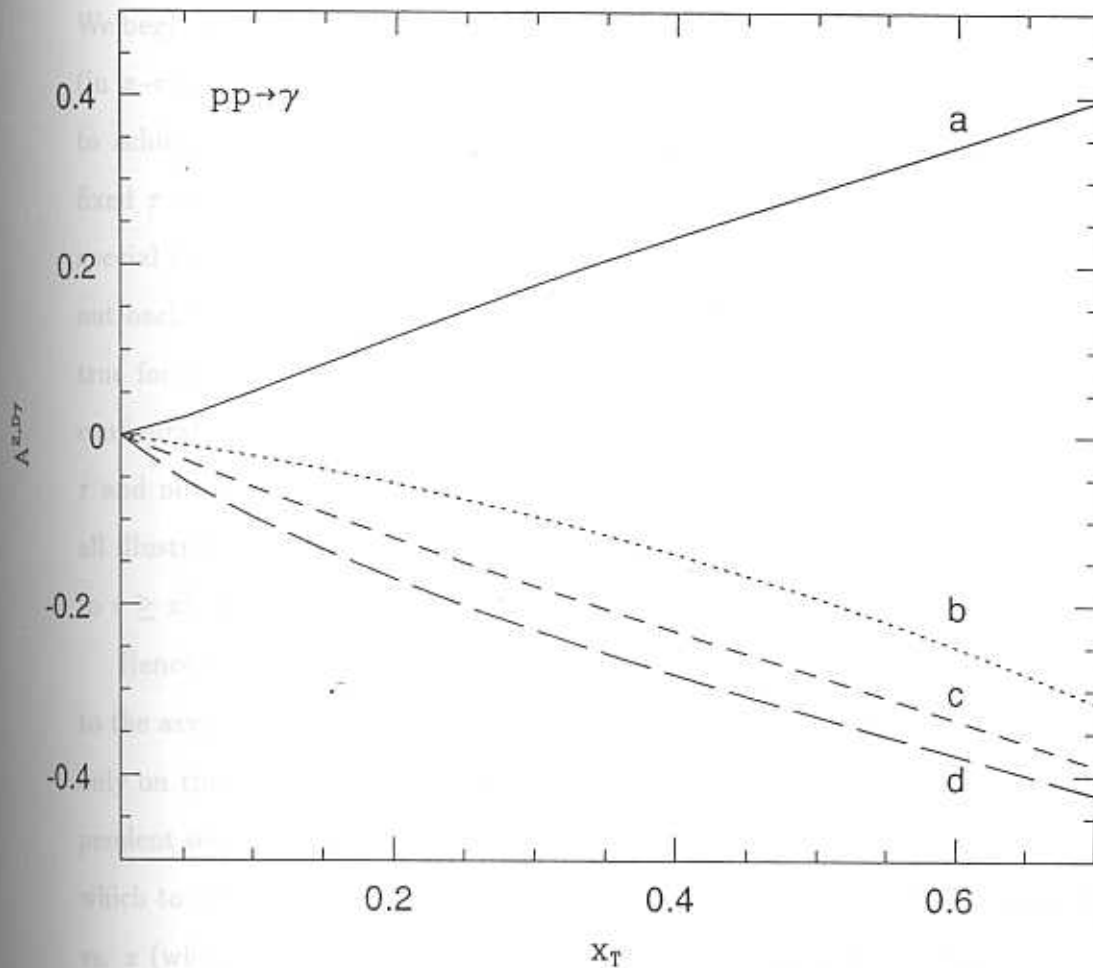


Fig. 4.8 The total semi-integrated $D\gamma$ asymmetry, $A^{2,D\gamma}$, is plotted as a function of x_T for different parametrisation types.

This means that a fixed target experiment (where the jet is difficult to define) should also be able to extract the spin dependent gluon densities. This is useful as these experiments are easier to perform than the collider experiments; in fact FermiLab [10] has already announced preliminary results for polarised proton antiproton scattering. We see that the semi-integrated asymmetries are atleast as large as the unintegrated ones and have similar form.

We now go on to an analysis of the Drell-Yau asymmetries. This follows closely along the lines of the direct photon case. The $\hat{\phi}$ behaviour is the same and we do not reproduce the graph for the $\hat{\phi}$ dependence of the asymmetry. We begin with Fig. (4.9) for β in order to decide the allowed kinematical region (in x - τ space). The approximation $x_1 = x_2 = x$ that we have used in order to achieve the factorisation of the asymmetry in eq. (4.14) is possible for a fixed τ only at a given value of x and not throughout phase space. In the special case when $y_1 = y_2 = 0$, that is, when the jet and virtual photon come out back-to-back at $\pi/2$ to the beam direction, the asymmetry in eq. (4.15) is true for all x -values. (This is also true in direct photon production.) In this configuration, as stated before, the asymmetry depends only on the variable τ and not on the beam energy. We therefore choose always, $y_1 = y_2 = 0$ for all illustrations here after. With this choice, the physical region is restricted to $\tau \geq x^2$. We see $\beta \leq 0.1$ in most of this physically allowed region.

Hence the leading order asymmetry is sufficiently accurate (as corrections to the asymmetry are small when β is small). Again this asymmetry depends only on the spin dependent gluon density and is independent of the spin dependent sea quark distribution. Hence, the DY process is also a good place in which to study the gluon polarisation. We then plot the β -order asymmetry vs. x (where $x_\tau = (x - \tau/x)$) in Fig. (4.10) where the zero-order asymmetry is also plotted for comparison. (As in $D\gamma$, the β asymmetry equals the total asymmetry to a very good approximation over a large kinematical range.) We see that the zero order asymmetry is a good approximation to the total DY

asymmetry for $x \geq 0.5$ which corresponds to $x_T = 0.3$.

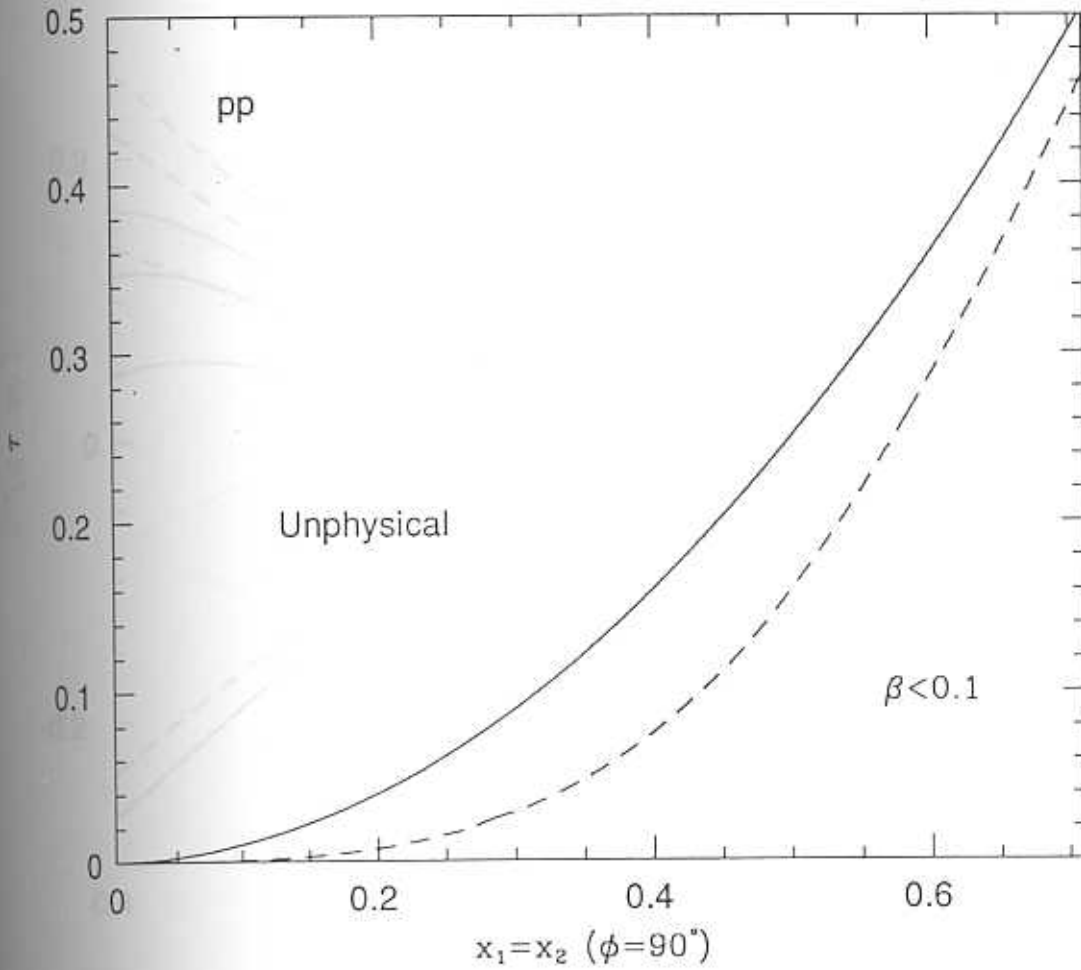


Fig. 4.9 The physically allowed region in x - τ space is shown for the DY process in pp collisions for $\hat{\phi} = 90^\circ$. The region where $\beta \leq 0.1$ is indicated.

At smaller values of x the correction due to the (negative) spin dependent sea densities in the β -order asymmetry causes it to differ from the zero-order asymmetry.

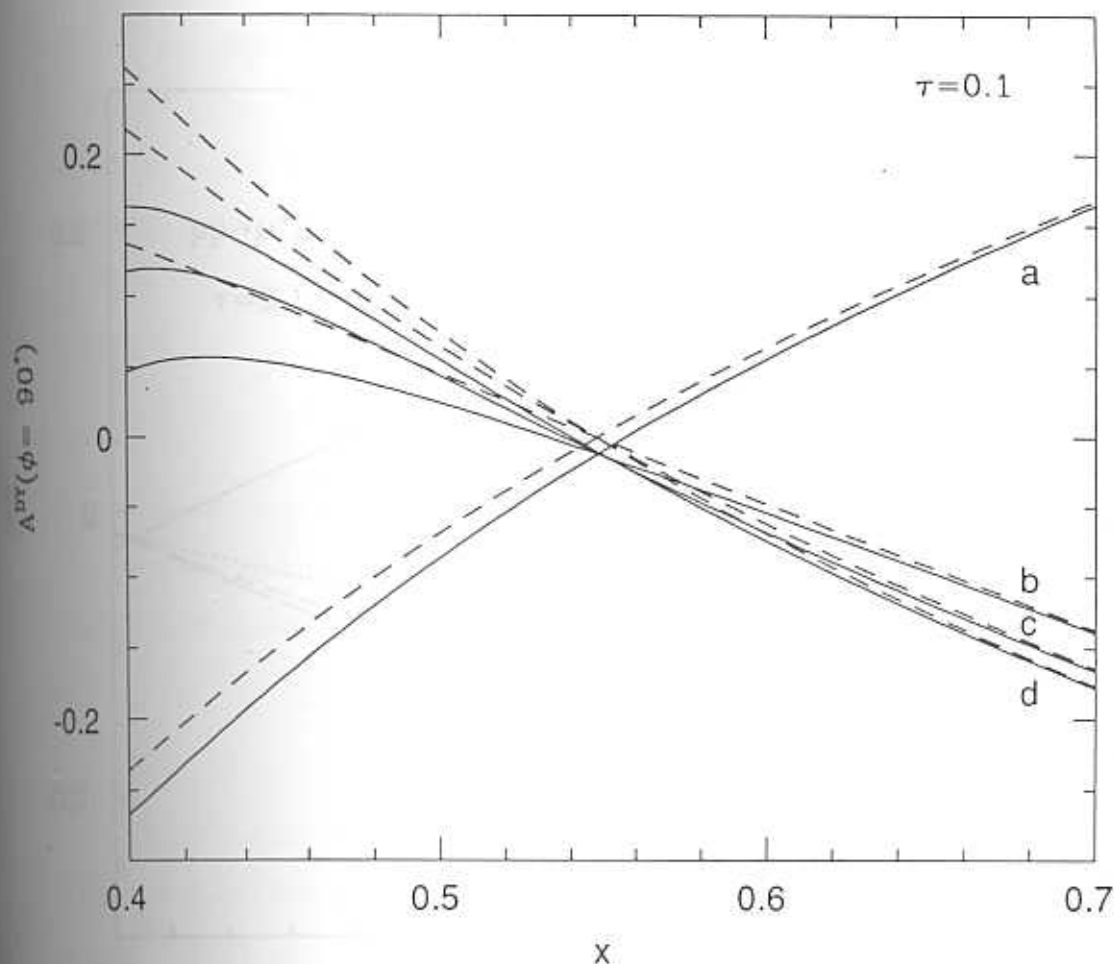


Fig. 4.10 The zero order asymmetry (dashed curves) in pp DY process is plotted for parametrisation types (a)–(d) as a function of $x = x_1 = x_2$ for $\phi = 90^\circ$ and $\tau = 0.1$. Also shown for comparison are the corresponding β -order asymmetries (solid lines).

Finally, we plot the semi-integrated asymmetry in Fig. (4.11) just as in Fig. (4.8) for the $D\gamma$ case. The cross-sections involved in this asymmetry are defined as in eq. (4.19) but are further differential with respect to the physical variable, τ . The limits on y_2 are now $\pm \ln((2 - \bar{x}_T)/x_T)$ and we have chosen $y_1 = 0$ and $\tau = 0.1$.

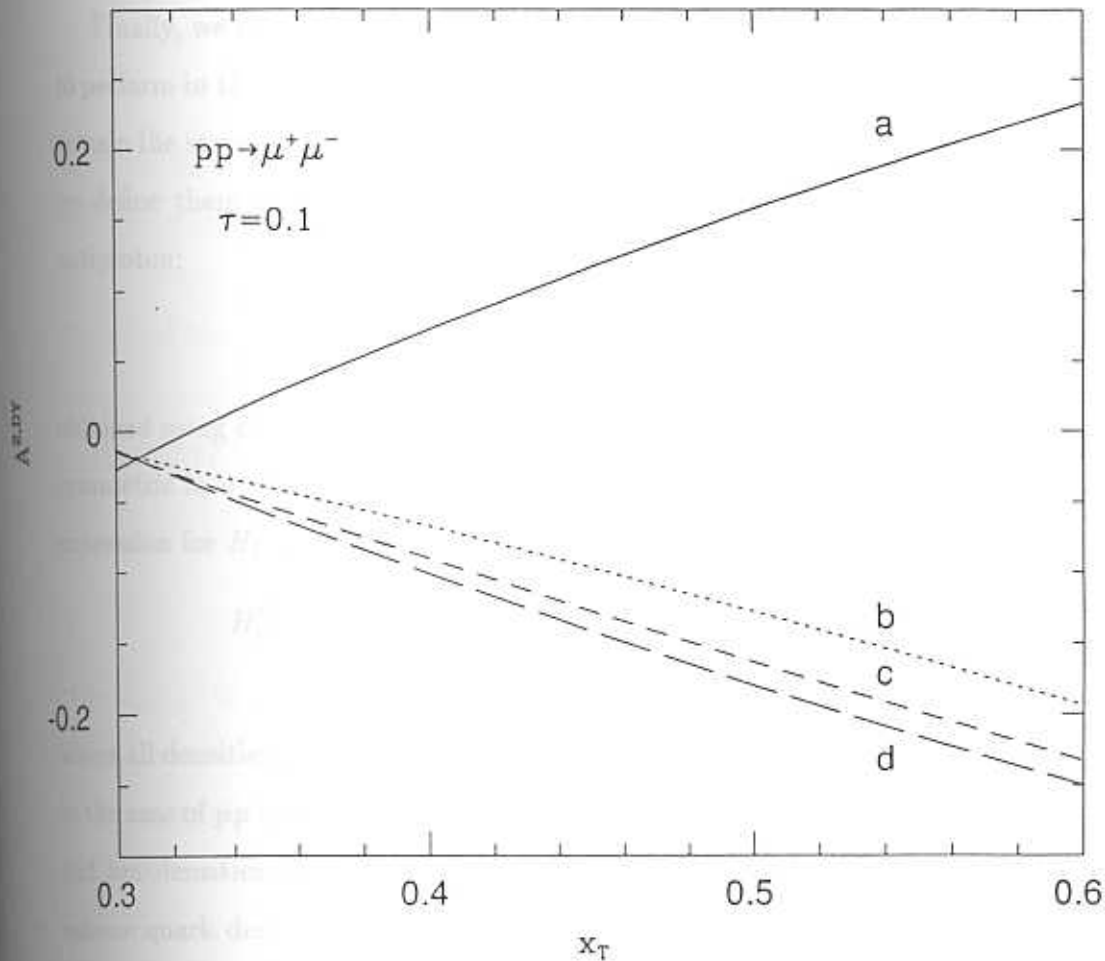


Fig. 4.11 The total semi-integrated DY asymmetry, $A^{2,DY}$, is plotted as a function of x_T for different parametrisation types for $y_1 = 0$ and $\tau = 0.1$.

Again, we see that the semi-integrated asymmetry which now contains no information on the balancing jet, is sensitive to differences in gluon parametrisation. We emphasise that the quantity plotted in Fig. (4.11) is the total asymmetry and not the zero-order one.

This concludes our numerical analysis of the asymmetries in $D\gamma$ and DY production in polarised pp collisions.

4.3 The $p\bar{p}$ collision process

Finally, we deal with polarised $p\bar{p}$ collisions. The experiments are harder to perform in this case; however, the subprocess cross-sections, $d\hat{\sigma}^\alpha$; $\alpha = C, A$, remain the same as in the pp case. The structure function factors are different; we define them using the following definitions of the parton densities in an antiproton:

$$\begin{aligned} q^{\bar{p}}(x) &= \bar{q}^p x ; \\ \bar{q}^{\bar{p}}(x) &= q^p x , \end{aligned} \tag{4.20}$$

obtained using charge conjugation symmetry. Since G_1 and G_2 in eq. (4.6) are symmetric in q and \bar{q} , they remain unaffected by this redefinition, while the expression for H_0 becomes

$$\begin{aligned} H_0^{\bar{p}} &= \sum_f e_f^2 \left[q^p(x_1) \bar{q}^{\bar{p}}(x_2) + \bar{q}^p(x_1) q^{\bar{p}}(x_2) \right] \\ &= \sum_f e_f^2 \left[q^p(x_1) q^p(x_2) + \bar{q}^p(x_1) \bar{q}^p(x_2) \right] , \end{aligned} \tag{4.21}$$

where all densities are with reference to a proton in the latter equation. Unlike in the case of pp collisions, $H_0^{\bar{p}}$ can be written in terms of structure functions and sea densities only under some assumption about the relation between valence quark densities for different flavours. To begin with, we assume that these are flavour independent, *i.e.*,

$$u_V(x) = 2V(x) ; \quad d_V(x) = V(x) ,$$

with the relationship between the sea densities as before ($u_s = d_s$; $s_s = \eta u_s$).

Then,

$$2F_1(x) = V(x) + \frac{(10 + 2\eta)}{9} \sigma(x) .$$

Substituting for $V(x)$ in eq. (4.21) we find an expression for $H_0^{p\bar{p}}$ in terms of F_1 and σ alone:

$$H_0^{p\bar{p}}(x_1, x_2) = \frac{68}{9} F_1^p(x_1) F_1^p(x_2) - \frac{212}{81} (F_1(x_1) \sigma(x_2) + \sigma(x_1) F_1(x_2)) + \frac{2251}{1458} \sigma(x_1) \sigma(x_2). \quad (4.22)$$

Similarly, the corresponding spin dependent term turns out to be

$$\widetilde{H}_0^{p\bar{p}}(x_1, x_2) = \frac{68}{9} g_1^p(x_1) g_1^p(x_2) - \frac{212}{81} (g_1(x_1) \bar{\sigma}(x_2) + \bar{\sigma}(x_1) g_1(x_2)) + \frac{2251}{1458} \bar{\sigma}(x_1) \bar{\sigma}(x_2). \quad (4.23)$$

Since the leading term of H_0 (or \widetilde{H}_0) is proportional to the product of two valence quark densities, we expect it to dominate over the compton terms. Hence, we shall write the asymmetry for $p\bar{p}$ collisions, neglecting the compton terms and find the valid region of phase space later (just as we did in the pp case, where the annihilation term was neglected instead).

Neglecting the sea densities in comparison with the valence ones, we find that for both $D\gamma$ and DY , the asymmetry is

$$A_0^{p\bar{p}} = \frac{g_1(x_1) g_1(x_2) d\bar{\sigma}^A}{F_1(x_1) F_1(x_2) d\hat{\sigma}^A} = A^{\mu p}(x_1) A^{\mu p}(x_2) \phi^A. \quad (4.24)$$

Note that ϕ^A for both $D\gamma$ and DY equals one. We stress that the factorisation of the asymmetry in terms of $A^{\mu p}$ does not require $x_1 = x_2 = x$ (unlike the pp case) as there is only one term in the leading contribution.

Corrections to the leading order asymmetry in eq. (4.24) coming from compton contributions can now be estimated. We follow the same procedure as before. We consider phase space regions where $y_1 = y_2 = 0$. Then $d\hat{\sigma}^C = d\hat{\sigma}^{C'}$ (or $\hat{i} = \hat{u}$; $x_1 = x_2$, as before). To leading order in the new expansion parameter,

$$\beta_A = \frac{9}{17} \frac{d\hat{\sigma}^C}{d\hat{\sigma}^A} \frac{g(x)}{F_1(x)},$$

the asymmetry is given by

$$A_{\beta}^{p\bar{p}} = A^{\mu p}(x) A^{\mu p}(x) \phi^A + \beta_A A^{\mu p}(x) \left\{ A^y(x) \phi^C - A^{\mu p}(x) \phi^A \right\}. \quad (4.25)$$

Again, since all the quantities multiplying powers of β_A are bounded by unity, our approximation is good if β_A is small. Further, β_A depends only on unpolarised quantities and can be estimated from known data.

Finally, corrections due to flavour differences between u - and d -valence quark distributions are checked by writing

$$u_V(x) = 2 f(x) d_V(x) ; \quad \widetilde{u}_V(x) = 2 \widetilde{f}(x) \widetilde{d}_V(x) .$$

Neglecting the compton term and sea densities, we get

$$A^{p\bar{p}} = \frac{(16\widetilde{f}^2 + 1) (8f + 1)^2}{(16f^2 + 1) (8\widetilde{f} + 1)^2} A_{\mu p}^2(x) .$$

All previous computations are therefore seen to be valid not only for the case when the x -dependence of the different flavour densities are the same ($f = \widetilde{f} = 1$), but whenever $f = \widetilde{f}$, no matter what values they assume. Since (u_V, \widetilde{u}_V) and (d_V, \widetilde{d}_V) must (at large x) go as the same power of $(1-x)$ as discussed in Chapter 2, this is not an unreasonable requirement. In fact, flavour corrections are sub-dominant compared to gluonic corrections and can be ignored.

4.3.1 Numerics

As usual, we begin by displaying the region where our approximation for the asymmetry holds: we indicate the region where $\beta_A \leq 0.1$ in a plot of τ vs. $x_1 = x_2 = x$ in Fig. (4.12). The x -axis where $\tau = 0$ corresponds to the result for the $D\gamma$ case. We see that our approximation of neglecting the compton contribution is valid only for large τ . In other words, this approximation does not hold in the Direct Photon case where $\tau = 0$. Hence we expect that the $D\gamma$ asymmetry in $p\bar{p}$ should exhibit substantial dependence on the spin dependent gluon densities. Indeed, we find this to be the case as is seen in Fig. (4.13) where the total $D\gamma$ asymmetry has been plotted as a function of τ for the configuration with $y_1 = y_2 = 0$. Although the dependence on the gluon density is weaker than in the case of pp collisions (for example the asymmetry is always positive, whether or not the gluon polarisation is positive

or negative for a given parametrisation) in the intermediate x_T region it may still be able to distinguish the various parametrisation types. In the past, it has been assumed that the $p\bar{p} D\gamma$ process is dominated by the annihilation channel. We find therefore, that this is not true. In fact, in the regions where the annihilation term dominates (large x_T), the EMC experiment can already fix the asymmetry as this is just dependent on the EMC DIS asymmetry.

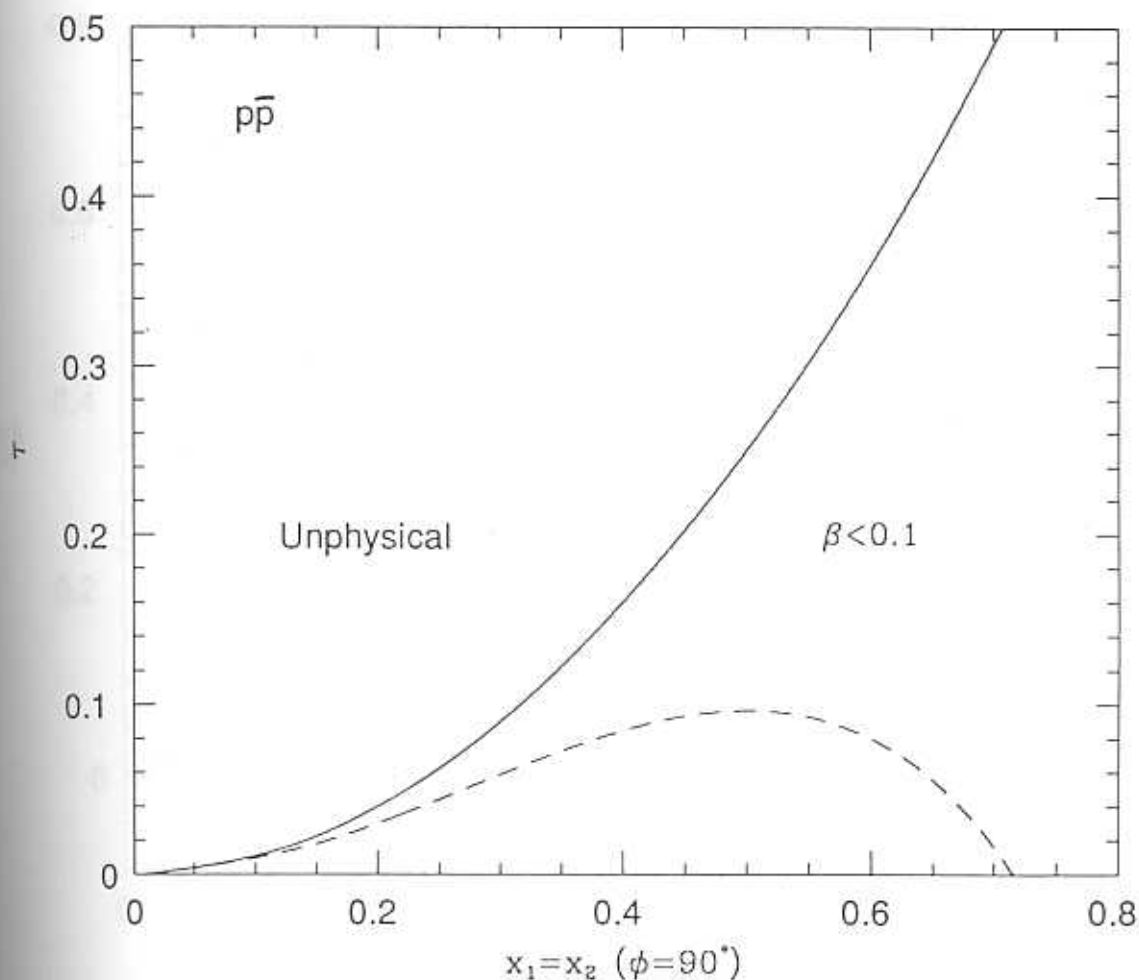


Fig. 4.12 The physically allowed region in x - τ space is shown for the DY process in $p\bar{p}$ collisions for $\hat{\phi} = 90^\circ$. The region where $\beta \leq 0.1$ is indicated.

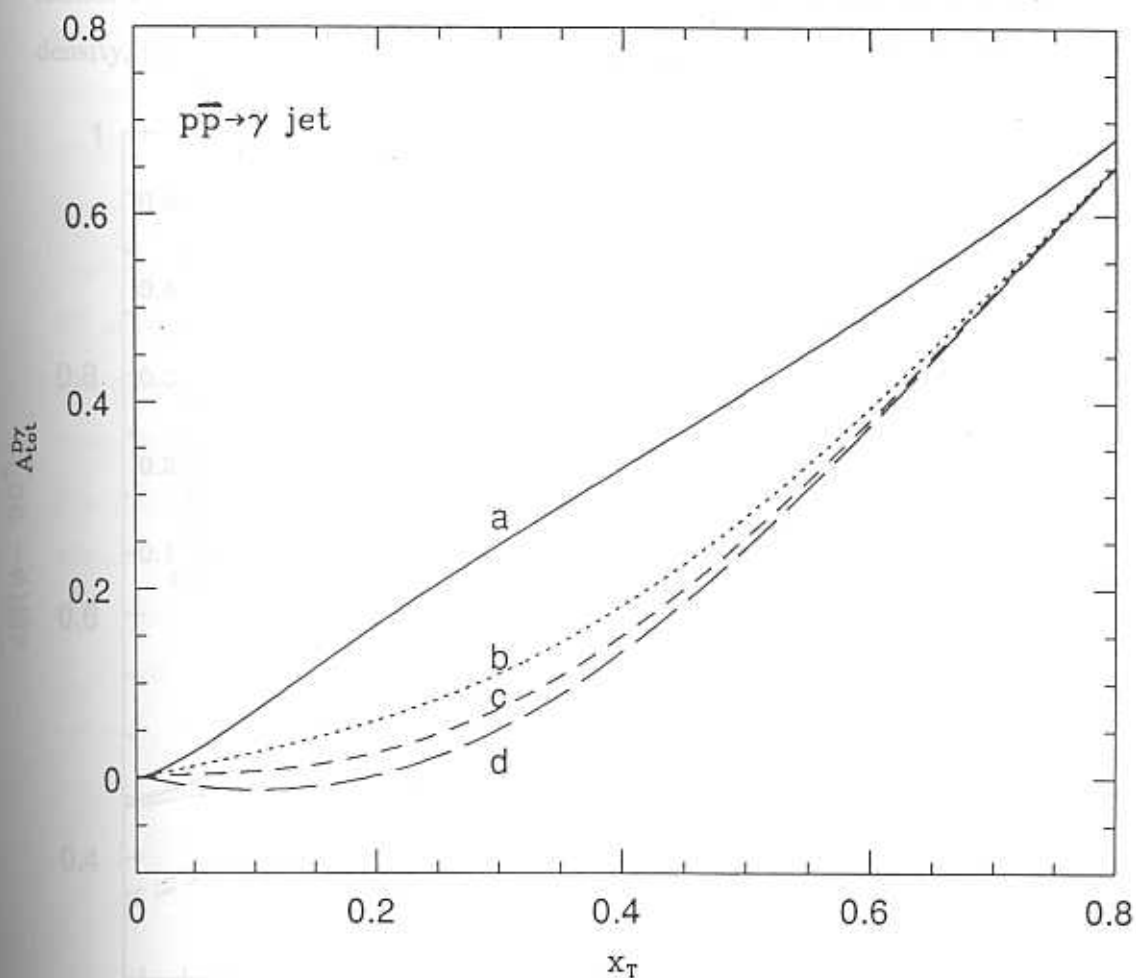


Fig. 4.13 The total $D\gamma$ asymmetry in $p\bar{p}$ collisions is plotted as a function of x_T for different parametrisation types.

On the other hand, in the DY process where β_A is small over a larger region, we expect the asymmetry to be largely independent of the spin dependent gluon density. We find this to be true, as evidenced by Fig. (4.14) where the total asymmetry for $y_1 = y_2 = 0$ and $\tau = 0.2$ for all parametrisation types are seen to be very close to each other over the entire x region. (Again, $x = x_1 = x_2$ and $x_T = x - \tau/x$). However, for smaller τ values where the correction terms cannot be ignored (as β_A is large), the asymmetry does depend on the gluon density, just as in the $D\gamma$ case. This is shown in the inset in Fig. (4.14).

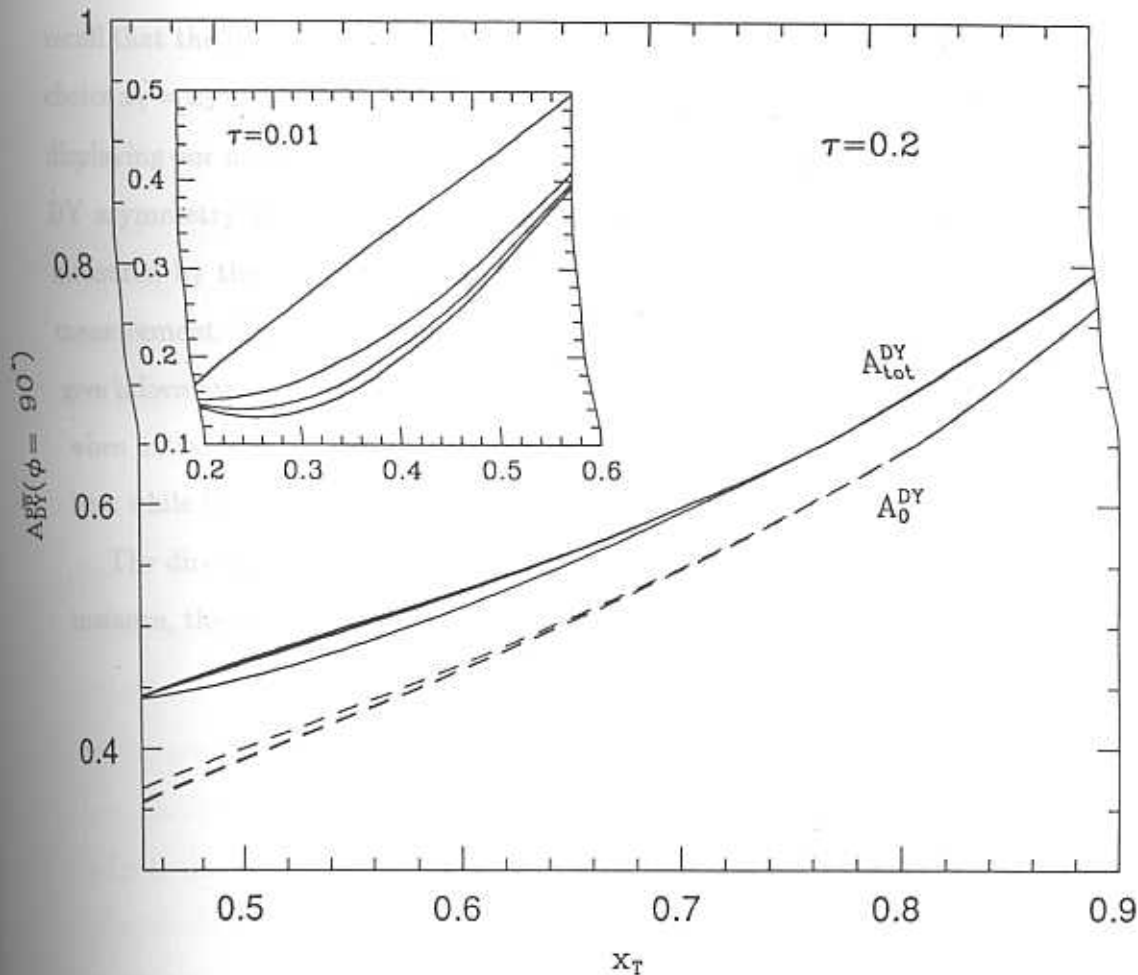


Fig. 4.14 The total DY asymmetry in $p\bar{p}$ collisions is plotted as a function of x_T for different parametrisation types for $\tau = 0.2$. The corresponding curves for $\tau = 0.01$ is shown in the inset.

In general, in phase space regions where τ is large, the asymmetry can be approximated by the square of the DIS asymmetry, while in regions of smaller τ , this approximation is not valid and the asymmetry depends on the value of the spin dependent gluon density. The reason for the importance of gluonic corrections in these regions is not hard to find: although the gluon density falls off with x as $(1-x)^6$, while F_1 goes as $(1-x)^3$, the value of the (unpolarised) gluon density at $x=0$ is so much larger that its faster fall with x does not reduce the ratio g/F_1 significantly till $x=0.7$ or so. However the ratio of parton cross-sections for large τ helps in reducing the value of β_A . Finally we recall that the factorisation of the asymmetry in eq. (4.24) did not require the choice $x_1=x_2$ unlike in the pp case; we used this for the sake of simplicity when displaying our numerical results. Even without this assumption, therefore, the DY asymmetry at large τ is given entirely in terms of the DIS asymmetry measured by the EMC. This can therefore be used as a check on the EMC measurement. The same experiment, in different kinematical regions can also give information on $\hat{g}(x)$. This would help reduce overall normalisation errors when extracting the two quantities. We must remember, however, that it may be a while before data obtained from such processes are sufficiently accurate.

The direct photon process, especially, has been studied by several; see, for instance, the references listed in [11].

THE GLUON DENSITIES: THE SMALL- x REGION

CONTENTS

The 2-jet production processes

Formalism

Numerics

5.0 The 2-jet production processes

We present here an analysis of 2-jet production in polarised $\vec{p}\vec{p}$ scattering. We show that this process provides a way of measuring the spin dependent gluon density in the experimentally accessible region of $x_T \leq 0.6$, and especially in the small- x region [12]. Further, being a strongly interacting process (where the jet is not identified as being either a quark or a gluon jet), this process has a larger cross-section than any others suggested so far using polarised proton beams, like direct photon production. As in the $D\gamma$ and DY cases, the spin dependent quark and gluon densities appear, in the leading order, *at the same order in α_s* , so that (unlike in the EMC experiment) the gluon contribution is not suppressed by an α_s factor when compared to the quark contribution. In fact, all subprocesses, whether qq , qg or gg scattering, appear at the same order in α_s . Since Δq and $(\alpha_s/2\pi)\Delta g$ are of the same order according to the Q^2 evolution equations (see Chapter 2), we expect that the gluons will play an important rôle in this process.

We therefore expect that this is a good process with which to study the gluon spin-dependent density. Further, as is well-known, quark densities dominate at large- x values; hence the large- x asymmetries will be largely independent of the gluon density or its parametrisation. However, at small and

intermediate x values, the cross-sections and asymmetries will depend sensitively on the gluon density and, this, anyway, is the experimentally accessible kinematic region. We will show that these results complement those of $D\gamma$ and DY production which, as we have seen, are sensitive to the spin dependent gluon density in regions where $x_T \geq 0.2$.

We begin with a description of the term *jet*. In a collision process with large momentum transfer, a struck parton (q or g) is ejected from the nucleon with great momentum. Over distances greater than about a fermi (typical proton sizes) the colour interactions between this parton and the others in the nucleon become very strong (equivalently, α_s becomes large) and these strong, attractive forces cause the parton to decelerate rapidly. The parton therefore radiates hadrons in a shower—hadron bremsstrahlung occurs. These *jets* are emitted in a narrow cone in the same direction as the original parton. The jets narrow out with increasing Q^2 , but this narrowing is logarithmic, not linear [13]. For our purposes, it is sufficient to say that, given a parton in the final state with large p_T , it will exhibit itself as a jet.

We now discuss this 2-jet production process in more detail. Since this chapter closely follows along the lines of discussion of the direct photon production process (of Chapter 4), we omit details that already have appeared earlier.

5.1 Formalism

We discuss the process

$$\vec{p}\vec{p} \rightarrow jet + jet + X, \quad (5.1)$$

where \vec{p} indicates a longitudinally polarised proton beam/target. As usual, the hadronic cross-section is expressed as a sum of contributions from various partonic sub-processes. The contributions, in the leading order, to this process are shown in Fig. (5.1). Quark-quark (qq), quark-gluon (qg) and gluon-gluon (gg) processes all contribute. The quantity of interest is the asymmetry, A , which is defined in eq. (4.0.4) in terms of the differential cross-sections for the

process. These cross-sections are expressed as a sum over the cross-sections for the various sub-processes, multiplied by corresponding parton density distributions.

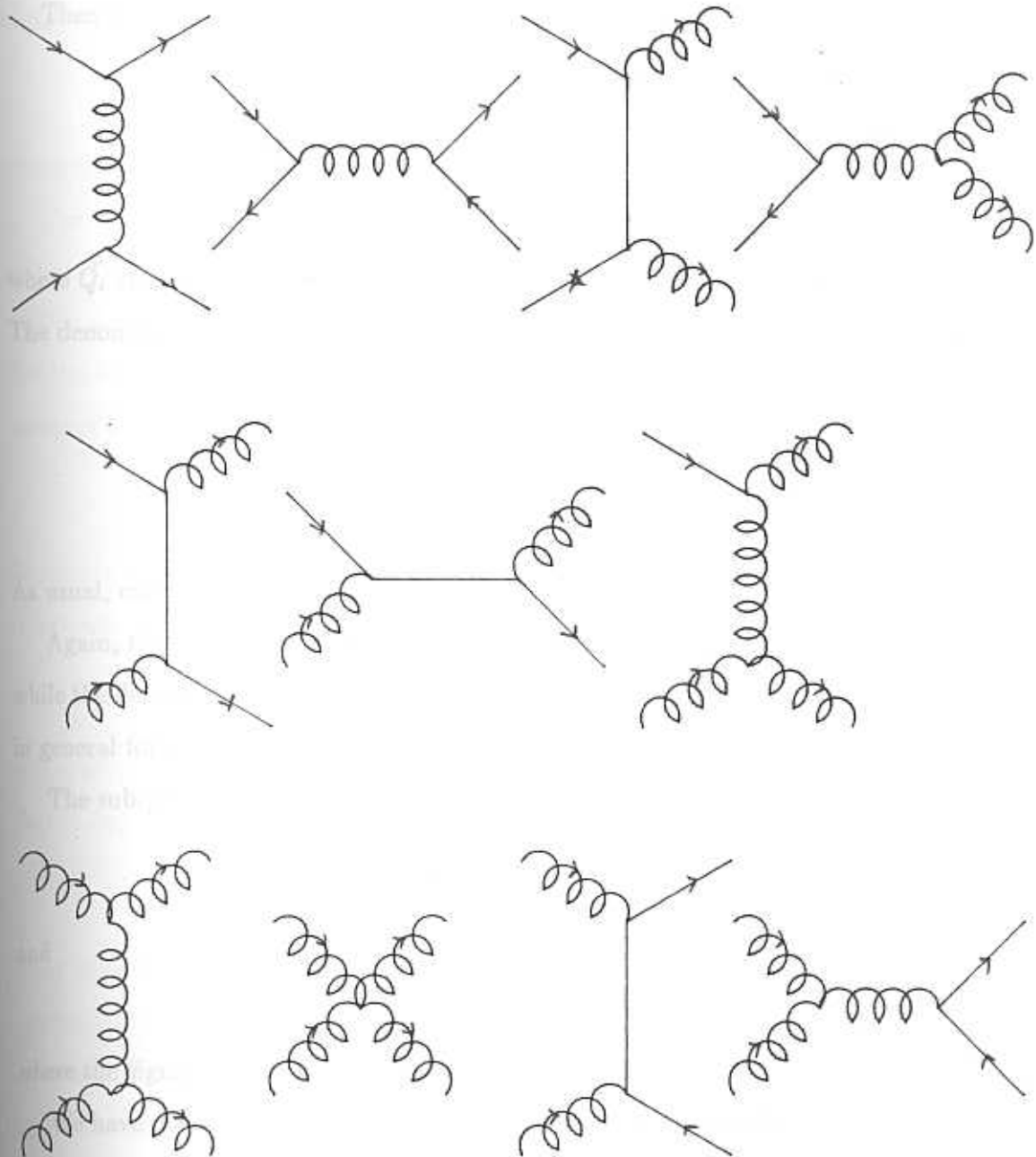


Fig. 5.1 The leading order contributions to $p\bar{p} \rightarrow \text{jet} + \text{jet} + X$.

We see that all the subprocesses are of the $2 \rightarrow 2$ type. With x_1 and x_2 defined as the momentum fractions of the incident partons with respect to their parent hadrons, the cross-section is differential with respect to the variables (x_1, x_2, \hat{t}) , just as in direct photon scattering.

Then the numerator of the asymmetry can be written as

$$\begin{aligned} \bar{d}\sigma &\equiv \frac{d^3\sigma(\uparrow\downarrow)}{dx_1 dx_2 d\hat{t}} - \frac{d^3\sigma(\uparrow\uparrow)}{dx_1 dx_2 d\hat{t}} \\ &= \sum_{ij} \bar{Q}_i(x_1) \bar{Q}_j(x_2) \frac{d\bar{\hat{\sigma}}_{ij}}{d\hat{t}} \end{aligned} \quad (5.2)$$

where \bar{Q}_i stands for any parton, $\bar{q}_i, \bar{\bar{q}}_i, i = u, d, s$ or \bar{g} .

The denominator of the asymmetry is

$$\begin{aligned} d\sigma &\equiv \frac{d^3\sigma(\uparrow\uparrow)}{dx_1 dx_2 d\hat{t}} + \frac{d^3\sigma(\uparrow\downarrow)}{dx_1 dx_2 d\hat{t}} \\ &= \sum_{ij} Q_i(x_1) Q_j(x_2) \frac{d\hat{\sigma}_{ij}}{d\hat{t}}. \end{aligned} \quad (5.3)$$

As usual, carets refer to sub-process variables.

Again, the numerator depends exclusively on the spin-dependent densities while the denominator depends on the spin-independent ones. This fact is true in general for asymmetries as defined in eq. (4.0.3) for $2 \rightarrow 2$ processes [3].

The sub-process cross-sections in eqs. (5.2) and (5.3) are as usual given by

$$\bar{d}\hat{\sigma} \equiv \frac{d\hat{\sigma}(+-)}{d\hat{t}} - \frac{d\hat{\sigma}(++)}{d\hat{t}}; \quad (5.4)$$

and

$$d\hat{\sigma} \equiv \frac{d\hat{\sigma}(+-)}{d\hat{t}} + \frac{d\hat{\sigma}(++)}{d\hat{t}}, \quad (5.5)$$

where the signs refer to the incident parton helicities.

We have not given details of cross-section calculations for the several subprocesses; the calculations follow along the lines of the demonstrated ones ($D\gamma$ or DY) with the help of the feynman rules listed in Appendix B. [14], [15] and have been listed in Table 5.1 for both the spin-independent and the spin-dependent case.

Again, the physical observables in this process are x_T ($= 2p_T/\sqrt{s}$ where p_T is the transverse momentum of either of the jets and \sqrt{s} is the energy in the C.M. of the hadrons), y_1 and y_2 (the rapidities of the two jets in the C.M. of the hadrons). However, reexpressing the cross-sections in terms of these variables just gives a Jacobean factor,

$$\frac{d^3\sigma}{dx_T dy_1 dy_2} = x_T \frac{\hat{s}}{2} \frac{d^3\sigma}{dx_1 dx_2 d\hat{t}},$$

which cancels in the asymmetry, exactly as in the $D\gamma$ or DY case.

The cross-sections in Table (5.1) have been expressed in terms of the variable $\chi = \hat{u}/\hat{t}$, *a la* Combridge and Maxwell [15]. These cross-sections have been written as a sum of two terms—a 'leading contribution' and a 'correction' term. For the unpolarised case, the leading term in all dominant sub-processes is a constant factor times a function, $F(\chi)$, where

$$F(\chi) = \chi^2 + \chi + 1 + \frac{1}{\chi} + \frac{1}{\chi^2}; \quad \chi = \hat{u}/\hat{t}.$$

Combridge and Maxwell in their pioneering work took advantage of this fact to express the spin-independent cross-section as

$$\frac{1}{2}d\sigma = \frac{\pi\alpha_s^2}{\hat{s}^2} P(x_1)P(x_2) a F(\chi), \quad (5.6)$$

where $d\sigma$ is defined in eq. (5.5) and a is a constant. Here, $P(x)$ is the generic parton density function, defined for three flavours by

$$P(x) = q(x) + \frac{C_A}{C_F} g(x); \quad C_A = 3, \quad C_F = 4/3. \quad (5.7)$$

They showed that the correction terms were negligible and hence the 2-jet production cross-section can be parametrised in terms of a single density combination, $P(x)$, which can be 'measured' in this process. This is a remarkable result considering the number of diagrams that contribute: the complicated parton density dependence of the cross-section is reduced to dependence on a single generic parton density to a very good approximation. This form of $d\sigma$ was later used to experimentally confirm the vector nature of the gluon. In fact, such a factorisation is not possible if the gluon were a scalar boson.

Subprocess	$d\hat{\sigma}_{ij}$
$q_i q_j \rightarrow q_i q_j,$ $q_i \bar{q}_j \rightarrow q_i \bar{q}_j$	$2F(x) + 0$
$q_i q_i \rightarrow q_i q_i$	$2F(x) - \frac{2}{N} \left\{ x + 2 + \frac{1}{x} \right\}$
$q_i \bar{q}_i \rightarrow q_i \bar{q}_i$	$2F(x) + \left\{ \frac{2}{N} \left(x - 1 + \frac{1}{x} \right) + \frac{2(1+x^2)}{(1+x)^2} \right\}$
$q_i \bar{q}_i \rightarrow q_j \bar{q}_j$	$0 + \left\{ \frac{2(1+x^2)}{(1+x)^2} \right\}$
$q_i \bar{q}_i \rightarrow g g$	$0 + \frac{N_g}{N} \left\{ x + \frac{1}{x} - \frac{h(1+x^2)}{(1+x)^2} \right\}$
$q g \rightarrow q g,$ $\bar{q} g \rightarrow \bar{q} g$	$h 2F(x) + \left\{ x + 3 + \frac{1}{x} \right\}$
$g g \rightarrow g g$	$h^2 2F(x) + h^2 \left\{ 4 - \frac{2x}{(1+x)^2} \right\}$
$g g \rightarrow q \bar{q}$	$0 + \frac{N}{N_g} \left\{ 2 \left(x + \frac{1}{x} \right) - \frac{2h(1+x^2)}{(1+x)^2} \right\}$
Subprocess	$d\tilde{\sigma}_{ij}$
$q_i q_j \rightarrow q_i q_j,$ $q_i \bar{q}_j \rightarrow q_i \bar{q}_j$	$-2G(x) + 0$
$q_i q_i \rightarrow q_i q_i$	$-2G(x) + \frac{2}{N} \left\{ x + 2 + \frac{1}{x} \right\}$
$q_i \bar{q}_i \rightarrow q_i \bar{q}_i$	$-2G(x) + \left\{ \frac{2}{N} \left(x - 1 + \frac{1}{x} \right) - \frac{2(1+x^2)}{(1+x)^2} \right\}$
$q_i \bar{q}_i \rightarrow q_j \bar{q}_j$	$0 + \left\{ \frac{2(1+x^2)}{(1+x)^2} \right\}$
$q_i \bar{q}_i \rightarrow g g$	$0 + \frac{N_g}{N} \left\{ x + \frac{1}{x} - \frac{h(1+x^2)}{(1+x)^2} \right\}$
$q g \rightarrow q g,$ $\bar{q} g \rightarrow \bar{q} g$	$-h 2G(x) - \left\{ x + 1 + \frac{1}{x} \right\}$
$g g \rightarrow g g$	$-h^2 2G(x) - h^2 \left\{ x + \frac{1}{x} + \frac{2x}{(1+x)^2} \right\}$
$g g \rightarrow q \bar{q}$	$0 + \frac{N}{N_g} \left\{ 2 \left(x + \frac{1}{x} \right) - \frac{2h(1+x^2)}{(1+x)^2} \right\}$

Table 5.1 Subprocess cross-sections, $d\hat{\sigma}_{ij}$ and $d\tilde{\sigma}_{ij}$ in 2-jet production in polarised $\vec{p}\vec{p}$ scattering in units of $a\pi\alpha_s^2/\hat{s}^2$. Here, $a = 4C_F^2/N_g$, $h = C_A/C_F$, $N = 3$ and $N_g = 8$.

We see from Table (5.1) that such a factorisation is possible in the spin-dependent case also. The corresponding χ -dependent function that factorises out here is

$$G(\chi) = \chi + 1 + \frac{1}{\chi}$$

so that the spin-dependent cross-section approximates to

$$\frac{1}{2} \widetilde{d\sigma} = \frac{\pi\alpha_s^2}{\hat{s}^2} \tilde{P}(x_1) \tilde{P}(x_2) aG(\chi). \quad (5.8)$$

Here, analogous to the spin-independent case, we may define

$$\tilde{P}(x) = \tilde{q}(x) + \frac{C_A}{C_F} \tilde{g}(x) \quad (5.9)$$

as the "generic spin dependent parton density" such that the $q_i q_j \rightarrow q_i q_j$ cross-section has no correction, i.e., it is correctly represented by $aG(\chi)$. On the other hand, we find that

$$\tilde{P}(x) = \tilde{q}(x) + \left(\frac{C_A}{C_F} + \frac{1}{2} \right) \tilde{g}(x) \quad (5.10)$$

is a better approximation as can be seen from Table (5.2), as the correction to the qg term also becomes zero in this case. The approximation is not very good for the $q_i q_i$ process and, in fact, quite bad for the $q\bar{q}$ subprocess. This is because the spin-dependent cross-sections (i.e., $G(\chi)$) are very much smaller than the spin-independent ones ($F(\chi)$) for all χ so the correction terms appear to be relatively large in the former case. However, the approximation still holds since the $q\bar{q}$ contribution is greatly reduced on multiplying the subprocess cross-section with appropriate densities. In fact, gluon terms are expected to dominate the cross-section. We shall explicitly demonstrate this in a later section. We stress here that this factorisation of the cross-section *a la* Combridge and Maxwell is not at all obvious in the spin dependent case and is a remarkable feature of the 2-jet production mechanism.

5.2 Numerics

For simplicity, we have chosen the configuration in which the jets are back-to-back in the C.M. of the hadrons, i.e., $y_1 = -y_2$ or $x_1 = x_2$. Further, we choose

$y_1 = 0$ (90° scattering) so that $x_1 = x_2 = x_T$. The parametrisations of the densities are as discussed in Chapter 2.

ϕ	Leading	$q_1 q_2$	$q_1 q_1$	$q_1 \bar{q}_1$	qg		gg	
					(a)	(b)	(a)	(b)
The Spin Independent Subprocess Cross sections								
60	23.90	23.90	20.74	32.07	26.40	21.60	27.38	18.33
65	17.96	17.96	15.08	24.83	20.28	16.59	21.36	14.30
70	14.10	14.10	11.41	20.01	16.28	13.32	17.43	11.67
75	11.59	11.59	9.05	16.82	13.68	11.19	14.87	9.96
80	10.02	10.02	7.58	14.81	12.05	9.86	13.27	8.88
85	9.16	9.16	6.77	13.69	11.15	9.12	12.39	8.30
90	8.89	8.89	6.52	13.33	10.86	8.89	12.12	8.11
The Spin Dependent Subprocess Cross sections								
60	-7.70	-7.70	-4.54	0.47	-9.42	-7.70	-13.71	-9.18
65	-6.88	-6.88	-3.99	-0.02	-8.41	-6.88	-12.14	-8.13
70	-6.28	-6.28	-3.59	-0.36	-7.67	-6.28	-11.00	-7.36
75	-5.84	-5.84	-3.30	-0.61	-7.14	-5.84	-10.18	-6.82
80	-5.55	-5.55	-3.11	-0.77	-6.79	-5.55	-9.63	-6.45
85	-5.39	-5.39	-3.00	-0.86	-6.59	-5.39	-9.32	-6.24
90	-5.33	-5.33	-2.96	-0.89	-6.52	-5.33	-9.22	-6.17

Table 5.2 The subprocess cross-sections of Table 5.1 evaluated for different scattering angles, ϕ ($\chi = \cot^2(\phi/2)$) in comparison with the Combridge Maxwell approximation, $2F(\chi)$ (spin-independent) and $2G(\chi)$ (spin-dependent). Column (a) of the qg term is the cross-section with the quantity (C_A/C_F) factored out, while (b) has $(C_A/C_F + 1/2)$ factored out. The squares of these quantities have been factored out of the corresponding expressions in the gg case.

Fig. (5.2) shows the various contributions to the spin dependent hadronic cross-section, $\widetilde{d\sigma}$. Figures labeled (a)–(d) correspond to parametrisation types (a)–(d) for the spin dependent densities, as parametrised in Chapter 2. We see that the gg contribution in Figs. (5.2a), (5.2c) and (5.2d) is fairly large.

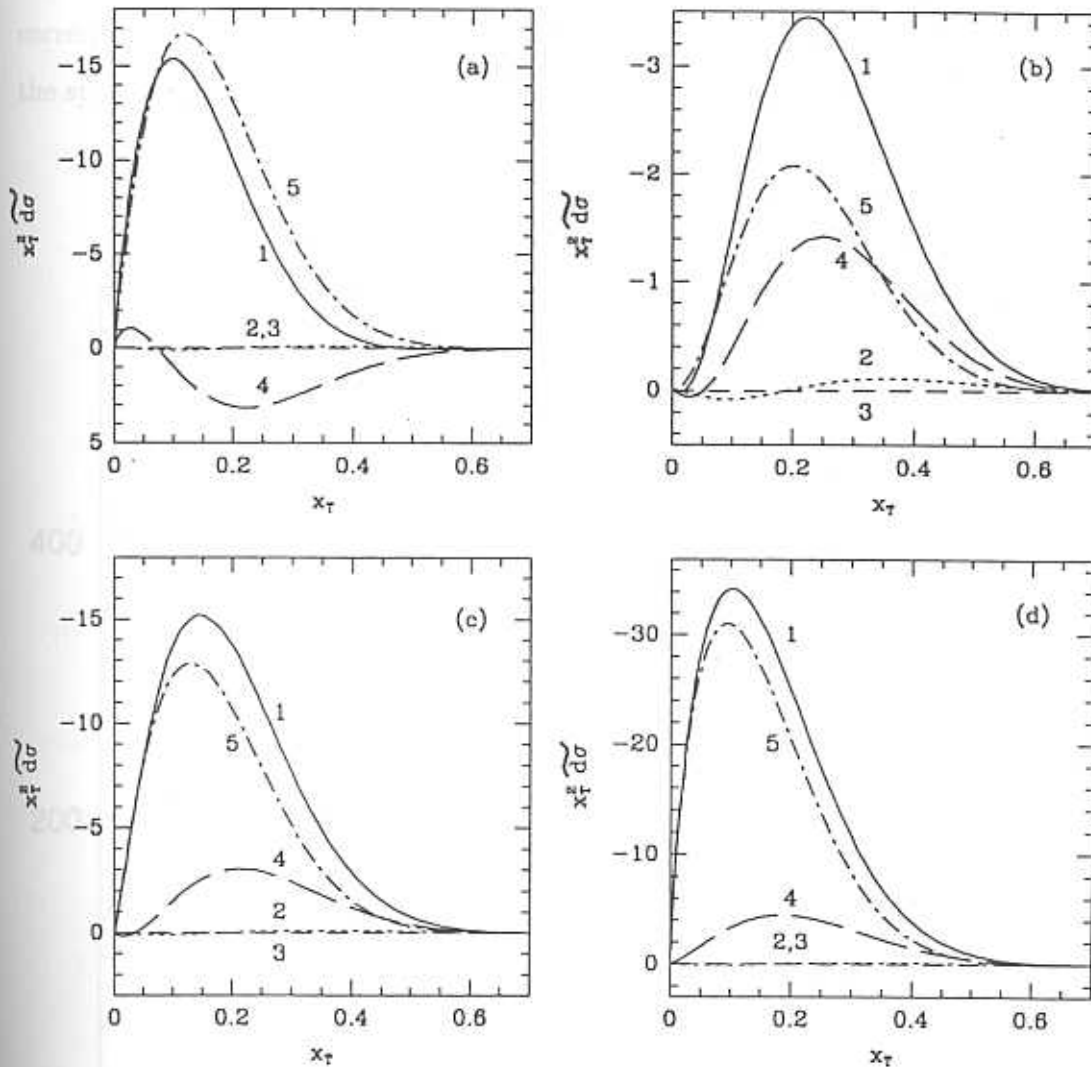


Fig. 5.2 The total spin-dependent cross-section, $x_T^2 \widetilde{d\sigma}$, in units of $(\pi \alpha_s^2 / \hat{s}^2)$, and the contributions to it are plotted as a function of x_T . The graphs (a)–(d) correspond to the parametrisation type (a)–(d) for the spin dependent densities. The labels on the curves correspond to (1): total (2): qq , (3): $q\bar{q}$, (4): qg and (5): gg contributions.

Furthermore, the sum of the qg and gg terms approximately equals the total cross-section as the qq and $q\bar{q}$ contributions (curves (2) and (3)) are negligibly small. Also, $\bar{d}\sigma$ remains mostly positive over the entire x_T region even for negative Δg since the gg contribution is always positive. Fig. (5.3) shows the corresponding spin independent cross-section, $d\sigma$, which is much larger than the spin-dependent cross-section.

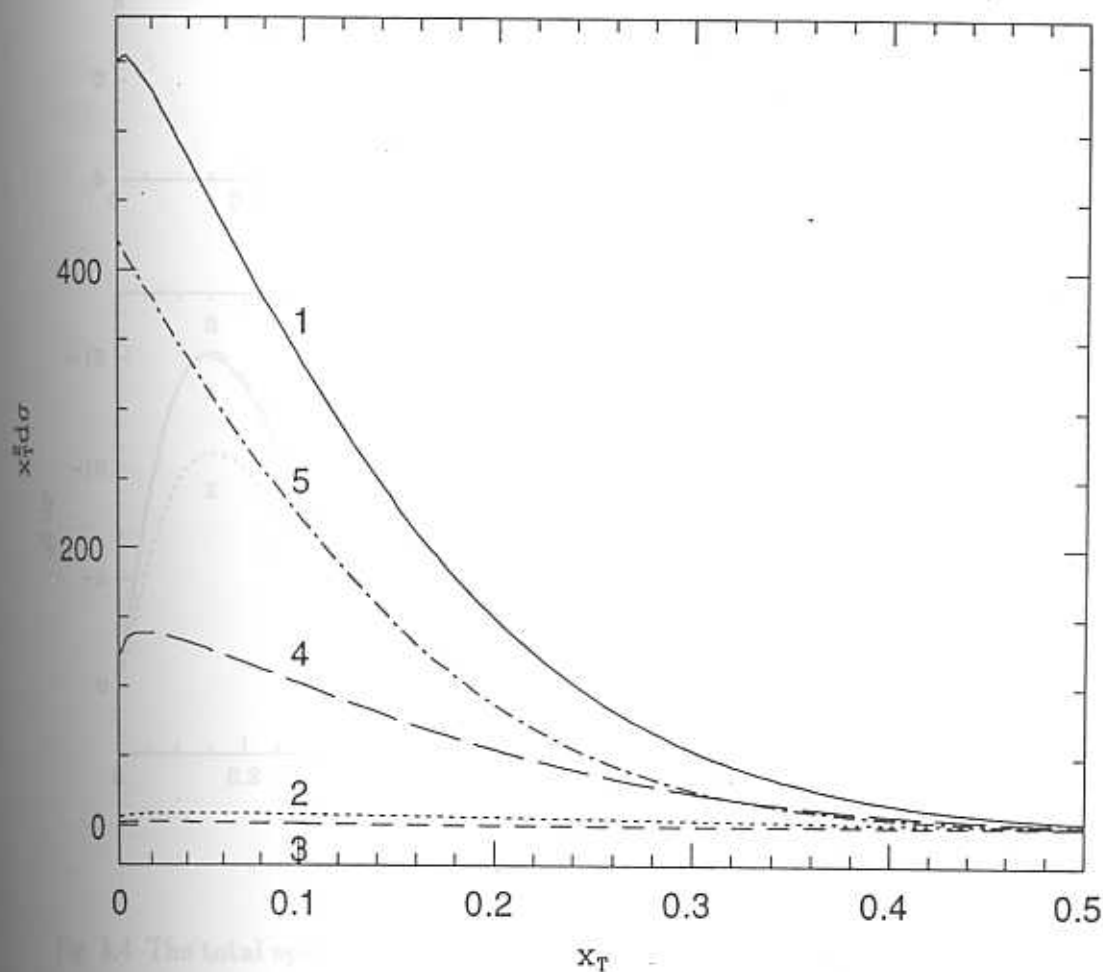


Fig. 5.3 This is the same as Fig. (5.2) for the spin-independent cross-section, $x_T^2 d\sigma$.

Fig. (5.4) shows the same spin-dependent cross-section, $\tilde{d}\sigma$, but this time in comparison with the approximations discussed in Section 5.1. Fig. (5.5) shows the same for the spin independent cross-section.

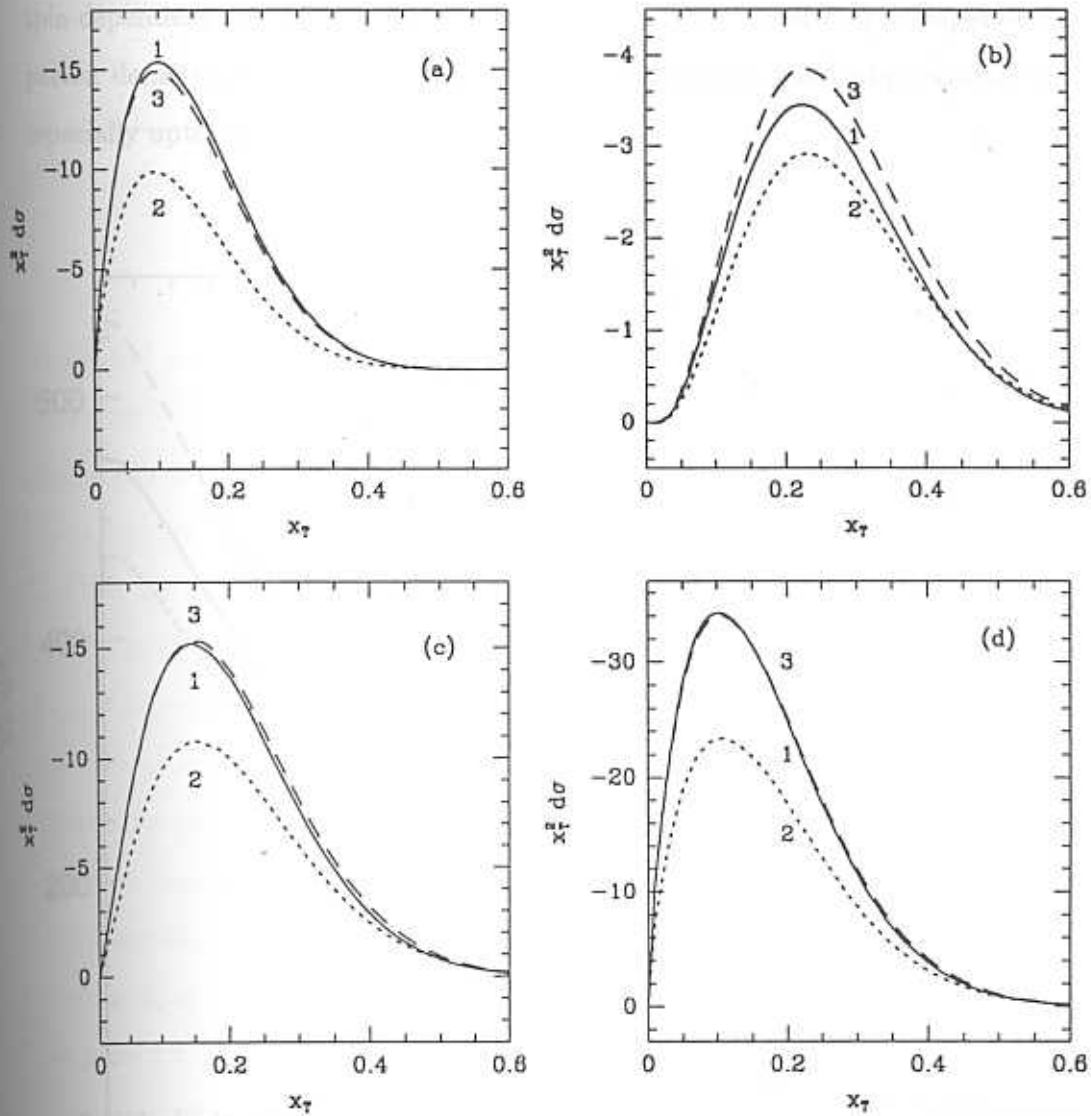


Fig. 5.4 The total spin-dependent cross-section shown in Fig. (5.2) is plotted as a function of x_T for different parametrisation of densities. The curves (2) and (3) correspond to the use of eqs. (5.9) and (5.10) respectively for \tilde{P} in eq. (5.8) and are the two approximations to curve (1), which is the total cross-section.

We see that both approximations, eq. (5.9) (Cambridge Maxwell choice) as well as eq. (5.10) for the generic parton density fit the spin independent cross-section quite well; however, the latter provides an excellent fit to the spin dependent cross-section (see also Table 5.2). A fit of this kind to the spin-dependent jet cross-sections will thus yield the generic spin-dependent parton density, $\tilde{P}(x) = \tilde{q}(x) + (C_A/C_F + 1/2) \tilde{g}(x)$ to a good approximation, especially upto $x_T \sim 0.6$.

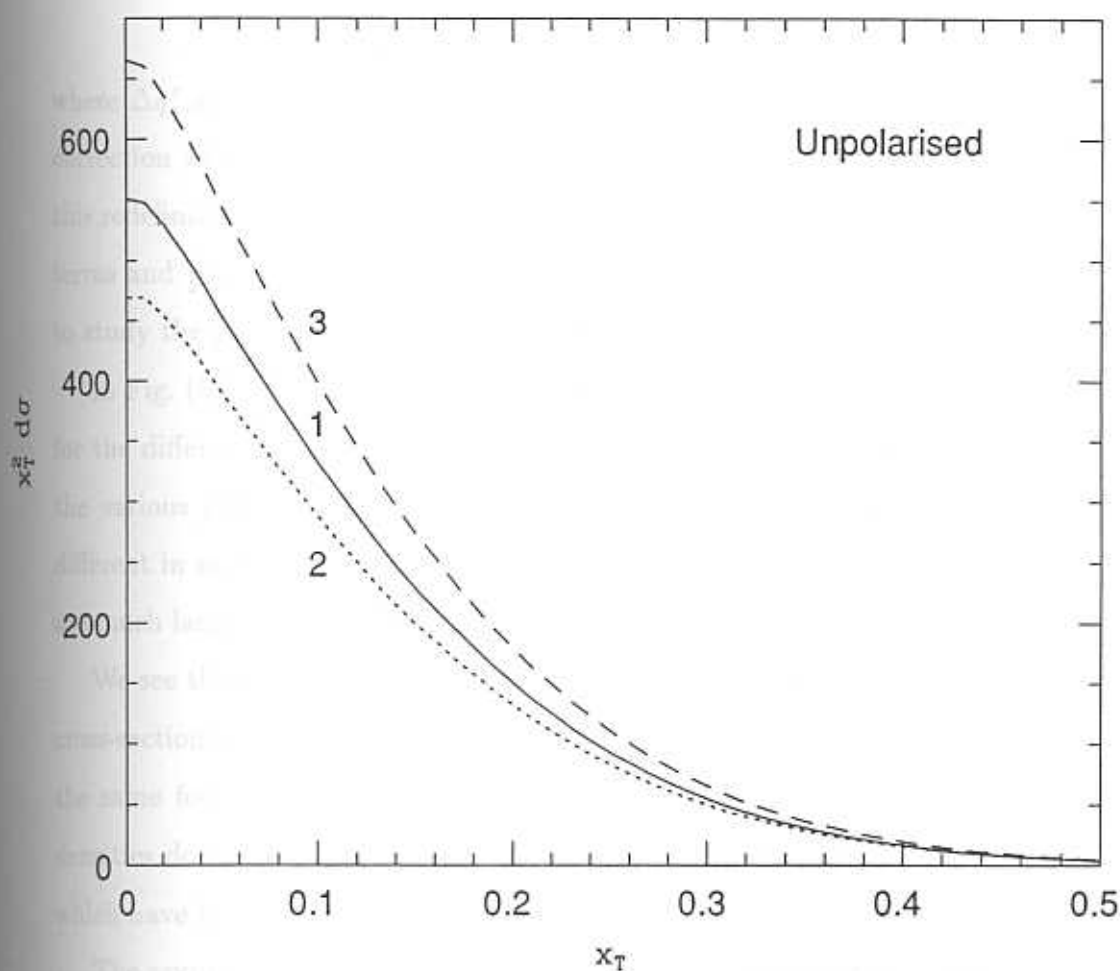


Fig. 5.5 This is the same as Fig. 5.4 for the spin-independent case.

This will therefore simplify the job of extracting the spin-dependent gluon densities from such a measurement. Note that for small values of Δg as is the case in parametrisation type (b), both eqs. (5.9) and (5.10) provide a good fit. However such a cross-section can be identified through its small magnitude in comparison with the other parametrisation sets. At this point, we note that, according to our definition of the parton densities, $\tilde{q}(x)$ automatically carries along with it an order $\mathcal{O}(\alpha_s)$ gluonic correction; this is usually referred to as a reinterpretation of the spin content of the quarks [16]:

$$\Delta q \equiv \Delta q' - \frac{\alpha_s}{2\pi} \Delta g ,$$

where $\Delta q'$ and not Δq is the true quark spin contribution. However, such a correction will not affect the jet results. This is because the gluon term from this redefinition will just be a next-to-leading order correction to the qg or gg terms and will be small. This is the big advantage of using 2-jet production to study the gluon spin-dependent density.

In Fig. (5.6), we plot the total asymmetry, $A = \tilde{d}\sigma/d\sigma$ as a function of x_T for the different parametrisations. Notice the tremendous difference between the various curves. Also, though the asymmetries themselves are not very different in magnitude from the $D\gamma$ or DY ones, recall that the cross-sections are much larger in the 2-jet process.

We see that the large- x asymmetries tend to equalise. This is because the cross-sections are mostly determined by the quark densities which are about the same for all the parametrisations at large- x values (where the valence densities dominate) and are thus independent of the gluon and sea densities which have become negligible in this region.

The asymmetry in the intermediate- x region, however, varies considerably depending on the type of parametrisation. For types (b), (c) and (d), which have a positive Δg , we see that the larger the Δg , the larger is the asymmetry. Hence, large asymmetries in this x_T region in 2-jet production experiments typically indicate the presence of a large 'anomaly-like' contribution in the

expression for G_1^p . Type (a), on the other hand, with a negative Δg , depends on the magnitude of Δg . The $g-g$ term always dominates upto $x_T \sim 0.2$. In this region, a small- Δg parametrisation resembles Type (b), while a large- Δg resembles Type (c). However, for larger x_T values, the $q-g$ term begins to compete with the $g-g$ term and the asymmetry becomes very small on account of their opposing signs. Here, although the asymmetry may become negative, it never becomes large.

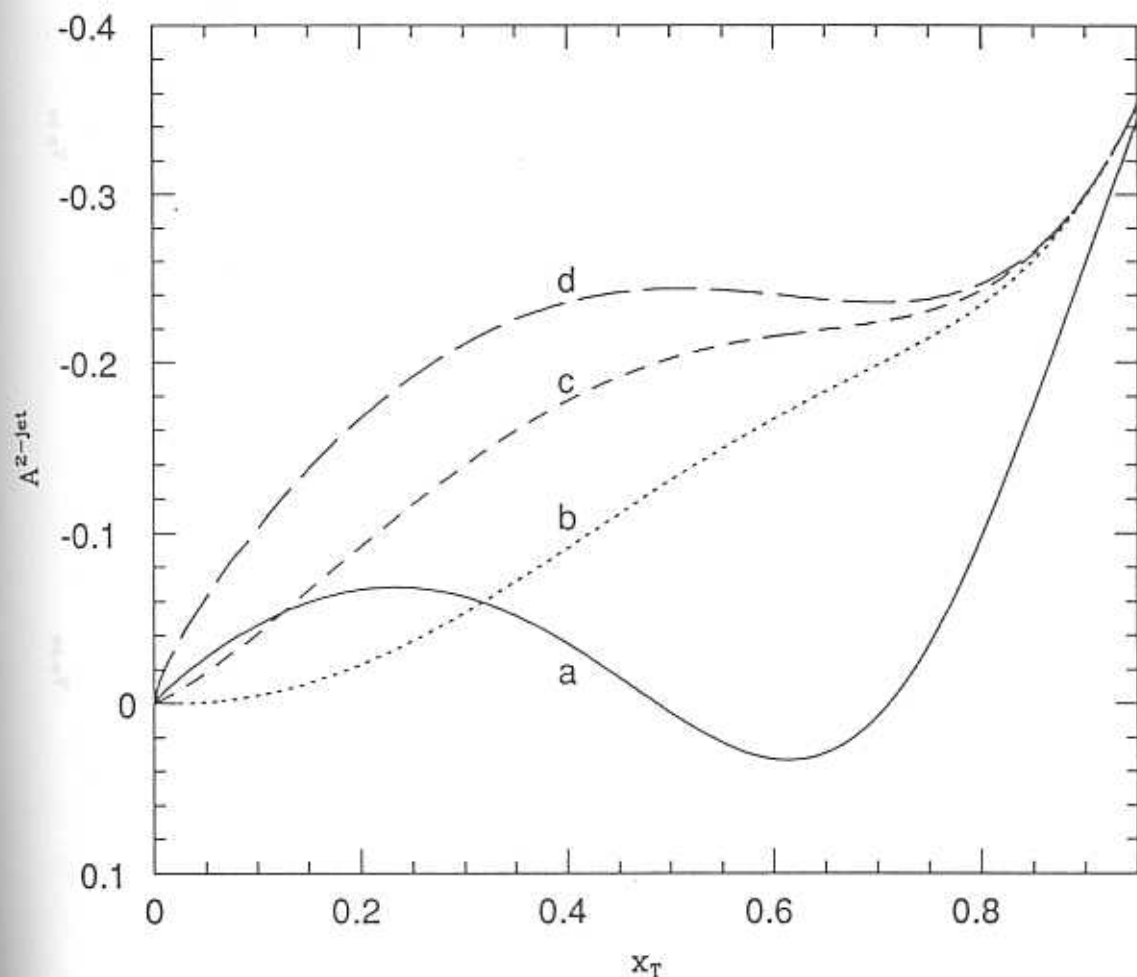


Fig. 5.6 The total asymmetry in 2-jet production is plotted vs x_T for different parametrisations as set up in Chapter 2. The curves labeled (a)-(d) refer to Type (a)-(d) parametrisations respectively.

In Fig. (5.7), we have plotted the total asymmetry as well as the approximations due to Cambridge-Maxwell and its variations (see Table 5.1). As expected, the fit is good in the intermediate x_T region upto $x_T \sim 0.6$, after which, the poorness of the approximation for the $q-q$ case causes it to deviate from the true curve.

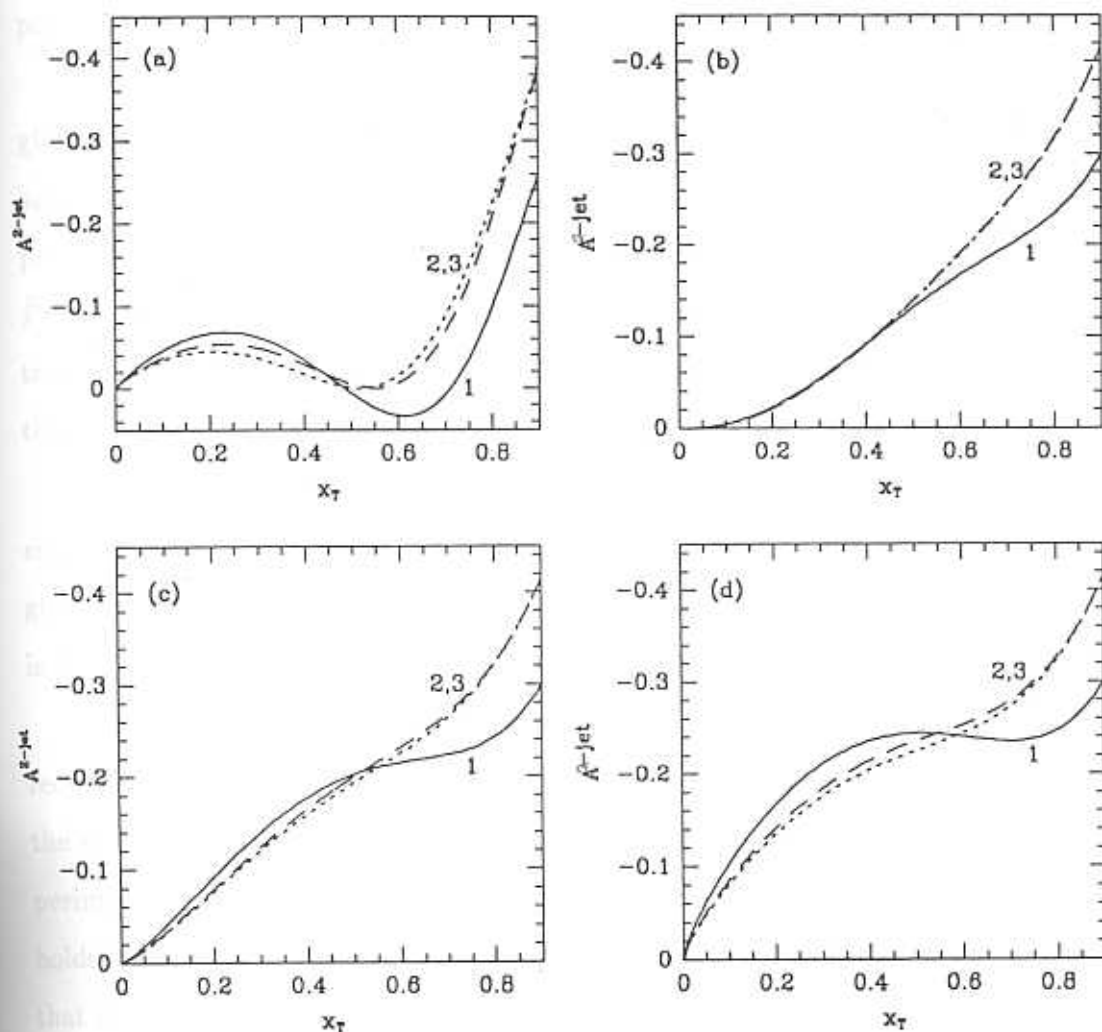


Fig. 5.7 The Cambridge Maxwell approximations for the asymmetry in 2-jet production for different parametrisation of the densities. Notice that this holds only in the region, $x_T \leq 0.6$. The labels are the same as in Fig. 5.5, where curve (1) is the total asymmetry.

To sum up, a large, positive asymmetry in the experimentally accessible region upto $x_T \sim 0.6$ constitutes a clear, unambiguous signal for the existence of a large gluon polarisation. A small value of the asymmetry (≤ 0.1) cannot distinguish the two cases, while a negative asymmetry anywhere in the x_T domain indicates that Δg is negative but may not be able to fix the magnitude of Δg or provide any information on the gluon spin-dependent parametrisation. In any case, the 2-jet production asymmetry can be expected to be mostly positive, or, if negative, small in magnitude.

Hence the asymmetry in 2-jet production can yield information on the gluon spin-dependent density. We also have extended the work of Cambridge and Maxwell to the spin-dependent sector; applying this, we see that this process yields a measurement of the generic spin dependent parton density, $\tilde{P}(x) = \tilde{q}(x) + (C_A/C_F + 1/2)\tilde{g}(x)$, to a good approximation. This is especially true in the small- x region, $x_T \leq 0.3$ where \tilde{g} dominates and thus complements the results of the previous chapter.

We however stress that these parametrisations and corresponding conclusions are only indicative of the character of the problem; the result that the gluon contribution forms a significant part of the 2-jet production cross-section is true, *independent* of the specific form of parametrisation.

At this point, we note that 2-jet production in polarised pp collisions has recently been discussed by several others [17]. However, none of them discusses the crucial issue of actually extracting the gluon densities from such an experiment. By demonstrating that a Cambridge-Maxwell type of factorisation holds in the spin dependent case also, we pin down a specific combination, viz., that in eq. (5.8), that is effectively measured to a good accuracy in this experiment. If such a factorisation is not assumed, there exist so many significant contributions in different kinematical regions that disentangling of the various terms and extraction of the gluonic (or any other) density is an almost hopeless task. Since one does not *a priori* know the magnitude of the gluon density, there is no justification for arbitrarily ignoring terms coming from quark-quark

or quark-gluon interactions. The point that really needs to be emphasised is that the gluonic terms not only appear at the *same order* in α_s as the quark terms (unlike in the DIS experiment of the EMC), but also that Δq and $\alpha_s \Delta g$ are comparable in magnitude. Ramsey, Richard and Sivers in ref [18] *do* use the Cambridge Maxwell technique of reexpressing the cross-section in terms of the universal densities; unfortunately, as the EMC data was not yet available, they did not consider the possibility of a large gluon contribution.

Num:

The

6.0

in the

at large

cross-

photon

studio

to this

photon

the rel

that (4)

inform

6.1.1

We are

The con

THE SEA DENSITIES

CONTENTS

The Direct Diphoton process

Formalism

Numerics

The $p\bar{p}$ process**6.0 The Direct Diphoton process**

In this Chapter, we study the process of direct double photon production at large transverse momentum in polarised pp collisions. The spin-averaged cross-section for this process is much smaller than for the corresponding single photon process. Nevertheless, this process has already been observed and studied in the unpolarised case [19]. There are potentially large backgrounds to this process coming from bremsstrahlung off quarks involved in the single photon process. Here, we assume that these corrections can be made and that the relevant hard-scattering cross-section can be extracted. We demonstrate that [4], atleast in some kinematic domains, this process is capable of providing information on the spin dependent sea quark densities.

6.1 Formalism

We are interested in the hadronic 2-photon production process,

$$\vec{p} + \vec{p} \rightarrow \gamma + \gamma + X .$$

The contributing subprocesses are shown in Fig. (6.1) . These are

$$q\bar{q} \rightarrow \gamma\gamma ;$$

$$gg \rightarrow \gamma\gamma .$$

Again, both processes are of the $2 \rightarrow 2$ type and the entire procedure developed in Chapter 4 can be carried through here. We see that the former (annihilation) subprocess is identical to that in single photon production with the gluon being replaced by a photon in the final state. Hence the cross-section for this process is the same, apart from charge and colour factors.

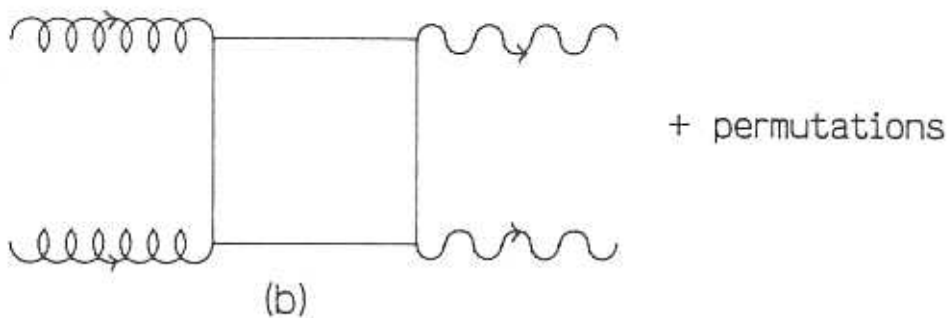
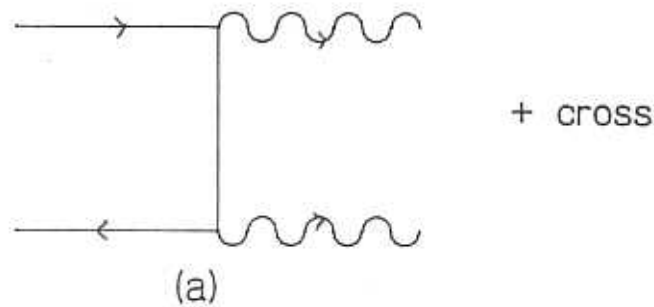


Fig. 6.1 This shows the leading order large- p_T subprocesses contributing to the direct diphoton process.

Putting in the right charge (e_f^4) and colour ($C_F = 3$) factors gives the annihilation contribution to the diphoton ($\gamma\gamma$) process:

$$\frac{d\hat{\sigma}^A}{dt}(\lambda, \lambda') = \sum_f e_f^4 \frac{\pi\alpha^2}{s^2} \frac{2}{3} (1 - \lambda\lambda') \left(\frac{\hat{u}}{\hat{t}} + \frac{\hat{t}}{\hat{u}} \right), \quad (6.1)$$

where λ and λ' are the helicities of the quark and antiquark and \hat{s} , \hat{t} and \hat{u} are the subprocess Mandelstam variables.

As usual, we are interested in the combinations

$$\begin{aligned} d\hat{\sigma}^\alpha &\equiv \frac{d\hat{\sigma}}{dt}(+-) + \frac{d\hat{\sigma}}{dt}(++); \\ \widetilde{d\hat{\sigma}}^\alpha &\equiv \frac{d\hat{\sigma}}{dt}(+-) - \frac{d\hat{\sigma}}{dt}(++) , \end{aligned} \quad (6.2)$$

for the subprocesses, $\alpha = A, G$. These are listed in Table 6.1.

The second contribution comes from the "box diagram" and is somewhat more complicated owing to the fermion loop-integration required.

α	$d\hat{\sigma}^\alpha$	$\widetilde{d\hat{\sigma}}^\alpha$
A	$\frac{4}{3} \left(\frac{u}{t} + \frac{t}{u} \right)$	$\frac{4}{3} \left(\frac{u}{t} + \frac{t}{u} \right)$
G	$\left[\frac{1}{8} (A_1^2 + A_2^2 + A_{2'}^2) + \frac{1}{2} (A_1 + A_2 + A_{2'}) + \frac{\pi^2}{2} (A_3^2 + A_{3'}^2) + 4 \right]$	$\left[-\frac{1}{8} (A_1^2 - A_2^2 - A_{2'}^2) - \frac{1}{2} (A_1 - A_2 - A_{2'}) + \frac{\pi^2}{2} (A_3^2 + A_{3'}^2) \right]$
where $A_1 = 2 \frac{t-u}{s} \ln \left(\frac{t}{u} \right) + \frac{t^2+u^2}{s^2} \left\{ \ln^2 \left(\frac{t}{u} \right) + \pi^2 \right\};$ $A_2 = 2 \frac{s-t}{u} \ln \left(\frac{-s}{t} \right) + \frac{s^2+t^2}{u^2} \ln^2 \left(\frac{-s}{t} \right);$ $A_3 = \frac{s-t}{u} + \frac{s^2+t^2}{u^2} \ln \left(\frac{-s}{t} \right);$ $A_{2'} = A_2 (t \leftrightarrow u);$ $A_{3'} = A_3 (t \leftrightarrow u).$		

Table 6.1 The cross-sections, $d\hat{\sigma}^\alpha$ and $\widetilde{d\hat{\sigma}}^\alpha$, as defined in eq. (6.2) for the processes $\alpha = A, G$. The cross-sections are expressed in units of $\pi\alpha^2/\hat{s}^2$ for $\alpha = A$ and in units of $(\sum_f e_f^2)^2(\alpha^2\alpha_s^2/4\pi\hat{s}^2)$ for $\alpha = G$ and f runs over the flavours u, d, s, c of the virtual quark in the loop. Carets on the subprocess variables have been dropped for clarity.

There are six contributing diagrams (permutations of Fig. (6.1b)) contributing to this cross-section, which can be expressed as

$$\frac{d\hat{\sigma}^G}{dt} = \left[\frac{\alpha^2 \alpha_s^2}{16\pi \hat{s}^2} \right] \left[\text{Tr} \frac{\lambda^a \lambda^b}{2} \right]^2 \frac{1}{8^2} \left[\sum_f e_f^2 \right]^2 |M|^2. \quad (6.3)$$

The first factor in square brackets is the usual kinematical factor for a $2 \rightarrow 2$ process, the second is the colour factor which evaluates to 2, a factor (1/8) is included for each gluon in the initial state (colour averaging) and the last quantity in square brackets is the flavour factor. Finally, the matrix element, M , for different helicity combinations, (h, h') , of the initial state gluons (with final state helicities summed over) is given by [20]

$$\begin{aligned} M_{++}^2 &= M_1^2 + 3 M_3^2; \\ M_{+-}^2 &= M_2^2 + M_2'^2 + 2 M_3^2, \end{aligned}$$

where

$$\begin{aligned} M_1 &= -4 \left[2 + 2 \frac{\hat{t} - \hat{u}}{\hat{s}} \ln \frac{\hat{t}}{\hat{u}} + \frac{\hat{t}^2 + \hat{u}^2}{\hat{s}^2} \left\{ \ln^2 \left(\frac{\hat{t}}{\hat{u}} \right) + \pi^2 \right\} \right]; \\ M_2 &= -4 \left[2 + 2 \frac{\hat{s} - \hat{t}}{\hat{u}} \ln \left(\frac{-\hat{s}}{\hat{t}} \right) + \frac{\hat{s}^2 + \hat{t}^2}{\hat{u}^2} \ln^2 \left(\frac{-\hat{s}}{\hat{t}} \right) \right] \\ &\quad + 8i\pi \left[\frac{\hat{s} - \hat{t}}{\hat{u}} + \frac{\hat{s}^2 + \hat{t}^2}{\hat{u}^2} \ln \left(\frac{-\hat{s}}{\hat{t}} \right) \right]; \\ M_2' &= M_2 (\hat{t} \leftrightarrow \hat{u}); \\ M_3 &= 8. \end{aligned} \quad (6.3a)$$

Within the approximation used, the gg cross-section seems to diverge as $\hat{t}, \hat{u} \rightarrow 0$. This is because we have neglected the parton masses. However, this is a problem only at $\phi \rightarrow 0^\circ, 180^\circ$, which does not come under the purview of "large p_T processes;" this, in fact, corresponds to forward (or backward) scattering. Hence, we shall not worry about regulating this cross-section.

We should point out that the box diagram is "down" by a factor of α_s^2 compared to the $q\bar{q}$ contribution. There is a similar diagram, $gg \rightarrow g\gamma$, that can contribute to the single photon cross-section, and which is also down by a factor of α_s^2 when compared to the diagrams we have considered for this case. However, we neglected this contribution to the single photon case as the total cross-section includes a folding over with the incident parton density

distributions. This results in an expression which is like $\alpha_s (\alpha_s \times g)^2$ for the 3-gluon box diagram and is like $(\alpha_s \times g)^2$ for the 2-gluon box diagram. Since the evolution equations for the spin dependent densities evolve such that $\alpha_s \Delta g$ is approximately constant, the 3-gluon cross-section is seen to be further down by a factor of α_s , and we feel justified in dropping it. Strictly speaking, however, we are discussing density distributions and *not* their moments for which the above statement is valid, but even if we do a naïve α_s count, this diagram still remains sub-dominant.

Coming back to the process of interest, namely, the 2-gluon box diagram, again, we are interested in the sum and difference cross-sections, $d\hat{\sigma}^G$ and $\widetilde{d\hat{\sigma}}^G$. These are listed in Table 6.1 .

Finally, we put in the structure function factors:

$$\begin{aligned} H_0(x_1, x_2) &= \sum_f e_f^4 \left(q^P(x_1) \bar{q}^T(x_2) + \bar{q}^P(x_1) q^T(x_2) \right); \\ G(x_1, x_2) &= g^P(x_1) g^T(x_2) \end{aligned}$$

The corresponding spin dependent quantities are

$$\begin{aligned} \widetilde{H}_0(x_1, x_2) &= \sum_f e_f^4 \left(\tilde{q}^P(x_1) \tilde{\bar{q}}^T(x_2) + \tilde{\bar{q}}^P(x_1) \tilde{q}^T(x_2) \right); \\ \widetilde{G}(x_1, x_2) &= \tilde{g}^P(x_1) \tilde{g}^T(x_2). \end{aligned}$$

Notice that the cross term which appeared in the $D\gamma$ and DY processes discussed in Chapter 4 (for the compton diagram) does not appear here as the structure function factors are the same: $d\hat{\sigma}^G$ is symmetric with respect to $\hat{i} \leftrightarrow \hat{u}$. We can now write down the asymmetry in this process,

$$A^{\gamma\gamma} = \frac{\widetilde{H}_0 \widetilde{d\hat{\sigma}}^A + \widetilde{G} \widetilde{d\hat{\sigma}}^G}{H_0 d\hat{\sigma}^A + G d\hat{\sigma}^G}. \quad (6.4)$$

As before, we study the back-to-back geometry in order to simplify the kinematics. We restrict ourselves to the central rapidity region ($y_1 = y_2 = 0$). Then $x_1 = x_2 = x_T = x$. In this configuration, the structure function factors can be re-written as

$$\begin{aligned} H_0(x) &= \frac{2}{81} [(16u_V + d_v) \sigma + (17 + \eta^2) \sigma^2] \\ &\simeq \frac{2}{81} (16u_V(x) + d_V(x)) \sigma(x) \end{aligned}$$

if we neglect squares of the sea densities, while the structure function factor for the box diagram is

$$G(x) = g^2(x).$$

While the annihilation subprocess cross-section for the unpolarised case (which is half of $d\tilde{\sigma}^A$) is much larger than that of the box diagram due to kinematical factors, it was observed [21], [20] that the parton densities compensate a great deal for this difference in the overall hadronic cross-section, *i.e.*, the box diagram cannot be neglected in comparison with the annihilation graph. As a result, no single diagram dominates the unpolarised cross-section.

In the asymmetry in eq. (6.4)), \bar{g} appears as a square, $\tilde{g}^2(x)$; hence the asymmetry is insensitive to the *sign* of $\tilde{g}(x)$. Even when $x_1 \neq x_2$, since the spin dependent gluon density $\tilde{g}(x)$ for a given parametrisation type has the same sign for all x , the quantity $\tilde{G}(x_1, x_2) = \tilde{g}(x_1)\tilde{g}(x_2)$ is always positive. On the other hand, H_0 contains a product of an overwhelmingly positive valence density and the spin dependent sea quark density. Since $\bar{d}\tilde{\sigma}^G$ is negative, while $\bar{d}\tilde{\sigma}^A$ is positive in sign, the asymmetry has effectively a difference of annihilation and box diagrams in the numerator. If both contributions are of the same order (as the unpolarised case seems to indicate) then the asymmetry will be extremely sensitive to the *sign* as well as the magnitude of the spin dependent sea quark contribution as we can write

$$A^{\gamma\gamma} \sim \frac{\bar{u}_v\tilde{\sigma} - \chi\tilde{g}\tilde{g}}{u_v\sigma + \chi g g}, \quad \chi > 0.$$

If $\tilde{\sigma}$ is positive, the asymmetry will be small (nearly zero if the two terms are of the same order) while it will be large and negative if $\tilde{\sigma}$ is negative. We shall study this more carefully in the next section.

6.2 Numerics

We again use the parametrisations for the spin dependent densities developed in Chapter 2 in order to quantify the statements we have made about the asymmetry in direct diphoton production in pp collisions. We use the EHLQ

parametrisation for the spin independent densities and Type 1 parametrisation for the spin dependent ones (see Chapter 2 for details). We first show the unpolarised (half the spin independent) subprocess cross-sections for the annihilation and box diagrams in Fig. (6.2) as a function of the scattering angle $\hat{\phi}$ in the CM of the partons. (These are independent of the parton densities).

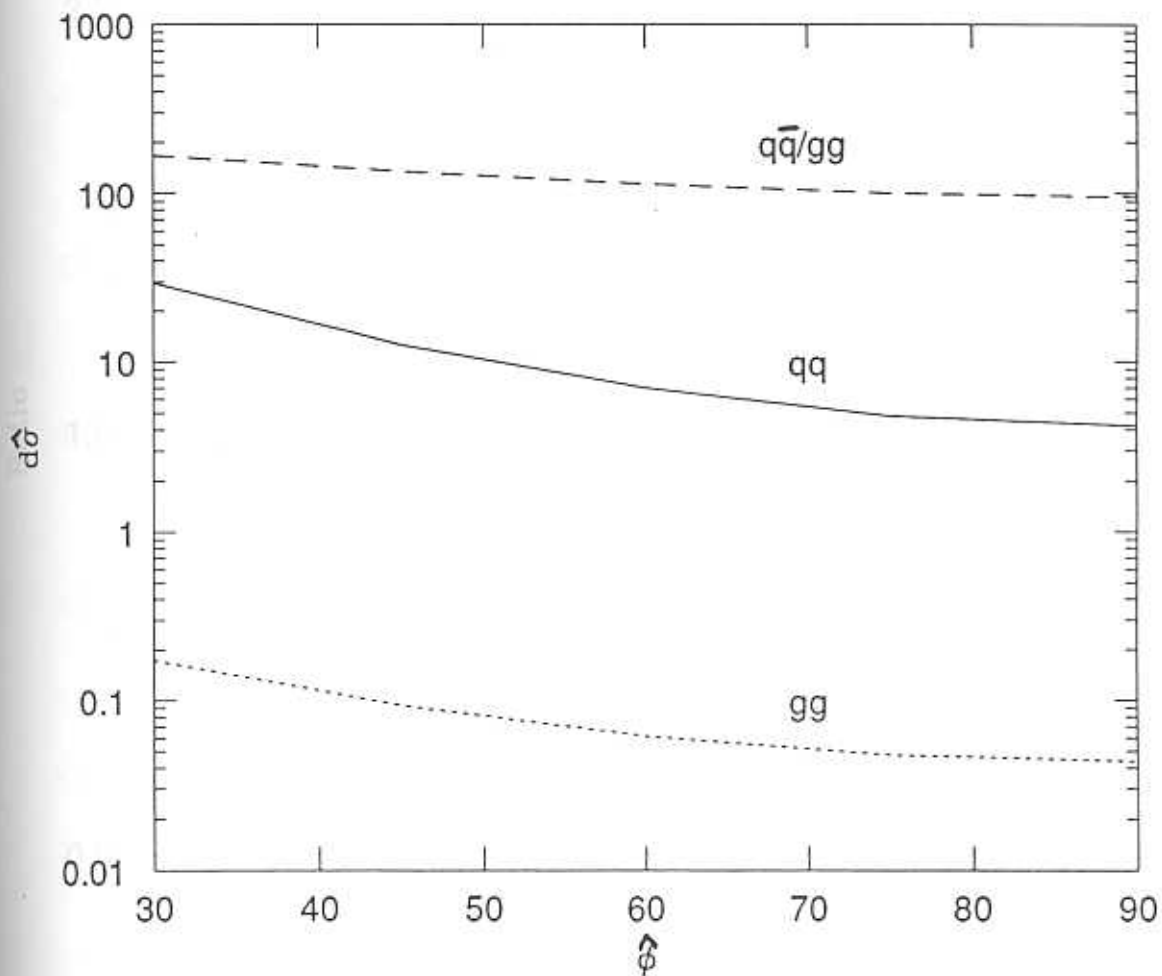


Fig. 6.2 The unpolarised annihilation and box subprocess cross-sections and their ratio are plotted as a function of the scattering angle $\hat{\phi}$.

The annihilation cross-section is about two hundred times the gluonic cross-section for all angles. However, the *contributions* to the hadronic diphoton production cross-section of these subprocesses involves a folding over of the subprocess cross-sections with corresponding parton densities. The ratio of these contributions in the spin independent case is plotted as a function of $x = x_1 = x_2 = x_T$ for different $\hat{\phi}$ in Fig. (6.3). (What is plotted is the ratio of the gluonic to annihilation terms).

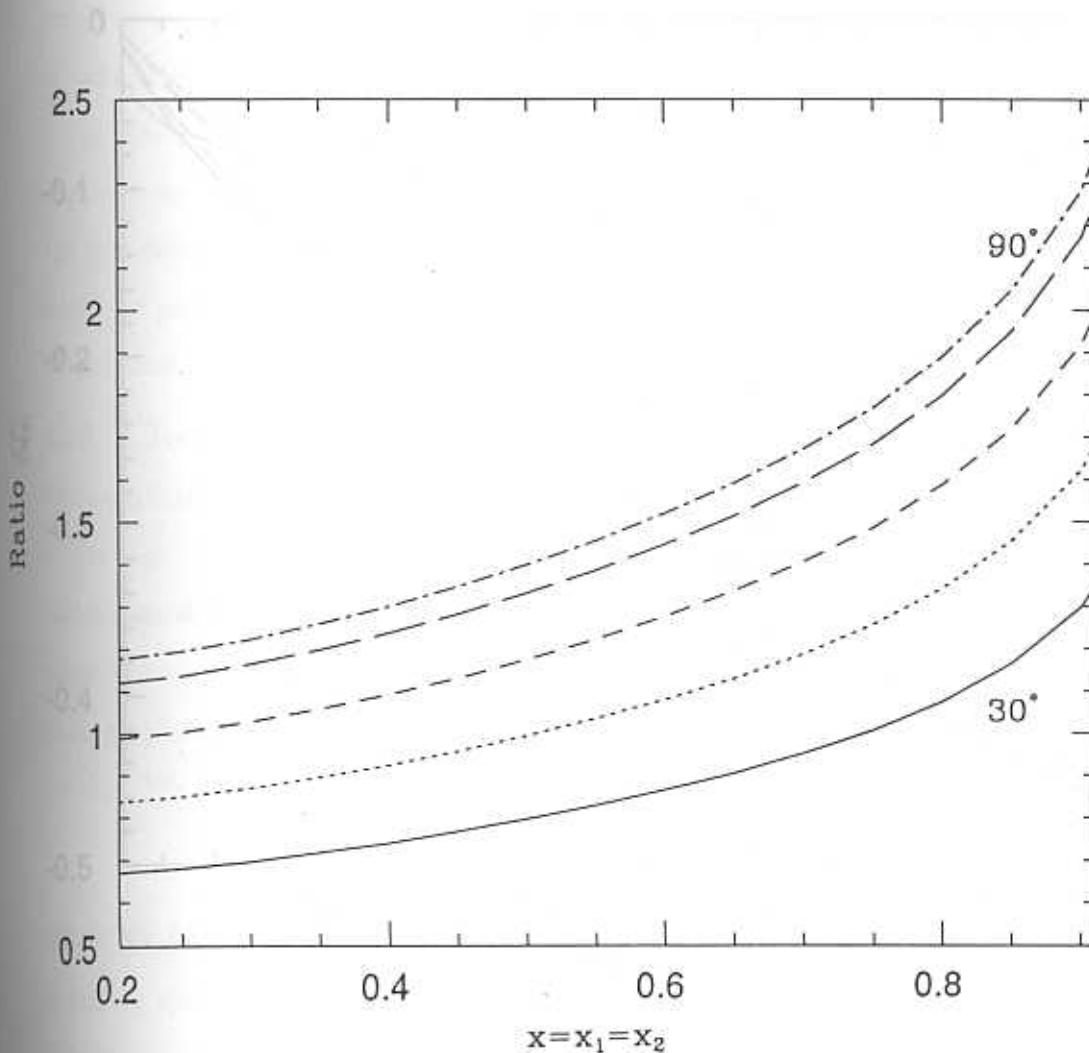


Fig. 6.3 The ratio of the box to the annihilation contribution to the unpolarised hadronic diphoton production cross-section is plotted as a function of x for different scattering angles from 30° to 90° in steps of 15° .

We see that the inclusion of parton densities with the subprocess cross-sections completely changes the result as now, in fact, the gluonic term is larger, although they are of the same order of magnitude. Hence it is not possible to ignore either term in the asymmetry equation. Retaining both terms, the total asymmetry is plotted as a function of x_T for $\hat{\phi} = 90^\circ$ in Fig. (6.4).

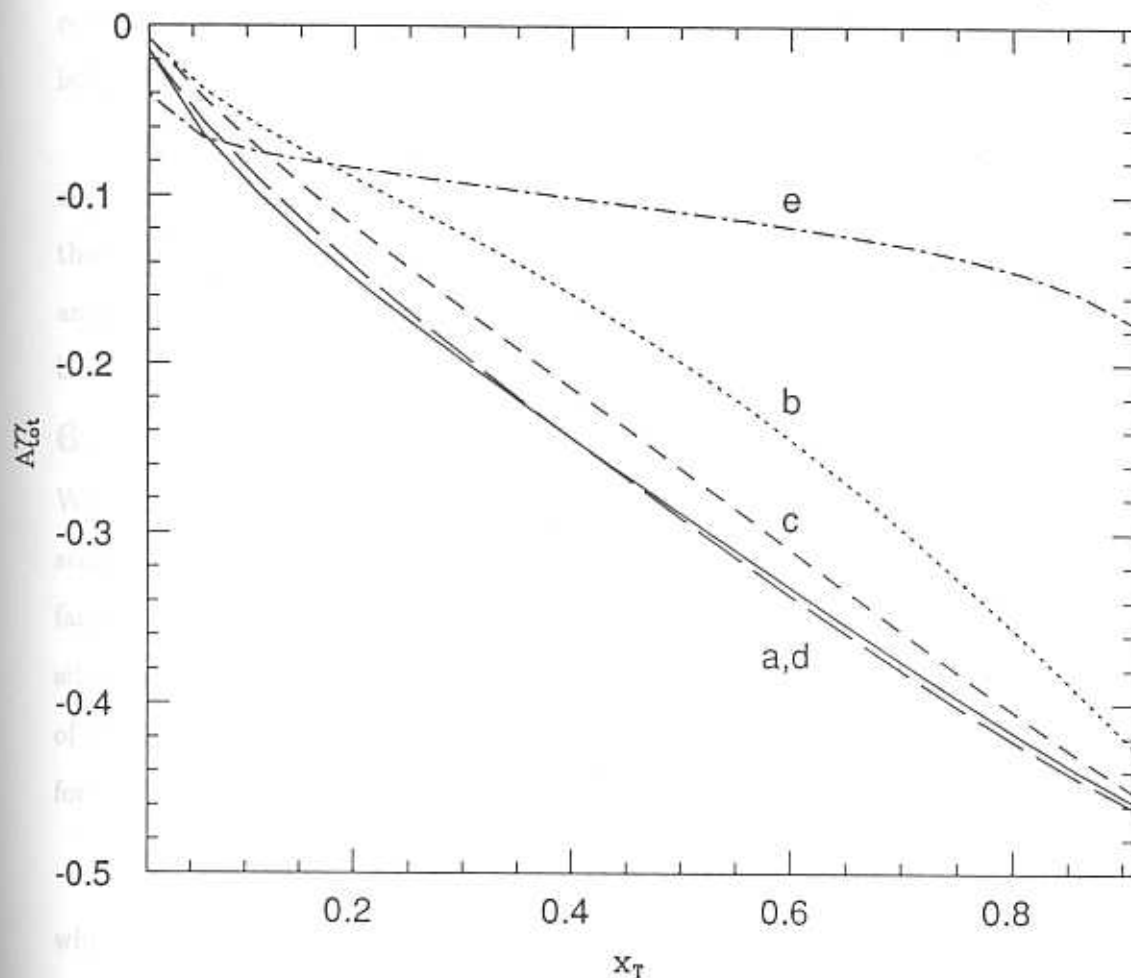


Fig. 6.4 The total asymmetry in $pp \gamma\gamma$ process is plotted as a function of x_T for $\hat{\phi} = 90^\circ$ for spin dependent parametrisation types (a)-(e). Recall that (e) corresponds to positive spin dependent sea density while the rest have negative sea density.

We notice the following interesting behaviour: for the same (negative) sign for the spin dependent sea density, \tilde{u}_s , parametrisations corresponding to a larger $|\Delta g|$ result in larger magnitudes for the asymmetry, while a flip in the sign of \tilde{u}_s to positive causes a sharp fall in the asymmetry to nearly zero (even for large Δg , as seen in curve (e)). Hence small asymmetries in diphoton production signal positive sea quark polarisation. Furthermore, curves (a) and (d) which correspond to parametrisations with large gluon polarisation of opposite signs result in the same value for the asymmetry; this indicates that this asymmetry is insensitive to the sign of the gluon polarisation.

In short, large negative asymmetries in diphoton production indicate large negative sea polarisation and large gluon polarisation of either sign. Knowing the spin dependent gluon density from other experiments such as direct photon and 2-jet production will then enable the spin dependent sea quark density to be extracted from a measurement of the asymmetry in diphoton production.

6.3 The $p\bar{p}$ collision process

We complete this Chapter by discussing diphoton production in polarised $p\bar{p}$ scattering. The subprocess cross-sections remain the same; but the density factors are different. We use charge conjugation symmetry to relate the densities in an antiproton to those in a proton, using eq. (4.20). As in the case of single photon or Drell-Yan production, the only change is in the expression for H_0 . We get

$$H_0(x) \simeq \frac{1}{81} \left\{ (16u_v^2 + d_v^2) + 2(16u_v + d_v)\sigma \right\},$$

where we have dropped terms containing σ^2 as in Chapter 4. The corresponding spin dependent structure function factor, \bar{H}_0 , is given by replacing spin independent densities by corresponding spin dependent ones in the above equation:

$$\bar{H}_0(x) \simeq \frac{1}{81} \left\{ (16\tilde{u}_v^2 + \tilde{d}_v^2) + 2(16\tilde{u}_v + \tilde{d}_v)\bar{\sigma} \right\}.$$

The annihilation term dominates here due to the presence of the valence densities. Hence, the asymmetry can be approximated as the ratio \bar{H}_0/H_0 to a

good accuracy, especially at larger- x values. (Here we have used $x_1 = x_2 = x$. As in the case of Direct Photon and Drell Yan processes, we point out that the approximation to the asymmetry holds without making this choice.) The total asymmetry is plotted as a function of x_T in Fig. (6.5).

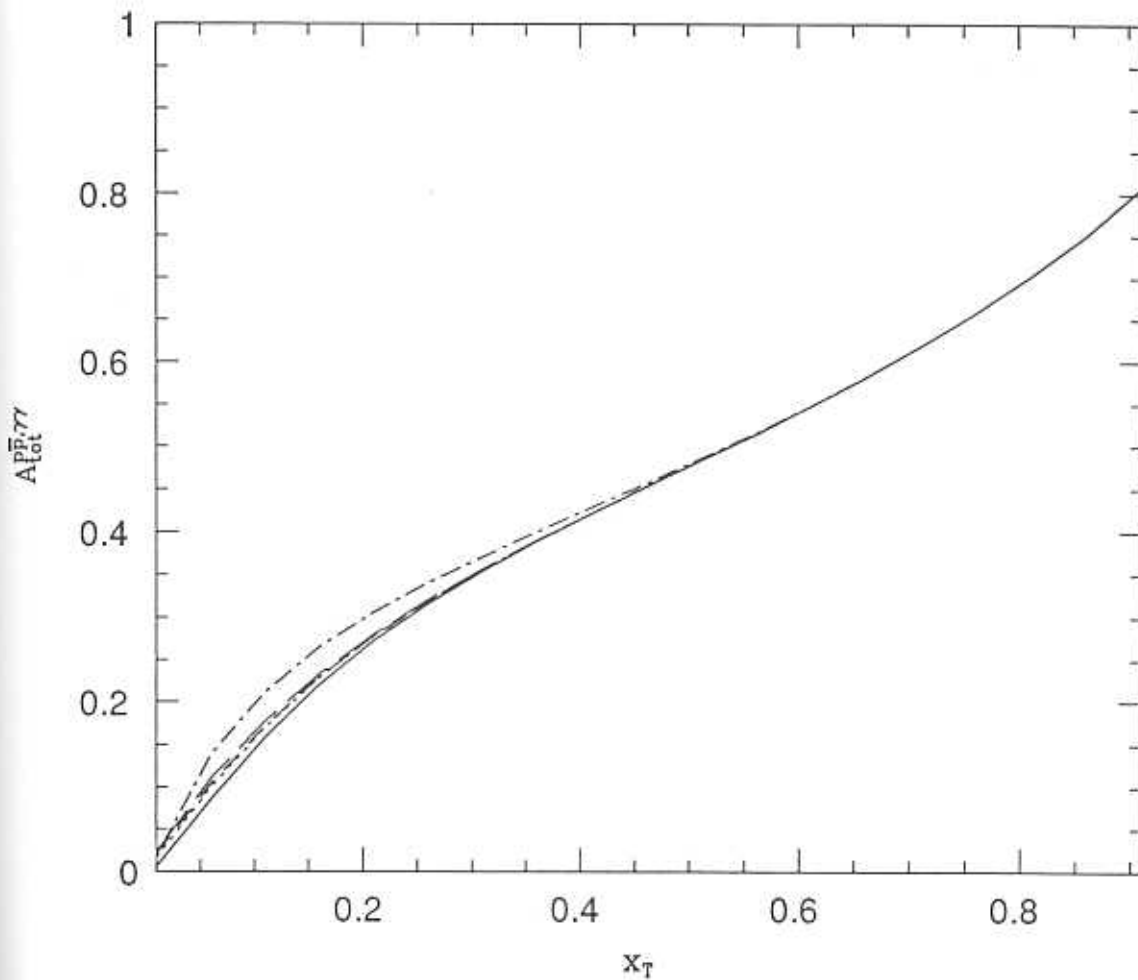


Fig. 6.5 The total asymmetry in $p\bar{p} \gamma\gamma$ process is plotted as a function of x_T for $\hat{\phi} = 90^\circ$ for spin dependent parametrisations type (a)-(e).

The asymmetry is seen to be insensitive to either the sea or the gluon spin dependent parametrisations and is completely dominated by the valence densities over most of the kinematical region. Hence it is a good measure of the spin dependent valence density, especially of the spin dependent valence u -quark density as its contribution is enhanced by a large charge factor (e_u^4).

This concludes our discussion of polarised pp and $p\bar{p}$ collision processes.

pp COLLISION PROCESSES: CONCLUSION

We have studied the cross-sections and the asymmetry in various processes in polarised proton–polarised proton collisions. Recently, FermiLab [10] has measured the asymmetry for π^0 production in such $\vec{p}\vec{p}$ and $\vec{p}\bar{p}$ collisions in fixed-target experiments. Hence we believe that these experiments can be performed in the near future. Though the kinematical region is limited, (unlike in collider experiments, which are, however, difficult to perform), they will certainly be able to probe the intermediate- x_T region, wherein all the interesting physics lies.

Chapter 3 demonstrated that spin dependent valence quark densities can be extracted from semi-inclusive DIS experiments. This then enabled us to select processes which were sensitive to the gluon and sea densities, without the valence densities clouding the issue. Chapters 4–6 were devoted to such a study. All processes that were discussed here are seen to occur in polarised pp and $p\bar{p}$ collisions. In particular, the asymmetry in direct photon and the Drell-Yan process shows a peculiar factorisation in certain highly accessible kinematical regions which directly allows extraction of the spin dependent gluon density, without need for the specific forms of either the valence or the sea quark densities. The inclusive 2-jet production process is equally sensitive to the spin dependent gluon density, though in a different kinematical region. Finally there is the ambivalent di-photon process, which is sensitive to the gluon as well as sea quark densities, although it is more sensitive to the sea quark density.

Experimentally, all these processes have been very well studied in unpolarised pp collisions. We wish to emphasise at this point that a great deal more information is required before results in the spin dependent sector match those in the spin independent sector. Hopefully, the processes listed above will go a long way in deciding some issues like convenient definition of densities at

next-to-leading order and the rôle of gluons in a polarised proton. The sea quark densities will be harder to fix accurately, especially in view of the fact that the only process (direct diphoton production) which is sensitive to it in the leading order is still not entirely dependent on the sea quark alone. In fact, determination of the spin dependent sea quark densities is likely to pose the maximum amount of problem in any scheme of complete determination of polarised parton densities. An alternative process, namely, νp DIS has a cross-section that is directly proportional to the singlet quark density; unfortunately, it is very difficult to obtain mono-energetic neutrino beams so that data from these experiments will have large error bars even though the problems involved in polarising proton beams do not apply here. This is true even in the spin independent case.

We have thus demonstrated a set of processes which, when taken together, will throw more light on the controversies in polarised DIS experiments as well as on the spin content of the nucleon. Although we have used lowest order perturbative QCD cross-sections in this analysis, the results are unlikely to undergo large modifications at higher order. This is because higher order corrections for the unpolarised processes are small at central rapidity [22] ($y = 0$). We expect a similar behaviour for the polarised case also.

Preliminary data in polarised $p\bar{p}$ fixed target experiments has recently been obtained by the FermiLab Collaboration. This leads us to believe that all the experiments involving pp collision processes that we have considered here can be performed shortly.

Finally, we note that apart from the processes we have considered here in order to probe the spin content of the nucleon, other experiments that have been suggested are J/ψ production via both photoproduction [23] as well as leptonproduction [24]. In the former, photon-gluon fusion occurs with the formation of a heavy quark-antiquark pair. The subprocess that contributes is exactly the order $\mathcal{O}(\alpha_s)$ gluonic contribution to the spin dependent structure function, $g_1^p(x)$. Since this is the troublesome quantity in the analysis of the

EMC result, such an experiment would directly probe this quantity and settle once and for all its contribution to the structure function. Note however, that the step from the quark pair production to J/ψ formation is model dependent. Both the suggested J/ψ experiments will be sensitive to the spin dependent gluon density. So also is the charmonium production process recently suggested in ref. [25]. Another process involving gluons is jet production in DIS processes rather than in pp processes. This has been studied in ref. [26].

References

- [1] N. Craigie et al. Phys. Rep. **99** (1983) 69 and references therein
- [2] E. Anasontzis et al. FermiLab preprint, 87/217-E
- [3] S. Gupta, D. Indumathi and M.V.N. Murthy, Z. Phys. **C42** (1989) 493
- [4] S. Gupta, D. Indumathi and M.V.N. Murthy, Z. Phys. **C47** (1990) 227
- [5] K. Hidaka, Nucl. Phys. **B192** (1981) 369; Phys. Rev. **D21** (1980) 1316
H.S. Mani, M. Noman, Phys. Rev. **D24** (1981) 1223
- [6] G. Altarelli, R.K. Ellis and G. Martinelli, Nucl. Phys. **B143** (1978) 521
- [7] Prakash Mathews and V. Ravindran, to appear in the August issue of J. Mod. Phys. Lett. 1992
- [8] Eichten et al. EHLQ, Rev. Mod. Phys. **56** (1984) 579.
- [9] T. Sloan, G. Smadja and R. Voss, Phys. Rep. **162** (1988) 45
- [10] D.L. Adams et al., FNAL E581/704 Collaboration, FermiLab preprint Fermilab-Pub-91/13-16-E.
- [11] E.L. Berger and J. Qiu, Phys. Rev. **D40** (1989) 778
H.Y. Cheng and C. N. Lai, Phys. Rev. **D41** (1990) 91
Prakash Mathews and R. Ramachandran, Z. Phys. **C53** (1992) 409

- [12] D. Indumathi, M.V.N. Murthy and V. Ravindran, preprint, IMSc/91/31, to appear in *Z. Phys. C* 1992
- [13] Yu. L. Dokshitzer, D. I. Dyakanov and S. I. Troyan, *Phys. Rep.* **58** (1980) 269
- [14] J. Babcock, E. Monsay and E. Sivers, *Phys. Rev.* **D19** (1979) 1483
- [15] B.L. Combridge and C.J. Maxwell, *Nucl. Phys.* B239 (1984) 429.
- [16] M. Glück and E. Reya, *Z. Phys* C39 (1988) 569; the smallness of the quark contribution to the proton spin was first discussed here.
C.S. Lam and Bing-An Li, *Phys. Rev.* D25 (1982) 683.
R.D. Carlitz, J.C. Collins and A.H. Mueller, *Phys. Lett.* B214 (1988) 229.
G. Altarelli and G.G. Ross, *Phys. Lett* B212 (1988) 391.
A.V. Efremov and O.V. Teryaev, Preprint JINR EL-88-287.
T.P. Cheng and L.-F. Li, *Phys. Rev. Lett* 62 (1989) 1441.
- [17] S.J. Brodsky, J. Ellis and M. Karliner, *Phys. Lett.* **B206** (1988) 209
H-Y. Cheng, S-R. Hwang and S-N. Lai, *Phys. Rev.* D42 (1990) 2243
C. Bourrely, J.Ph. Guillet and J. Soffer, *Nucl. Phys.* B361 (1991) 72
C. Bourrely, J. Soffer, F.M. Renard and P. Taxil, *Phys. Rep.* 177 (1989) 319
- [18] G.P. Ramsey, D. Richard and D. Sivers, *Phys. Rev.* D37 (1988) 3140
Other work on jet production in polarised $\vec{p} - \vec{p}$ experiments that predates the EMC experiment:
C. Bourrely, J. Soffer and Tai Tsun Wu, *Phys. Rev. Lett.* 59 (1987) 2009
M.B. Einhorn and J. Soffer, *Nucl. Phys.* B274 (1986) 714
P. Chiapetta, J.Ph. Guillet and J. Soffer, *Nucl. Phys.* B262 (1985) 187;
Phys. Lett. B183 (1987) 215

- [19] J.F. Owens, *Rev. Mod. Phys.* **59** (1987) 465 and references therein
- [20] B.L. Combridge, *Nucl. Phys.* **B174** (1980) 243
- [21] E.L. Berger, E. Braaten and R.D. Field, *Nucl. Phys.* **B239** (1984) 52
- [22] P. Aurenche et al., *Z. Phys.* **C29** (1985) 459
- [23] M. Gluck and E. Reya, *Z. Phys.* **C39** (1988) 569
P. Kalyniak, M.K. Sundaresan and P.J.S. Watson, *Phys. Lett.* **B216**
(1989) 397
J. Ph. Guillet, *Z. Phys.* **C39** (1988) 75
B. Lampe, *Phys. Lett.* **B227** (1989) 469
- [24] R.M. Godbole, S. Gupta and K. Sridhar, *Phys. Lett.* **B255** (1991) 120
- [25] R.W. Robinett, *Phys. Rev.* **D45** (1991) 113
- [26] R.D. Carlitz, J.C. Collins and A.H. Mueller, *Phys. Lett.* **B214** (1988) 229

PART II

THE SPIN DEPENDENT
STRUCTURE FUNCTION,
REVISITED

OPE APPROACH TO THE MOMENTS OF THE SPIN DEPENDENT STRUCTURE FUNCTION

C O N T E N T S

The Operator Product Formalism
Effective Equation of Motion
Numerical Estimates of m_{eff}
Model Calculation of Matrix Elements
Conclusions

In this Chapter, we briefly discuss the moments of the spin dependent proton structure function, $g_1^p(x)$, in the operator product expansion (OPE) approach. We find that ratios of successive moments can be expressed so that they are independent of the unknown hadronic matrix elements involved and are therefore calculable. Details of this work can be found in refs. [1], [2], [3].

The operator product expansion predicts logarithmic violations of scaling, which is clearly supported by experiments. In particular, the Q^2 evolution of the moments of the structure functions computed in this framework involve products of hadronic matrix elements of gauge invariant, local operators of well-defined twist and their coefficient functions. While the latter are computed perturbatively in QCD, predictions for the nonperturbative matrix elements do not exist. Consider the two lowest moments of the structure function $g_1(x)$, in $e(\mu)p$ scattering. Their measured values (without including errors) are [4]

$$G_1 \equiv \int dx g_1(x) \simeq 0.126; \quad G_3 \equiv \int dx x^2 g_1(x) \simeq 0.011; \quad \langle Q^2 \rangle \simeq 10 \text{ GeV}^2 .$$

In fact, in both the polarised as well as the unpolarised case, the ratio of successive moments is around 0.1. We show that the ratios of successive moments

can be written as m_{eff}^2/M_p^2 , where M_p is the proton mass and m_{eff} is some dynamically generated quark mass. Substituting the relevant numbers, we find this mass to be of the order of 300 MeV, which is very close to the constituent quark mass. We support our statements using a simple bag model.

7.1 The OPE Formalism

We start with the expression for the hadronic tensor that we have defined earlier:

$$\begin{aligned} W_{\mu\nu} &\equiv \frac{1}{2\pi M_p} \int d^4y e^{iq \cdot y} \langle p, S | [j_\mu(y), j_\nu(0)] | p, S \rangle \\ &\equiv W_{\mu\nu}^S + W_{\mu\nu}^A. \end{aligned} \quad (7.1)$$

Here p and S are the momentum and spin of the proton, q is the momentum transfer at the hadronic vertex and j_μ is the electromagnetic current. Using Wilson's OPE, the nonlocal product of two electromagnetic currents can be expanded near the light cone ($y^2 \sim 0$) leading to separation of the perturbatively calculable "Wilson coefficient" functions and unknown, renormalised operators in the theory. Hence, the matrix element in eq. (7.1) can be expressed in terms of singular, calculable coefficients and nonperturbative matrix elements of local operators in the theory. We are interested in the moments of the spin dependent structure function that appears in the expression for $W_{\mu\nu}^A$ (see Appendix C). These moments, which are taken with respect to the Bjorken variable, defined as $x = (Q^2/2\nu)$, are expressed in the OPE as

$$\begin{aligned} G_n^{NS}(Q^2) &\equiv \int dx x^{n-1} g_1^{NS}(x, Q^2) = \frac{1}{2} \sum_i a_n^{i,NS} E_{1,i}^{n,NS}(Q^2, g); \\ G_n^S(Q^2) &\equiv \int dx x^{n-1} g_1^S(x, Q^2) = \frac{1}{2} \sum_i a_n^{i,S} E_{1,i}^{n,S}(Q^2, g); \quad n \text{ odd}, \end{aligned}$$

where the superscripts NS and S (which have different behaviour under Q^2 evolution) refer to the non-singlet and singlet contributions respectively [5]. We have not outlined the details of calculation of this result. For our purposes it suffices to know that the E^i are the calculable perturbative coefficient functions (of Q^2 and the QCD coupling constant g). The hadronic matrix elements are contained in the $a_{n,i}$ for different relevant local operators in the theory, of

correct dimension and twist. Furthermore, in the asymptotic limit,

$$\lim_{Q^2 \rightarrow \infty} E_{1,i}^n(Q^2, g=0) = 1 ,$$

so that in the leading order, the combined singlet and non-singlet moment is

$$G_n \equiv \int dx x^{n-1} g_1(x) = \frac{1}{2} \sum_{i=1}^f e_i^2 a_{n,i}(\mu^2) ; \quad i = u, d, s . \quad (7.2)$$

The matrix elements of the local operators which are renormalised at the scale μ^2 are defined as follows:

$$\langle p, S | i^{n-1} \bar{\psi}_i \gamma_5 \{ \gamma^{\mu_1} D^{\mu_2} \dots D^{\mu_n} \} \psi_i | p, S \rangle = -\alpha_n^i \{ S^{\mu_1} p^{\mu_2} \dots p^{\mu_n} \} , \quad (7.3)$$

where $(\{ \dots \})$ implies symmetrisation over the enclosed indices and D^μ is the gauge covariant derivative. In eq. (7.3) we have neglected less divergent terms containing operators like $g^{\mu_1 \mu_2}$, etc., as their contribution will be suppressed in the scaling limit. Using eq. (7.3), we obtain for the first two moments of g_1 (i.e., G_1 and G_3 for $n = 1, 3$),

$$\begin{aligned} G_1 &= -\frac{1}{2} \frac{S^\mu}{S^2} \sum_i e_i^2 \langle p, S | \bar{\psi}_i \gamma_5 \gamma_\mu \psi_i | p, S \rangle ; \\ G_3 &= \frac{S^\mu}{2S^2 M_p^2} \sum_i e_i^2 \left[\langle p, S | \bar{\psi}_i \gamma_5 (\gamma_\mu D^2 + \not{D} D_\mu + D_\mu \not{D}) \psi_i | p, S \rangle \right] . \end{aligned} \quad (7.4)$$

In obtaining eq. (7.4) we have made use of the fact that $p^2 = M_p^2$ and $S \cdot p = 0$, where M_p is the proton mass.

7.2 Effective equation of Motion

Our aim is to obtain the ratios of moments. We do not, at this stage, know how to compute the hadronic matrix elements in eq. (7.4). In order to proceed, we introduce the effective equation of motion,

$$\left(i \not{D} - m_{\text{eff}}^i(\mu^2) \right) \psi_i = 0 ; \quad \left(\partial^2 + \left[m_{\text{eff}}^i(\mu^2) \right]^2 \right) \psi_i = 0 , \quad (7.5)$$

where $m_{\text{eff}}^i(\mu^2)$ is the effective mass of the i -th quark evaluated at the same scale μ^2 at which the operator in the hadronic matrix element is renormalised. We henceforth replace the covariant derivatives by ordinary derivatives. We

assume that at this scale all effects of interactions may be included in m_{eff} . In taking this step, we are guided by the spirit of quark model calculations with "constituent quarks." In fact, the m_{eff} appearing in this equation hides our ignorance or inability to calculate the soft gluon contributions which probably dominate the non-perturbative matrix elements. We thus anticipate that this m_{eff} will be of the order of the dynamical quark mass, rather than the current quark mass, just as in the case of the spontaneous chiral symmetry breaking of the QCD vacuum [6].

We now put this equation of motion, eq. (7.5), back in the moments eq. (7.4). We see that

$$G_3 = -\frac{S^\mu}{2S^2 M_p^2} \sum_i e_i^2 \left(m_{\text{eff},i}^2 \langle p, S | \bar{\psi}_i \gamma_5 \gamma_\mu \psi_i | p, S \rangle + 2 m_{\text{eff},i} \langle p, S | \bar{\psi}_i \gamma_5 i \partial_\mu \psi_i | p, S \rangle \right). \quad (7.6)$$

Notice that the first term in G_3 , apart from mass factors, is very similar to G_1 in eq. (7.4). Equations (7.4) and (7.6) form the basic set of equations. In the next section, we numerically estimate m_{eff} in as model independent a way as possible and later check our calculations in a bag model with massive quarks.

7.3 Numerical estimates of m_{eff}

As pointed out before, the matrix element appearing in the first term of G_3 in eq. (7.6) is the same as that in eq. (7.4) for G_1 , apart from mass factors. The second term typically gets contributions from the transverse momentum of the quarks and may be expected to be small in comparison with the first term. We shall therefore ignore this term for the moment and justify this step later. Then, we immediately see that the moments of $g_1(x)$ satisfy the following relation:

$$\mathcal{R}_G \equiv \frac{G_3}{G_1} = \frac{m_{\text{eff}}^2(\mu^2)}{M_p^2}, \quad (7.7)$$

where we have used the assumption that all flavours have equal mass. The measured $g_1(x)$ is positive everywhere for $0.01 \leq x \leq 0.7$ [4]. The quoted value of G_1 is

$$G_1 = 0.126 \pm 0.010 \text{ (stat)} \pm 0.015 \text{ (syst)}. \quad (7.8)$$

To consistently obtain both G_1 and G_3 from the same set of parametrisations, we use the parametrisations in refs. [4], [7] which yield

$$G_1 = 0.125 \quad \text{and} \quad G_3 = 0.011 . \quad (7.9)$$

Hence,

$$\mathcal{R}_G = 0.091 \quad \text{or equivalently,} \quad m_{\text{eff}} = 283 \text{ MeV}. \quad (7.10)$$

This is close to the constituent quark mass. However, caution should be exercised in interpreting this result, as the approximation we have made in the expression for G_3 can only be justified in a model dependent way. The fact that the EMC result yields a positive value for G_3 already indicates that m_{eff} is of the order of the constituent quark mass rather than the current quark mass. (If current quark masses were used in eq. (7.14) for the third moment, the strange quark contribution would dominate as its (current) mass is the largest. Since this is believed to be a negative quantity ($\Delta s \leq 0$), it would make G_3 negative rather than positive as obtained from the EMC measurement).

The result is completely parametrisation independent and only depends on the (reasonable) assumption that all flavours have equal masses. Furthermore, this is a leading order result, as we have dropped $\mathcal{O}(\alpha_s)$ terms in the Wilson coefficients; the resulting error in the estimates is not more than 10% to 15% for the various moments. In order to include perturbative Q^2 corrections in the Wilson coefficients, we need to know the individual spin dependent parton densities as the non-singlet and singlet densities evolve differently in Q^2 ; these are unfortunately, as yet unknown. If we assume that the nonsinglet terms dominate the moments, and correct \mathcal{R}_G for finite Q^2 , we have

$$\frac{G_3(Q^2)}{G_1(Q^2)} \left(\frac{\ln \left(\frac{Q^2}{\Lambda^2} \right)}{\ln \left(\frac{\mu^2}{\Lambda^2} \right)} \right)^{d^3 - d^1} = \frac{m_{\text{eff}}^2(\mu^2)}{M_p^2} ,$$

where d^3 and d^1 are related to the anomalous dimensions for the non-singlet terms in the third and first moment of $g_1(x)$ and Λ is the QCD scale parameter.

Using the known values for d^1 and d^3 [8] for $Q^2 \simeq 10 \text{ GeV}^2$ (corresponding to the EMC central value), we find that $m_{\text{eff}} \simeq 318 \text{ MeV}$ (up from 283 MeV without Q^2 corrections). In general, finite Q^2 corrections tend to increase the effective mass. More importantly, this mass lies in the range of the constituent quark mass.

7.4 Model Calculation of Matrix Elements

In the previous section, we have seen that the relation between the hadronic matrix elements obtained using a simple assumption regarding the effective mass of quarks can be made consistent with deep inelastic scattering data on moments. However, we were unable to calculate the moments themselves. We may now ask whether these matrix elements can be calculated in a model which admits an equation of motion similar to eq. (7.5). The simplest model we can use is the MIT bag model with massive, non-strange quarks which is a modification of the original model and is due to Golowich [9].

We quickly review the main results of the model. The quarks of mass m satisfy the equation

$$(i \not{\partial} - m)\psi_\alpha(x) = 0 \quad (7.11)$$

inside the bag and the following boundary conditions on the surface:

$$\begin{aligned} i n \cdot \gamma \psi_\alpha(x) &= \psi_\alpha(x), \\ \sum_\alpha n \cdot \partial [\bar{\psi}_\alpha(x) \psi_\alpha(x)] &= 2B. \end{aligned} \quad (7.12)$$

The normal, $n_\mu = (0, -\hat{r})$, points into the bag at the surface and B is the bag pressure.

We are interested in solutions corresponding to the proton (ground state) which is completely symmetric in spin, isospin and spatial indices, while being completely antisymmetric in the colour index. These solutions are functions of the three model parameters, namely, the quark mass, m , the bag radius, R , and ω , the mode frequency (here that of the quark ground state). These parameters are constrained by the linear boundary condition in eq. (7.12). The model thus requires two input parameters to consistently determine m , R and

ω . We choose these to be the (known) nucleon axial vector coupling constant, g_A and the charge square radius of the proton, $\langle r^2 \rangle_p$. (See ref. [9] for details of the calculation of g_A and $\langle r^2 \rangle_p$ within the model).

It suffices for us to state that, given the input g_A and using the linear boundary condition in eq. (7.12), the parameter ω and the product mR are fixed. The input $\langle r^2 \rangle_p$ then separately determines m and R , so that the three parameters are uniquely fixed for a given g_A and $\langle r^2 \rangle_p$. In Fig. (7.1) we show the variation of the mass (the parameter of interest) with the input parameters g_A and $\langle r^2 \rangle_p$. We see that for a given g_A , the effective quark mass decreases with increasing $\langle r^2 \rangle_p$.

We now evaluate the matrix elements occurring in the OPE which are required in the model calculation. We need to evaluate two different matrix elements, namely $S^\mu \langle p, S | \bar{\psi} \gamma_5 \gamma_\mu \psi | p, S \rangle$ which occurs in G_1 as well as in G_3 and $S^\mu \langle p, S | \bar{\psi} \gamma_5 \partial_\mu \psi | p, S \rangle$ which occurs in G_3 alone. The first of these is given by

$$G_1 = \frac{5}{54} \left(\frac{2\omega^2 + 4mR\omega - 3mR}{2\omega^2 - 2\omega + mR} \right), \quad (7.13)$$

where we have identified G_1 as the (charge weighted) sum of the u - and d -quark contributions as this is a model with non-strange quarks:

$$G_1 = \frac{1}{18} (4\Delta u + \Delta d).$$

Since G_1 depends on ω and the product mR alone, the value of g_A is sufficient to evaluate it. Then, using eq. (7.4), the first term in G_3 is

$$G_3^{(1)} = \frac{m^2}{M_p^2} G_1. \quad (7.14)$$

The second term of G_3 can be written as

$$\begin{aligned} G_3^{(2)} &= \frac{m}{M_p^2} \sum_q e_q^2 g_q \left[\int d^3x \bar{\psi}(x) \gamma_5 i \partial_3 \psi(x) \right]_{\text{bag}} \\ &= -\frac{10}{54 M_p^2} \frac{m}{R} \frac{\omega^2 - m^2 R^2}{2\omega^2 - 2\omega + mR}, \end{aligned} \quad (7.15)$$

where $g_u = 4/3$ and $g_d = -1/3$. The ratio of the second and first terms in G_3

is then given by

$$\mathcal{R}_3 \equiv \frac{G_3^{(2)}}{G_3^{(1)}} = -\frac{2}{mR} \frac{\omega^2 - m^2 R^2}{2\omega^2 + 4mR\omega - 3mR}, \quad (7.16)$$

which is fixed by the value of g_A alone, just as is G_1 . We however need one more input in order to evaluate the terms in G_3 .

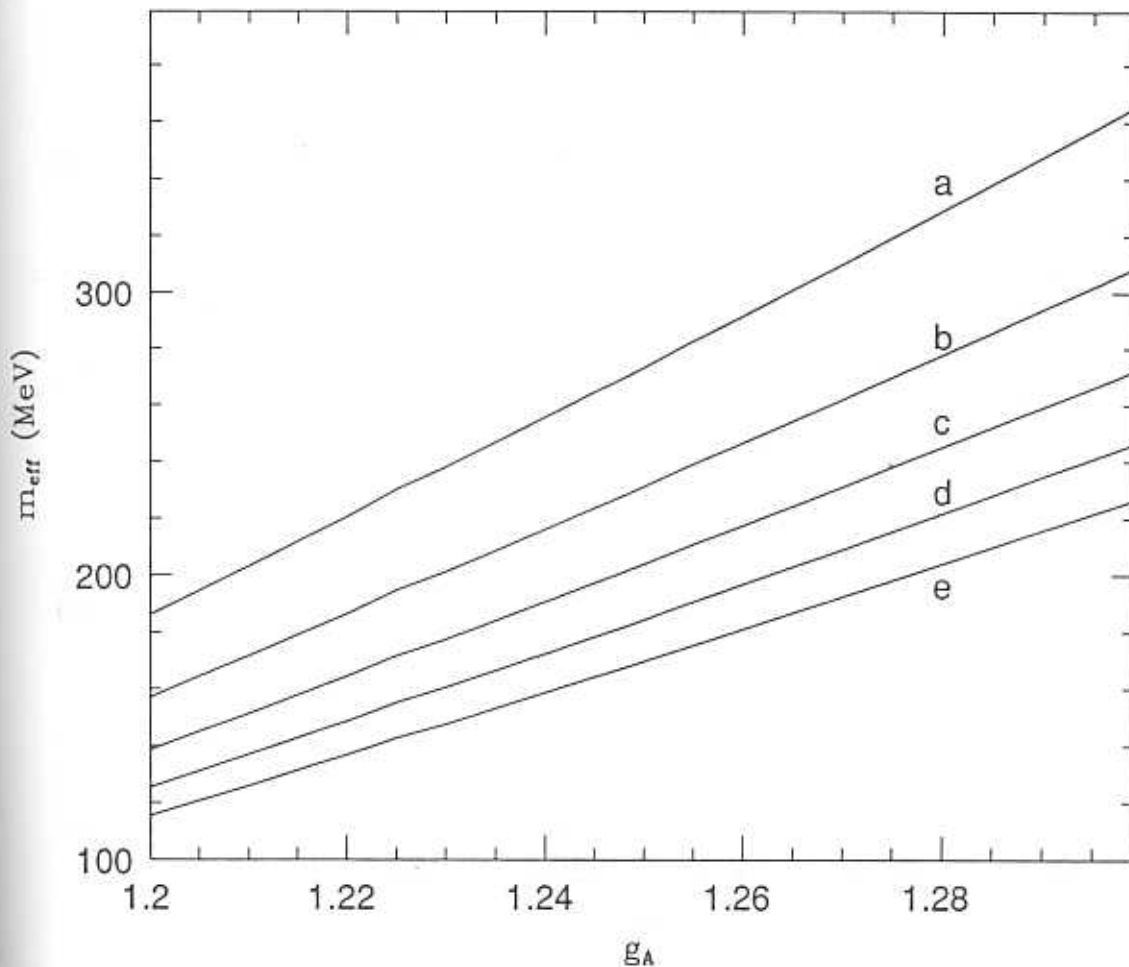


Fig. 7.1 This shows the variation of quark mass with the input parameters in the bag model. g_A is plotted along the x -axis, while labels (a) to (e) correspond to $\langle r^2 \rangle_p$ values from 0.25 to 0.65 in steps of 0.1.

The behaviour of G_1 is shown in Fig. (7.2). We see that G_1 is a slowly varying function of g_A . For $g_A = 1.26$, which is the experimental value, $G_1 \simeq 0.21$. We discuss the significance of this value later.

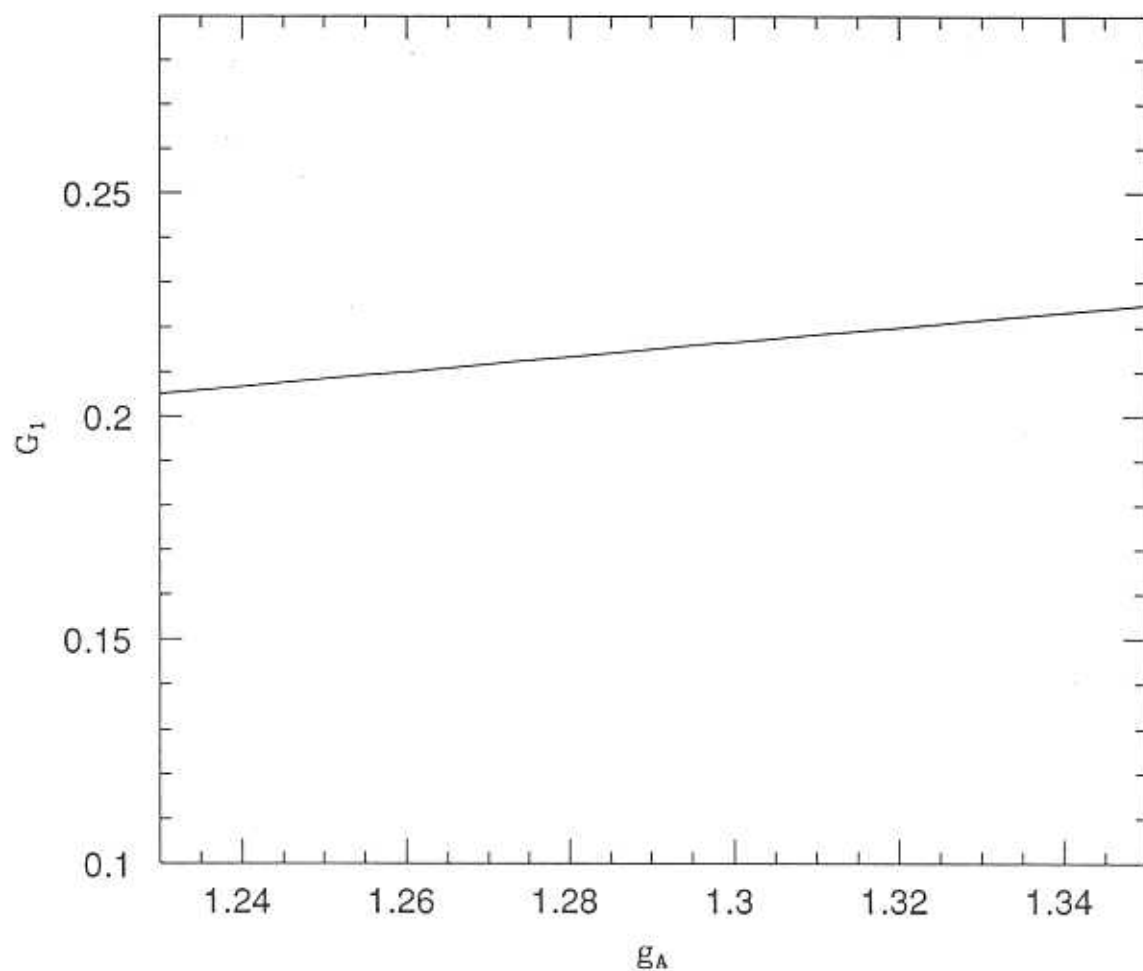


Fig. 7.2 G_1 is plotted as a function of g_A in the bag model.

The ratio of the two terms of the third moment, G_3 , however, varies rapidly with g_A as can be seen from Fig. (7.3). The second term is always smaller than the first term, so that \mathcal{R}_3 is always less than one; for $g_A = 1.26$, the second term is less than half the first. To obtain the actual values of these terms requires one more input—we choose $\langle r^2 \rangle^{0.5} = 0.5$ fm.

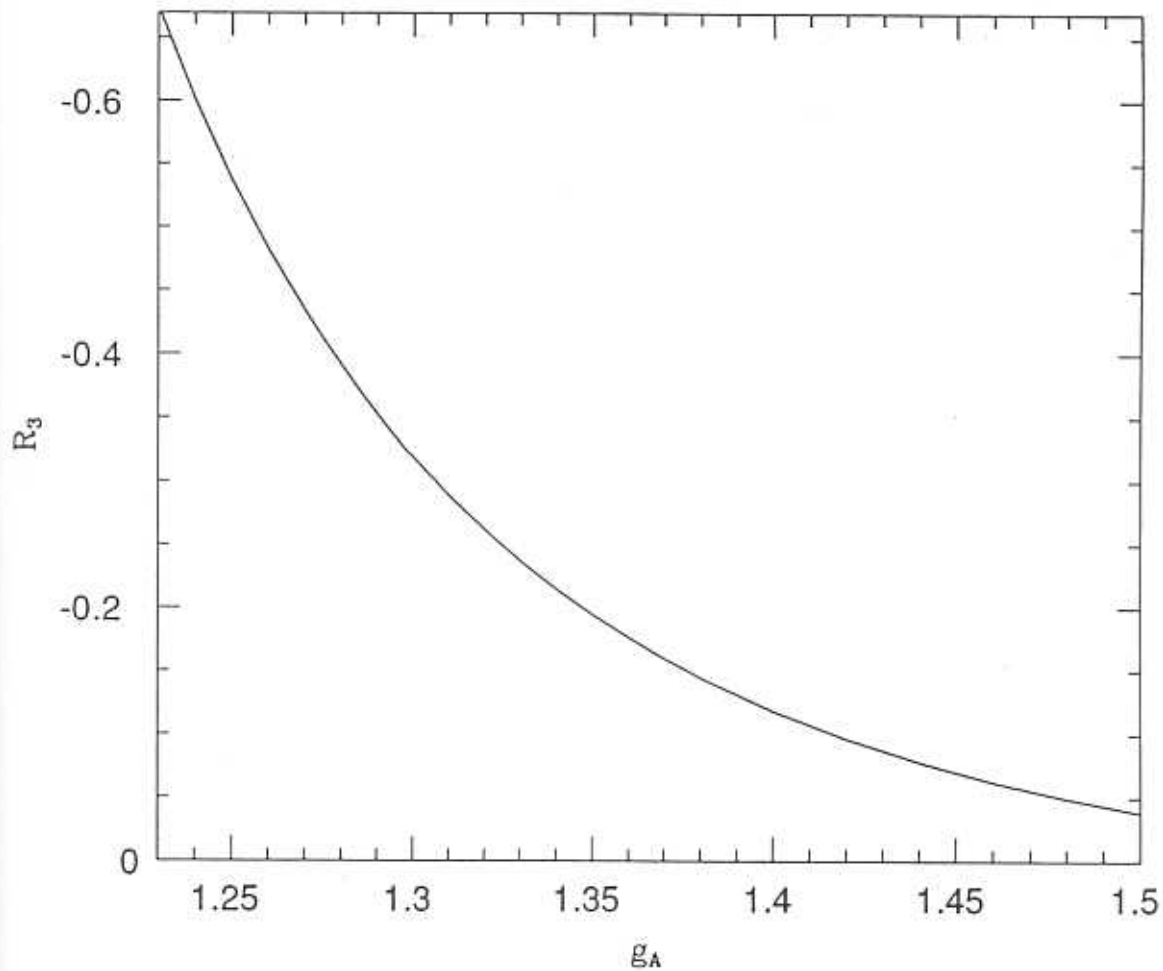


Fig. 7.3 The ratio, \mathcal{R}_3 , of the two terms of G_3 is plotted as a function of g_A in the bag model.

Although this is smaller than the measured value of 0.83 fm for the proton charge radius, we prefer this choice as it results in a mass of about 300 MeV when g_A is close to its experimentally measured value of 1.26. The behaviour of the two terms of G_3 for this choice of parameters is shown in Fig. (7.4). For large mass values, the first term dominates the nearly constant second term.

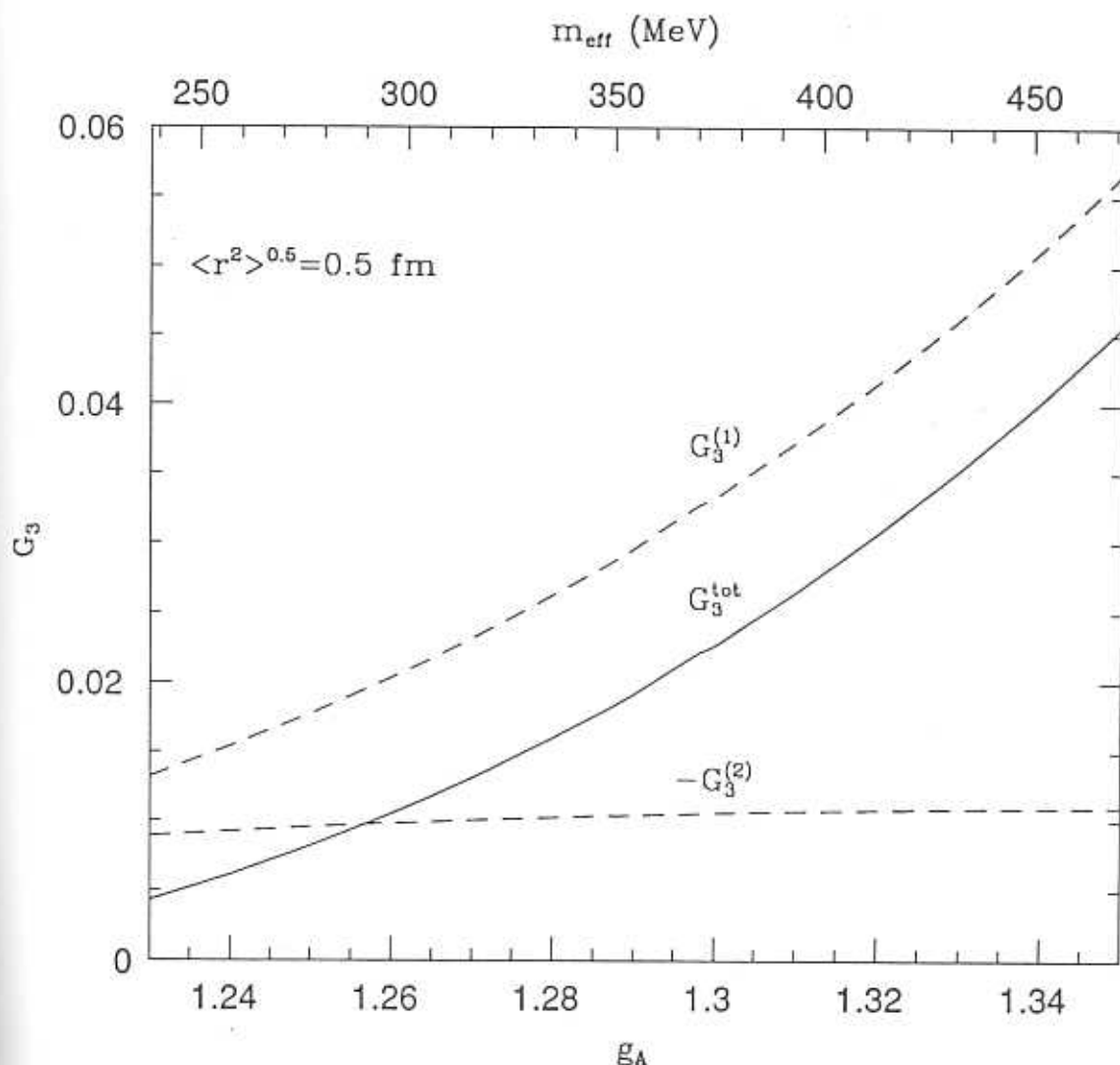


Fig. 7.4 The two terms of G_3 are plotted as a function of g_A (or equivalently m_{eff} for a constant r.m.s. charge radius of 0.5 fm.

Hence, we feel justified in ignoring the second term in our analysis. At $g_A = 1.26$, the total third moment is $G_3 \simeq 0.01$, which is close to that obtained from parametrisation of the data.

We now return to a discussion of the bag model value obtained for G_1 ,

$$G_1 = 0.21,$$

which is very different from the value $G_1 = 0.126$ quoted by the EMC. The reason for the discrepancy in G_1 is not hard to find, especially when we notice that the leading order Ellis-Jaffe Sum Rule [10] gave a strikingly similar result:

$$G_1 \simeq 0.19 .$$

(The difference between this and the value quoted in Chapter 1 is that α_s corrections have not been incorporated here since the entire calculation is a leading order one). Recall that this value was predicated upon the assumption that the strange quark contribution was zero and using SU(3) Current Algebra. The singlet piece in the first moment of $g_1(x)$, which includes the sea (and hence the strange) quark and gluon contributions, cannot be handled within the bag model. Hence, the bag model reproduces the Ellis Jaffe result rather than the observed value. A large value of this singlet contribution may explain why the experimental value of G_1 deviates so sharply from the Ellis Jaffe result. If this is true, and, indeed, such is expected to be the solution to the "proton spin puzzle," then the contribution of the singlet term to the higher moments of $g_1(x)$ must be small. This is because the singlet contribution is a small- x effect. On the other hand, by taking higher moments of $g_1(x)$, the small- x contributions naturally get suppressed; hence, we would expect the value of the third moment of $g_1(x)$ obtained in the bag model to be closer to the experimental value than the first moment is to its corresponding measured value. We find this to be indeed the case, with G_3 approaching $\simeq 0.010$, as mentioned before.

Hence, our simple model with massive non-strange quarks already reflects

(albeit somewhat crudely) the complicated nature of the contribution to the small- x region of $g_1(x)$.

It would seem that the failure of the bag model to predict correctly the first moment of the spin dependent structure function $g_1(x)$, while providing reasonable estimates for the third moment, combined with the knowledge that gluonic effects are not included in this model, points to the inclusion of the gluon contribution as being a prime candidate to the resolution of the discrepancy. It also seems reasonable to expect a generic quark model, or, in fact, *any* nonperturbative model capable of evaluating the moments of $g_1(x)$, to give fairly accurate predictions for the third moment and to reproduce the Ellis Jaffe result for the first moment.

7.5 Conclusions

We have analysed the moments of the (experimentally) known proton structure function, $g_1(x)$, via the operator product expansion. An effective quark mass, $m_{\text{eff}}(\mu^2)$, is introduced through an equation of motion, where μ^2 is the scale at which the operators whose matrix elements occur in the operator product expansion are renormalised. Being nonperturbative matrix elements, we expect that the corresponding mass occurring in these is of the order of the constituent quark mass rather than the current quark mass. We set up ratios of the various moments and evaluate this mass, which turns out to be around 300 MeV, thus reinforcing our expectation. Certain approximations are made which are justified within a bag model with massive, non-strange quarks. We also evaluate the absolute values of the moments themselves in this bag model. The first moment, G_1 , reproduces the value calculated by Ellis and Jaffe, while the third moment is consistent (within errors) with the measured one. We can understand the discrepancy in the first moment as due to the absence of gluon terms in the bag model. Since this is basically a small- x contribution, this conclusion is consistent with the fact that the third moment comes out alright, as higher moments suppress small- x contributions. Hence our analysis gives credence to the view that a bag model with massive

quarks is probably closer to reality.

We add that the corresponding spin independent calculation has also been done [2], [3], where *even* moments of the spin independent structure function, $F_1(x)$, are defined analogous to eq. (7.2). Here, the bag model fits both the second and fourth moment quite well. Furthermore, there is only one term in the expressions for both the moments so that the expression analogous to eq. (7.7) is exact in the spin independent sector. Hence, the extraction of a mass scale (which also turns out to be around 300 MeV) from the ratio of these moments is more reliable.

References

- [1] D. Indumathi, M.V.N. Murthy and V. Ravindran, *Mod. Phys. Lett.* **A14** (1990) 1125
- [2] D. Indumathi, M.V.N. Murthy and V. Ravindran, *Int. J. Mod. Phys.* **A6** (1991) 3933
- [3] V. Ravindran, Ph. D. Thesis
- [4] SLAC, G. Baum et al., *Phys. Rev. Lett.* **51** (1983) 1135;
EMC, J. Ashman et al., *Nucl. Phys.* **B293** (1987) 740
- [5] J. Kodaira et al., *Nucl. Phys.* **B159** (1979) 99;
J. Kodaira, *Nucl. Phys.* **B165** (1980) 129
- [6] V.E. Elias, *Phys. Rev.* **D34** (1986) 3537
- [7] T. Sloan, *Phys. Rep.* **162** (1988) 45
- [8] A.J. Buras, *Rev. Mod. Phys.* **52** (1980) 199
- [9] E. Golowich, *Phys. Rev.* **D12** (1975) 2108 and references therein
- [10] J. Ellis and R.L. Jaffe, *Phys. Rev.* **D9** (1974) 1444; *Phys. Rev.* **D10** (1974) 1669

THE SPIN DEPENDENT STRUCTURE FUNCTIONS: QCD SUM RULE APPROACH

C O N T E N T S

The Sum Rule

Calculation of $\text{Im } \mathcal{T}_{\mu\nu}$ via the OPE

Conclusions

The QCD Sum Rule technique was first proposed and applied to the study of meson properties by Shifman, Vainshtein and Zakharov [1]. The Sum Rule approach attempts to incorporate nonperturbative corrections into perturbative calculations in QCD. The Sum Rule itself may be simply written as

$$LHS = RHS .$$

The right hand side (RHS) of the Sum Rule involves calculating a time-ordered product of currents and use of Wilson's operator product expansion (OPE) in order to evaluate the matrix elements of this time-ordered product. This results in separating the long-distance and short-distance effects. The latter, *viz.*, the Wilson coefficients, are calculated perturbatively while the long-distance part, which is unknown, involves non-vanishing expectation values of quark and gluon operators such as $\langle 0|q\bar{q}|0\rangle$ and $\langle 0|G_{\mu\nu}^a G_{\mu\nu}^a|0\rangle$, which vanish in standard perturbation theory. Here q is the quark field and $G_{\mu\nu}^a$ is the gluon field strength tensor. These local operators all have different dimensions, hence the OPE consists in writing an expansion in terms of operators of increasing dimension such that their (perturbatively calculable) coefficients increase as the inverse power of Q^2 , the momentum squared, when Q^2 is large. The most dominant (lowest dimension) operator thus has the most singular

coefficient. This being an asymptotic expansion, we do not expect it to be convergent, but rather we expect that the first few terms yield a reasonable approximation to the RHS. We therefore have a result for the matrix element of the time-ordered product of currents between vacuum states (also called the correlation function) in terms of quark and gluon degrees of freedom.

On the other hand side (left hand side or LHS), this correlation function can be computed as an integral over its absorptive part, using a dispersion relation. In general, the dispersion relation can be written as

$$\Pi(Q^2) = \frac{1}{\pi} \int ds \frac{\text{Im} \Pi(s)}{s + Q^2}$$

where $\text{Im} \Pi(s)$ is proportional to measurable cross-sections involving physical quantities like mass, coupling constant, etc. Equating the QCD-based perturbative OPE calculation of the correlator with its dispersed form yields the required Sum Rule, from which the required hadronic property (mass, coupling, etc.) can be extracted. The validity of this method needs some justification, which we shall not attempt to provide here, but merely refer to existing work in refs. [1],[2].

As a simple example, consider the ρ -meson current, written in terms of quark fields as

$$j_\mu^\rho = \frac{1}{2} (\bar{u}\gamma_\mu u - \bar{d}\gamma_\mu d) .$$

The correlator of interest is the fourier transform of the time ordered product:

$$\begin{aligned} \Pi_{\mu\nu} &= i \int d^4x e^{iq \cdot x} \langle 0 | T(j_\mu(x)j_\nu(0)) | 0 \rangle \\ &= (q_\mu q_\nu - q^2 g_{\mu\nu}) \Pi^\rho(q^2) , \end{aligned}$$

where $q^2 = -Q^2$ is large and negative. Using the OPE and the definition of j_μ^ρ , $\Pi^\rho(q^2)$ can be related to the vacuum matrix elements of relevant operators like \mathbb{I} , $\langle \bar{q}q \rangle$, $\langle G_{\mu\nu}^a G_{\mu\nu}^a \rangle$, etc., with perturbatively calculable coefficients. This forms the RHS. On the other hand, since Π^ρ is seen to have a pole at $q^2 = 0$, it satisfies the once-subtracted dispersion relation,

$$\Pi^\rho(Q^2) = \Pi^\rho(0) - \frac{Q^2}{12\pi^2} \int ds \frac{R(s)}{s(s + Q^2)} ,$$

where R is related to the imaginary part of Π^ρ :

$$\begin{aligned} R &= \frac{\sigma(e^+e^- \rightarrow \text{hadrons})}{\sigma(e^+e^- \rightarrow \mu^+\mu^-)} \\ &= 12\pi^2 \frac{m_\rho^2}{g_\rho^2} \delta(s - m_\rho^2) \end{aligned}$$

in the resonance approximation. Comparison of the dispersed form of Π^ρ with its OPE evaluation yields an expression for the ρ meson coupling constant [1],

$$\frac{g_\rho^2}{4\pi} \simeq \frac{2\pi}{e} \simeq 2.3,$$

and this result improves to 2.41 when continuum corrections to R are included. As a technical point, we note that the two sides of the Sum Rule are usually Borel-transformed to suppress excited state contributions.

The method is less accurate in the case of nucleon calculations, but has still met with considerable success in computing the masses and coupling constants of low-lying hadron states [1], including the mass of the nucleon [3], [4] and its octet partners as well as the isobar and the decimet members. This was later extended [5], [6] to a computation of the magnetic moments of the proton and neutron to $\sim 10\%$ accuracy. This was done by considering the correlation function of the baryon current in an external magnetic field, $F_{\mu\nu}$. By calculating the term *linear* in $F_{\mu\nu}$ in the current correlation function, they were able to calculate the magnetic moments. This idea was used to compute [7] the nucleon axial vector coupling constant, g_A , by looking at the propagation of the baryon current in an external axial vector field, Z_μ , and evaluating the terms linear in Z_μ in the correlator. A similar calculation was done in the case of hyperons. This technique was put to good use when the controversial result for the proton spin dependent structure function was announced by the EMC: the calculation was extended to include a computation of the isoscalar axial vector renormalisation constant, g_s . Using the experimentally known value for the other non-singlet coupling constant, g_8 , and the results for g_A and g_s from the QCD Sum Rule method, the authors [8] obtained a result for

the first moment of this structure function,

$$G_1^p \equiv \int dx g_1^p(x) \simeq 0.135 ,$$

which is compatible, within errors, with the EMC measurement of 0.126. Furthermore, they obtained a value of $g_s = 0.35$, while $g_8 = 0.6$. The difference between these two can be understood on one hand as being due to large gluon contributions and on the other, as the strange quark matrix element acquiring nonzero value through loop corrections. (Although there is no direct use of the axial anomaly in the analysis, the phenomenological value of the chiral symmetry breaking condensate, $\langle \bar{q}q \rangle$ that is used, arises from the anomaly in instanton-based models of the QCD vacuum [9], [10]. This can be thought to be the cause of the large gluon contribution in the first moment of the structure function).

With these successes of the technique in mind, we now address the question of computation of, not just the moment, but the x dependent structure functions themselves. Calculation of the structure function at individual x (the Bjorken scaling variable) is a much harder task. This was done for the *spin independent* case by Belyaev and Ioffe [2]. The extension to the spin dependent case was first done by Singh and Pasupathy [11] where they considered chiral-odd structures contributing to the sum rule. Later, a similar calculation was performed by Belyaev and Ioffe [12] for the chiral-even structures. Here, we will discuss these features—that of the choice of nucleon current and gauge invariance properties of the four-point function—and the inter-relation between them [13] for the chiral-even case.

8.1 The Sum Rule

The physical quantity of interest is the antisymmetric part of the forward virtual Compton scattering amplitude:

$$T_{\mu\nu}^A(p, q, S) = i \int d^4x e^{iq \cdot x} \langle p, S | T (j_\mu(x) j_\nu(0))^A | p, S \rangle , \quad (8.1)$$

where $j_\mu(x)$ is the electromagnetic current, given in terms of the quark fields by

$$j_\mu(x) = \frac{2}{3} (\bar{u}(x)\gamma_\mu u(x)) - \frac{1}{3} (\bar{d}(x)\gamma_\mu d(x)) ,$$

and p, q are the four-momenta of the (on-shell) nucleon and the virtual photon; M_N and S are the mass and spin of the nucleon with $S^2 = -1$, $S \cdot p = 0$ and $\nu \equiv p \cdot q$. The absorptive part of $T_{\mu\nu}^A$ is related to the spin-dependent part of the deep inelastic lepton-proton scattering cross-section and hence, to the spin-dependent structure functions. We have [14]

$$\begin{aligned} \text{Im } T_{\mu\nu}^A(p, q, S) = & \frac{\pi}{2} \bar{u}(p, S) \left[\left\{ p_\mu [\gamma_\nu, \not{q}] - p_\nu [\gamma_\mu, \not{q}] + p \cdot q [\gamma_\mu, \gamma_\nu] \right\} G_1(q^2, \nu) \right. \\ & \left. + \left\{ q_\mu [\gamma_\nu, \not{q}] - q_\nu [\gamma_\mu, \not{q}] + q^2 [\gamma_\mu, \gamma_\nu] \right\} G_2(q^2, \nu) \right] u(p, S) \end{aligned} \quad (8.2)$$

where the nucleon spinor is normalised according to

$$\bar{u}(p, S) u(p, S) = 2M_N.$$

The two structure functions exhibit scaling behaviour in the Bjorken limit,

$$\begin{aligned} (M_N \nu) G_1(q^2, \nu) & \xrightarrow[-q^2, \nu \rightarrow \infty]{-q^2/2\nu = x, \text{finite}} g_1(x) , \\ (\nu^2/M_N) G_2(q^2, \nu) & \xrightarrow{\hspace{1.5cm}} g_2(x) . \end{aligned} \quad (8.3)$$

Following Belyaev and Ioffe, to compute $\text{Im } T_{\mu\nu}^A$, we start with the antisymmetric part of the four-point function,

$$T_{\mu\nu}^A(p, q) = -i \int d^4x d^4y d^4z e^{iqx + ip(y-z)} \langle 0 | T [\eta(y) j_\mu(x) j_\nu(0) \bar{\eta}(z)]^A | 0 \rangle , \quad (8.4)$$

where the nucleon current, $\eta(y)$, is taken to be [2]

$$\eta^n(y) = \epsilon^{abc} \left[(d^n)^T(y) C \gamma_\alpha d^b(y) \right] \gamma_5 \gamma^\alpha u^c(y) \quad (8.5)$$

for the neutron, with the interchange of d and u (isospin symmetry) for the proton. Here, T stands for transpose and C for the charge conjugation operator. The current has a coupling strength, λ_N to the nucleon state defined

by

$$\langle 0 | \eta(y) | N \rangle = \lambda_N u(p, M_N) . \quad (8.6)$$

We are interested in the imaginary part of $T_{\mu\nu}$ calculated in the Mandelstam variable, $s = (p + q)^2$, the centre of mass energy squared. The divergence of the four-point function is given by

$$q^\mu T_{\mu\nu} = \int d^4x d^4y d^4z e^{iq \cdot x + ip \cdot (y-z)} \partial^\mu \left\{ \langle 0 | T (\eta(y) j_\mu(x) j_\nu(0) \bar{\eta}(z)) | 0 \rangle \right\} ;$$

where $\partial^\mu \equiv \partial / \partial x_\mu$ and we have

$$\begin{aligned} \partial^\mu \left\{ \langle 0 | T (\eta(y) j_\mu(x) j_\nu(0) \bar{\eta}(z)) | 0 \rangle \right\} &= \langle 0 | T \left\{ \eta(\partial^\mu j_\mu) j_\nu \bar{\eta} + \delta(x_0) \eta [j_0, j_\nu] \bar{\eta} \right. \\ &\quad \left. + \delta(x_0 - y_0) [j_0, \eta] j_\nu \bar{\eta} \right. \\ &\quad \left. + \delta(x_0 - z_0) \eta j_\nu [j_0, \bar{\eta}] \right\} | 0 \rangle . \end{aligned}$$

The first term vanishes as $\partial^\mu j_\mu = 0$; the second term anyway has no imaginary part. To evaluate the remaining terms, we use the equal time commutation relations:

$$\begin{aligned} [j_0(x), \eta(y)]_{x_0=y_0} &= -e_\eta \eta(y) \delta^3(\vec{x} - \vec{y}) ; \\ [j_0(x), \bar{\eta}(y)]_{x_0=y_0} &= e_{\bar{\eta}} \bar{\eta}(y) \delta^3(\vec{x} - \vec{y}) , \end{aligned}$$

where e_η is the charge of η . Hence,

$$q_\mu T_{\mu\nu} = e_\eta \int d^4x d^4y \left[e^{ip \cdot x - i(p-q) \cdot y} - e^{i(p+q) \cdot x - ip \cdot y} \right] \langle 0 | T (\eta(x) j_\nu(0) \bar{\eta}(y)) | 0 \rangle , \quad (8.7)$$

and is therefore proportional to the charge of η . Hence, it is zero for the charge-neutral neutron. For the proton, however, it is, in general, different from zero.

The spin-dependent structure functions are obtained from the four-point function in eq. (8.4) by inserting a complete set of physical intermediate states of which the nucleon, of course, has the lowest mass and by making use of eqs. (8.6) and (8.1). The term of interest (see Appendix E for details), is

$$\begin{aligned} &\frac{\lambda_N^2}{(p^2 - M_N^2)^2} u(p, S) \text{Im} \left[i \int d^4x e^{iq \cdot x} \langle p, S | T (j_\mu(x) j_\nu(0))^A | p, S \rangle \bar{u}(p, S) \right] \\ &= \frac{\pi M_N \lambda_N^2}{2(p^2 - M_N^2)^2} \left[\{ p^2 \Gamma_{\mu\nu} + \not{p} \Gamma_{\mu\nu} \not{p} \} G_1 + \{ \not{p} \Gamma_{\mu\nu} \not{p} + \not{q} \Gamma_{\mu\nu} \not{p} \} G_2 \right] , \end{aligned} \quad (8.8)$$

where $\Gamma_{\mu\nu} \equiv (\gamma_\mu \not{\epsilon}\gamma_\nu - \gamma_\nu \not{\epsilon}\gamma_\mu)$ and we have made use of eqs.(8.1) and (8.2). Hence, on using the dispersion, the imaginary part of the four-point function, $\mathcal{T}_{\mu\nu}$, is related to the imaginary part of the two-point function, $T_{\mu\nu}$. While the divergence of the four-point function need not be zero, $q_\mu \text{Im} \mathcal{T}_{\mu\nu}$ as defined in eq.(8.1) is always zero as it only has terms corresponding to the first two terms of eq.(8.6). Hence, the presence of time ordering induces nontrivial changes with respect to gauge invariance, when going from 2-point to 4-point functions. In the next section, we shall evaluate $\text{Im} \mathcal{T}_{\mu\nu}$ via the OPE and explicitly show that $q_\mu \text{Im} \mathcal{T}_{\mu\nu}$ is not zero for the proton case. Here, we shall proceed to set up the Sum Rule for the neutron, as it is well defined.

$\text{Im} \mathcal{T}_{\mu\nu}$, evaluated using the Wilson OPE approach, consists of various tensor structures in accordance with Lorentz invariance, gauge invariance, CP invariance, etc. The most general gauge invariant expression for $\text{Im} \mathcal{T}_{\mu\nu}$ in terms of the tensor structures appearing in eq. (8.8) are

$$\text{Im} \mathcal{T}_{\mu\nu}^A = A'_1 \not{\epsilon}\Gamma_{\mu\nu} \not{\epsilon} + A'_2 p^2 \Gamma_{\mu\nu} + C'_1 \not{\epsilon}\Gamma_{\mu\nu} \not{\epsilon} + C'_2 \not{\epsilon}\Gamma_{\mu\nu} \not{\epsilon}.$$

For later convenience, we write this as

$$\text{Im} \mathcal{T}_{\mu\nu}^A = A_1 B_{1,\mu\nu} + A_2 B_{2,\mu\nu} + C_1 B_{3,\mu\nu} + C_2 B_{4,\mu\nu} \quad (8.9)$$

where

$$\begin{aligned} B_{1,\mu\nu} &= \frac{1}{2} (p^2 \Gamma_{\mu\nu} + \not{\epsilon}\Gamma_{\mu\nu} \not{\epsilon}) \quad ; \quad B_{2,\mu\nu} = p^2 \Gamma_{\mu\nu} \\ B_{3,\mu\nu} &= \not{\epsilon}\Gamma_{\mu\nu} \not{\epsilon} \quad ; \quad B_{4,\mu\nu} = \not{\epsilon}\Gamma_{\mu\nu} \not{\epsilon}. \end{aligned}$$

Matching eqs. (8.8) and (8.9) at the proton pole thus yields the required Sum Rule. In eq. (8.8), there are only two independent coefficients, G_1 and G_2 . We can identify A'_1 with G_1 and $(C'_1 = C'_2)$ with G_2 when we set up the Sum Rule at the proton pole, where we have the condition, $p^2 = M_N^2$. Note however, that $\not{\epsilon} \neq M_N$ as we do not have spinors in $\mathcal{T}_{\mu\nu}$. We have

$$\frac{\pi M_N \lambda_N^2}{(p^2 - M_N^2)^2} G_1 = A_1 ;$$

$$\frac{\pi M_N \lambda_N^2}{2(p^2 - M_N^2)^2} G_2 = C_1 = C_2 .$$

$\text{Im } \mathcal{T}_{\mu\nu}$ also contains excited state contributions from (proton + resonance) and (resonance + resonance) poles; hence, the coefficients A_i, C_i pick out not only terms proportional to $\frac{1}{(p^2 - M_N^2)^2}$, but also to $\frac{1}{(p^2 - M_N^2)(p^2 - M_N'^2)}$ and $\frac{1}{(p^2 - M_N'^2)^2}$. To suppress these excited state contributions, the usual procedure is to Borel transform both the LHS and the RHS. The Borel transform is defined as

$$B(f(p^2)) = \lim_{\substack{-p^2, n \rightarrow \infty \\ -p^2/n \rightarrow M^2, \text{finite}}} \frac{(-p^2)^{n+1}}{n!} \left(\frac{d}{dp^2} \right)^n f(p^2).$$

The procedure for the RHS of the Sum Rule is now clear: evaluate the Wilson coefficients of the various operators in the OPE for the four-point function, $\text{Im } \mathcal{T}_{\mu\nu}$ and identify in them the tensor structures B_i defined earlier. Their coefficients, which correspond to the structure functions we are seeking to compute, are then Borel transformed and equated to the Borel transform of corresponding terms in the LHS. The LHS is the dispersed form of the four-point function, where the lowest lying state (proton) contribution is expressed in terms of the structure functions we are interested in evaluating and some excited state contributions which the Borel transform suppresses. This gives the Sum Rule for these structure functions.

8.2 Calculation of $\text{Im } \mathcal{T}_{\mu\nu}$ via the OPE

The LHS of the Sum Rule has a pole at $p^2 = M_N^2$. Hence, we perform the calculations at a large, negative p^2 and later, do an analytic continuation to time-like p^2 . (This, in fact, is accomplished by the Borel transformation).

The leading contribution to the RHS of the Sum Rule (for the chiral-even case that we are considering) comes from the coefficient of the Identity operator, while the next-to-leading order contribution is from the $\langle q \bar{q} \rangle^2$ operator. The $\langle \bar{q} q \rangle$ term contributes to the chiral-odd Sum Rule). We calculate terms which are singular in $-p^2$ for p^2 large and negative such that $|q^2| \gg |p^2| \gg |1/R^2|$, where R is the confinement radius [2]. These are the terms that survive the Borel transformation, when $-p^2$ is replaced by the Borel variable,

M^2 . The two sides of the Sum Rule are then matched at $M^2 \simeq M_N^2$. The leading u -quark contribution to the neutron structure function, $G_{1,2}^n(Q^2, \nu)$, is shown in Fig. (8.1). Using the form of the neutron current given in eq. (8.5), the contribution of Fig. (8.1) to the antisymmetric part of $\text{Im} T_{\mu\nu}$ is given by

$$-\frac{2e_u^2}{(2\pi)^5} \epsilon^{abc} \epsilon^{abc} \int \frac{d^4 k}{k^4} d^4 \ell \delta(k+q)^2 \delta(\ell^2) \delta(p-k-\ell)^2 \left\{ \text{Tr} [\not{\ell} \gamma_\alpha (\not{p} - \not{k} - \not{\ell}) \gamma_\beta] \times \right. \\ \left. \gamma_5 \gamma^\alpha \not{k} (\gamma_\mu (\not{k} + \not{q}) \gamma_\nu - \gamma_\nu (\not{k} + \not{q}) \gamma_\mu) \not{k} \gamma^\beta \gamma_5 \right\}. \quad (8.10)$$

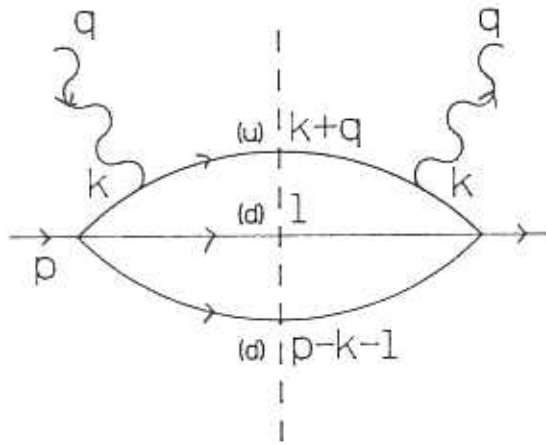


Fig. 8.1 This shows the diagram contributing to $\text{Im} T_{\mu\nu}$ where the u -quark interacts with the (virtual) photon.

The ℓ -integration can be done by going to a frame where the three-momenta \vec{p} and \vec{q} are back-to-back. This introduces a function $\theta(p-k)^2$, with which constraint the k -integration is performed (see Appendix E). The result is

$$\begin{aligned} \text{Im } \mathcal{T}_{\mu\nu}^{A,u} &= \frac{e_u^2}{4(2\pi)^3} \frac{p^2}{\nu} \ln(-p^2) \left\{ B_{1,\mu\nu} \left[4(1-x)^2(1+2x) + \frac{2p^2}{\nu}(1-x) \times \right. \right. \\ &\quad \left. \left. (1-6x-4x^2+18x^3) \right] - B_{2,\mu\nu}(1-x)(4+4x-2x^2) \right. \\ &\quad \left. - (B_{3,\mu\nu} + B_{4,\mu\nu}) \frac{p^2}{2\nu}(1-x)(1+x-8x^2) \right\} . \end{aligned} \quad (8.11)$$

Note that the coefficients A'_1 and A'_2 are not equal. In that case the coefficient of $B_{2,\mu\nu}$, which does not contribute to either of the structure functions, would have been zero. Using eq. (8.9), we have

$$\begin{aligned} (A_1)^u &= -\frac{e_u^2}{4(2\pi)^3} \frac{p^2}{\nu} \ln(-p^2) 4(1-x)^2(1+2x) , \\ (C_1 = C_2)^u &= -\frac{e_u^2}{8(2\pi)^3} \frac{p^4}{\nu^2} \ln(-p^2)(1-x)(1+x-8x^2) \end{aligned} \quad (8.12)$$

where we have ignored non-singular pieces (in p^2) as they will vanish on Borel transforming. Then, to this order, the QCD Sum Rule for the u -quark contribution to the neutron structure function is (after Borel transforming)

$$\begin{aligned} M_N \nu G_1^u &\xrightarrow{\text{scaling}} g_1^u(x) = \frac{e_u^2}{\lambda_N^2} M^6 e^{M_N^2/M^2} 4(1-x)^2(1+2x) + \mathcal{E} ; \\ \frac{\nu^2}{M_N} G_2^u &\xrightarrow{\text{scaling}} g_2^u(x) = \frac{e_u^2}{\lambda_N^2} \frac{M^8}{M_N^2} e^{M_N^2/M^2} 2(1-x)(1+x-8x^2) + \mathcal{E} , \end{aligned} \quad (8.13)$$

where $\widetilde{\lambda}_N^2 = (32\pi^4 \lambda_N^2)$ and \mathcal{E} stands for the excited state contributions. The d -quark contribution to the neutron spin dependent structure function coming from Fig. (8.2) can be similarly evaluated. We get

$$\begin{aligned} \text{Im } \mathcal{T}_{\mu\nu}^{A,d} &= \frac{e_d^2}{4(2\pi)^3} \frac{p^2}{\nu} \ln(-p^2) \left\{ B_{1,\mu\nu} \left[4(1-x)^2(1-4x) + \frac{2p^2}{\nu}(1-x) \times \right. \right. \\ &\quad \left. \left. (1-18x+50x^2-36x^3) \right] + B_{2,\mu\nu}(1-x)(2-4x-4x^2) \right. \\ &\quad \left. - (B_{3,\mu\nu} + B_{4,\mu\nu}) \frac{p^2}{2\nu}(1-x)(7+29x+16x^2) \right. \\ &\quad \left. - q^2 (\gamma_\mu \not{p} \gamma_\nu - \gamma_\nu \not{p} \gamma_\mu) \frac{p^2}{\nu} 3(1-x)^2 \right\} . \end{aligned} \quad (8.14)$$

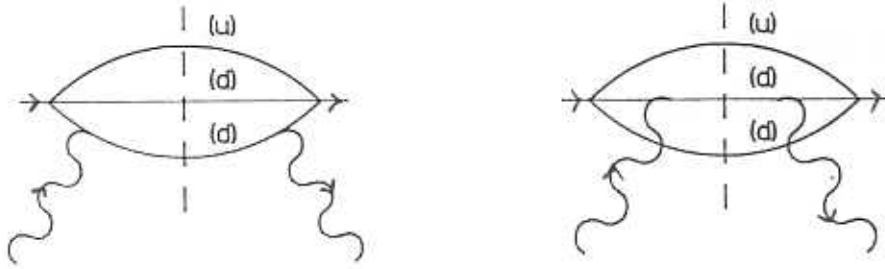


Fig. 8.2 This shows the diagrams contributing to $\text{Im}\mathcal{T}_{\mu\nu}$ where the d -quark interacts with the (virtual) photon.

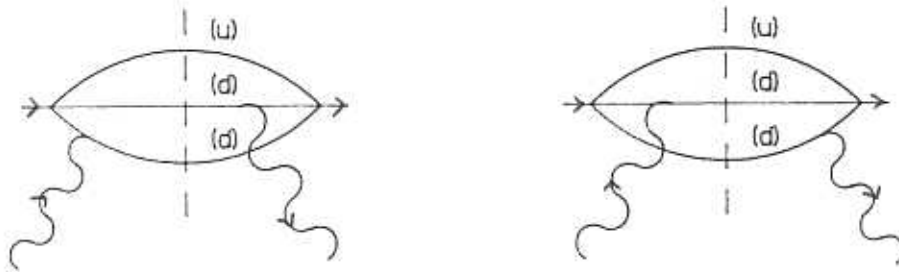


Fig. 8.3 This shows the “cross” diagrams contributing to $\text{Im}\mathcal{T}_{\mu\nu}$ where the d -quark that absorbs the (virtual) photon is not the same as the d -quark that emits it.

Hence,

$$\begin{aligned} (A_1)^d &= \frac{e_d^2}{4(2\pi)^3} \frac{p^2}{\nu} \ln(-p^2) 4(1-x)^2(1-4x), \\ (C_1 = C_2)^d &= -\frac{e_d^2}{8(2\pi)^3} \frac{p^4}{\nu^2} \ln(-p^2)(1-x)(7-29x+16x^2). \end{aligned} \quad (8.15)$$

G_1 is of order $\mathcal{O}(p^2/\nu)$ while G_2 is of order $\mathcal{O}(p^4/\nu^2)$. This is to be contrasted with the spin-independent Sum Rule where both $F_1(x)$, $F_2(x)$ are of the same order, $\mathcal{O}(p^2/\nu)$.

We notice an extra structure in the expression for the d -quark contribution to $\text{Im} \mathcal{T}_{\mu\nu}$, which is absent in the u -quark term. This structure, namely,

$$B_{5,\mu\nu} \equiv q^2 (\gamma_\mu \not{p} \gamma_\nu - \gamma_\nu \not{p} \gamma_\mu) \quad (8.16)$$

contributes at $\mathcal{O}(p^4/\nu)$ and survives in the scaling limit. In fact, it corresponds to the third tensor structure contributing to G_2 in eq. (8.2). What is more, this is not a gauge invariant structure as its product with q_μ is non-zero. Eq. (8.7) demands that such structures do not contribute to $\text{Im} \mathcal{T}_{\mu\nu}$ for the neutron. Obviously, we have not exhausted the list of contributing diagrams. There exist "cross-diagrams" wherein the quark that absorbs the virtual photon is not the same as the quark that emits it. One such set of diagrams that adds to the d -quark contribution of $\text{Im} \mathcal{T}_{\mu\nu}$ is shown in Fig. (8.3) above. These "cross-diagrams" were shown to vanish in the scaling limit in the spin independent case [2]. It is possible that inclusion of these diagrams in the spin dependent case may lead to a cancellation of the non gauge invariant terms of Fig. (8.2). We find the term of interest to be

$$\begin{aligned} q_\mu \text{Im} \mathcal{T}_{\mu\nu}^A [\text{Fig.}(8.3)] &= -\frac{e_d^2}{4(2\pi)^3} \frac{p^2}{\nu} \ln(-p^2) q^2 (\gamma_\mu \not{p} \gamma_\nu - \gamma_\nu \not{p} \gamma_\mu) \frac{p^2}{\nu} 3(1-x)^2 \\ &= q_\mu \text{Im} \mathcal{T}_{\mu\nu}^A [\text{Fig.}(8.2)] \neq 0. \end{aligned} \quad (8.17)$$

This reinforces, rather than cancels the non gauge invariant pieces in eq. (8.14). Similarly evaluating the corresponding tensor structure for the remaining set of cross diagrams shown in Fig. (8.4), we find the result to be the same as eq. (8.17) with the charge factor e_d^2 being replaced by $e_u e_d$. However, we

emphasise that the requirement of gauge invariance is on the total $\text{Im}\mathcal{T}_{\mu\nu}$, not on individual contributions. We immediately see that the divergence of $\text{Im}\mathcal{T}_{\mu\nu}^{\text{neutron}}$ vanishes, as it should.

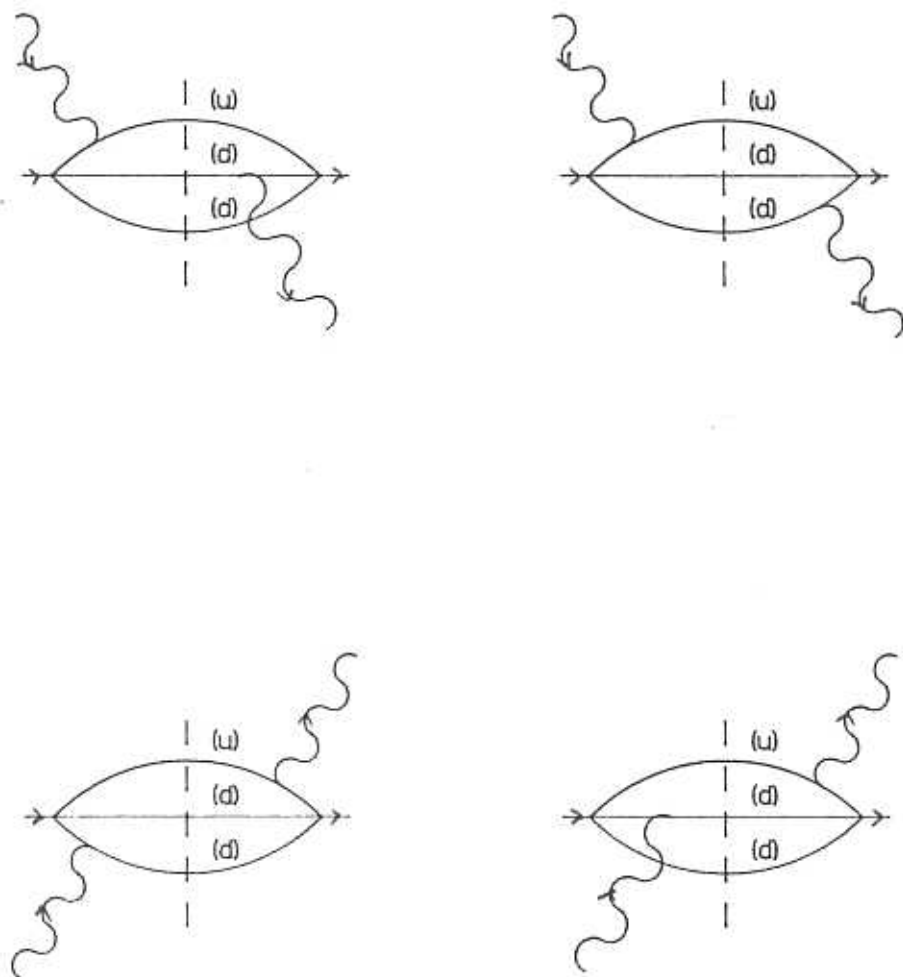


Fig. 8.4 This shows the “cross” diagrams contributing to $\text{Im}\mathcal{T}_{\mu\nu}$ where the quark that absorbs the (virtual) photon does not have the same flavour as the quark that emits it.

This is because $\text{Im} \mathcal{T}_{\mu\nu}^{\text{neutron}}$ is the sum of the contributions from Figs. (8.1)–(8.4). Since Fig. (8.1) is gauge invariant and the gauge noninvariant pieces of Figs. (8.2)–(8.4) are the same apart from charge factors, the derivative of $\text{Im} \mathcal{T}_{\mu\nu}^{\text{neutron}}$ is proportional to

$$(0 \cdot e_u^2 + e_d^2 + e_d^2 + e_u e_d) = e_d(2e_d + e_u) = 0. \quad (8.18)$$

However, $q_\mu \text{Im} \mathcal{T}_{\mu\nu}^{\text{proton}}$ (which is obtained by interchanging e_u and e_d in the neutron computation) is proportional to

$$e_u(2e_u + e_d) \propto e_{\text{proton}} \neq 0. \quad (8.19)$$

With this, we exhaust the list of possible diagrams contributing to the identity coefficient of the Sum Rule. To summarise our results so far, the u -quark structure is gauge invariant, but the d -quark structure is not. Further, the “cross diagrams” involving terms proportional to e_d^2 as well as to $e_u e_d$ are also not gauge invariant. Also, all gauge non invariant structures appear at $\mathcal{O}(p^4/\nu)$ and hence survive in the scaling limit. Taken together, the diagrams are gauge invariant, by which we mean that they satisfy the condition in eq. (8.7). Explicitly, this means that while the derivative of the neutron correlator in the RHS vanishes, that for the proton does not. It is proportional to e_{proton} as required by eq. (8.7); however, the dispersed form of the proton correlator (LHS) involves the two-point function, $T_{\mu\nu}$, with zero divergence. We also point out here that this situation does not occur in any meson calculation.

We now ask whether there exists any other nucleon current that yields a divergence-free result for the proton calculation to $\mathcal{O}(p^4/\nu^2)$. There are only two independent, local currents without derivatives with quantum numbers of the nucleon [15]. Denoting them as $O_1(y)$ and $O_2(y)$ we have, for the proton,

$$\begin{aligned} O_1(y) &= \epsilon^{abc} \left((u^a)^T C d^b \right) \gamma_5 u^c ; \\ O_2(y) &= \epsilon^{abc} \left((u^a)^T C \gamma_5 d^b \right) u^c . \end{aligned} \quad (8.20)$$

Let us consider, for the proton current, a generalised linear combination:

$$\eta_t(y) = O_1(y) + t O_2(y) . \quad (8.21)$$

The current, $\eta(y)$, defined in eq.(8.5), is

$$\eta(y) = 2(O_1(y) - O_2(y)) . \quad (8.22)$$

We shall only calculate the four-divergence, $q_\mu \text{Im} \mathcal{T}_{\mu\nu}$ using the current η_t as we are interested here in its gauge invariance properties. Specifically, we wish to see if there exists a (real) value of t that satisfies the condition,

$$q_\mu \text{Im} \mathcal{T}_{\mu\nu}^{t,A} = 0 .$$

However, it is more convenient to evaluate the trace of $\text{Im} \mathcal{T}_{\mu\nu}^{t,A}$ with $\gamma_5 \not{p}$. Hence we shall check for the condition,

$$q_\mu \text{Tr}(\gamma_5 \not{p} \text{Im} \mathcal{T}_{\mu\nu}^{t,A}) = 0 . \quad (8.23)$$

This has terms of the form

$$A + t^2 B + t(C + D) ,$$

where A , B , C and D are the contributions from the $O_1 \bar{O}_1$, $O_2 \bar{O}_2$, $O_1 \bar{O}_2$ and $O_2 \bar{O}_1$ terms respectively. Further, each of these terms gets contributions from each of the diagrams in Figs. (8.1)–(8.4). However, many of these terms are equal; in particular, we have

$$A = B; \quad C = D$$

and further, for each term, the contributions of Figs. (8.2) and (8.3) are equal, while that of Fig. (8.4) equals the sum of the contributions of Figs. (8.1) and (8.2). With this, we obtain,

$$q_\mu \text{Tr} \left[\gamma_5 \not{p} \text{Im} \mathcal{T}_{\mu\nu}^{t,A} \right] = e_u^2 I + e_u e_d II + e_d^2 III ,$$

where

$$\begin{aligned} I &= 2 \{ (1+t^2)A_2 + 2tC_2 \} , \\ II &= \{ [(1+t^2)A_2 + 2tC_2] + [(1+t^2)A_1 + 2tC_1] \} , \\ III &= 2 \{ (1+t^2)A_1 + 2tC_1 \} . \end{aligned} \quad (8.24)$$

Here, the subscripts 1 and 2 stand for the contributions to the terms A and C coming from the Figs. (8.1) and (8.2). These evaluate to

$$A_1 = 3X_\nu ; \quad C_1 = 3X_\nu ; \quad A_2 = -9X_\nu ; \quad C_2 = -3X_\nu ,$$

$$\text{where } X_\nu = \frac{i}{4(2\pi)^3} \frac{p^4}{\nu} \ln(-p^2) x(1-x)^2 q_\mu \epsilon_{\mu\nu\lambda\sigma} p_\lambda S_\sigma .$$

Substituting in eq. (8.24), we have

$$\begin{aligned} I &= -2(9t^2 + 6t + 9)X_\nu , \\ II &= -6(1 + t^2)X_\nu , \\ III &= 3(t^2 + 2t + 1)X_\nu . \end{aligned} \quad (8.25)$$

Hence, for the proton, we get

$$q_\mu \text{Tr} \left[\gamma_5 \not{S} \text{Im} \mathcal{T}_{\mu\nu}^{A,t} \right] = 3X_\nu \left[(t^2 + 1)(e_d^2 - 2e_u e_d - 6e_u^2) + 2t(e_d^2 - 2e_u^2) \right] . \quad (8.26)$$

We see at once that $t = -1$ is a unique solution to the condition $III = 0$ for the d -quark contribution in eq.(8.25), while there does not exist any real t that satisfies $II, III = 0$ for either the e_u^2 or the $e_u e_d$ contributions. This is true for the neutron case also, since this just involves an interchange of e_u and e_d . We see from eq. (8.26) that no real value of t in eq. (8.26) can satisfy the condition in eq. (8.23). However, we know from our earlier analysis that the solution for the charge-neutral neutron should necessarily satisfy eq. (8.23). Interestingly, we see that (on interchanging e_u and e_d to obtain the neutron solution using isospin symmetry), in eq.(8.26)), there exists exactly one value of t , namely, $t = -1$, that does this. Hence, the condition of gauge invariance in the calculation of the neutron structure functions implies the existence of exactly one valid form of nucleon current, which is the one displayed in eq. (8.5). Also, the

“cross-diagrams” are essential in obtaining a gauge invariant result. However, the problem of different nature of divergence of the RHS and LHS in the proton case persists.

It is interesting at this point to do a similar analysis of the unpolarised case. This can be done by computing the $(\mu\nu)$ symmetric terms of these diagrams, *i.e.*, $\mathcal{T}_{\mu\nu}^S$. At order $\mathcal{O}(p^2/\nu)$ (at which both F_1 and F_2 get contributions), the corresponding results are

$$A = B = C = D = 0$$

i.e., every arbitrary combination of O_1 and O_2 for both the neutron and proton yields a gauge invariant result in the spin-independent sector! In fact, every diagram is gauge invariant by itself, so that there is no restriction on the value of t from the spin independent sector. Furthermore, every contribution is divergence-free. We conclude that the form of nucleon current specified in eq.(2.5) is most suitable as it satisfies the requirement of gauge invariance for the nucleon, both proton and neutron, for both the spin independent and spin dependent cases.

8.3 Conclusion

We have attempted to discuss some of the problems and technicalities involved in applying the QCD Sum Rule technique to evaluate nucleon spin dependent structure functions. We first show the conditions under which the two sides of the Sum Rule can be matched. The condition of gauge invariance severely restricts the choice of nucleon current and in fact, makes it unique. Such a constraint cannot come from a study of the spin independent case where all possible choices of nucleon current are allowed. Recall that the $(\mu\nu)$ antisymmetric part of $\mathcal{T}_{\mu\nu}$ is also the spin dependent part. $\mathcal{T}_{\mu\nu}^S$ sums over spins and hence it is not sensitive to the spinor structure of the nucleon current. Since $\mathcal{T}_{\mu\nu}^A$ probes the spin content of the nucleon, it is perhaps not surprising that the spin dependent calculation restricts the choice of the spinorial current, η , while the spin independent calculation is indifferent to the tensor structure of

η . The spin dependent calculation of the nucleon structure function therefore provides a convincing argument for the choice of current shown in eq. (8.5), namely,

$$\eta^n(y) = \epsilon^{abc} \left[(d^a)^T(y) C \gamma_\alpha d^b(y) \right] \gamma_5 \gamma^\alpha u^c(y),$$

as claimed by Ioffe in [15].

References

- [1] M.A. Shifman, A.I. Vainshtein and V.I. Zakharov, Nucl. Phys. **B147** (1979) 385 ; **B147** (1979) 448
V.A. Novikov, M.A. Shifman, A.I. Vainshtein, M.B. Voloshin and V.I. Zakharov, Nucl. Phys. **B237** (1984) 525
- [2] V.M. Belyaev and B.L. Ioffe, Nucl. Phys. **B310** (1988) 548
- [3] B.L. Ioffe, Nucl. Phys. **B188** (1981) 317 ; Nucl. Phys. **B191** (1981) 591E
- [4] V.M. Belyaev and B.L. Ioffe, Sov. Phys. JETP **56** (1982) 493 ; **57** (1983) 716
- [5] B.L. Ioffe and A.V. Smilga, Nucl. Phys. **B232** (1984) 109
- [6] I.I. Balitsky and A.V. Yung, Phys. Lett. **B129** (1983) 328
- [7] V.M. Belyaev and Y.I. Kogan, JETP Lett. **37** (1983) 730; Phys. Lett. **B136** (1984) 273; for an independent calculation, see C.B. Chiu, J. Pasupathy and S.L. Wilson, Phys. Rev. **D32** (1985) 1786
- [8] V.M. Belyaev, B.L. Ioffe and Y.I. Kogan, Phys. Lett. **B151** (1985) 290
S. Gupta, M.V.N. Murthy and J. Pasupathy, Phys. Rev. **D39** (1989) 2547
E.M. Henley, W.-Y.P. Hwang and L.S. Kisslinger, Phys. Rev. **D46** (1992) 431

- [9] P. Pascual and R. Tarrach, Lec. Notes in Physics **194**, *QCD: Renormalisation for the Practitioner*, Springer-Verlag, 1984
- [10] E.V. Shuryak, World Scientific Lec. Notes in Physics **8**, *The QCD vacuum, hadrons and the Superdense matter*, World Scientific, 1988
- [11] J.P. Singh and J. Pasupathy, Phys. Lett. **B198** (1987) 239
- [12] V.M. Belyaev and B.L. Ioffe, Int. J. Mod. Phys. **A6** (1991) 1533
- [13] D. Indumathi, Inst. of Mathematical Sciences, preprint IMSc/92/47
- [14] J.D. Bjorken, Phys. Rev. **148** (1966) 1467
- [15] B.L. Ioffe, Nucl. Phys. **B188** (1981) 317; **E B191** (1981) 591; Z. Phys **C18** (1983) 67
- D. Espriu, P. Pascual and R. Tarrach, Nucl. Phys. **B214** (1983) 285
- See also,
- Y. Chung, H.G. Dosch, M. Krenmer and D. Schall, Phys. Lett. **B102** (1981) 175 ; Nucl. Phys. **B197** (1982) 55

2 → 2 KINEMATICS

CONTENTS

Introduction

The Cross-section

Mandelstam Variables

A.0 Introduction

We discuss here, the kinematics of the scattering of two particles of 4-momenta p_1 and p_2 ,

$$p_1 + p_2 \rightarrow p_3 + p_4 ,$$

in their centre-of-mass (CM) frame. All results are well known and have been presented for the sake of completeness. Let E_i and \vec{p}_i , $i = 1, \dots, 4$, denote the energy and 3-momentum (vector) of the particles respectively. Then there are 16 variables in the problem, but not all are independent. There are four constraints coming from the mass-shell condition on the four external line momenta, *i.e.*,

$$p_i^2 = M_i^2 ,$$

where M_i is the mass of the i -th particle. Overall energy-momentum conservation eliminates four more variables as

$$p_1 + p_2 = p_5 = p_3 + p_4 ,$$

where p_5 is the 4-momentum of the intermediate off-shell state; this condition typically eliminates the variables corresponding to one of the final state particles, say, p_4 . In the CM of p_1 and p_2 ,

$$\vec{p}_1 = -\vec{p}_2 . \tag{A.1}$$

This eliminates three more variables. Freedom of choice of the coördinate axes eliminates two more variables. We choose them to be

$$p_{1z} = p_{2y} = 0$$

or equivalently, $\theta = \phi = 0$ in spherical coördinates, where an arbitrary momentum is represented as

$$k = (E, |k|(\sin \theta \cos \phi, \sin \theta \sin \phi, \cos \theta)) .$$

The interaction vertex is the origin of the coördinate system. Finally, eq. (A.1) implies that

$$\vec{p}_3 = -\vec{p}_4 .$$

Hence, the process is planar (with the interaction plane defined by the two vectors \vec{p}_1 and \vec{p}_3) and is invariant under rotation of the plane of interaction about the interaction vertex. In other words, the final state azimuthal angle, ϕ_3 , is irrelevant.

These 15 constraints leave only one variable in $2 \rightarrow 2$ processes, namely, $\theta_3 (= \theta_4 - 180^\circ \equiv \theta)$. Note that the total initial energy in the interaction,

$$s = (p_1 + p_2)^2 ,$$

is fixed.

We can now write down the various momenta explicitly:

$$\begin{aligned} p_1 &= (E_1, 0, 0, p) , \\ p_2 &= (E_2, 0, 0, -p) , \\ p_3 &= (E_3, p'(\sin \theta, 0, \cos \theta)) , \\ p_4 &= (E_4, -p'(\sin \theta, 0, \cos \theta)) , \end{aligned} \tag{A.4}$$

where we have used $\phi = 0$. p_1 and p_2 are completely fixed in terms of (known) quantities, s , M_1^2 and M_2^2 as follows:

$$\begin{aligned} 2\sqrt{s}E_1 &= s \pm M_1^2 \mp M_2^2 , \\ p^2 &= \frac{s^2 + (M_1^2 - M_2^2)^2}{2s} , \end{aligned} \tag{A.5}$$

and

$$p'^2 = \frac{s^2 + (M_3^2 - M_4^2)^2}{2s} ,$$

so that θ is the only unknown quantity, once \sqrt{s} is fixed.

In the limit of massless particles, which we shall most often use, the specific forms for the various momenta are

$$\begin{aligned} p_1 &= \frac{\sqrt{s}}{2} (1, 0, 0, 1) ; \\ p_2 &= \frac{\sqrt{s}}{2} (1, 0, 0, -1) ; \\ p_3 &= \frac{\sqrt{s}}{2} (1, 0, \sin \theta, \cos \theta) ; \\ p_4 &= \frac{\sqrt{s}}{2} (1, 0, -\sin \theta, -\cos \theta) . \end{aligned} \tag{A.2}$$

A.1 The Cross-section

The differential cross-section for the process is symbolically written as

$$d\sigma = \frac{|M|^2}{F} dQ , \tag{A.3}$$

where $|M|^2$ is the square of the invariant amplitude for the process to occur, F is the incident flux and dQ is the Lorentz invariant phase space factor. $|M|^2$ is process dependent while the flux is a measure of the number of beam and target particles interacting per unit time so that the cross-section is independent of the number of particles in beam or target. For the $2 \rightarrow 2$ process under consideration, the flux in the lab. frame is given by the product of the density of target particles and the density of beam particles traversing a unit area perpendicular to the beam direction per unit time. More generally, the flux is given by the manifestly Lorentz invariant quantity,

$$F = 4 \left((p_1 \cdot p_2)^2 - M_1^2 M_2^2 \right)^{1/2} . \tag{A.4}$$

Finally, dQ is a measure of the number of available final states and is given by (the Lorentz invariant quantity)

$$dQ = (2\pi)^4 \delta^4(p_1 + p_2 - p_3 - p_4) \frac{d^3 p_3}{(2\pi)^3 2E_3} \frac{d^3 p_4}{(2\pi)^3 2E_4} \tag{A.5}$$

where the energy momentum conservation condition is expressed by means of the δ -function. Eqs. (A.4) and (A.5) ensure that the expression for the cross-section in eq. (A.3) is Lorentz invariant.

We will now evaluate eq. (A.3) for the $2 \rightarrow 2$ process in the CM frame.

Use

$$\frac{d^3 p}{(2\pi)^3 2E} \equiv \frac{d^4 p}{(2\pi)^3} \delta^+(p^2 - M^2);$$

$$\text{where } \delta^+(p^2 - M^2) \equiv \delta(p^2 - M^2) \theta(p_0),$$

(obtained by performing the integration over p_0) to eliminate p_4 . Then, we have

$$dQ = \frac{1}{(2\pi)^2} \frac{d^3 p_3}{2E_3} \delta^+((p_1 + p_2 - p_3)^2 - M_4^2).$$

It is straight-forward to show that in the CM frame,

$$\delta(E_4^2 - (E_1 + E_2 - E_3)^2) \equiv \frac{1}{2E_4} \delta(E_1 + E_2 - E_3 - E_4).$$

We now need to simplify

$$d^3 p_3 = p'^2 dp' d\Omega.$$

We know that p' is not an independent variable and so we can integrate it out.

We use the mass-shell condition which gives

$$d(E_3 + E_4) = p' dp' \left(\frac{1}{E_3} + \frac{1}{E_4} \right).$$

On changing variables from p' to $(E_3 + E_4)$, we can use the δ -function to perform the integration. This yields

$$dQ = \frac{1}{16\pi^2} \frac{p'}{\sqrt{s}} d\Omega, \quad (\text{A.6})$$

where we have used $(E_1 + E_2) = \sqrt{s}$.

The flux factor in the CM frame is similarly evaluated to be

$$F = 4p\sqrt{s}. \quad (\text{A.7})$$

Hence, the differential cross-section in the CM frame is

$$\frac{d\sigma}{d\cos\theta} = \frac{1}{32\pi s} \frac{p'}{p} |M|^2, \quad (\text{A.8})$$

where we have used $d\Omega \equiv d\cos\theta d\phi$ and have performed the (trivial) ϕ integration.

A.2 Mandelstam variables

It is more convenient to compute the cross-section in terms of Lorentz invariant variables. These are defined as

$$s = (p_1 + p_2)^2 ; \quad t = (p_1 - p_3)^2 ; \quad u = (p_1 - p_4)^2 .$$

Since there are only two independent variables in a $2 \rightarrow 2$ scattering process, only two of these are independent. The constraint equation is

$$s + t + u = \sum_{i=1}^4 M_i^2 , \quad \text{or}$$
$$s + t + u = 0 \quad \text{in the massless case.}$$

For the massless case, in the CM frame,

$$t = -\frac{s}{2} (1 - \cos \theta) ,$$
$$u = -\frac{s}{2} (1 + \cos \theta) ,$$
$$s = 4p^2 ,$$

where p is fixed for a given experimental setup.

For more details, see *Quarks and Leptons: An Introductory Course in Modern Particle Physics* by F. Halzen and A.D. Martin, New York, Wiley, 1984 and *An Introduction to Quarks and Partons* by F.E. Close, London, Academic Press, 1979.

COLLECTION OF USEFUL FORMULÆ

CONTENTS

- The QCD Lagrangian
 Definitions and Normalisation Conventions
 γ Matrix Algebra
 Some Colour Traces and Identities
 Feynman Rules for QCD

B.0 The QCD Lagrangian

Quantum Chromodynamics (QCD) is a renormalisable quantum field theory of strong interactions. The fundamental fermionic fields of spin half and fractional charge are called quarks and possess the SU(3) quantum number called *colour*, which is gauged, as well as *flavour*. The mediators of the colour (strong) interactions, called *gluons*, are spin-1 massless particles with zero electric charge and no flavour which also undergo self-interactions.

Let $q_f^\alpha(x)$ denote a quark field of colour α and flavour f , $\alpha = 1, 2, 3$ and $f = u, d, s, \dots$. Typically, we shall assume three flavours for the purpose of our calculations. Let B_μ^a denote the gauge fields, $a = 1, \dots, 8$ (in the adjoint representation of SU(3)) where μ is the Lorentz index.

The Lagrangian density can be expressed as

$$L = \frac{1}{2g^2} \text{Tr} F^{\mu\nu} F_{\mu\nu} + \frac{i}{2} \bar{q}_f \gamma_\mu D^\mu q_f(x), \quad (B.1)$$

where the covariant derivative, D^μ , given by

$$D_{\alpha\beta}^\mu \equiv \delta_{\alpha\beta} \partial^\mu - ig T_{\alpha\beta}^a B_a^\mu(x), \quad (B.2)$$

is introduced in order to make the Lagrangian density invariant under *local* gauge (colour) transformation:

$$q_f^{\alpha'}(x) = G_{\alpha\beta}(x) q_f^\beta(x) \equiv \left(e^{-igT_a\theta_a(x)} \right)_{\alpha\beta} q_\beta(x). \quad (B.3)$$

Here $\theta_a(x)$ are real, space-time dependent functions, g is a real dimensionless coupling constant and T_a are the generators of the SU(3) algebra in its fundamental representation. Denote

$$\begin{aligned} B^\mu(x) &\equiv igT_a B_a^\mu(x) \\ D^\mu &\equiv I\partial^\mu - B^\mu(x), \end{aligned} \quad (B.4)$$

where B^μ and D^μ are now $N \times N$ (here 3×3) matrices. Introduce the antisymmetric field strength tensor,

$$\begin{aligned} F^{\mu\nu}(x) &\equiv igT_a F_a^{\mu\nu}(x) \equiv -[D^\mu, D^\nu] \\ &= \partial^\mu B^\nu(x) - \partial^\nu B^\mu(x) - [B^\mu(x), B^\nu(x)], \end{aligned}$$

$$\text{where } F_a^{\mu\nu}(x) = \partial^\mu B_a^\nu(x) - \partial^\nu B_a^\mu(x) + gf_{abc} B_b^\mu(x) B_c^\nu(x).$$

The last term reflects the non-abelian character of SU(3). In general, the Lagrangian density in eq. (B.1) can be expressed as

$$L = L_{\text{gauge}} + L_q + L_{qg} + L_{gg}, \quad (B.5)$$

where L_{gauge} and L_q are the kinetic term for the gluon and quark fields given by

$$\begin{aligned} L_{\text{gauge}} &= \frac{1}{2g^2} \text{Tr } F^{\mu\nu}(x) F_{\mu\nu}(x), \\ L_q &= i\bar{q}_f^\alpha(x) \gamma^\mu \partial_\mu q_f^\alpha(x) - m_f \bar{q}_f^\alpha(x) q_f^\alpha(x). \end{aligned} \quad (B.6)$$

and are invariant under local gauge transformations. A mass term for the quark field does not break this invariance, but one for the gluons will. The qg interaction piece is given by

$$L_{qg} = \frac{g}{2} \bar{q}_f^\alpha(x) \lambda_{\alpha\beta}^a \gamma_\mu q_f^\beta(x) B_a^\mu(x); \quad T_a = \lambda_a/2, \quad (B.7)$$

while the gluon self-interaction is described by

$$L_{gg} = -\frac{g}{2} f_{abc} (\partial^\mu B_a^\nu - \partial^\nu B_a^\mu) B_b^\mu B_c^\nu(x) - \frac{g^2}{4} f_{abc} f_{ade} B_b^\mu B_c^\nu B_d^\mu(x) B_e^\nu(x). \quad (B.8)$$

The equations of motion are

$$\begin{aligned} (i \not{D} - m_f)q_f(x) &= 0; & \not{D} &\equiv D_\mu \gamma^\mu \\ [D^\mu, F_{\mu\nu}(x)] &= -ig^2 T_a \sum_f \bar{q}_f(x) \gamma_\nu q_f(x). \end{aligned} \quad (B.9)$$

B.1 Definitions and normalisation conventions

The Lagrangian density is invariant with respect to various symmetries and conservation laws; in particular, it satisfies Lorentz and translational invariance. P_μ is the energy-momentum operator and is the infinitesimal generator of translations, while $\mathcal{J}_{\mu\nu}$ is the angular momentum operator and is the infinitesimal generator of Lorentz transformations.

From these can be constructed the two invariant Casimirs, P^2 and W^2 , where W_μ is the Pauli-Lubanski vector given by

$$W_\mu = -\frac{1}{2} \varepsilon_{\mu\nu\rho\sigma} \mathcal{J}^{\nu\rho} P^\sigma. \quad (B.10)$$

Since $P^2 = m^2$, W^2 takes only values of the form $W^2 = -m^2 S(S+1)$ where S denotes the spin (integer or half-integer) of the particle. For both the Dirac as well as Klein-Gordon field, $P_\mu = -i\partial_\mu$ so $P^2 = -\partial^2 = m^2$. For the Dirac case we are interested in, $\mathcal{J}_{\mu\nu}$, as we have said, is the (infinitesimal) generator of Lorentz transformations:

$$\begin{aligned} x' &= \Lambda x, \\ \psi'(x') &= S(\Lambda)\psi(x), \end{aligned}$$

where $\partial x^\nu / \partial x'^\mu = (\Lambda^{-1})^\nu_\mu$ and S is constrained to satisfy

$$S(\Lambda)\gamma^\mu S^{-1}(\Lambda) = (\Lambda^{-1})^\mu_\nu \gamma^\nu \quad (B.11)$$

in order that both ψ as well as the transformed ψ' satisfy the Dirac equation. A proper transformation may be written as

$$\Lambda^\mu_\nu = g^\mu_\nu + \omega^\mu_\nu$$

with ω^μ_ν being an infinitesimal antisymmetric matrix. Hence, $S(\Lambda)$ can be expanded as

$$S(\Lambda) = I - \frac{i}{4} \sigma^{\mu\nu} \omega_{\mu\nu} + \dots \quad (B.12)$$

where the matrices σ_ν^μ are also antisymmetric and a choice of them that satisfies the constraint eq. (B.11) is

$$\sigma_{\alpha\beta} = \frac{i}{2} [\gamma_\alpha, \gamma_\beta] .$$

In terms of this matrix, the transformation can be expressed as

$$\begin{aligned} \psi'(x) &\equiv \left(I - \frac{i}{2} \mathcal{J}_{\mu\nu} \omega^{\mu\nu} \right) \psi(x) = \left(I - \frac{i}{4} \sigma_{\mu\nu} \omega^{\mu\nu} \right) \psi(x^\rho - \omega_\nu^\rho x^\nu) \\ &= \left(I - \frac{i}{4} \sigma_{\mu\nu} \omega^{\mu\nu} + x_\mu \omega_\nu^\mu \partial_\nu \right) \psi(x) \end{aligned}$$

from which we deduce

$$\mathcal{J}_{\mu\nu} = \frac{1}{2} \sigma_{\mu\nu} + i(x_\mu \partial_\nu - x_\nu \partial_\mu) .$$

Hence, we have

$$W_\mu = -\frac{1}{4i} \varepsilon_{\mu\nu\rho\sigma} \sigma^{\nu\rho} \partial^\sigma ; \quad W^2 = -\frac{1}{2} \left(\frac{1}{2} + 1 \right) m^2 . \quad (B.12)$$

We see that W_μ has no orbital contribution so that it corresponds to intrinsic angular momentum and that it describes spin-half particles.

The positive energy Dirac spinor with momentum p and mass m , satisfying $(\not{p} - m)u(p) = 0$ is normalised according to

$$\bar{u}^\alpha(p) u(p)^\beta = 2m \delta_{\alpha\beta} \quad (B.13)$$

while the negative energy one (corresponding to an antiparticle) is normalised according to

$$\bar{v}^\alpha(p) v(p)^\beta = -2m \delta_{\alpha\beta} \quad (B.13)$$

where $\alpha, \beta = 1, 2$ are polarisation indices while the projectors are given by

$$\begin{aligned} \Lambda_+(p) &= \sum_\alpha u^\alpha(p) \otimes \bar{u}^\alpha(p) = (\not{p} + m) . \\ \Lambda_-(p) &= \sum_\alpha v^\alpha(p) \otimes \bar{v}^\alpha(p) = (-\not{p} + m) . \end{aligned} \quad (B.14)$$

The states are normalised according to

$$\langle p, S | p', S' \rangle = \delta^{SS'} 2E (2\pi)^3 \delta^3(\vec{p} - \vec{p}') , \quad E = \sqrt{|\vec{p}|^2 + m^2} . \quad (B.15)$$

Given a space-like normalised four-vector, $n, n^2 = -1$, orthogonal to the momentum p , we can write the projection of W_μ in eq. (B.12), as

$$W \cdot n = -\frac{1}{4i} \epsilon_{\mu\nu\rho\sigma} n^\mu p^\nu \sigma^{\rho\sigma} = -\frac{1}{2} \gamma_5 \not{n} \not{p}. \quad (B.16)$$

Hence, in the rest frame, $p = (m, \vec{0})$,

$$W_0 = 0; \quad \vec{W} = \frac{m}{2} \gamma_5 \gamma^0 \vec{\gamma} \equiv \frac{m}{2} \vec{\Sigma}, \quad (B.17)$$

where $\vec{\Sigma}$ is the matrix $\text{diag}(\vec{\sigma}, \vec{\sigma})$ where $\vec{\sigma}$ are the Pauli matrices.

To define states of definite polarisation, which is the quantity of central interest in the thesis, we construct the projection operators along the z -direction. In this case, we choose n along the z -axis, $n = (\vec{0}, 1)$ so that the Dirac spinors are eigen states of the operator $-(W \cdot n)/m$ with eigen values $\pm 1/2$. In general,

$$P(n) = \frac{1}{2} (1 + \gamma_5 \not{n}) \quad (B.18)$$

projects onto the state which has a spin $(\sigma \cdot n)/2 = 1/2$ for a positive energy solution and $-1/2$ for a negative energy one, thus removing the degeneracy between the two solutions. With the particular choice of n such that \vec{n} is proportional to the momentum \vec{p} , the polarisation is called helicity and is such that

$$P(n) \Lambda_\pm(p) = \left(I \pm \frac{\Sigma \cdot \vec{p}}{|\vec{p}|} \right) \Lambda_\pm(p)$$

so that $P(n)$ projects over positive energy, positive helicity and negative energy, negative helicity states. The spin of the particle, S^μ can be identified with the vector n . When n is along the z -axis, in the nonrelativistic limit, $P_\pm = (1 \pm \sigma_z)/2$, while in the extreme relativistic limit, $m/p_0 \rightarrow 0$, $S^\mu \rightarrow p^\mu/m$, the projections yield

$$\begin{aligned} P(\pm S)(\not{p} + m) &= \frac{1 \pm \gamma_5}{2} (\not{p} + m) \\ &= \frac{1 \pm \lambda \gamma_5}{2} (\not{p} + m); \quad \lambda = \pm 1. \end{aligned} \quad (B.19)$$

The eigen states of $P(S)$ with $\lambda = \pm 1$ (i.e., with spin along or opposed to the momentum direction) are known as positive and negative helicity eigen

states. Helicity is defined as the component of spin along the 3-momentum, generalising the case of Dirac particles and the notion extends to massless particles. This immediately implies that the matrix element for a right handed fermion denoted by

$$u_R(p, S) \equiv \left(\frac{1 + \gamma_5}{2} \right) u(p, S)$$

to scatter into a left handed one, denoted by

$$u_L(p, S) \equiv \left(\frac{1 - \gamma_5}{2} \right) u(p, S)$$

with interaction γ^μ (electromagnetic) is zero. Hence fermion helicity is conserved in electromagnetic processes at the photon-fermion vertex.

A spin-one space-like gluon (or photon) has three polarisation vectors, the transverse, $\epsilon^\mu(\pm)$ with helicity ± 1 and the longitudinal (or scalar) one, $\epsilon^\mu(0)$, with zero helicity. These and the momentum vector of the boson are orthogonal to one another and satisfy the condition $q_\mu \epsilon_\lambda^\mu = 0$, for $\lambda = \pm 1, 0$. An example of such a basis for $q^2 < 0$ is

$$\begin{aligned} \epsilon(\pm 1) &= \mp \frac{1}{\sqrt{2}}(0, 1, \pm i, 0) \\ \epsilon(0) &= \frac{i}{\sqrt{-q^2}}(|\vec{q}|, 0, 0, q_0) \end{aligned}$$

In particular, this vector can be re-written in terms of Dirac spinors as

$$\epsilon_\mu^\lambda(q) = \frac{1}{(4q \cdot p)^{1/2}} \bar{u}_\lambda(q) \gamma_\mu u_\lambda(p)$$

where p is an arbitrary time-like vector such that $q \cdot p \neq 0$ and $p^2 = 0$. In fact, p can be chosen to be any vector in the problem, especially external line momenta which are on-shell and therefore satisfy the requirements on p . Note that the arbitrariness allowed in the choice of p is equivalent to the gauge freedom we have and is a choice of gauge. Matrix elements, when computed, will be independent of p . Hence, the polarisation tensor,

$$T_{\mu\nu}^\lambda \equiv \epsilon_\mu^\lambda \epsilon_\nu^{\lambda*}$$

can be written as

$$T_{\mu\nu}^{\lambda} = -\frac{1}{2}g_{\mu\nu} + \frac{q_{\mu}p_{\nu} + q_{\nu}p_{\mu}}{2q \cdot p} + \frac{i\lambda}{2q \cdot p}\epsilon_{\mu\nu\rho\sigma}q^{\rho}p^{\sigma}$$

where we have used the relations for $u(p)\bar{u}(p)$ as given earlier and traced over the γ matrices as prescribed in the next section. Here λ denotes the helicity of the boson. When we sum over the polarisation states, we obtain

$$\sum_{\lambda} T_{\mu\nu}^{\lambda} = -g_{\mu\nu} + \frac{q_{\mu}p_{\nu} + q_{\nu}p_{\mu}}{q \cdot p}$$

as in the axial gauge where the antisymmetric piece has dropped out of the expression. This form of $T_{\mu\nu}^{\lambda}$ is useful when we consider scattering of definite helicity gluons.

B.2 γ -matrix algebra

The metric is defined as $g^{\mu\nu} = \text{diag}(1, -1, -1, -1)$. The gamma matrices satisfy

$$\{\gamma^{\mu}, \gamma^{\nu}\} = 2g^{\mu\nu}.$$

γ_0 is hermitian while the γ^i are antihermitian and

$$\begin{aligned}\gamma_5 &= i\gamma^0\gamma^1\gamma^2\gamma^3, \\ &= -\frac{i}{4!}\epsilon_{\mu\nu\rho\sigma}\gamma^{\mu}\gamma^{\nu}\gamma^{\rho}\gamma^{\sigma},\end{aligned}$$

with

$$\gamma_5^2 = 1 \quad \text{and} \quad \{\gamma_5, \gamma^{\nu}\} = 0.$$

Here $\epsilon_{\mu\nu\rho\sigma}$ is the totally antisymmetric Levi-Civita tensor with $\epsilon^{0123} = +1$.

We have the following useful relations:

$$\begin{aligned}\gamma^0\gamma^{\mu}\gamma^0 &= \gamma^{\mu\dagger} \\ \gamma^0\gamma_5\gamma^0 &= -\gamma_5^{\dagger} = -\gamma_5 \\ C\gamma_{\mu}C^{-1} &= -\gamma_{\mu}^T \\ C\gamma_5C^{-1} &= -\gamma_5^T\end{aligned}$$

where C stands for the Charge conjugation matrix and T for transpose. Note $C = -C^{-1} = -C^\dagger = -C^T$; $C^2 = -1$. Finally, we have

$$\begin{aligned}\gamma_\mu \gamma^\mu &= 4 \\ \gamma_\mu \gamma^\lambda \gamma^\mu &= -2\gamma^\lambda \\ \gamma_\mu \gamma^\lambda \gamma^\rho \gamma^\mu &= 4g^{\lambda\rho} \\ \dots &= \dots\end{aligned}$$

Furthermore, we can express the product of three γ -matrices in terms of its symmetric and antisymmetric components as

$$\gamma_\mu \gamma_\rho \gamma_\nu = [g_{\mu\rho} \gamma_\nu + g_{\nu\rho} \gamma_\mu - g_{\mu\nu} \gamma_\rho] - i\epsilon_{\mu\rho\nu\eta} \gamma_5 \gamma_\eta.$$

Traces of odd numbers of γ matrices vanish. Traces of even number of γ matrices or traces of γ_5 and an even number of γ matrices can be evaluated using standard relations; we show a few below:

$$\begin{aligned}\text{Tr}(\gamma_\mu \gamma_\nu) &= 4g_{\mu\nu} \\ \text{Tr}(\gamma_\mu \gamma_\nu \gamma_\rho \gamma_\lambda) &= 4(g_{\mu\nu} g_{\rho\lambda} + g_{\mu\lambda} g_{\nu\rho} - g_{\mu\rho} g_{\nu\lambda}) \\ \text{Tr}(\gamma_5 \gamma_\mu \gamma_\nu \gamma_\rho \gamma_\lambda) &= -4i\epsilon^{\mu\nu\rho\lambda}\end{aligned}$$

B.3 Some Colour Traces and Identities

There are $N^2 - 1$ generators in $SU(N)$, $T_a = \lambda_a/2$, $a = 1, \dots, N^2 - 1$, which close a Lie algebra:

$$\begin{aligned}[\lambda_a, \lambda_b] &= 2if_{abc} \lambda_c; \\ \{\lambda_a, \lambda_b\} &= \frac{4}{N} \delta_{ab} I + 2d_{abc} \lambda_c.\end{aligned}$$

The d_{abc} are real and symmetric while the f_{abc} are real and totally antisymmetric and satisfy

$$f_{abc} f_{dbc} = N \delta_{ad}.$$

The gluon fields transform as its adjoint representation; then

$$(T_a)_{bc} = -if_{abc}.$$

The quark fields transform under SU(3) as the fundamental representation and here $T_a = \lambda_a/2$. The λ_a are traceless hermitian matrices such that

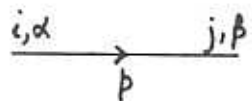
$$(\lambda_a)_{\alpha\beta}(\lambda_a)_{\gamma\delta} = 2 \left\{ \delta_{\alpha\delta}\delta_{\beta\gamma} - \frac{1}{N}\delta_{\alpha\beta}\delta_{\gamma\delta} \right\} .$$


Some useful colour traces are

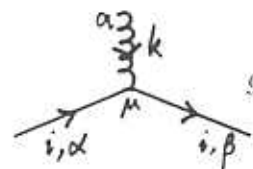
$$\begin{aligned} \text{Tr}(\lambda_a) &= 0 , \\ \text{Tr}(\lambda_a\lambda_b) &= 2\delta_{ab} \\ \text{Tr}(\lambda_a\lambda_b\lambda_c) &= 2(d_{abc} + if_{abc}) \\ \dots &= \dots \end{aligned}$$

For $N = 3$, the diagonal λ_a are $\lambda_3 = \text{diag}(1, -1, 0)$, $\lambda_8 = \text{diag}(1, 1, -2)/\sqrt{3}$. Explicit values of the f 's and d 's are listed in the references given at the end.

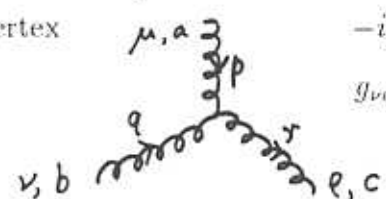
B.4 Feynman Rules for QCD

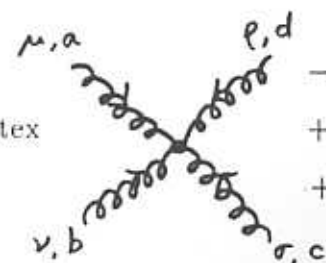
Quark Propagator  $\frac{i}{\not{p} - m_i} \delta_{ij} \delta_{\alpha\beta}$

Gluon Propagator  $\frac{-ig_{\mu\nu} \delta_{ab}}{k^2}$

Fermion Gluon Vertex  $g \left(\frac{\lambda_a}{2} \right)_{\beta\alpha} \gamma^\mu$

Fermion Photon Vertex  $-ie e_q \gamma^\mu$

Triple Gluon Vertex  $-ig f_{abc} [g_{\mu\nu}(p-q)_\sigma + g_{\nu\sigma}(q-r)_\mu + g_{\sigma\mu}(r-p)_\nu]$

Quartic Gluon Vertex  $-g^2 [f_{abe} f_{cde} (g_{\mu\sigma} g_{\nu\rho} - g_{\mu\rho} g_{\nu\sigma}) + f_{ace} f_{bde} (g_{\mu\nu} g_{\sigma\rho} - g_{\mu\rho} g_{\nu\sigma}) + f_{ade} f_{cbe} (g_{\mu\sigma} g_{\nu\rho} - g_{\mu\nu} g_{\sigma\rho})]$

Propagators are attached to each internal line while spinors (u or v) are attached to every external quark or antiquark line and the polarisation vector (ϵ_μ^λ) to every external gluon line. Finally, overall momentum conservation is represented by the δ -function.

For details, see the books on

Quantum Field Theory by C. Itzykson and J-B. Zuber, McGraw-Hill, 1980 and *Lecture Notes in Physics* Vol. 194, QCD: Renormalisation for the practitioner by P. Pascual and R. Tarrach, Springer-Verlag 1984.

DEEP INELASTIC SCATTERING PHENOMENA

C O N T E N T S

Introduction
 The Leptonic Tensor, $\mathcal{L}_{\mu\nu}$
 The Hadronic Tensor, $W^{\mu\nu}$
 The Cross-section
 The Asymmetry
 Parton Model Interpretation

C.0 Introduction

Consider deep inelastic electromagnetic scattering¹ (DIS) of muons (or any leptons) on protons. In this process, which can be represented as

$$\ell p \rightarrow \ell X ,$$

the high energy lepton probe causes the proton to break-up and so probes the structure of the proton. Here X is the hadron debris which remains experimentally unobserved.

The momenta are indicated in Fig. (C.1). The initial lepton of momentum k and spin s scatters into the final state lepton of momentum k' and spin s' while the nucleon of momentum p and spin S breaks up into a number of final states, p_i , of spin S'_i , $i = 1, \dots, N$, with invariant mass, W , given by

$$W^2 = (p + k - k')^2 \equiv (p + q)^2 = M_p^2 + 2\nu + q^2 ,$$

where $q \equiv (k - k')$ is the momentum flowing into the hadronic vertex (the momentum of the virtual intermediate state photon), $\nu \equiv p \cdot q$ and M_p is the

¹We do not consider weakly interacting DIS processes here

nucleon mass. This is no longer just a $2 \rightarrow 2$ process as there are a number of final states.

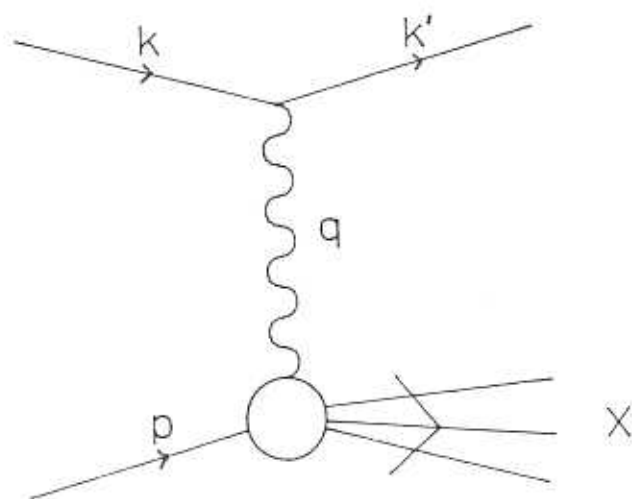


Fig. C.1 This illustrates the DIS process and the break-up of the proton due to the collision.

However, of these, only the lepton is detected. This means that we need to integrate out the p_i . Then, in the CM of μ and p , we choose the momenta as follows:

$$\begin{aligned} k &= E(1, 0, 0, 1), \quad p = E(1, 0, 0, -1), \\ k' &= E'(1, \hat{n}); \quad \hat{n} = (\sin \theta, 0, \cos \theta), \end{aligned}$$

where we have chosen the azimuthal scattering angle to be zero and have neglected the masses of the lepton as well as the proton in comparison with the incident beam energy. Hence $E = \sqrt{s}/2$, s is the Mandelstam variable, not to be confused with spin.

In the lab. frame, the kinematical invariants are

$$\begin{aligned} q^2 &= -4EE' \sin^2(\theta/2) \\ \text{and } \nu &= p \cdot q = M_p(E - E'), \end{aligned}$$

where θ is the lab. scattering angle. Hence there are two independent variables, (E', θ) or equivalently, (q^2, ν) in DIS. Note that $q^2 = -Q^2$ is negative for this t -channel DIS process but will be positive for, say, the e^+e^- annihilation process. The phase space factor is given by

$$dQ = (2\pi)^4 \delta^4 \left(k + p - k' - \sum_i p_i \right) \frac{d^3 k'}{(2\pi)^3 2E'} \prod_i \frac{d^3 p_i}{(2\pi)^3 2E_i}.$$

$$\text{We shall denote } \widetilde{dQ} \equiv \frac{d^3 k'}{(2\pi)^3 2E'} = \frac{E' dE' d\Omega'}{2(2\pi)^3}. \quad (C.1)$$

Then from eq. (A.3), we have

$$d\sigma = \frac{|\widetilde{M}|^2}{F} \widetilde{dQ}, \quad (C.2)$$

where we have included the hadronic phase space factors in $|\widetilde{M}|^2$, viz.,

$$|\widetilde{M}|^2 \equiv (2\pi)^4 \delta^4 \left(k + p - k' - \sum_i p_i \right) \prod_i \frac{d^3 p_i}{(2\pi)^3 2E_i} |M|^2,$$

where M is the matrix element as usual and the flux, $F = 2s$. The Mandelstam variable, s , is the (Lorentz invariant) CM energy squared ($= 4M_p E$ in the lab frame with the proton at rest).

The lepton-photon vertex is an elementary one characterised by γ_μ , while the interaction of the photon with the composite proton is non-trivial and unknown. Let us express the matrix element as

$$-iM = \bar{u}(k', s') (-ie\gamma_\mu) u(k, s) \frac{-i}{q^2} \langle p, S | (iej^\mu) | p_i, S' \rangle ,$$

where j^μ is the electromagnetic current and $u(k, s)$ is the lepton spinor. We can then separate out the lepton and hadron dependent parts:

$$|M|^2 \equiv \frac{e^4}{q^4} \mathcal{L}_{\mu\nu} M^{\mu\nu} , \quad (C.3)$$

where $\mathcal{L}_{\mu\nu}$ represents the known leptonic part and the hadronic part, $M^{\mu\nu}$, will be expressed in terms of *structure functions*. We begin with a discussion of the leptonic tensor.

C.1 The Leptonic Tensor, $\mathcal{L}_{\mu\nu}$

The leptonic term can be expressed as

$$\mathcal{L}_{\mu\nu}(k, k', s) = \sum_{s'} \text{Tr} (\gamma_\mu S_\ell(k, s) \gamma_\nu S_\ell(k', s')) , \quad (C.4)$$

where

$$S_\ell(k, s) = u(k, s) \bar{u}(k, s)$$

is known (see App. B). The helicity contributions to $\mathcal{L}_{\mu\nu}$ can be expressed in terms of the symmetric and antisymmetric combinations:

$$\mathcal{L}_{\mu\nu}^\pm = \mathcal{L}_{\mu\nu}^S + \mathcal{L}_{\mu\nu}^{\pm, A} . \quad (C.5)$$

The spin independent piece is given by the terms symmetric in the indices $(\mu\nu)$. Neglecting mass terms, we have

$$\mathcal{L}_{\mu\nu}^S = \frac{1}{2} \text{Tr} (\gamma_\mu \not{k} \gamma_\nu \not{k}') = 2 \{ k_\mu k'_\nu + k_\nu k'_\mu - g_{\mu\nu} k \cdot k' \} \quad (C.6)$$

where the last step comes from using the identities in App. B. The piece that is antisymmetric in the indices $(\mu\nu)$ is linear in the lepton spin:

$$\mathcal{L}_{\mu\nu}^A = -\frac{\lambda_\ell}{2} \text{Tr} (\gamma_5 \gamma_\mu \not{k} \gamma_\nu \not{k}') = -2i\lambda_\ell \epsilon_{\mu\nu\rho\sigma} k_\rho k'_\sigma . \quad (C.7)$$

Here, we have used the relativistic limit of $S_\ell(k, s)$ as given in eqs. (B.14) and (B.19):

$$S_\ell(k, s) = \frac{(1 \pm \gamma_5)}{2} (\not{k} + m) \rightarrow \frac{(1 + \lambda_\ell \gamma_5)}{2} (\not{k} + m),$$

where $\lambda_\ell = \pm 1$ represents the helicity state of the particle.

C.2 The Hadronic Tensor, $W^{\mu\nu}$

The hadronic tensor is

$$M^{\mu\nu} \equiv \sum_{S'} \langle p, S | j_\mu | p_i, S' \rangle \langle p_i, S' | j_\nu | p, S \rangle, \quad (C.8)$$

where the sum is over intermediate state spins, S' and j^μ is the usual electromagnetic current given by

$$j^\mu = \bar{\psi} \gamma^\mu \psi, \quad (C.9)$$

where ψ is the proton wave function. As in eq. (C.2), we shall include the hadronic phase space factors with $M^{\mu\nu}$ and define a new quantity,

$$W^{\mu\nu} \equiv \frac{1}{4\pi M_p} \prod_{i=1}^N \int \frac{d^3 p_i}{(2\pi)^3 2E_i} (2\pi)^4 \delta^4(p + q - \sum_i p_i) M^{\mu\nu}, \quad (C.10)$$

where p_i runs over all possible allowed physical intermediate states. Then, analogous to eq. (C.3), we can write

$$|\widetilde{M}|^2 \equiv \frac{e^4}{q^4} \mathcal{L}_{\mu\nu} W^{\mu\nu}. \quad (C.11)$$

Performing the sum over the complete set of final states, we have

$$\begin{aligned} W^{\mu\nu} &= \frac{1}{4\pi M_p} \int d^4 x e^{iq \cdot x} \langle p, S | j^\mu(x) j^\nu(0) | p, S \rangle \\ &= \frac{1}{4\pi M_p} \int d^4 x e^{iq \cdot x} \langle p, S | [j^\mu(x), j^\nu(0)] | p, S \rangle, \end{aligned} \quad (C.12)$$

where we have used the completeness property,

$$\sum_i \int \frac{d^3 p_i}{(2\pi)^3 2E_i} |p_i\rangle \langle p_i| \equiv \sum_X |X\rangle \langle X| = 1.$$

We are able to introduce the current commutator in the definition for $W^{\mu\nu}$ because the $j_\nu j_\mu$ term (which is the extra piece added in, in the last step

of eq. (C.12)) is physically disallowed and identically vanishes. However, expressing $W^{\mu\nu}$ as a current commutator enables it to be written in terms of the imaginary part of the forward (virtual) photon-proton scattering amplitude, $T^{\mu\nu}$, defined by

$$T^{\mu\nu} = i \int d^4x e^{iq \cdot x} \langle p, S | T(j^\mu(x)j^\nu(0)) | p, S \rangle, \quad (C.13)$$

where T stands for the time-ordered product of the currents. Using the optical theorem, we have

$$W^{\mu\nu} = \frac{1}{\pi} \text{Im} T^{\mu\nu}, \quad (C.14)$$

The hadronic tensor also has components which are both symmetric as well as antisymmetric with respect to the interchange of indices ($\mu\nu$),

$$W^{\mu\nu} = W^{\mu\nu,S} + W^{\mu\nu,A}.$$

Then the symmetric part of $\mathcal{L}_{\mu\nu}$ contracts with the symmetric part of $W^{\mu\nu}$ to yield the spin independent cross-section and the antisymmetric part of $\mathcal{L}_{\mu\nu}$ contracts with the antisymmetric part of $W^{\mu\nu}$ to give the spin dependent cross-section. The usual procedure is as follows: the hadronic tensor is unknown and is expressed in its most general form in terms of the available vectors and tensors of the theory. These are the metric, $g^{\mu\nu}$, p^μ , q^μ , the two independent momenta occurring at the hadron vertex and S^μ , the proton spin (axial) vector. $W^{\mu\nu}$ must satisfy constraints due to Lorentz invariance, hermiticity ($W^{\mu\nu} = W^{\nu\mu*}$) and gauge invariance ($q_\mu W^{\mu\nu} = q_\nu W^{\mu\nu} = 0$, which is a consequence of current conservation, $\partial_\mu j^\mu = 0$). Furthermore, $W^{\mu\nu}$ must respect parity and time reversal symmetry. (Note that parity can be violated in weak-DIS. In fact, gauge invariance also does not hold). All these constraints together yield the following form for the spin-symmetric part of the hadronic tensor:

$$\frac{1}{2} W^{\mu\nu,S} = W_1(q^2, \nu) \left(\frac{q^\mu q^\nu}{q^2} - g^{\mu\nu} \right) + \frac{W_2(q^2, \nu)}{M_P^2} \left(p^\mu - \frac{p \cdot q}{q^2} q^\mu \right) \left(p^\nu - \frac{p \cdot q}{q^2} q^\nu \right). \quad (C.15)$$

In other words, the unknown nature of the hadronic vertex is *parametrised* in terms of the unknown structure functions. There are two structure functions

in the spin independent case, W_1 and W_2 which are both functions of q^2 and ν . However, we are more interested in the spin dependent or antisymmetric piece,

$$W^{\mu\nu,A} = -i\epsilon^{\mu\nu\lambda\sigma} q_\lambda \left\{ S_\sigma \left(M_p G_1(q^2, \nu) + \frac{p \cdot q}{M_p} G_2(q^2, \nu) \right) - \frac{q \cdot S}{M_p} p_\sigma G_2(q^2, \nu) \right\}. \quad (C.16)$$

G_1 and G_2 are the two spin dependent structure functions.

C.3 The Cross-section

Combining the results in eqs. (C.6) and (C.7) for the leptonic tensor and in eqs. (C.15) and (C.16) for the hadronic tensor, we can write the differential DIS cross-section using eqs. (C.1) and (C.3) in terms of the two independent variables, E' and θ . The symmetric contribution is independent of either the lepton or proton spin and is also twice the total unpolarised cross-section, *i.e.*, the cross-section for the scattering of unpolarised leptons off unpolarised protons. This is because the symmetric term is the sum over the possible initial spin orientations which can be represented as

$$\frac{d\sigma^{\text{lab}}}{d\Omega' dE'} (\uparrow\downarrow + \uparrow\uparrow) = \left[\frac{2\alpha^2}{4E'^2 \sin^4(\theta/2)} \right] \left\{ 2W_1 \sin^2(\theta/2) + W_2 \cos^2(\theta/2) \right\}. \quad (C.17)$$

where $\alpha = e^2/(4\pi)$ is the fine structure constant. The arrows denote that the relative longitudinal polarisations of the initial lepton and proton are parallel ($\uparrow\uparrow$) or antiparallel ($\uparrow\downarrow$). Half the above sum indicates a spin average rather than a spin sum and so corresponds to the spin averaged (unpolarised) cross-section.

The quantity shown in square brackets is twice the Mott cross-section and has a typical $(1/\sin^4(\theta/2))$ behaviour as in the classic scattering of α particles off (gold) nuclei.

Experimentally, it is observed that the cross-section does not separately depend on q^2 and ν , but rather on the single Bjorken variable, $x = -q^2/2\nu$; $0 < x \leq 1$. The W_i are said to *scale* in the variable x and dimensionless *scaling*

structure functions are defined in the limit,

$$\lim_{\substack{-q^2 \rightarrow \infty \\ \nu \rightarrow \infty}} \frac{-q^2}{2\nu} = x, \text{ constant}, \quad (C.18)$$

by

$$\begin{aligned} (\nu/M_p) W_2(\nu, q^2) &\rightarrow F_2(x) \text{ (dimensionless)}; \\ M_p W_1(\nu, q^2) &\rightarrow F_1(x) \text{ (dimensionless)}. \end{aligned} \quad (C.19)$$

In terms of the invariants, s , t and u defined in Appendix A, we have

$$\frac{d\sigma}{dt du}(\uparrow\downarrow + \uparrow\uparrow) = \frac{8\pi\alpha^2}{t^2 s^2} \frac{1}{(s+u)} \left\{ (s+u)^2 x F_1(x) - us F_2(x) \right\}. \quad (C.20)$$

A third expression in terms of the dimensionless variables, x and $y = \nu/(M_p E)$ is

$$\frac{d\sigma}{dx dy}(\uparrow\downarrow + \uparrow\uparrow) = \frac{8\pi\alpha^2 s}{t^2} \left\{ xy^2 F_1(x) + (1-y) F_2(x) \right\}. \quad (C.21)$$

$x = 1$ corresponds to elastic ℓp scattering. Since experimentally $\sin^2(\theta/2) \ll 1$, it is hard to extract W_1 . However, the F_i satisfy the Callan-Gross relation, from which F_1 can be extracted.

We now consider the spin dependent case. Such a contribution can be measured in polarised DIS processes. The kinematics of the polarised process is the same as that for the unpolarised case, except that the initial state particles are both longitudinally polarised along a reference axis (here, the beam direction or the z -axis):

$$\vec{\mu}\vec{p} \rightarrow \mu X$$

and cross-sections are measured when their spins are parallel as well as antiparallel to each other. Eq. (C.17) still holds for the sum of the two polarisation configurations, while the spin dependent cross-section is obtained by evaluating the difference in the cross-section when the spins are parallel and antiparallel with respect to each other. The result can be simply obtained by contracting the antisymmetric part of $\mathcal{L}_{\mu\nu}$ with the antisymmetric part of $W^{\mu\nu}$. Hence, probing the spin dependent piece is equivalent to selecting the $(\mu\nu)$ antisymmetric piece. Note also that *both* the initial particles need to

be polarised in order to obtain information on the proton spin, as otherwise the cross-section vanishes. (Equivalently, it is possible to have a single initial particle polarised, but we need to maintain information on the polarisation of at least one of the final state particles). We obtain

$$\frac{d\sigma^{\text{lab}}}{d\Omega'dE'}(\uparrow\downarrow - \uparrow\uparrow) = \left[\frac{\alpha^2}{E^2 \sin^2(\theta/2)} \right] \left\{ (E + E' \cos \theta) M_p G_1(q^2, \nu) + q^2 G_2(q^2, \nu) \right\}. \quad (\text{C.22})$$

Notice that the symmetric combination in eq. (C.17) involves only the spin independent structure functions, $F_{1,2}$ while the antisymmetric combination in eq. (C.22) depends only on the spin dependent functions $G_{1,2}$. Again in the scaling limit defined in eq. (C.18), the spin dependent structure functions can be written in terms of the dimensionless scaling structure functions,

$$\begin{aligned} M_p \nu G_1(\nu, q^2) &\rightarrow g_1(x) \text{ (dimensionless);} \\ (\nu^2/M_p) G_2(\nu, q^2) &\rightarrow g_2(x) \text{ (dimensionless).} \end{aligned} \quad (\text{C.23})$$

It is useful to express these cross-sections (or $W^{\mu\nu}$) in terms of helicity amplitudes in polarised virtual photo-absorption using the optical theorem. Keeping in mind parity and time reversal invariance, there are four such independent helicity amplitudes, $W_{i,j;i',j'}$ for the process

$$\gamma(i)N(j) \rightarrow \gamma(i')N(j')$$

where i and j are spin projections of the photon and nucleon. The independent amplitudes are

$$\begin{aligned} a &\equiv W_{1,1/2;1,1/2}, & b &\equiv W_{1,-1/2;1,-1/2}, \\ c &\equiv W_{0,1/2;0,1/2}, & d &\equiv W_{1,-1/2;0,1/2}. \end{aligned}$$

In terms of these amplitudes, we can write the various structure functions as follows:

$$\begin{aligned} W_1 &= \frac{A}{2} (b + a) \sim \sigma_{1/2}^T + \sigma_{3/2}^T; \\ W_L &\equiv (1 + \frac{\nu^2}{M_p^2 Q^2}) W_2 - W_1 = A c \sim \sigma_{1/2}^L; \\ \nu G_1 - Q^2 G_2 &= \frac{A}{2} (b - a) \sim \sigma_{1/2}^T - \sigma_{3/2}^T; \\ \sqrt{Q^2} (M_p G_1 + \frac{\nu}{M_p} G_2) &= A d \sim \sigma_{1/2}^{TL}. \end{aligned} \quad (\text{C.24})$$

Here, $A = K/(4\pi^2\alpha)$ where K is the photon flux factor and σ are the photo-absorption cross-sections into states with $J_z = 1/2, 3/2$ and with transverse (T , helicity = ± 1) or scalar (L , helicity = 0) photons. In terms of these photo-absorption cross-sections, the DIS cross-section can be written as

$$\begin{aligned} \frac{d\sigma}{d\Omega dE'}(\uparrow\downarrow + \uparrow\uparrow) &= (\sigma_{1/2}^T + \sigma_{3/2}^T) [1 + \epsilon R] \Gamma ; \\ \frac{d\sigma}{d\Omega dE'}(\uparrow\downarrow - \uparrow\uparrow) &= \left[(\sigma_{1/2}^T - \sigma_{3/2}^T) \left\{ 1 - \frac{E'}{E} \epsilon \right\} + \sigma_{1/2}^{TS} \left\{ \frac{\sqrt{Q^2}}{E} \epsilon \right\} \right] \Gamma , \end{aligned} \quad (C.25)$$

where we have introduced the quantities,

$$\begin{aligned} \epsilon &= \left[1 + 2 \left(1 + \frac{\nu^2}{M_p^2 Q^2} \right) \tan^2(\theta/2) \right]^{-1} \quad \text{and} \\ \Gamma &= \frac{K\alpha}{\pi^2 Q^2} \frac{E'}{E} \frac{1}{(1 - \epsilon)} . \end{aligned} \quad (C.26)$$

Note that ϵ is small as it has a $1/\nu$ behaviour which vanishes in the scaling limit. The final form of the cross-sections given in eq. (C.25) is what we need to use.

C.4 The Asymmetry

This is the quantity that is actually measured in experiments. It is defined as

$$A^{\mu p(DIS)} \equiv \frac{d\sigma(\uparrow\downarrow - \uparrow\uparrow)}{d\sigma(\uparrow\downarrow + \uparrow\uparrow)} , \quad (C.27)$$

where the cross-section can be differential with respect to any convenient set of independent variables. The asymmetry is independent of the photon flux factor and can be put into the form

$$A^{\mu p} = D (A_1 + \eta A_2) , \quad (C.28)$$

where the depolarisation factor, D , is of order unity and is given by

$$D = \frac{1 - \epsilon E'/E}{1 + \epsilon R} ; R = \sigma^L / \sigma^T , \quad (C.29)$$

where $\sigma^T = \sigma_{1/2}^T + \sigma_{3/2}^T$. The transverse asymmetry, A_1 , is given by

$$A_1 = \frac{\sigma_{1/2}^T - \sigma_{3/2}^T}{\sigma_{1/2}^T + \sigma_{3/2}^T} = \frac{1}{F_1(x)} \left(g_1(x) - \frac{2xM_p^2}{\nu} g_2(x) \right) \quad (C.30)$$

in terms of the scaling structure functions while

$$\eta = \frac{\epsilon \sqrt{Q^2}}{E - \epsilon E'}$$

and

$$A_2 = \frac{\sigma_{1/2}^{TS}}{\sigma^T} = \frac{M_p \sqrt{Q^2}}{\nu} \frac{(g_1(x) + g_2(x))}{F_1(x)}.$$

There exist bounds, $|A_1| \leq 1$ and $|A_2| \leq R$ on these asymmetries. Since $R \rightarrow 0$, A_2 vanishes in the scaling limit. Furthermore, η , which is the coefficient of A_2 in the equation for the asymmetry, $A^{\mu p}$, (eq. (C.28)), is also small. Hence, the EMC has used, in the analysis of its polarised DIS data, the approximation,

$$A^{\mu p}(x) \simeq D A_1(x) \simeq D \frac{g_1(x)}{F_1(x)}. \quad (C.31)$$

This neglect of A_2 is equivalent to the assumption $g_2(x) = 0$, which is expected to hold in the parton model.

C.5 Parton Model Interpretation

Historically, scaling behaviour was anticipated by Bjorken and Feynman and was later experimentally observed. This suggests an interpretation of the scattering target in terms of point-like, nearly non-interacting constituents, most of which have spin-1/2. This idea is incorporated into the parton model, which is formulated in the infinite momentum frame where the masses of both proton as well as parton are ignored in comparison with the (large) 3-momentum of the proton. Within the parton model, the structure functions are expressed in terms of the density distributions, $f^\pm(x)$, of the partons, where x is now interpreted to be the fraction of the parent proton momentum that is carried by the parton. Specifically, $f^\pm(x)$ is the probability of finding, in a proton with its spin polarised along a specified direction, a parton of flavour f with momentum fraction between x and $(x + dx)$ and with its spin aligned (+) or opposed (-) to that of the parent hadron. The combination

$$q_f(x) = f^+(x) + f^-(x)$$

is identified as the number density corresponding to flavour type, f , while the difference

$$\bar{q}_f(x) = f^+(x) - f^-(x)$$

is the net positive helicity or spin density of f -flavour quarks along the proton spin direction.

The structure function, F_2 , is then defined as a (charge weighted) sum of the momentum fractions, $xq_f(x)$, of partons of various flavours:

$$F_2(x) = \sum_f e_f^2 xq_f(x) \quad (C.32)$$

and the Callan-Gross relation is expressed as

$$2xF_1 = F_2; \quad R \equiv \frac{\sigma_L}{\sigma_T} = 0. \quad (C.33)$$

Hence, DIS is pictured as incoherent elastic scattering of the lepton off the constituent quarks so that the total cross-section is a sum over individual cross-sections, not over individual amplitudes. The parton model predicts

$$\frac{d\sigma}{dx dy} (\uparrow\downarrow + \downarrow\uparrow) = \frac{4\pi\alpha^2}{q^4} s \{1 + (1-y)^2\} \sum_f e_f^2 xq_f(x). \quad (C.34)$$

If quarks had zero spin, the scaling behaviour of the structure functions would still hold, but R would tend to infinity rather than zero. This is not the observation and lends support to the parton model hypothesis of spin-half charged quarks. The parton model predictions are identical to the lowest order QCD result; they are however, modified at the next order.

Analogously, for the spin dependent case, we have

$$g_1(x) = \frac{1}{2} \sum_f e_f^2 \bar{q}_f(x) \quad \text{and} \quad g_2(x) = 0. \quad (C.35)$$

The expression for the asymmetry is

$$A^{np} = \frac{\sum_{f,\bar{f}} e_f^2 \bar{q}_f(x)}{\sum_{f,\bar{f}} e_f^2 q_f(x)}; \quad A(x=0) = 0; \quad A(x=1) = 1.$$

The last ($A(1) = 1$) is an assumption, implying that as $x \rightarrow 1$, when all the momentum of the proton is carried by a single quark, the entire spin is also carried by that same quark.

The Bjorken Sum Rule [1] is derived from current algebra considerations; it states that assuming isospin symmetry, the proton and neutron spin dependent structure functions are related to the axial vector coupling constant as follows:

$$\int_0^1 (g_1^p(x) - g_1^n(x)) dx = \frac{1}{6} g_A (1 - \alpha_S/\pi) , \quad (C.36)$$

where the expression has been corrected up to first order in QCD. The Ellis-Jaffe Sum Rule [2] makes the stronger assumption of $SU(3)_f$ symmetry as well as that of zero strange quark polarisation to obtain individual expressions for the moments of the proton and neutron spin dependent structure functions:

$$\int_0^1 g_1^{p(n)}(x) dx = \frac{g_A}{12} \left[\pm 1 \left(1 - \frac{\alpha_s}{\pi} \right) + \frac{1}{3} \frac{3F - D}{F + D} \left\{ 5 - \left(1 + 4 \frac{33 - 8f}{33 - 2f} \right) \frac{\alpha_s}{\pi} \right\} \right] , \quad (C.37)$$

where F and D are the antisymmetric and symmetric $SU(3)$ couplings, related to the observed octet coupling constants by

$$g_A = F + D , \quad g_8 = 3F - D$$

and f is the number of quark flavours. Eq. (C.37) has also been QCD-corrected to $\mathcal{O}(\alpha_s)$; note that the corrections to the two terms are different because of different Q^2 dependence of the nonsinglet (first term) and singlet (second term) contributions. If we use the central values for g_A and g_8 as given in the text: $g_A = 1.261$, $g_8 = 0.584$ and $\alpha_s(Q^2 = 10.7 \text{ GeV}^2) = 0.27$, we get a value $\int dx g_1^p(x) = 0.174$ using the Ellis-Jaffe result, which is very different from the EMC result of 0.126. Furthermore, the moment of the neutron structure function comes out to be -0.018 and is very sensitive to the choice of g_8 .

We have just provided the basic equations for DIS scattering; details can be had from several standard text books, including that of Halzen and Martin and Close referenced in Appendix A.

References

- [1] J.D. Bjorken, Phys. Rev. **148** (1966) 1467
- [2] J. Ellis and R.L. Jaffe, Phys. Rev. **D9** (1974) 1444; E: **D10** (1974) 1669;
for an independent derivation using $SU(6)$ current algebra, see
A.S. Joshipura and P. Roy, Nucl. Phys. **B116** (1976) 591

KINEMATICS OF pp PROCESSESC O N T E N T SVariables in pp processesThe cross-section for $2 \rightarrow 3$ processes

Choice of reference frame

D.0 Variables in pp processes

The *hadronic* pp collision process, as we have seen, can be expressed as a sum over all possible contributing *partonic* subprocesses. Consider Drell-Yan (DY) or Direct Photon ($D\gamma$) production. We shall present the variables in the centre of mass of hadrons (CMH), in DY, for example,

$$\begin{aligned} p_1 p_2 &\rightarrow \gamma^* X, \\ &\hookrightarrow \mu^+ \mu^-, \end{aligned}$$

as well as in the centre of mass of partons (CMP):

$$\begin{aligned} q_1 q_2 &\rightarrow \gamma^* q_3 \\ &\hookrightarrow \mu^+ \mu^-. \end{aligned}$$

All CMP variables are distinguished by carets; we have

$$\begin{aligned} \hat{s} &\equiv (q_1 + q_2)^2 = 2q_1 \cdot q_2; \\ \hat{t} &\equiv (q_1 - q_\gamma)^2 = M^2 - 2q_1 \cdot q_\gamma; \\ \hat{u} &\equiv (q_1 - q_3)^2 = -2q_1 \cdot q_3; \\ \hat{s} + \hat{t} + \hat{u} &= M^2. \end{aligned} \tag{D.1}$$

The partons, q_i , $i = 1, \dots, 3$, have been assumed to be massless while the off-shell photon has a "mass" M^2 . Furthermore, $M^2 = 0$ for $D\gamma$. We shall consider the DY case in general; unless otherwise specified, corresponding results for $D\gamma$ are obtained by simply setting $M^2 = 0$.

q_1 and q_2 carry a fraction of momentum, x_1 and x_2 , of their parent hadron momenta, p_1 and p_2 . Hence, the Mandelstam variables in the CMp and CMH are related by

$$\hat{s} = x_1 x_2 s; \quad \hat{t} = \frac{(M^2 - \hat{s})}{2} (1 - \cos \hat{\phi}); \quad \hat{u} = \frac{(M^2 - \hat{s})}{2} (1 + \cos \hat{\phi}), \quad (D.2)$$

where $\hat{\phi}$ is the CMp scattering angle ($= \hat{\phi}_\gamma = \hat{\phi}_3 - 180^\circ$).

There are four independent variables in DY: x_1 , x_2 , $\cos \hat{\phi}$ and $\tau = M^2/s$ in the CM of partons, in terms of which we have expressed the cross-section in Chapter 4. These are *not* the physically observed variables in the CM of hadrons (or the lab frame). One such set of observables is (x_T, y_1, y_2, τ) . x_T is a dimensionless measure of the transverse momentum picked up by the final state particles in the collision process:

$$x_T = \frac{2p_T}{\sqrt{s}} = \frac{(x_1 x_2 - \tau)}{\sqrt{(x_1 x_2)}} \sin \hat{\phi}; \quad 0 < x_T \leq 1. \quad (D.3)$$

Note that since the initial states had no transverse momentum, x_T (or p_T) is the same in either the CMp or CMH (as they are related by a boost along the longitudinal direction). The rapidities of the photon and jet, y_1 and y_2 , are defined by

$$y_i = \frac{1}{2} \ln \left(\frac{E_i + p_{L_i}}{E_i - p_{L_i}} \right) = \frac{1}{2} \ln \frac{E_i + |p| \cos \theta_i}{E_i - |p| \cos \theta_i}, \quad (D.4)$$

where E , p_L are the energy and longitudinal momentum (z -component) and θ_i are the scattering angles in the hadron CM. Rapidities are preferred to angles as they obey an additive law under Lorentz transformations, unlike velocities or angles. In the CMp, we have

$$y_i^{CMp} = \frac{1}{2} \ln \frac{E_i + |\vec{p}_i| \cos \hat{\phi}_i}{E_i - |\vec{p}_i| \cos \hat{\phi}_i}. \quad (D.5)$$

Since $\hat{\phi}_1 = 180^\circ + \hat{\phi}_2$, we have $y_1^{CMp} = -y_2^{CMp}$. In other words, the γ^* and jet are always back-to-back in the parton CM. This is not so in the hadronic CM, where

$$y_\gamma^{CMH} = \frac{1}{2} \ln \frac{(\hat{s} + M^2 + (\hat{s} - M^2) \cos \hat{\phi}_i)}{(\hat{s} + M^2 - (\hat{s} - M^2) \cos \hat{\phi}_i)} + \frac{1}{2} \ln \frac{x_1}{x_2}, \quad (D.6)$$

obtained by boosting eq. (D.5) to the CMH, and

$$y_2 = y_{jet}^{CMH} = \frac{1}{2} \ln \frac{(1 - \cos \hat{\phi}_i)}{(1 + \cos \hat{\phi}_i)} + \frac{1}{2} \ln \frac{x_1}{x_2}. \quad (D.7)$$

Define, for convenience,

$$\overline{x_T}^2 = x_T^2 + 4\tau.$$

Then the variables x_1 , x_2 , \hat{l} or equivalently $\cos \hat{\phi}$ and M^2 can be written in terms of the physical set of variables x_T , y_1 , y_2 and τ as

$$\begin{aligned} x_1 &= \frac{1}{2} (\overline{x_T} e^{y_1} + x_T e^{y_2}); & x_2 &= \frac{1}{2} (\overline{x_T} e^{-y_1} + x_T e^{-y_2}); \\ \cos \hat{\phi} &= \frac{\overline{x_T} \sinh(y_1 - y_2)}{x_T + \overline{x_T} \cosh(y_1 - y_2)}; & \tau &= M^2/s; \end{aligned}$$

while the Mandelstam variables defined in eq. (D.2) can be reexpressed more conveniently in terms of the mixed set of variables as

$$\begin{aligned} \hat{l} &= -\frac{s}{2} x_2 x_T e^{y_2} = M^2 - \frac{s}{2} x_1 \overline{x_T} e^{-y_1}; \\ \hat{u} &= -\frac{s}{2} x_1 x_T e^{-y_2} = M^2 - \frac{s}{2} x_2 \overline{x_T} e^{y_1}. \end{aligned} \quad (D.8)$$

Furthermore, $\hat{s} + \hat{l} + \hat{u} = M^2$ implies that $M_{max}^2 = \hat{s} = x_1 x_2 s$ or the physically allowed region is $\tau_{max} = x_1 x_2$. The corresponding results for $D\gamma$ are obtained by setting $M^2 = 0$.

In the special case when $x_1 = x_2 \equiv x$, we have $y_1 = -y_2$ and θ_i and ϕ_i (the CMP and CMH scattering angles) collapse to the same angle. So although $\hat{\phi}$ is not a physically observed variable, the choice $\hat{\phi} = 90^\circ$ in this special frame implies 90° scattering in the lab (CMH) also. With this choice, we obtain

$$\begin{aligned} x &= \frac{1}{2} (x_T \cosh y_2 + \overline{x_T} \cosh y_1); \\ \text{where } \overline{x_T} &= -x_T \frac{\sinh y_2}{\sinh y_1}. \end{aligned}$$

Then the cross-section for the $D\gamma$ process is differential with respect to either of the sets of variables and the two are related by

$$\frac{d\sigma}{dx_T dy_1 dy_2} = \mathcal{J} \frac{(x_1, x_2, \hat{l})}{(x_T, y_1, y_2)} \frac{d\sigma}{dx_1 dx_2 d\hat{l}}, \quad (D.9)$$

where the Jacobean factor is given by

$$\mathcal{J} \frac{(x_1, x_2, \hat{l})}{(x_T, y_1, y_2)} = \frac{x_T}{2} \hat{s} \quad (D.10)$$

for both direct photon as well as the Drell Yan process. For the DY process, there is an additional derivative with respect to τ (or M^2). The kinematics of direct diphoton production and 2-jet production are exactly like in $D\gamma$ as both final state particles are massless here.

D.1 Cross-section for $2 \rightarrow 3$ processes

The cross-section for the subprocesses contributing to the direct photon process can be simply evaluated using the equations for $2 \rightarrow 2$ processes given in Appendix A. The Drell Yan process, however, being a $2 \rightarrow 3$ process, is a little more complicated. It can be thought of as a combination of a $2 \rightarrow 2$ collision process producing a large- p_T (off-shell) photon and a balancing jet, followed by a $1 \rightarrow 2$ decay process in which the photon goes into a lepton pair; in the CMp frame, we have

$$\begin{aligned} q_1 q_2 &\rightarrow \gamma^* q_3, \\ &\hookrightarrow \mu^+ \mu^-. \end{aligned}$$

In general, any $2 \rightarrow 3$ process

$$p_a + p_b \rightarrow p_1 + p_2 + p_3$$

can be decomposed in this manner:

$$\begin{aligned} p_a + p_b &\rightarrow p_1 + p_{23}; \\ p_{23} &\rightarrow p_2 + p_3. \end{aligned}$$

The corresponding differential cross-section is given by

$$d\sigma = \frac{|\mathcal{M}|^2}{F} R_3, \quad (D.11)$$

where F is the flux factor which can be expressed in terms of the Mandelstam invariant, s , as $F = 2s$. (This is the same as in the $2 \rightarrow 2$ process as the flux factor depends on the number of initial states which is the same in both cases.) The matrix element \mathcal{M} , is calculable from the theory, while the phase space factor is given by

$$R_3 = \int \frac{d^3 p_1}{(2\pi)^3 2E_1} \frac{d^3 p_2}{(2\pi)^3 2E_2} \frac{d^3 p_3}{(2\pi)^3 2E_3} (2\pi)^4 \delta^4(p_a + p_b - p_1 - p_2 - p_3). \quad (D.12)$$

All the $\vec{p}_i, i = 1, \dots, 3$ are not independent; for such a process there are four independent variables (the delta function removes four variables of the nine variables and the rotation of the system about the beam axis is trivial). Note that the three final state particles lie in a plane called the production plane. If we introduce the intermediate state explicitly, there are two variables describing each—the collision and the decay—process. To see this, we introduce the intermediate state mathematically into eq. (D.12) by using the identity

$$1 = \int ds_2 \int \frac{d^3 p_{23}}{(2\pi)^3 2E_{23}} \delta^4(p_{23} - p_2 - p_3), \quad (D.13)$$

where $s_2 = (p_2 + p_3)^2 = M^2$ can be thought of as the Mandelstam s variable for the decay process. Hence we can write

$$R_3(s) = \int \frac{ds_2}{(2\pi)^5} R_2(s; m_1^2; s_2) R_2(s_2; m_2^2; m_3^2). \quad (D.14)$$

We therefore have a convolution of two processes, the first a collision process characterised by the Mandelstam variable s where the intermediate state (23), is produced from a collision of particles a and b and the second when this state decays to the particles 2 and 3 characterised by the variable, s_2 which is the mass squared of the intermediate state. The integral over s_2 implies that all possible masses of the intermediate state satisfying the delta-function in eq. (D.13) are allowed. Hence, we can use the procedure developed for $2 \rightarrow 2$ processes to evaluate R_2 for the collision process; on integrating out the dependent variables, we know that this is a function of a single variable, $t = (p_a - p_1)^2$. We get

$$R_2(s; m_1^2; s_2) = \frac{\pi}{4\sqrt{s}P} \int dt, \quad (D.15)$$

where P is the 3-momentum of either of the initial particles (a or b) in their CM frame. The phase space factor coming from the decay process is best evaluated in the rest frame of the intermediate state (23), which evaluates to

$$R_2(s_2; m_2^2; m_3^2) = \frac{P_2^{R23}}{4\sqrt{s_2}} \int d\Omega_2^{R23}, \quad (D.16)$$

where $(R23)$ denotes the rest frame of (23) and P_2 is the magnitude of the 3-momentum of the second (or the third) particle in this frame. Use of eqs. (D.15) and (D.16) in the expression for R_3 in eq. (D.14) and setting

$$P_2^{R23} = \frac{1}{2} (s_2 - 4m_\ell^2)^{1/2},$$

where m_ℓ is the mass of the lepton, yields

$$R_3(s) = \frac{1}{(2\pi)^4 32s} \int dt dM^2 d\Omega_2^{R23}, \quad (D.17)$$

where we have used $s_2 = M^2$ and dropped terms of the order of $\mathcal{O}(m_\ell^2/M^2)$ as the lepton mass is small in comparison with the large momentum-square of the photon.

Hence, the cross-section for the Drell Yan process is

$$\frac{d\sigma}{dt dM^2} = \frac{\sqrt{1 - 4m_\ell^2/M^2}}{(2\pi)^4 64s^2} \int d\Omega_2^{R23} |\mathcal{M}|^2, \quad (D.18)$$

where the matrix element can be calculated for the various contributing subprocesses.

D.2 Choice of Reference Frame

In order to evaluate the integral over the solid angle, Ω_2 in the rest frame of the massive intermediate photon, we have to specify a choice of co-ordinates. We choose arbitrarily, but for later simplicity, p_b to be the z -axis and let p_1 lie in the $(x - z)$ plane. Then in the rest frame of the photon, *viz.*,

$$p_{23} = (M, \vec{0}); \quad \text{or} \quad \vec{p}_2 + \vec{p}_3 = 0,$$

$$\text{we have,} \quad \vec{p}_1 = \vec{p}_a + \vec{p}_b$$

or p_a is fixed. Then the components of the various momenta in this frame are as follows:

$$\begin{aligned} p_b &= E_b(1, 0, 0, 1), \\ p_1 &= E_1(1, \sin \theta_1, 0, \cos \theta_1), \\ p_a &= (E_a, E_1 \sin \theta_1, 0, E_1 \cos \theta_1 - E_b), \\ p_2 &= E(1, \hat{n}), \\ p_3 &= E(1, -\hat{n}), \end{aligned}$$

and we use the mass shell conditions on the particles to obtain

$$\begin{aligned} E_a &= \frac{M^2 - t}{2M}, \\ E_b &= \frac{M^2 - u}{2M}, \\ E_1 &= \frac{s - M^2}{2M}, \\ \cos \theta_1 &= \frac{su - M^2 t}{su + M^2 t}, \\ E &= \frac{M}{2}. \end{aligned}$$

The unit vector, $\hat{n} = (\sin \theta \cos \phi, \sin \theta \sin \phi, \cos \theta)$ denotes the arbitrary orientation of \vec{p}_2 (or \vec{p}_3) in the rest frame of (23) where (θ, ϕ) are to be integrated over. In terms of these variables, the solid angle is given by

$$d\Omega_2^{R23} = d \cos \theta d\phi.$$

Hence, there are four variables (t, M^2, θ, ϕ) with respect to which the cross-section for the $2 \rightarrow 3$ process is differential; in the expressions given in Chapter 4 for Drell Yan subprocesses, we have integrated out the angular variables and retained only (\hat{t}, M^2) . The total hadronic cross-section is then differential with respect to these subprocess variables as well the boost variables to the hadron CM, namely, x_1 and x_2 . Everywhere we have assumed the leptons to be massless.

SOME DETAILS OF THE SUM RULE METHOD

C O N T E N T S

The LHS

The RHS

List of Integrals

E.1 The LHS

We discuss here, some details of the dispersion relation satisfied by the four-point function, $\mathcal{T}_{\mu\nu}^A$, defined as the antisymmetric part of

$$\mathcal{T}_{\mu\nu}(p, q) = -i \int d^4x d^4y d^4z e^{iqx + ip(y-z)} \langle 0 | T [\eta(y) j_\mu(x) j_\nu(0) \bar{\eta}(z)] | 0 \rangle, \quad (E.1)$$

where $\eta(y)$ is the nucleon current and j_μ is the electromagnetic current.

We now make use the identity

$$I = \sum_X |X\rangle \langle X|,$$

which is expressed in momentum space as

$$I = \int \frac{d^3p}{(2\pi)^3 2p_0} |X\rangle \langle X| = \int \frac{d^4p}{(2\pi)^4} 2\pi \delta(p^2 - M_X^2) \theta(p_0) |p_X\rangle \langle p_X|. \quad (E.2)$$

Here X runs over the complete set of physically allowed states. The insertions of unity as expressed in eq. (E.2) in the matrix element in eq. (E.1) are at the positions marked by the arrows:

$$\langle 0 | T \eta \uparrow j_\mu j_\nu \uparrow \bar{\eta} | 0 \rangle.$$

We then use eq. (E.2) as well as the translation property:

$$\eta(y) = e^{+i\mathcal{P} \cdot y} \eta(0) e^{-i\mathcal{P} \cdot y}, \quad \mathcal{P}|0\rangle = 0.$$

where \mathcal{P} is the momentum operator, and perform the integrals over y and z as the matrix element no longer contains any y, z dependence. Ignoring the x -integral, summations and various δ -functions for the sake of clarity, the coördinate space matrix element can be written as

$$\langle 0|\eta(0)|X\rangle \times \langle X|j_\mu(x)j_\nu(0)|Y\rangle \times \langle Y|\bar{\eta}(0)|0\rangle. \quad (E.3)$$

We now use the fact that η couples to the nucleon state with a strength given by λ_N , *i.e.*,

$$\langle 0|\eta(0)|N\rangle = \lambda_N u(p, M_N), \quad (E.4)$$

where u is the proton spinor. We see that for $X = Y = N$, that is, for the ground state nucleon, eq. (E.3) can be written as a product of three terms,

$$\lambda_N u(p) \times \langle p|Tj_\mu j_\nu|p\rangle \times \bar{u}(p)\lambda_N.$$

Putting back the x -dependent factors and defining

$$T_{\mu\nu} = i \int d^4x e^{iq \cdot x} \langle p|Tj_\mu j_\nu|p\rangle,$$

we get

$$\text{Im}T_{\mu\nu}^{\text{ground state}} = \frac{\lambda_N^2}{(p^2 - M_N^2)^2} \text{Im}[u(p)T_{\mu\nu}\bar{u}(p)],$$

which is the result obtained in eq. (8.8). The second expression in eq. (8.8) is obtained by using eq. (8.2) for $\text{Im}T_{\mu\nu}$ and using $u\bar{u} = \not{p} + M_N$.

E.2 The RHS

We now outline the calculation for the result of Fig. (8.1) shown in eq. (8.11). We use the identities for γ -matrices as well as colour traces as set up in Appendix B. For the u -quark diagram corresponding to the calculation with the neutron current, namely,

$$\eta(y) = \epsilon^{abc} [(d^a)^T C \gamma_\alpha d^b] \gamma_5 \gamma^\alpha u^c,$$

we get

$$\mathcal{P} \equiv \eta(y)\bar{\eta}(0) = 2\epsilon^{abc}\epsilon^{a'b'c'} \text{Tr} [\gamma_\alpha S_d^{bb'} \gamma_\beta C (S_d^{aa'})^T C] \gamma_5 \gamma_\alpha S_u^{cc'} \gamma_\beta \gamma_5, \quad (E.5)$$

where S_q is the quark propagator and the factor 2 appears as the two possible contractions yield identical contributions. The quark propagator corresponding to the quark which interacts with the photon is given by

$$S_u^{cc'} = \frac{ie_u^2 \delta^{cc'}}{k^4 (k+q)^2} [k\gamma_\mu (k + \not{q})\gamma_\nu k] , \quad (E.6)$$

where the momenta are as indicated in Fig. (8.1) and γ matrices are the vertex functions. The other quark propagators are simple ones and have been given in Appendix B *i.e.*,

$$\begin{aligned} S_d^{aa'} &= \frac{i}{\ell^2} \not{\ell} \delta^{aa'} ; \\ S_d^{bb'} &= \frac{i}{(p-k-\ell)^2} (\not{p} - \not{k} - \not{\ell}) \delta^{bb'} . \end{aligned} \quad (E.7)$$

Then the contribution to $\mathcal{T}_{\mu\nu}$ of this diagram is

$$\mathcal{T}_{\mu\nu}^{A,u} = \int \frac{d^4 k}{(2\pi)^4} \frac{d^4 \ell}{(2\pi)^4} \mathcal{P} . \quad (E.8)$$

Taking the imaginary part of this correlation function involves putting the “cut” lines in Fig. (8.1) on mass-shell as per the Cutkosky rules. In other words, for every quark line with momentum, q , that is put on-shell, we make the replacement,

$$\frac{1}{q^2} \rightarrow (-2\pi i) \delta(q^2) ,$$

as we have made the assumption of massless quarks. Hence, on substituting the propagators in eqs. (E.6) and (E.7) in eq. (E.5), the product of momenta that appears in the denominator, namely,

$$\frac{1}{\ell^2} \frac{1}{(p-k-\ell)^2} \frac{1}{(k+q)^2}$$

is replaced by the δ -functions,

$$(-2\pi i)^3 \delta(\ell^2) \delta(p-k-\ell)^2 \delta(k+q)^2 .$$

Putting together all these results, the expression for $\text{Im}\mathcal{T}_{\mu\nu}$ from Fig. (8.1) for the neutron is as shown in eq. (8.10):

$$\begin{aligned} & -\frac{2e_u^2}{(2\pi)^5} \epsilon^{abc} \epsilon^{abc} \int \frac{d^4 k}{k^4} d^4 \ell \delta(k+q)^2 \delta(\ell^2) \delta(p-k-\ell)^2 \left\{ \text{Tr} [\not{\ell} \gamma_\alpha (\not{p} - \not{k} - \not{\ell}) \gamma_\beta] \times \right. \\ & \left. \gamma_5 \gamma^\alpha k (\gamma_\mu (\not{k} + \not{q}) \gamma_\nu - \gamma_\nu (\not{k} + \not{q}) \gamma_\mu) k \gamma^\beta \gamma_5 \right\} . \end{aligned} \quad (E.9)$$

The trace can be computed using the identities in Appendix B. The k and ℓ integrations can be performed using the Identities listed in the next section. The result of such a computation is shown in eq. (8.11). Calculations for the other diagrams in Chapter 8 (Figs. (8.2)–(8.5)) follow similarly.

E.3 List of Integrals

We present, without details, the list of integrals that we have used in the computation of the various terms in the Sum Rule calculation. Note that only the terms singular in p^2 have been listed. The integrals also have terms constant in p^2 , but we ignore them as these vanish on taking the Borel transformation. We begin with a list of the ℓ -integrals (see Section 8.2).

Table of Integrals of the δ - δ Type

$$\begin{aligned} \int d^4\ell \delta(\ell^2) \delta(p-k-\ell)^2 \ell_\rho &= \frac{\pi}{4} (p-k)_\rho \theta(p-k)^2 \\ \int d^4\ell \delta(\ell^2) \delta(p-k-\ell)^2 \ell_\rho \ell_\lambda &= \frac{\pi}{6} \left\{ (p-k)_\rho (p-k)_\lambda \right. \\ &\quad \left. -(p-k)^2 g_{\rho\lambda} \right\} \theta(p-k)^2 \\ \int d^4\ell \delta(\ell^2) \delta(p-k-\ell)^2 \ell_\rho (p-k-\ell)_\lambda &= \frac{\pi}{24} \left\{ 2(p-k)_\rho (p-k)_\lambda \right. \\ &\quad \left. +(p-k)^2 g_{\rho\lambda} \right\} \theta(p-k)^2 \\ \int d^4\ell \delta(\ell^2) \delta(p-k-\ell)^2 \ell \cdot (p-k-\ell) &= \frac{\pi}{4} \left\{ (p-k)^2 \right\} \theta(p-k)^2 \end{aligned}$$

Table of Integrals of the δ - θ Type

We list results for integrals of the form

$$\begin{aligned} \mathcal{I}_n^m \equiv \int \frac{d^4k}{k^{2n}} \delta(k+q)^2 \theta(p-k)^2 \{k_{\rho_1} k_{\rho_2} \dots k_{\rho_m}\} &= \left\{ \left\{ A_{m0}^m [p_{\rho_1} p_{\rho_2} \dots p_{\rho_m}] \right. \right. \\ &\quad \left. \left. + A_{m1}^m [q_{\rho_1} p_{\rho_2} \dots p_{\rho_m}]_S + \dots + A_{mm}^m [q_{\rho_1} q_{\rho_2} \dots q_{\rho_m}] \right\} \right. \\ &\quad \left. + \left\{ B_{m2}^m [g_{\rho_1 \rho_2} p_{\rho_3} p_{\rho_4} \dots p_{\rho_m}]_S + B_{m3}^m [g_{\rho_1 \rho_2} q_{\rho_3} p_{\rho_4} \dots p_{\rho_m}]_S \right. \right. \\ &\quad \left. \left. + \dots + B_{mm}^m [g_{\rho_1 \rho_2} q_{\rho_3} q_{\rho_4} \dots q_{\rho_m}]_S \right\} + \dots + Z^m \right] \ln \left(\frac{-xp^2}{2\nu} \right), \end{aligned} \tag{E.10}$$

for $n = 1, 2$. Here $[\]_S$ implies symmetrisation over enclosed indices, with

$$\begin{aligned} Z^m &= \left[g_{\rho_1 \rho_2} g_{\rho_3 \rho_4} \cdots g_{\rho_{m-1} \rho_m} \right]_S C^m \quad \text{for } m \text{ even} \\ Z^m &= \left[g_{\rho_1 \rho_2} g_{\rho_3 \rho_4} \cdots g_{\rho_{m-2} \rho_{m-1}} \left\{ C_p^m p_{\rho_m} + C_q^m q_{\rho_m} \right\} \right]_S \quad \text{for } m \text{ odd} \end{aligned} \quad (E.11)$$

When $n = 0$, the resulting integral is nonsingular:

$$\mathcal{I}_0^0 \equiv \int d^4 k \delta(k+q)^2 \theta(p-k)^2 = \text{nonsingular} .$$

We begin with the case when $n = 1$. The basic result for $m = 0$ is

$$\mathcal{I}_1^0 \equiv \int \frac{d^4 k}{k^2} \delta(k+q)^2 \theta(p-k)^2 = \frac{\pi p^2}{4\nu} \left[1 - x - \frac{p^2 x}{2\nu} (1 - 2x) \right] \ln\left(\frac{-xp^2}{2\nu}\right) .$$

For the case when $m \neq 0$, we present results for the coefficients, A, B, \dots , as defined in eqs. (E.10) and (E.11). We have

$$\begin{aligned} A_{10}^1 &= \left[\frac{\pi p^2}{4\nu} \left(x(1-x) + \frac{p^2}{2\nu} x(1-5x+5x^2) \right) \right] \\ A_{11}^1 &= \left[\frac{\pi p^4}{16\nu^2} (1-x)(1-3x) \right] \\ \\ A_{20}^2 &= \left[\frac{\pi p^2}{4\nu} \left(x^2(1-x) + \frac{p^2}{2\nu} x^2(3-11x+9x^2) \right) \right] \\ A_{21}^2 &= \left[\frac{\pi p^4}{8\nu^2} x(1-x)(1-2x) \right] \\ A_{22}^2 &= [0 + \mathcal{O}(p^6/\nu^3)] \\ B_{22}^2 &= - \left[\frac{\pi p^4}{16\nu} x(1-x)^2 \right] \\ \\ A_{30}^3 &= \left[\frac{\pi p^2}{4\nu} \left(x^3(1-x) + \frac{p^2}{2\nu} x^3(6-19x+14x^2) \right) \right] \\ A_{31}^3 &= \left[\frac{\pi p^4}{16\nu^2} x^2(1-x)(3-5x) \right] \\ A_{32}^3 &= [0 + \mathcal{O}(p^6/\nu^3)] \\ A_{33}^3 &= [0 + \mathcal{O}(p^6/\nu^3)] \\ B_{32}^3 &= - \left[\frac{\pi p^4}{16\nu} x^2(1-x)^2 \right] \\ B_{33}^3 &= [0 + \mathcal{O}(p^6/\nu^3)] \end{aligned}$$

For the case where $n = 2$ and $m = 0$, we have

$$I_2^0 \equiv \int \frac{d^4 k}{k^4} \delta(k+q)^2 \theta(p-k)^2 = -\frac{\pi}{4x\nu} \ln\left(\frac{-xp^2}{2\nu}\right) \left[1-x - \frac{p^2 x}{2\nu} (1-2x) - \frac{p^4 x}{4\nu^2} (1-4x+6x^2) \right]$$

Notice that the leading order term in this case is of $\mathcal{O}(1/\nu)$ rather than of $\mathcal{O}(p^2/\nu)$ as in the case when $n = 1$. As in the earlier case, the $m \neq 0$ results for $n = 2$ are

$$A_{10}^1 = -\left[\frac{\pi}{4\nu} \left((1-x) + \frac{p^2}{2\nu} (1-6x+6x^2) - \frac{9p^4}{4\nu^2} x(1-4x+4x^2) \right) \right]$$

$$A_{11}^1 = \left[\frac{\pi p^2}{4\nu^2} \left(1-x + \frac{p^2}{4\nu} (3-13x+12x^2) \right) \right]$$

$$A_{20}^2 = -\left[\frac{\pi}{4\nu} \left(x(1-x) + \frac{p^2}{2\nu} x(4-15x+12x^2) + \frac{3p^4}{4\nu^2} x(1-15x+41x^2-30x^3) \right) \right]$$

$$A_{21}^2 = -\left[\frac{\pi p^2}{8\nu^2} \left((1-x)(1-3x) + \frac{p^2}{2\nu} (1-16x+43x^2-30x^3) \right) \right]$$

$$A_{22}^2 = \left[\frac{3\pi p^4}{16\nu^3} (1-x)(1-2x) \right]$$

$$B_{22}^2 = \left[\frac{\pi p^2}{8\nu} \left((1-x)^2 + \frac{p^2}{4\nu} (1-10x+21x^2-12x^3) \right) \right]$$

$$A_{30}^3 = -\left[\frac{\pi}{4\nu} \left(x^2(1-x) + \frac{p^2 x^2}{2\nu} (9-28x+20x^2) + \frac{p^4}{4\nu^2} x^2 (18-155x+338x^2-216x^3) \right) \right]$$

$$A_{31}^3 = -\left[\frac{\pi p^2}{4\nu^2} \left(x(1-x)(1-2x) + \frac{p^2 x}{4\nu} (6-49x+101x^2-60x^3) \right) \right]$$

$$A_{32}^3 = -\left[\frac{\pi p^4}{16\nu^3} (1-x)(1-8x+10x^2) \right]$$

$$A_{33}^3 = [0 + \mathcal{O}(p^6/\nu^4)]$$

$$C_p^3 = \left[\frac{\pi p^2}{8\nu} \left(x(1-x)^2 + \frac{p^2 x}{2\nu} (1-6x+10x^2-5x^3) \right) \right]$$

$$C_q^3 = \left[\frac{\pi p^4}{32\nu^2} ((1-x)^2(1-4x)) \right]$$

$$\begin{aligned}
A_{40}^4 &= -\left[\frac{\pi}{4\nu}(x^3(1-x))\right] \\
A_{41}^4 &= -\left[\frac{\pi p^2}{8\nu^2}x^2(1-x)(3-5x)\right] \\
A_{42}^4 &= -\left[\frac{3\pi p^4 x}{16\nu^3}((1-x)(3-9x+7x^2))\right] \\
A_{43}^4 &= [0 + \mathcal{O}(p^6/\nu^4)] \\
A_{44}^4 &= [0 + \mathcal{O}(p^6/\nu^4)] \\
B_{42}^4 &= \left[\frac{\pi p^2}{8\nu}x^2(1-x)^2\right] \\
B_{43}^4 &= \left[\frac{\pi p^4}{32\nu^2}x(1-x)^2(5-8x)\right] \\
B_{44}^4 &= [0 + \mathcal{O}(p^6/\nu^4)] \\
C^4 &= -\left[\frac{\pi p^4}{32\nu}x(1-x)^3\right]
\end{aligned}$$

Finally, we point out that there exist several recursion relations between the set of $n = 1$ and the set of $n = 2$ integrals. These were used to verify many of these integrals. In particular, we have

$$\begin{aligned}
g_{\rho_1\rho_2}\mathcal{I}_2^2(\rho_1,\rho_2) &= \mathcal{I}_1^0 \\
g_{\rho_1\rho_2}\mathcal{I}_2^3(\rho_1,\rho_2,\rho_3) &= \mathcal{I}_1^1(\rho_3) \\
g_{\rho_1\rho_2}\mathcal{I}_2^4(\rho_1,\rho_2,\rho_3,\rho_4) &= \mathcal{I}_1^2(\rho_3,\rho_4) \\
&\dots = \dots,
\end{aligned}$$

and can be easily obtained from eq. (E.10).